THE ROLES OF PLATELET CLEC-2 AND PODOPLANIN IN SKIN WOUND HEALING

by

Surasak Wichaiyo

UNIVERSITY OF BIRMINGHAM

A thesis submitted to The University of Birmingham for the degree of

DOCTOR OF PHILOSOPHY

Institute of Cardiovascular Sciences

College of Medical and Dental Sciences

The University of Birmingham, UK

August 2019

Abstract

Platelet-expressed C-type lectin-like receptor-2 (CLEC-2) and glycoprotein (GP)VI play important roles in inflammation, in particular inflammatory haemostasis in the skin. The CLEC-2-ligand, podoplanin, is upregulated in the inflamed and wounded skin, but the role of the CLEC-2-podoplanin interaction and the signalling downstream of podoplanin in the repair process is unclear. I have addressed these questions by investigating skin wound healing in wild-type (WT) mice, transgenic mice that lack platelet GPVI or CLEC-2 or both receptors (double knockout; DKO), and podoplanin cytoplasmic tail-deficient (*PdpnCyto*) mice. Deletion of both CLEC-2 and GPVI impairs vascular integrity in the skin resulting in accelerated wound healing. The beneficial effect was due to increased plasma leakage in the tissue that promoted fibrin generation, enhanced re-epithelialisation and angiogenesis, and decreased immune cell infiltration. Accelerated wound healing also led to smaller scar formation. This healing phenotype is not due to developmental defects in DKO animals as similar results were obtained in podoplanin-blocking antibody-injected GPVI-deficient mice. Wound healing is independent of the signalling downstream of podoplanin as *PdpnCyto* mice had similar healing kinetics compared to WT mice. *PdpnCyto* mice were however capable of upregulating podoplanin during wound healing, suggesting further application of this model in inflammatory settings. Alongside wound repair, the *PdpnCyto* mice were characterised. I have shown that the cytoplasmic tail is dispensable for the separation of blood and lymphatic vessels. In addition, I have used a metabolomics approach to reveal an increase in M1 pro-inflammatory metabolites, i.e. glycolysis and inducible nitric oxide synthase (iNOS)-mediated arginine pathway, in bone marrow-derived podoplanin-deficient macrophages, which possibly support the anti-inflammatory activity of podoplanin in macrophages.

Acknowledgements

I wish to express my deep appreciation to those who give support along the way of my PhD study. Most importantly, I would like to thank my supervisor Prof. Steve Watson for being supportive and giving me the opportunity to learn several skills during the past three years. I genuinely thank Julie and Sian for being a great mentor and for doing me the favours on animal work, over the years. Thank you to Jerry and Sam for all guidance on wound experiments, Neil for sequencing stuff, Lizzie for embryo work, Jeremy for image analyses, Ying for providing recombinant CLEC-2, Alex Brill for productive discussion, Beata and Stef Watson for all general helps, and all other members of the Platelet Research Group for giving me the support, encouragement and friendship.

I would like to acknowledge the Ministry of Sciences and Technology of Thailand for providing me a PhD scholarship and the Office of Educational Affairs under the Royal Thai Embassy in London for welfare support during studying in the UK. Thank you research facilities at the University of Birmingham, including Biomedical Services Unit for all support with animal experiments, the Technology Hub for imaging assistance and the Phenome Centre for metabolomics collaboration.

I would also like to extend my gratitude to my teachers and colleagues at the Faculty of Pharmacy, Mahidol University, Thailand, particularly Assoc. Prof. Srichan and Assoc. Prof. Chuthamanee for giving me the opportunity to start my academic career at the Department of Pharmacology and for promoting my higher education.

Thank you to all Thai friends in the UK for making me feel at home. Last but not least, thank you to my mom and dad for all your unconditional and endless support and care.

Table of Contents

Page

List of Figures

Page

List of Tables

Page

List of Abbreviations

Term	Full name
ADAM	A Disintegrin and metalloproteinases
ADP	Adenosine diphosphate
ATP	Adenosine triphosphate
bp	Base pair
BSA	Bovine serum albumin
CD	Cluster of differentiation
CLEC-2	C-type lectin-like receptor-2
CRISPR/Cas9	Clustered regularly interspaced palindromic repeats/CRISPR-associated protein 9
DC	Dendritic cells
DETC	Dendritic epithelial T-cell
DKO	Double knockout
DVT	Deep vein thrombosis
E	Embryonic day
ECM	Extracellular matrix
ERM	Ezrin/radixin/moesin family proteins
F	Clotting factors
$FADH_2$	Flavin adenine dinucleotide
Fc	Fragment constant portion of IgG
FcRγ	γ-chain of Fc receptor
fMLP	N-Formyl-Methionyl-Leucyl-Phenylalanine
FRC	Fibroblastic reticular cell
GP	Glycoprotein

H&E	Haematoxylin and eosin
HEV	High endothelial venule
HILIC	Hydrophilic interaction liquid chromatography
HIV	Human immunodeficiency virus
HPF	High power field
HRP	Horseradish peroxidase
IDH	Isocitrate dehydrogenase
IFN	Interferon
Ig	Immunoglobulin
IL	Interleukin
iNOS	Inducible nitric oxide synthase
ITAM	Immunoreceptor tyrosine-based activation motif
LEC	Lymphatic endothelial cell
MS	Mass spectrometry
NADH	Nicotinamide adenine dinucleotide
NET	Neutrophil extracellular trap
NG2	Neuron-glial antigen 2
NK	Natural killer
NMR	Nuclear magnetic resonance spectroscopy
O.C.T.	Optimal cutting temperature
OXPHOS	Oxidative phosphorylation
P2X	Purinergic 2X receptor
P2Y	Purinergic 2Y receptor
PAR	Protease-activated receptor
PBST	Phosphate buffer saline with 0.1% Tween
PCR	Polymerase chain reaction

PDGF	Platelet-derived growth factor
PF4	Platelet factor 4
PLAG	Platelet aggregation-stimulating domains
PLC	Phospholipase C
Rbc	Red blood cell
rCLEC-2-Fc	Recombinant dimeric CLEC-2-Fc
rpA	Reverse passive Arthus reaction
S1P	Sphingosine-1-phosphate
SDH	Succinate dehydrogenase
SEM	Standard error of mean
SFKs	Src family kinases
Syk	Spleen tyrosine kinase
TCA	Tricarboxylic acid cycle
TGF	Transforming growth factor
TLR	Toll-like receptor
TNF	Tumour necrosis factor
TxA_2	Thromboxane A_2
UVB	Ultraviolet B
VEGF	Vascular endothelial growth factor
VTE	Venous thromboembolism
VWF	von Willebrand factor
WT	Wild-type
α-SMA	α-smooth muscle actin

Chapter 1 Introduction

1.1 An overview of platelet biogenesis

Platelets are small anucleate cells derived from megakaryocytes in bone marrow and in the lung vasculature. Platelets primarily circulate in blood vessels and senescent platelets are removed from blood by phagocytes in the reticuloendothelial system, mainly in the spleen (Semple et al., 2011, Yeung et al., 2018, Lefrancais et al., 2017, Li et al., 2017). A circulating lifespan of individual platelet in human is 7-10 days, thereby, leading to daily production of approximately 100 billion platelets to maintain normal platelet counts (150-400 x 10^9 cells per litre of blood). In mice, platelets live shorter (3-5 days) in blood circulation and the platelet counts (900-1,600 x 10^9 cells per litre of blood) are higher than in human (Semple et al., 2011). Platelets express numerous surface proteins, including receptors and adhesion molecules. In addition, platelets contain α-granules and dense granules (Figure 1.1), which collectively release over 300 molecules upon platelet stimulation, including secondary mediators of platelet activation, coagulation factors, growth factors, cytokines, and chemokines (Semple et al., 2011, Nurden, 2011, Yeung et al., 2018).

1.2 Platelet function in haemostasis and thrombosis

Platelets play a major physiological role in haemostasis, a process that stops bleeding (Lievens and von Hundelshausen, 2011, Yeung et al., 2018). Based on their size, platelets are marginated to the endothelial wall, which allows immediate detection and response to vascular damage (Xu et al., 2016). Initially after vessel injury, platelets tether at the vessel

wall via the binding of platelet-expressed GPIb-IX-V complex to immobilised von Willebrand factor (VWF) on exposed collagen (Jennings, 2009), leading to GPVI activation by collagen (Jennings, 2009). Thrombin generated through tissue factor-mediated initiation of the extrinsic pathway of coagulation also activates its receptors on platelets (Monroe et al., 2002). These subsequently result in the activation of integrin αIIbβ3 (GPIIb/IIIa) and integrin α2β1 (GPIa/IIa) which bind to VWF/fibrinogen and collagen, respectively (Figure 1.1), leading to firm adhesion. Activated platelets also release secondary mediators, e.g. thromboxane A_2 (TxA_2), and adenosine diphosphate (ADP), which stimulate their G protein-coupled receptors to further amplify platelet activation. The activation of integrin αIIbβ3 on platelets enables binding of fibrinogen that bridges platelet-platelet interaction, resulting in platelet aggregation (Jennings, 2009, Gale, 2011, Montalescot, 2011). In addition to primary haemostasis, platelets promote the coagulation cascade. Upon activation, platelets expose phosphatidylserine, a negatively charged molecule, on their outer layer of plasma membrane, which recruits coagulation factors (Xase and prothrombinase complexes), contributing to the propagation of thrombin generation. Thrombin then converts fibrinogen into fibrin, forming an insoluble stable haemostatic plug at the site of injury (i.e. secondary haemostasis) (Gale, 2011, Xu et al., 2016).

In contrast to normal haemostasis, excessive platelet activation/aggregation leads to a detrimental occlusion of blood vessels, which contributes to the pathogenesis of arterial thrombosis (Rivera et al., 2009, Yeung et al., 2018). Arterial thrombosis, including coronary artery disease, cerebrovascular artery disease, and peripheral arterial disease, occurs at sites of medium to high shear flow (500-1500 s^{-1}) and is associated with the

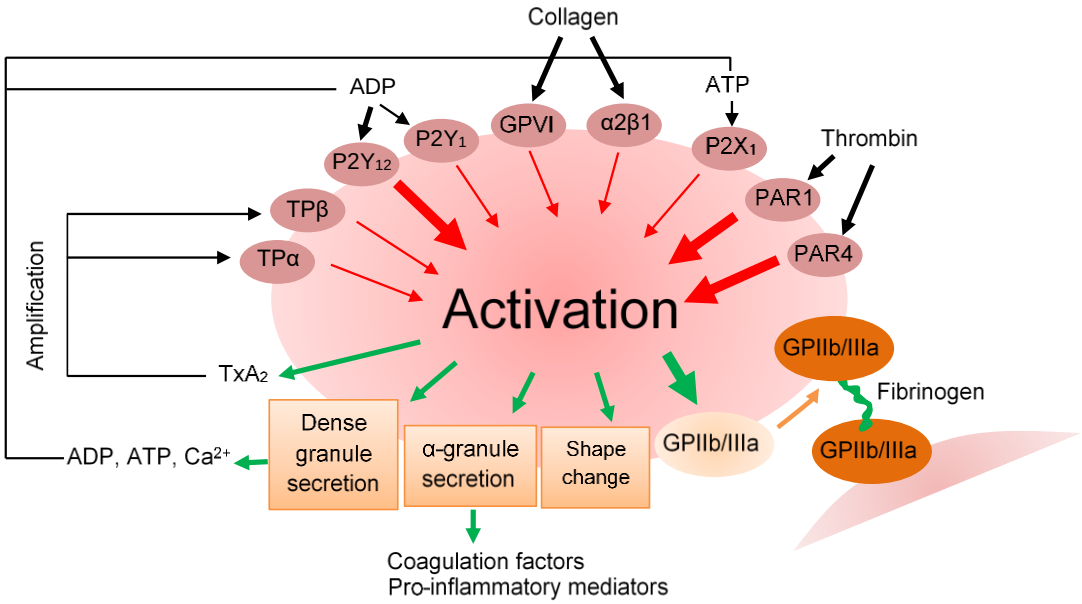

Figure 1. 1. Simplified mechanism of platelet activation and aggregation. After initial adhesion to endothelium during vascular injury, platelets via GPVI and integrins (α2β1 and αIIbβ3) mediate platelet activation and adhesion. Thrombin, generated by the extrinsic pathway of coagulation (tissue factor-dependent), also activates platelets. The activated platelets release secondary mediators, such as thromboxane A_2 (TxA_2), adenosine diphosphate (ADP), adenosine triphosphate (ATP), which subsequently amplify platelet activation. Integrin αIIbβ3 allows fibrinogen binding, resulting in platelet-platelet interaction and the formation of stable platelet aggregates. Thick arrow = potent effect. PAR = protease-activated (thrombin) receptor, P2X = purinergic 2X (ATP) receptor, P2Y = purinergic 2Y (ADP) receptor, TP = TxA_2 receptor. Adapted from (Wallentin, 2009, Xu et al., 2016).

formation of platelet-rich thrombi (also called a white clot) (Ouriel, 2001, Xu et al., 2016, Yeung et al., 2018). The rupture of atherosclerotic plaque is the most common cause of acute arterial thrombosis, such as acute coronary syndrome and ischaemic stroke. In atherosclerosis, activated platelets not only support clot formation but also recruit neutrophils and monocytes to the site of vascular damage, which also promote the growth of thrombi. Accordingly, anti-platelet drugs, such as aspirin and P2Y12 receptor antagonists, are recommended for prophylactic prevention and treatment of acute arterial thrombotic events (Xu et al., 2016, Yeung et al., 2018).

Venous thromboembolism (VTE), including deep vein thrombosis (DVT) and pulmonary embolism, arises under low shear flow (10 - 500 s^{-1}) and represent as fibrin-rich thrombi (also called red clots), indicating an over-activation of blood coagulation. Therefore, anticoagulants, such as unfractionated and low-molecular-weight heparins, are mainly used for prophylaxis of occurrence, the treatment of acute episodes, and the prevention of recurrence in VTE (Yeung et al., 2018, Xu et al., 2016, Mackman, 2012). However, emerging evidence has demonstrated a crucial contribution of platelets in the pathogenesis of VTE. For example, a reduction in blood flow can cause hypoxia, which activates endothelial cells leading to exposure of P-selectin and VWF (Brill et al., 2011). Platelets adhere to the activated endothelium via GPIbα-VWF. In addition, platelets recruit leucocytes, which express tissue factor on activation, triggering the extrinsic pathway of coagulation cascade (Mackman, 2012, Xu et al., 2016). As mentioned, phosphatidylserine exposure on the surface of activated platelets also promotes coagulation (Xu et al., 2016). Polyphosphate released from activated platelets stimulates factor XII activation to XIIa which regulates an intrinsic pathway of blood coagulation, although the significance of this is unknown (Mackman, 2012). In mice, genetic ablation

of P2Y1 (Bird et al., 2012) or CLEC-2 on platelets (Payne et al., 2017) has been shown to decrease the occurrence of VTE. In addition, anti-platelet drugs, such as aspirin and clopidogrel reduce VTE in rats, rabbits, and dogs (Yeung et al., 2018). Clinical studies also support a role for platelets in VTE by demonstrating that aspirin lowers the rate of VTE recurrence in patients who are currently using anticoagulants (Yeung et al., 2018, Xu et al., 2016).

1.3 The role of platelets in maintaining vascular integrity

Vascular endothelium controls the homeostatic function of blood vessels, including the prevention of leakage and the regulation of blood flow, which is termed "vascular integrity" (Nachman and Rafii, 2008, Ho-Tin-Noe et al., 2018). Breakage of endothelial barrier leads to a loss of vascular integrity. Unlike classical haemostasis, platelets have been reported to support vascular integrity by stabilising the intercellular junctions of endothelial cells. Sphingosine-1-phosphate (S1P), angiopoietin-1, platelet-activating factor, vascular endothelial growth factor (VEGF)-A, brain-derived neurotrophic factor, and epidermal growth factor are examples of barrier-strengthening mediators secreted by platelets, contributing to this process (Nachman and Rafii, 2008, Rodrigues and Granger, 2015).

Petechiae, pinpoint red spots in skin due to the extravasation of red blood cells (Rbcs), in patients with thrombocytopenia is one of clinical examples pointing to the vasculoprotective role of platelets during steady-state condition (Nachman and Rafii, 2008). Moreover, sunburn (Carbo et al., 2009) and ultraviolet B (UVB) irradiation (Hillgruber et al., 2015) trigger petechiae in patients with thrombocytopenia whereas anti-inflammatory agents (e.g. glucocorticoids) prevent this reaction (Kitchens and

Pendergast, 1986), demonstrating that inflammation increases the risk of vascular leakage in the presence of low platelet counts (Ho-Tin-Noe et al., 2018).

Several experimental models also demonstrate intra-tissue haemorrhage during inflammation, especially in the skin and the lungs of platelet-depleted animals (Table 1.1) (Ho-Tin-Noe et al., 2018, Gros et al., 2015, Boulaftali et al., 2018, Rayes et al., 2018). Microscopic observation during inflammation reveals that at the site of increased vascular permeability, mainly post-capillary venules, platelets adhere to the vessel wall and prevent inflammatory bleeding by sealing small holes between endothelial junctions following leucocyte extravasation in a G protein-coupled receptor-independent mechanism (Ho-Tin-Noe et al., 2018, Gros et al., 2015). At least, four characteristic features for the contribution of platelets in safeguarding vascular integrity during inflammation have been described. Firstly, intra-tissue bleeding occurs only when the circulating platelets are substantially low (< 2-15 % of normal platelet counts in mice), suggesting that small numbers of platelets are required to prevent inflammatory bleeding. Secondly, single platelets (rather than aggregates) appear to seal an open gap at endothelial junctions in inflamed vasculature. Thirdly, this process may not need full activation of platelets as electron microscopy has shown residual granules in adhered cells. Fourthly, platelets protect vascular integrity during inflammation in an organ- and/or stimulus-dependent manner since there is no abnormal bleeding in thrombocytopenic mice with rheumatoid arthritis, peritonitis, and endotoxaemia (Ho-Tin-Noe et al., 2018).

Table 1. 1. Evidence of intra-tissue bleeding due to the impairment of vascular integrity during inflammation in thrombocytopenic mice

Skin:	reverse passive Arthus reaction (rpA; also called immune complex-induced dermatitis), irritant contact dermatitis, UVB-induced dermatitis
Lung:	LPS-induced lung inflammation, *Klebsiella*-induced pneumonia
Kidney:	immune complex-induced glomerulonephritis
Brain:	cerebral ischemia reperfusion injury, lymphocytic choriomeningitis viral infection
Cancer:	breast tumour (4T1), melanoma (B16F10), Lewis lung carcinoma (LLC)
Other:	ovalbumin and complete Freund's adjuvant-induced immunisation

Adapted from (Ho-Tin-Noe et al., 2018, Gros et al., 2015, Rayes et al., 2018, Boulaftali et al., 2013).

1.4 The role of platelets in other pathways

1.4.1 Platelets as immune cells

Platelets are now considered as immune cells, regulating both innate and adaptive responses. Platelets express toll-like receptors (TLRs) that recognise invading microorganisms. In the acute phase response, lipopolysaccharide (LPS) on the outer membrane of gram-negative bacteria has been reported to activate platelets via TLR4, which induces secretion of antimicrobial peptides and promotes platelet-neutrophil interaction, subsequently stimulating the release of neutrophil extracellular traps (NETs) for bacterial killing (Clark et al., 2007), although this has not been seen by other groups including the Watson laboratory (personal communication). This LPS-TLR4 interaction also contributes to sepsis-associated thrombocytopenia caused by platelet consumption (microthrombi) within end organs, such as in the lung (Xu et al., 2016, Morrell et al., 2014, Thomas and Storey, 2015). Moreover, platelets demonstrate host defense against parasitic infection by binding to *Plasmodium spp.*-infected Rbcs and releasing platelet factor 4 (PF4) to kill this parasite (Kho et al., 2018, Xu et al., 2016). In contrast, platelets directly interact dengue (Simon et al., 2015) and human immunodeficiency virus (HIV)-1 (Chaipan et al., 2006), which support dengue infection and HIV-1 transmission, respectively.

Activated platelets expose P-selectin on their cell surface, which binds P-selectin glycoprotein ligand 1 on leucocytes (Rinder et al., 1991). In addition, platelet GPIbα directly interacts with integrin αMβ2 (or macrophage-1 antigen; Mac-1) on leucocytes and indirectly through binding to fibrinogen (Wang et al., 2017). These interactions

facilitate leucocyte trafficking to the site of inflammation (Xu et al., 2016, Morrell et al., 2014, Thomas and Storey, 2015).

The interplay between platelets and the adaptive response has also been described. Platelets bind circulating lymphocytes to facilitate lymphocyte entry into lymph nodes in a P-selectin-dependent fashion (Diacovo et al., 1996). In addition, platelet-derived PF4 inhibits Th17 cell differentiation, reducing the inflammatory reaction (Shi et al., 2014, Guo et al., 2015). Moreover, a cluster of differentiation (CD) 40 ligand (CD40L) on platelets promote inflammatory responses of B- and T-lymphocytes. For example, CD40L mediates switching of immunoglobulin (Ig) production by B-cells (i.e. the increase in IgG relative to IgM). In addition, it enhances interferon (IFN)-γ secretion by T-cells (Elzey et al., 2003).

1.4.2 Platelets in lymphangiogenesis and angiogenesis

During embryonic development, platelets play a key role in prevention of mixing of blood and lymphatic vasculatures. The interaction of platelets with podoplanin, an endogenous CLEC-2 ligand, on lymphatic endothelial cells (LECs), has been shown to regulate this process (Xu et al., 2016, Schacht et al., 2003, Bertozzi et al., 2010, Finney et al., 2012).

Platelets also secrete growth factors to facilitate angiogenesis (i.e. the formation of new blood vessels from the existing ones), which is important for embryonic development, tissue repair, and tumour growth. Platelet-derived growth factor (PDGF), VEGF, insulin-like growth factor, and angiopoietin-1 are examples of pro-angiogenic factors released by activated platelets. In addition to these proteins, platelet-derived cytokines and chemokines promote the recruitment of leucocytes, fibroblasts, and endothelial cells during wound healing (Xu et al., 2016, Yang et al., 2011).

1.4.3 Platelets in cancer metastasis

Several lines of evidence suggest the role of platelets in tumour metastasis, a process of tumour cell migration from primary site to the distant tissues (Xu et al., 2016). For example, tumour spreading is limited in thrombocytopenia whereas it is reversed by transfusion of platelet-rich plasma (Gasic et al., 1968). Platelet-derived P-selectin and GPIIb/IIIa mediate aggregate formation between platelets and tumour cells within blood circulation. In addition, podoplanin on tumour cells has been shown to activate platelet CLEC-2 in the bloodstream (Leblanc and Peyruchaud, 2016, Lowe et al., 2012, Shirai et al., 2017). Intravascular platelet-tumour aggregate promotes survival of cancer cells by protecting against shear rate-induced damage and natural killer (NK) cell-mediated cytolysis. In addition, this aggregate activates endothelium to express adhesion molecules for cancer cell arrest at the vessel wall, facilitating extravasation of cancer cells to the target tissues (Xu et al., 2016, Leblanc and Peyruchaud, 2016).

1.5 Platelet (hemi)immunoreceptor tyrosine-based activation motif (ITAM) receptors

ITAMs are defined by the presence of two YxxL sequences separated by six to twelve amino acids, whereas the hemi-ITAM bears a single YxxL (Watson et al., 2010). In human platelets, three (hemi)ITAM-associated platelet activation receptors have been described, including FcγRIIA, GPVI, and CLEC-2 (Watson et al., 2010, Stegner et al., 2014). FcγRIIA is a receptor for the fragment constant (Fc) portion of IgG, which contributes to immune complexes-mediated thrombosis and thrombocytopenia, such as in heparin-induced thrombocytopenia in human (Kelton et al., 2013, Gitz et al., 2014,

Qiao et al., 2015). However, this receptor is not expressed on mouse platelets or indeed in the rodent genome (McKenzie et al., 1999).

1.5.1 Structure and function of GPVI

GPVI belongs to the Ig superfamily of receptors, and is only expressed on surface of megakaryocyte/platelet lineage (Dutting et al., 2012, Stegner et al., 2014). GPVI receptor density is approximately 5,586 ± 1155 copy numbers per mouse platelet (unpublished data from Watson laboratory) whereas the range of 3,730 ± 453 copy numbers is observed per human platelet (Best et al., 2003). On resting platelets, GPVI is present in both monomeric (Dutting et al., 2012) and dimeric forms (Jung et al., 2009). Monomeric GPVI is unable to bind collagen whereas dimerisation of GPVI has high affinity to this ligand (Dutting et al., 2012). To mediate its function, GPVI forms a complex structure with a homodimer of γ-chain of Fc receptor (FcRγ-chain) (Figure 1.2). The intracellular structure of GPVI itself consists of proline-rich region, which constitutively binds Src family kinases (SFKs), including Fyn and Lyn (Dutting et al., 2012, Watson et al., 2010) whereas the ITAM domain is located in cytoplasmic region of FcRγ-chain. Upon collagen ligation, GPVI dimer triggers tyrosine phosphorylation of ITAMs on FcRγ-chain by the SFK, which in turn recruits and activates spleen tyrosine kinase (Syk). This results in subsequent activation of downstream signalling molecules, adaptor proteins (e.g. SLP-76), and effector molecules, including phospholipase C (PLC)-γ2 that mediates platelet activation (Stegner et al., 2014, Dutting et al., 2012, Watson et al., 2010).

In addition to collagen, endogenous ligands of GPVI include fibrin (Alshehri et al., 2015), fibrinogen (Induruwa et al., 2018, Mangin et al., 2018), fibronectin (Bultmann et al., 2010), and laminin (Inoue et al., 2006). Convulxin, a snake venom toxin, can also activate

platelets via GPVI binding (Jandrot-Perrus et al., 1997). Furthermore, it has recently been demonstrated *in vitro* that GPVI dimers can form clusters (multimers) following platelet adhesion to collagen fibres or related substrates, which may potentiate platelet activation (Poulter et al., 2017).

The upregulation of surface GPVI has been reported in patients with acute coronary syndrome (Bigalke et al., 2010a, Bigalke et al., 2010c) and stroke (Bigalke et al., 2010b), which is associated with poor prognosis. On the other hand, the ectodomain of GPVI is rapidly cleaved from activated platelets by A disintegrin and metalloproteinases (ADAM) family sheddases, i.e. ADAM-10 and ADAM-17 (Dutting et al., 2012). Although the physiological function of GPVI shedding is unclear, a soluble form of GPVI is increased in the circulation of patients with thrombotic and thrombo-inflammatory diseases, including acute ischaemic stroke (Al-Tamimi et al., 2011), thrombotic microangiopathy (Yamashita et al., 2014), rheumatoid arthritis (Stack et al., 2017), gout (Conway et al., 2017), cirrhosis (Egan et al., 2017), and sepsis (Montague et al., 2018). Therefore, soluble GPVI is a marker of platelet activation in various pathological settings.

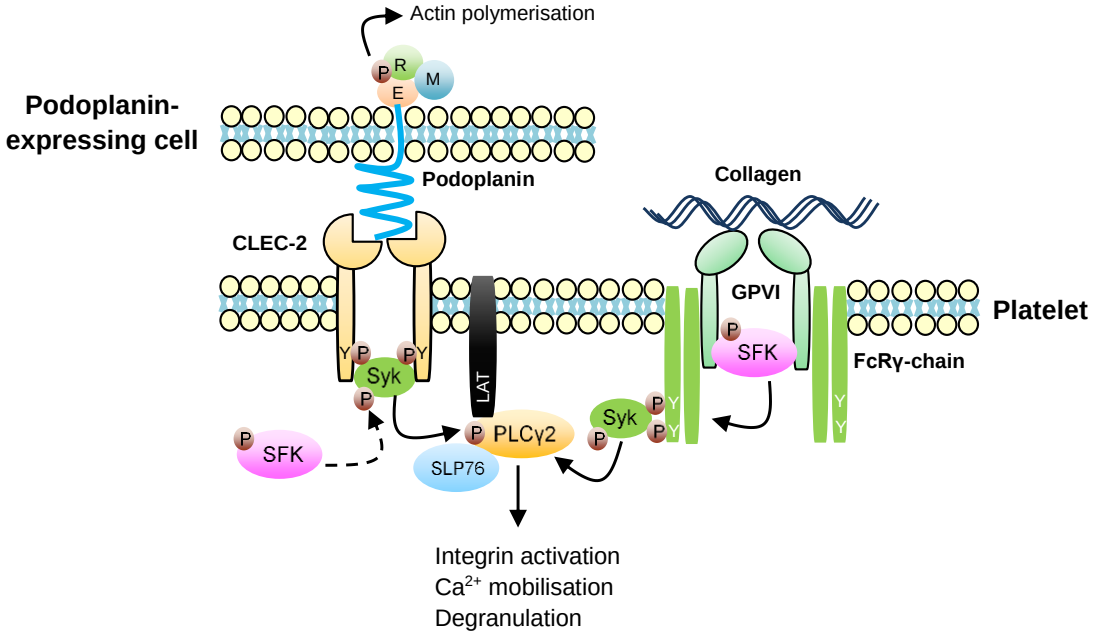

Figure 1. 2. Structure and signalling of platelet GPVI and CLEC-2. The binding of collagen to GPVI dimer allows tyrosine phosphorylation of ITAMs on FcRγ-chain by Src family kinases (SFKs), which subsequently recruit spleen tyrosine kinase (Syk). The phosphorylated Syk further stimulates downstream molecules, including adaptor protein SLP-76 and phospholipase C (PLC)-γ2, resulting in platelet activation. Upon podoplanin interaction, CLEC-2 dimer recruits Syk to the hemi-ITAMs, which leads to Syk-mediated autophosphorylation and the phosphorylation of hemi-ITAMs. SFKs mediate activation of Syk. The downstream events of CLEC-2-mediated platelet activation are similar to that of GPVI. Podoplanin signals through ezrin (E)/radixin (R)/moesin (M) phosphorylation, which modulates actin cytoskeleton and cell migration. "Y" represents the tyrosine residue in YxxL sequence on (hemi)ITAMs. "P" denotes phosphorylated state of proteins. LAT = membrane adaptor protein called "linker for activated T-cells". Adapted from (Watson et al., 2010, Dutting et al., 2012, Astarita et al., 2012).

1.5.2 Structure and function of platelet CLEC-2

CLEC-2 is a type II transmembrane protein, which is abundantly expressed on megakaryocytes and platelets (Watson et al., 2010, Suzuki-Inoue et al., 2011). Murine platelets contain approximately 41,652 ± 7,760 copy numbers of CLEC-2 (Zeiler et al., 2014) whereas 2,016 ± 239 copy numbers are present per human platelet (Gitz et al., 2014). A low level of CLEC-2 is also detected on Kupffer cells and sinusoidal endothelium within the liver (Chaipan et al., 2006, Tang et al., 2010). In mice, CLEC-2 has been reported on circulating B-lymphocytes and $CD11b^{hi}Gr\text{-}1^{hi}$ leucocytes (i.e. granulocytes, monocytes, and NK cells), although the presence on lymphocytes is in the form of microvesicles which are presumed to be platelet in origin (Lowe et al., 2015b). Reports of expression of CLEC-2 on neutrophils are due to off-target binding of the monoclonal antibody (mAb 17D9) (Kerrigan et al., 2009). CLEC-2 is also present on dendritic cells (DCs), especially within lymph node, and it is upregulated during LPS stimulation (Lowe et al., 2015b). DC-expressed CLEC-2 facilitates draining of DCs into lymph nodes (Acton et al., 2014), promotes DC motility within lymph nodes where it can present antigen to T-cells (Acton et al., 2014, Fletcher et al., 2015), and mediates lymph node expansion, which supports leucocyte migration and proliferation during immune responses (Acton et al., 2014, Astarita et al., 2015).

Unlike GPVI/FcRγ-chain complex, the cytoplasmic region of CLEC-2 has a hemi-ITAM, which does not directly bind to SFKs (Figure 1.2). CLEC-2 is constitutively expressed as homodimer. Following ligand engagement, Syk is recruited to the hemi-ITAMs of CLEC-2. Subsequently, SFKs activate Syk, which mediate phosphorylation of hemi-ITAMs.

Activated phosphorylated Syk triggers the similar downstream molecules to that of GPVI to mediate platelet activation (Watson et al., 2010, Suzuki-Inoue et al., 2011)

Currently, the only known endogenous CLEC-2 ligand is podoplanin (also known as aggrus, gp36, gp38, T1α, D2-40, OST-8, PA2.26, RANDAM-2, and transmembrane glycoprotein E11), which is expressed on LECs and a wide variety of cells outside of blood vessels, including type I lung epithelial cells and the choroid plexus (Table 1.2). The extracellular part of podoplanin is extensively O-glycosylated, and has platelet aggregation-stimulating domains (PLAGs), which interact with CLEC-2 (Pan and Xia, 2015, Astarita et al., 2012, Krishnan et al., 2018). Podoplanin has a short cytoplasmic tail that binds ezrin/radixin/moesin (ERM) family proteins (Figure 1.2). The cellular function of podoplanin remains inconclusive. However, the increase in podoplanin expression, including in cancer cells, has been demonstrated *in vitro* to enhance ERM phosphorylation and RhoA activation, which allows binding of other intracellular proteins, including actin, contributing to cell migration and function (Martin-Villar et al., 2006, Suchanski et al., 2017, Takemoto et al., 2017, Krishnan et al., 2018). In contrast, lymph node-derived fibroblastic reticular cells (FRCs) deficient in cytoplasmic tail of podoplanin show a defect in cell elongation despite an intact ERM phosphorylation (Astarita et al., 2015), suggesting ERM-independent regulatory downstream of podoplanin cytoplasmic tail in FRC elongation.

Table 1. 2. Distribution of podoplanin expression in various organs

Kidney:	podocytes, parietal epithelial cells of Bowman's capsule
Lung:	type I alveolar epithelial cells, pleura
Liver:	bile ducts, peritoneum
Skin, oesophagus, cervix:	basal keratinocytes
Salivary gland:	myoepithelial cells
Intestine:	peritoneum
Lymphoid organs:	fibroblastic reticular cells, follicular dendritic cells
Central nervous system:	choroid plexus, ependyma, meninges, neuro-epithelium
Bone:	osteocytes, periosteum
Bone marrow:	fibroblastic reticular-like cells
Heart:	epicardium, pericardium
Breast:	myoepithelial cells
Ovary:	follicular granulosa cells, germinal epithelium
Prostate:	myofibroblast
Testis:	fibromyocytes

Data was combined from human and murine tissues. Adapted from (Astarita et al., 2012, Hou et al., 2010, Hur et al., 2014, Kerrigan et al., 2012, Lowe et al., 2015a, Mahtab et al., 2008, Schacht et al., 2005, Tamura et al., 2016).

Podoplanin is also upregulated during inflammation, such as on macrophages following LPS stimulation (Kerrigan et al., 2012). Furthermore, skin keratinocytes show elevated levels of podoplanin in response to transforming growth factor (TGF)-β, interleukin (IL)-6, IL-22, and IFN-γ (Honma et al., 2012). In a similar fashion, synoviocytes express high levels of podoplanin after treating with IL-1β, tumour necrosis factor (TNF)-α, and TGF-β1 (Ekwall et al., 2011). Therefore, podoplanin is a marker of inflammation and tumour growth (Krishnan et al., 2018), although its function requires further investigation.

Exogenous ligands of CLEC-2 have also been introduced, including a snake venom toxin called 'rhodocytin' and brown seaweed-derived sulphated polysaccharide called 'fucoidan', both of which mediate platelet aggregation (Astarita et al., 2012, Pan and Xia, 2015). Historically, the discovery of CLEC-2 on platelets is based on studies identifying the receptor for rhodocytin-induced platelet aggregation (Suzuki-Inoue et al., 2011, Watson et al., 2010, Suzuki-Inoue et al., 2006). Moreover, HIV-1 is able to bind CLEC-2, despite platelet activation being unlikely to be involved in CLEC-2-mediated HIV-1 transmission (Chaipan et al., 2006).

1.6 Physiological functions of platelet ITAM receptors

Although GPVI mediates stable platelet adhesion and platelet activation, mice deficient in GPVI show no haemostatic defect (Bender et al., 2013). In human, the prevalence of GPVI defects are very rare and it is unclear to what extent loss of GPVI gives rise to bleeding as most cases are caused by autoimmune thrombocytopenia (Arthur et al., 2007). Several unrelated patients homozygous for a truncation mutant prior to the membrane domain in GPVI have been described in Chile and have a mild bleeding diathesis (Matus et al., 2013). Similar to that of GPVI, CLEC-2 deficient animals exhibit normal

haemostasis (Bender et al., 2013). However, combined deficiency of GPVI and CLEC-2 leads to prolonged bleeding time in mice although this is also associated with a reduction in platelet counts (Bender et al., 2013). Based on the observation in genetic ablation studies, GPVI-null mice demonstrate normal viability, fertility, and baseline haematological parameters (Kato et al., 2003), suggesting that GPVI deficiency may not affect developmental and physiological processes. However, it has recently been revealed that GPVI on megakaryocytes controls proplatelet formation in bone marrow (Semeniak et al., 2016) making it difficult to reconcile these observations. In addition, GPVI has been reported to contribute to postnatal closure of ductus arteriosus (Echtler et al., 2010).

1.6.1 CLEC-2-podoplanin in the separation of blood and lymphatic vasculatures

During embryonic day (E) 8.5-9.5 in mice, a subset of venous endothelial cells in cardinal veins are committed to change their fate by expressing prospero-related homeobox domain 1 (Prox-1) transcription factor and lymphatic vascular endothelial hyaluronan receptor-1 (LYVE-1), the markers of lymphatic endothelial cells (LECs) (Bautch and Caron, 2015). These lymphatic endothelial precursors migrate away from the vein and coalesce into primary lymph sac, the earliest form of lymphatic vessel, at E11.5-13.5 (Bautch and Caron, 2015, Pan and Xia, 2015). Podoplanin is expressed on LECs at E11.5-12.5 (Schacht et al., 2003). Platelets via CLEC-2 have been shown to interact with podoplanin-positive LECs and play a role in the separation of lymphatic and venous vasculatures during E11.5-14.5 (Bautch and Caron, 2015, Pan and Xia, 2015, Bertozzi et al., 2010). Mice deficient in podoplanin (Schacht et al., 2003, Bertozzi et al., 2010, Uhrin et al., 2010) or platelet CLEC-2 (Finney et al., 2012, Bertozzi et al., 2010) or downstream molecules following CLEC-2 activation, including Syk (Finney et al., 2012, Abtahian et

al., 2003) and adaptor protein SLP-76 (Abtahian et al., 2003, Bertozzi et al., 2010), exhibit blood-lymphatic mixing (also called blood-filled lymphatics) and commonly die *in utero*.

Although it remains inconclusive, at least five mechanisms of how CLEC-2-podoplanin mediates blood-lymphatic separation have been described:

1. Initially, it is demonstrated that CLEC-2-podoplanin interaction results in accumulation of platelet plug, which terminates blood and lymphatic connections (Bertozzi et al., 2010). However, mice deficient in GPIIb/IIIa have no evidence of blood-filled lymphatics (Hodivala-Dilke et al., 1999, Hess et al., 2014). In addition, blocking GPIIb/IIIa on platelets has no impact on proliferation, migration and tube formation of LECs *in vitro* (Osada et al., 2012), arguing against the role of platelet aggregation.
2. Moreover, the supernatant of activated platelets inhibits this blood-lymph connection (Osada et al., 2012), suggesting a GPIIb/IIIa-independent mechanism participating in platelet activation for the separation of blood and lymphatic vessels that involves platelet granule secretion.
3. Third, it has been proposed that binding of platelet CLEC-2 to podoplanin leads to clustering of both molecules. This stable interaction between platelets and LECs activates signalling downstream of podoplanin to inhibit LEC migration during contact with blood endothelium (Pollitt et al., 2014). However, transgenic mice lacking the cytoplasmic tail of podoplanin show no blood-filled lymphatics (Astarita et al., 2015).
4. Furthermore, once the mature lymphatic capillary has been generated (in late-gestation), platelets mediate thrombus formation at the bicuspid valve

(podoplanin-positive) in lymphovenous junction, where lymph is drained from thoracic duct (a main lymphatic vessel) to the vein, to prevent a reflux of blood into lymphatic vessel. CLEC-2 deficient embryos (E17.5) and adult mice, which lack platelet-containing thrombi at lymphovenous valve, display filling of Rbcs in thoracic duct and subsequent lymphatic network (Hess et al., 2014).

5. More recently, this blood-filled lymphatic phenotype has been linked to the impairment of vascular integrity during development. At E14, the murine mesenteric vein is temporarily leaky, defined by the presence of gaps between adjacent endothelial cells, associated with extravasation of Rbcs, which interact with LECs. Platelets are observed at the intercellular gaps of venous endothelium. Perivascular podoplanin is also detected on mural cells, including the fibroblasts, at E14, suggesting the role of CLEC-2-podoplanin interaction for the maintenance of mesenteric venous integrity during embryogenesis. The intercellular gaps disappear at E15 when the lymphatic vessel is formed. During this stage, Rbcs are transiently presence in developing lymphatic vessels whereas platelets are only observed in blood vasculature. At E16, Rbcs are no longer detected in lymphatic vessel, indicating the beginning of lymphatic drainage (Zhang et al., 2018). In CLEC-2 knockout embryos, there is extravascular localisation of both platelets and Rbcs, which interact with LECs at E14. A more pronounced blood-filled lymphatic vessel is observed at E15 of CLEC-2 deficient embryos. At E16, Rbcs remained in the lymphatic vasculature, suggesting a lack of lymph flow in CLEC-2 knockout embryos (Zhang et al., 2018).

1.6.2 Regulation of high endothelial venule (HEV) integrity by CLEC-2 and podoplanin

In the perivascular zone of lymph nodes (Figure 1.3 A), it has been shown that circulating lymphocytes generally enter into lymph nodes through HEV, a specialised blood vessel, for immune surveillance and this process is substantially increased during immune responses. Following leucocyte transmigration, platelet CLEC-2 binds podoplanin on fibroblastic reticular cells (FRCs) surrounding HEV, resulting in the secretion of platelet-derived S1P. Subsequently, S1P promotes the expression of vascular endothelial (VE)-cadherin to seal HEV cell-cell junctions, maintaining HEV barrier function (integrity) (Herzog et al., 2013). The spontaneous leakage of Rbcs into the extravascular space is observed in lymph nodes of FRC-specific podoplanin-knockout, platelet CLEC-2 deficient, and S1P-deficient mice, which is increased upon immunisation (Herzog et al., 2013). Moreover, histological analysis in mice bearing podoplanin-negative FRCs or CLEC-2-deficient platelets show Rbcs within lymphatic vessels (Herzog et al., 2013), suggesting that the impairment of HEV integrity may also contribute to blood-filled lymphatic phenotype in the absence of CLEC-2-podoplanin interaction (Zhang et al., 2018).

1.6.3 CLEC-2 and podoplanin regulate development and integrity of cerebral blood vessels

It has been reported that CLEC-2 deficient and neuroepithelium-specific podoplanin-knockout embryos exhibit cerebral haemorrhage, in association with a tortuous and discontinuous vascular structure, in the developing brain between E10.5 and E11.5. The evidence of bleeding is more apparent, especially in the ventricle, at E12.5. In addition,

histological examination reveals a decrease numbers of mural cells, including pericytes, around the developing vessel in these embryos, suggesting the defects in vascular development. Cerebral haemorrhage is also present at E12.5 of embryos deficient in integrin αIIb or platelet α- and dense-granules but not in platelet-specific S1P-knockout littermates. Collectively, it is proposed that the early-developed blood vessel is leaky, which allows transient extravasation of Rbcs and platelets into the perivascular area. The interaction of platelet CLEC-2 to podoplanin-expressing neuro-epithelium leads to platelet activation, subsequently releasing non-S1P pro-angiogenic factors to recruit mural cells for a full development of blood vessel (Figure 1.3 B). In addition, the activated platelets (via CLEC-2 stimulation) may form small platelet plugs at the vascular wall in a GPIIb/IIIa-dependent manner to prevent bleeding (maintain vascular integrity) during the development of cerebral blood vessels (Lowe et al., 2015a). This CLEC-2-podoplanin interaction may explain a role of platelets for the prevention of intraventricular haemorrhage in preterm infants (Lowe et al., 2015a).

1.6.4 CLEC-2-podoplanin interaction aids platelet formation in bone marrow

A low platelet count observed in megakaryocyte/platelet-specific CLEC-2 knockout mice raises the research question whether CLEC-2-podoplanin axis contributes to platelet biogenesis. In bone marrow, podoplanin is detected on stromal cells at the periarteriolar interface, defined as ‘bone marrow FRC-like cells’. Megakaryocytes are observed in proximity to these perivascular podoplanin-positive cells. CLEC-2 knockout mice had a reduction in total numbers and the association of megakaryocytes with bone marrow FRC-like cells. The *in vitro* experiments have revealed that either recombinant podoplanin or bone marrow FRC-like cells increases megakaryocyte expansion whereas

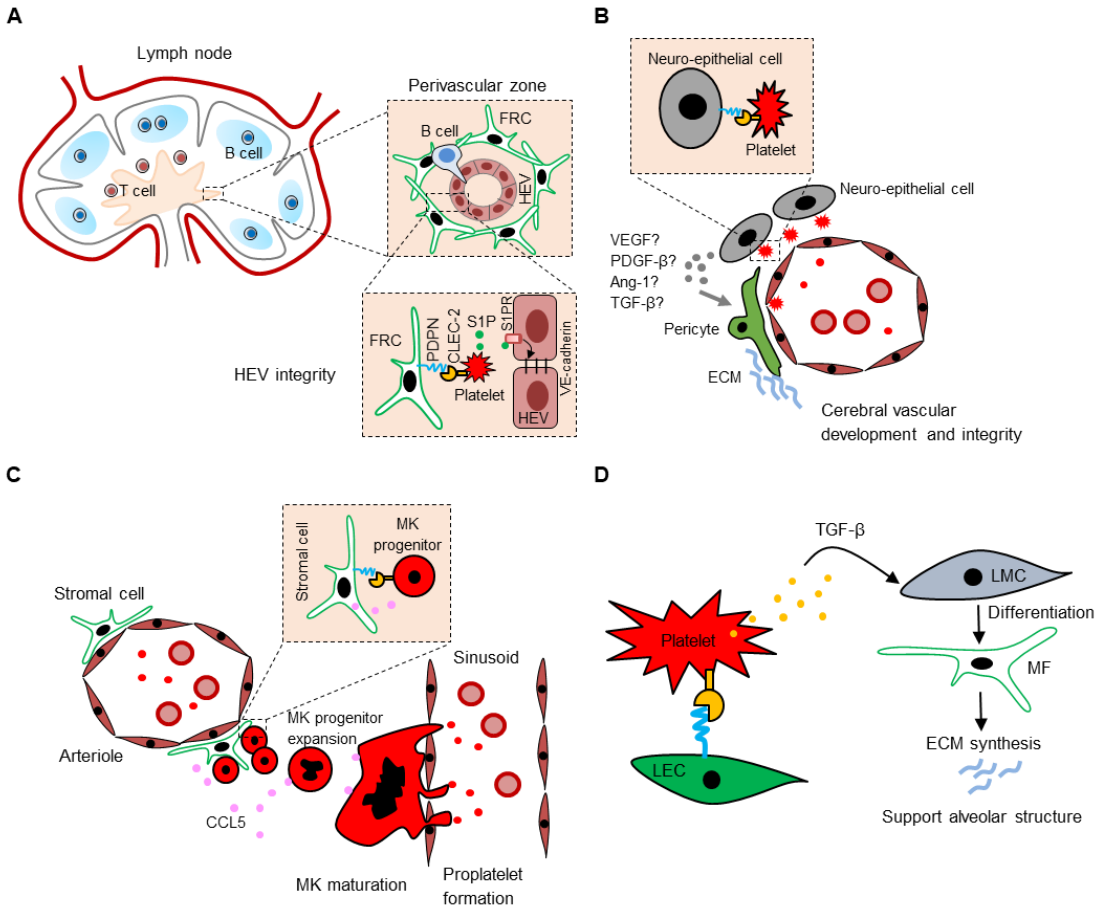

Figure 1. 3. Physiological functions of platelet CLEC-2 and podoplanin interaction. (A) Regulation of high endothelial venule integrity within lymph nodes (Herzog et al., 2013). (B) Cerebrovascular development and integrity (Lowe et al., 2015a). (C) Megakaryocyte expansion and proplatelet formation in bone marrow (Tamura et al., 2016). (D) Lung development (Tsukiji et al., 2018a). FRC = fibroblastic reticular cell, HEV = high endothelial venule, PDPN = podoplanin, S1P = sphingosine-1-phosphate, S1PR1 = sphingosine-1-phosphate receptor 1, VEGF = vascular endothelial growth factor, PDGF-β = platelet-derived growth factor-β, Ang-1 = angiogenin-1, TGF-β = transforming growth factor-β, ECM = extracellular matrix, MK = megakaryocytes, LEC = lymphatic endothelial cell, LMC = lung mesothelial cell, MF = myofibroblast. See text for details.

anti-podoplanin antibody inhibits this effect. These parameters are decreased using CLEC-2 knockout megakaryocytes. In addition, recombinant CLEC-2 enhances secretion of the chemokine (C-C motif) ligand 5 (CCL5) from bone marrow FRC-like cells *in vitro*, which is accompanied by an increase in proplatelet formation, supporting the significance of periarteriolar CELC-2-podoplanin interaction in megakaryocyte/platelet production (Figure 1.3 C) (Tamura et al., 2016). However, postnatal depletion of CLEC-2 in mice has no impact on platelet counts (Lowe et al., 2015b), which contradicts these data.

1.6.5 CLEC-2-podoplanin in lung development

As mentioned, constitutive deletion of CLEC-2 or podoplanin in mice commonly leads to death during development. Lung abnormalities are one of the suspected causes of embryonic or perinatal lethality (Ramirez et al., 2003, Finney et al., 2012). Recently, a detailed mechanism involving CLEC-2-podoplanin interactions in lung development has been proposed. Although podoplanin is expressed in alveolar type I cells, the interaction of platelet CLEC-2 and podoplanin on lymphatic endothelial cells (LECs) is likely to regulate this process by inducing transforming growth factor (TGF)-β1 secretion from activated platelets. Subsequently, TGF-β1 stimulates differentiation of lung mesothelial cells into alveolar duct myofibroblasts, which synthesise extracellular matrix (ECM) to support the normal lung structure and function (Figure 1.3 D). In mice, global CLEC-2 knockout and LEC-specific podoplanin knockout neonates show a similar lung malformation, including a smaller alveolar space, a thickening of alveolar septum, and a minimal extent of elastic fibres. This is in association with an increase in lung mesothelial cells but a decrease in alveolar duct myofibroblasts. In addition, CLEC-2 null mice demonstrate a reduction of TGF-β in the developing lung. However, a milder form of

lung malformation is observed in platelet-specific CLEC-2 deficient mice, which is possibly due to the 2% remaining of CLEC-2 on platelets in this model (Tsukiji et al., 2018a). Further treatment of the platelet-specific CLEC-2 deficient pregnant mice with anti-CLEC-2 or anti-TGF-β antibody shows lung malformation in neonates, which is identical to that of global CLEC-2 knockout littermates, suggesting that platelet CLEC-2 regulates normal lung development in part through TGF-β secretion (Tsukiji et al., 2018a). Moreover, *in vitro* and *ex vivo* incubation of platelet supernatant plus hydrochloric acid (to convert TGF-β into active form) promote differentiation of lung mesothelial cells into myofibroblasts, supporting the role of platelet-derived TGF-β in lung development (Tsukiji et al., 2018a).

1.7 Platelet ITAM receptors in pathological conditions

In addition to the regulation of normal physiological function, GPVI and CLEC-2 have been reported to participate in various pathological conditions, including in thrombosis and inflammation. These two ITAM receptors show additive or synergistic effect in certain circumstances whereas they may provide opposing activity in others. Moreover, even GPVI or CLEC-2 itself plays different role depending on the related pathological context, which is possibly because of the distribution and the specific function of their ligands.

1.7.1 The role of GPVI and CLEC-2 in thrombosis

It has been elucidated *ex vivo* that GPVI predominantly binds collagen at the core of human carotid atherosclerotic plaque. In addition, anti-human GPVI antibody (5C4) inhibits plaque-induced platelet aggregation *in vitro* (Schulz et al., 2008). In

apolipoprotein E knockout (*Apoe*$^{-/-}$) animals, the major mouse model of atherosclerosis, GPVI is also detected in atherosclerotic lesion on arterial wall, including at carotid artery and aortic arch (Schulz et al., 2008). Anti-mouse GPVI antibody (JAQ1) has been reported to reduce the size of thrombus following either ultrasound- or needle-induced acute plaque rupture in carotid artery of *Apoe*$^{-/-}$ mice (Kuijpers et al., 2009, Hechler and Gachet, 2011). Moreover, GPVI fusion protein (GPVI-Fc), which competitively binds collagen, has been shown to inhibit platelet adhesion and aggregation *in vitro* (Schonberger et al., 2012), attenuates the progression of atherosclerosis in *Apoe*$^{-/-}$ mice (Schulz et al., 2008), reduces infarct size and improves left-ventricular systolic function in a mouse model of myocardial infarction (temporary ligation of the left anterior descending artery) (Schonberger et al., 2012). In murine model of ischemic stroke (transient middle cerebral artery occlusion), JAQ1 has been demonstrated to reduce infarct volume in the absence of bleeding complication (Kleinschnitz et al., 2007). The association of GPVI in these thrombotic events is suggested in part by the regulation of inflammatory responses (Schonberger et al., 2012, Nieswandt et al., 2011). Moreover, a Syk inhibitor given orally shows a promising effect by prolonging time to arterial occlusion and reducing infract size in animal model of acute stroke (van Eeuwijk et al., 2016). GPVI-null mice are also protected against VTE by showing the increase in survival rate following pulmonary embolism compared to control (Lockyer et al., 2006).

CLEC-2 has also been investigated in thrombosis. In a mouse model of ferric chloride ($FeCl_3$)-induced thrombus formation at mesenteric arterioles, either JAQ1 or anti-CLEC-2 antibody (INU1) alone does not affect thrombosis and haemostasis (tail bleeding time). However, combined administration of both antibodies significantly reduces thrombus formation but prolongs bleeding time, suggesting that GPVI and CLEC-2 cooperate in

thrombosis whereas these two ITAM receptors play a redundant role in haemostasis (Bender et al., 2013). Moreover, CLEC-2-podoplanin axis protects against DVT in mice. Either CLEC-2 knockout or anti-podoplanin antibody-treated mice show a reduction in platelet recruitment and thrombus formation following partial ligation of inferior vena cava-induced DVT (Payne et al., 2017). A recent study, finding drug candidates for CLEC-2 inhibition, demonstrates that cobalt haematoporphyrin is able to inhibit rhodocytin- and podoplanin-induced platelet aggregation in a dose-dependent manner. Moreover, this compound shows a promising effect by reducing thrombus formation in murine models of arterial thrombosis and DVT (Tsukiji et al., 2018b).

1.7.2 GPVI and CLEC-2 mediate inflammatory haemostasis

Initially, the function of GPVI and CLEC-2 in maintaining vascular integrity during inflammation has been introduced in a murine model of cutaneous rpA (Boulaftali et al., 2013); bovine serum albumin (BSA) is intravenously injected into mice followed by intradermal injection of anti-BSA antibody to generate immune complex-mediated skin inflammation. Mice lacking the extracellular domain of GPIbα do not exhibit intra-skin haemorrhage following rpA unless they are thrombocytopenic, suggesting GPIbα-independent platelet function in rescuing vascular damage during skin inflammation. Adoptive transfusion of either normal platelets plus JAQ1 injection or CLEC-2 deficient platelets into these thrombocytopenic GPIbα deficient mice also results in rpA-mediated bleeding. Moreover, transfusion of CLEC-2 deficient platelets accompanied with JAQ1 treatment increases bleeding phenotype, which is identical to a reconstitution of SLP-76 knockout platelets, indicating the important role of these two ITAM-associated receptors and their signal transduction in preventing inflammatory bleeding (Boulaftali et al.,

2013). Subsequently, it has been revealed that neutrophil transmigration is a cause of vascular breaches during cutaneous and peritoneal rpA (Gros et al., 2015). GPVI contributes to neutrophil-mediated cytotoxic activity in both conditions whilst it has been shown to simultaneously seal vascular damage only in cutaneous but not peritoneal rpA. Intravital microscopy reveals that single platelets, rather than platelet aggregates, regulate this inflammatory haemostasis, which is unlike classical haemostasis (Gros et al., 2015). A more recent study elucidates that GPVI deficient mice show bleeding during cutaneous rpA whereas platelet-specific CLEC-2 knockout mice do not (Rayes et al., 2018). However, the degree of bleeding is increased in GPVI and CLEC-2 double deficient mice. Administration of anti-podoplanin antibody also increases vascular leakage in GPVI knockout mice but does not cause bleeding in GPVI-expressing controls (Rayes et al., 2018). These data suggest that GPVI has a primary role and that CLEC-2-podoplanin functions as a back-up in safeguarding vascular integrity during skin rpA. Binding of GPVI to its ligands (e.g. collagen) in subendothelial matrix, and CLEC-2 to podoplanin-expressing cells in proximity to blood vessel (proposed as fibroblasts and macrophages), mediate this vasculoprotective function during inflammation by sealing the gap following leucocyte extravasation (Figure 1.4) (Ho-Tin-Noe et al., 2018, Boulaftali et al., 2018, Rayes et al., 2018).

The role of GPVI and CLEC-2 in preventing vascular leakage during a model of intranasal *Pseudomonas aeruginosa* LPS-induced lung inflammation is controversial. Following LPS (7 µg) inhalation in adoptive transfusion experiment in mice lacking extracellular domain of GPIbα, intra-pulmonary haemorrhage is observed in all similar settings to that of cutaneous rpA, which supports the contribution of platelet GPVI and CLEC-2 in this inflammatory condition (Boulaftali et al., 2013). In contrast, a recent work

reveals that higher dose of LPS (20 µg) does not cause bleeding into bronchoalveolar space in GPVI-null mice (with or without anti-podolanin antibody) or platelet-specific CLEC-2 knockout mice, whereas GPIbα-ectodomain deficient mice present bleeding in the inflamed lung (Rayes et al., 2018), indicating that GPIbα-IX-V complex may play a role in maintaining vascular integrity during lung inflammation. Moreover, intra-bronchoalveolar bleeding during lung rpA model (intranasal anti-BSA antibody + BSA i.v.) only occurs in thrombocytopenic mice but not in mice deficient in GPVI or GPIbα-ectodomain, pointing to stimulus-dependent mechanism for the prevention of inflammatory bleeding (Rayes et al., 2018).

Dasatinib, an anti-cancer drug that inhibits tyrosine kinases (e.g. Src), has been reported to increase risk of bleeding in leukaemia patients, including in skin (petechiae) and the gastrointestinal tract (Kreutzman et al., 2017, Apperley et al., 2009). Dasatinib also inhibits *in vitro* ITAM-mediated platelet adhesion (Pollitt et al., 2014, Induruwa et al., 2018) and aggregation (Lorenz et al., 2015, Induruwa et al., 2018). Moreover, mice treated with this drug exhibits significant bleeding in the small intestine. Dasatinib shows no direct cytotoxicity, but reversibly disrupts cell-cell junctions between endothelial cells *in vitro,* supporting the mechanism of dasatinib-induced loss of vascular integrity (Kreutzman et al., 2017).

Although a loss of vascular integrity is suggested to cause detrimental consequences, including intra-tissue bleeding during inflammation, it may provide a beneficial effect in wound healing (Shaterian et al., 2009) and cancer chemotherapy (Demers et al., 2011). During skin wound healing model, extensive vascular leakage is observed at the initial phase of repair, in association with a progression of angiogenesis in later phases. The

increase in vascular permeability allows the release of growth factors, matrix proteins, and cells into the wound to facilitate healing process. Moreover, vascular leakage may aid in drug delivery to the wound site that would accelerate wound healing (Shaterian et al., 2009, Mendonca et al., 2010). There is no evidence of dasatinib-associated impaired wound healing relative to other tyrosine kinase inhibitors (Shah et al., 2014). On the other hand, dasatinib may facilitate the entry of other chemotherapeutic drugs into a solid tumour, which potentially enables effective cancer treatment (Kreutzman et al., 2017). The direct role of platelet GPVI and CLEC-2 has never been investigated in these settings.

1.7.3 Regulation of inflammatory responses by GPVI and CLEC-2

During recent years, GPVI and CLEC-2 have been shown to regulate inflammatory responses in various conditions. In addition, these two ITAM receptors can play an opposite role in inflammation. For example, GPVI promotes a pro-inflammatory phenotype during glomerulonephritis by increasing platelet and neutrophil recruitment to the inflamed glomeruli (Devi et al., 2010). Microparticles, which are released upon GPVI-mediated platelet activation, promote an inflammatory activity of synovial fibroblasts and exacerbate the progression of arthritic diseases (Boilard et al., 2010). As mentioned previously, GPVI contributes to neutrophil-mediated tissue damage in cutaneous rpA (Gros et al., 2015). More recently, it has been reported that GPVI ablation promotes switching of macrophages from a M1 pro-inflammatory to M2 anti-inflammatory phenotype, which reduces inflammation and pain in an inflamed paw skin model (Pierre et al., 2017). However, this pro-inflammatory activity of GPVI supports innate immunity, which is beneficial for bacterial killing during gram-negative bacterial pneumonia-induced sepsis (Claushuis et al., 2018).

CLEC-2-podoplanin interaction has been demonstrated to protect against organ damage and reduce inflammation during lung injury (Lax et al., 2017b) and sepsis (Rayes et al., 2017). In addition, *in vitro* ligation of CLEC-2 with podoplanin-positive T cells inhibits the inflammatory response in Th17 cells (Nylander et al., 2017). However, CLEC-2 promotes M1 macrophage migration to the site of infection, resulting in efficient pathogen clearance during bacterial peritonitis (Rayes et al., 2017). On the other hand, the upregulation of podoplanin is also associated with the degree of inflammation in arthritis (Croft et al., 2016, Takakubo et al., 2017). Moreover, CLEC-2-podoplanin involves in infection-induced thrombosis, which occludes liver microvessels, despite the unaltered degree of inflammation (Hitchcock et al., 2015).

Dasatinib also produces anti-inflammatory activity, at least by reducing neutrophil recruitment (da Silva et al., 2016) and neutrophil-derived respiratory burst (Futosi et al., 2012) as well as enhancing M2 macrophage population (Ozanne et al., 2015, Cruz et al., 2016). However, these activities are suggested as a direct effect of dasatinib on leucocytes. There is no evidence demonstrating the cooperation of platelet GPVI and CLEC-2 in mediating inflammatory responses.

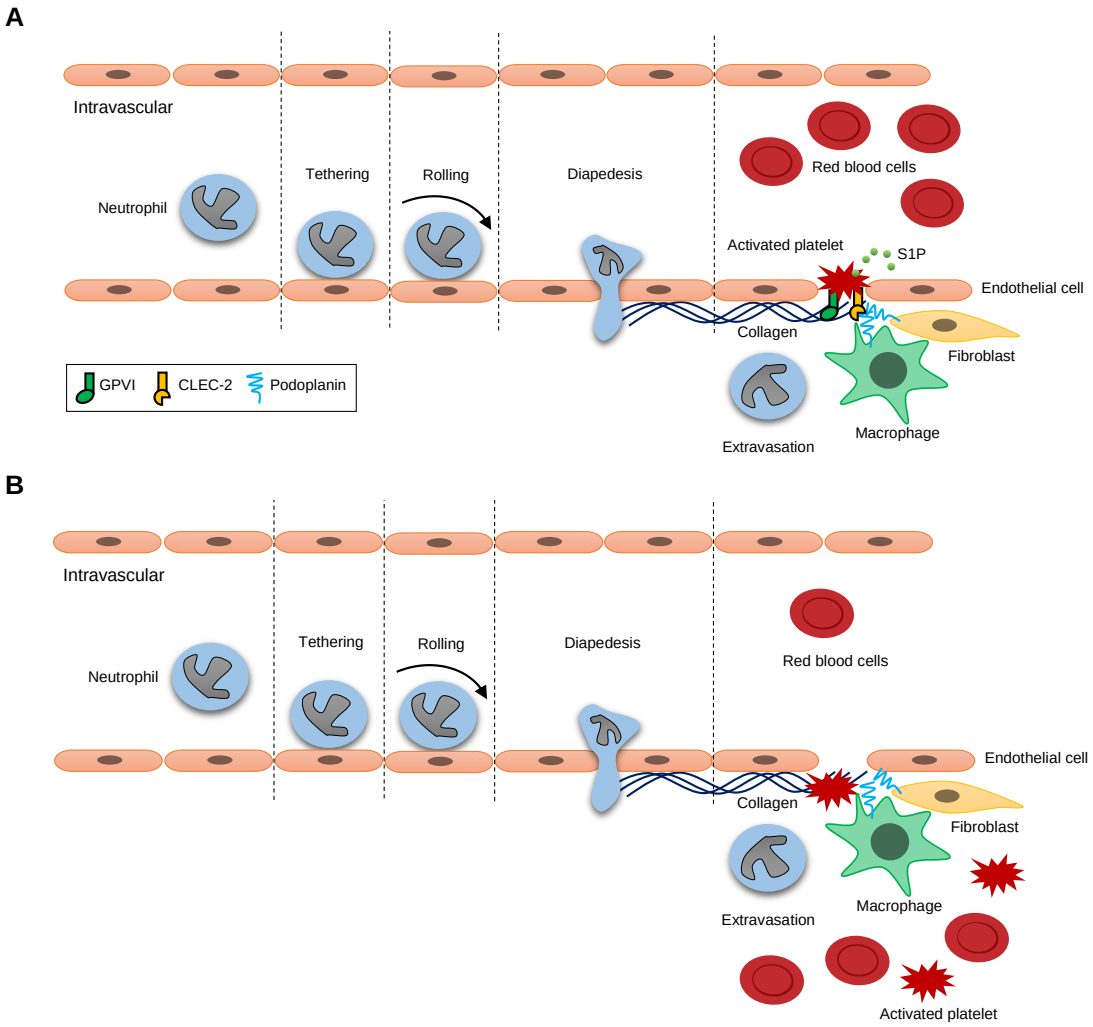

Figure 1. 4. Role of platelet GPVI and CLEC-2 in safeguarding vascular integrity during inflammation. (A) Platelets, primarily via GPVI (green), seal the small hole between endothelium following neutrophil extravasation. GPVI binds collagen in subendothelial matrix, leading to platelet activation and secretion of barrier-strengthening mediators, such as sphingosine-1-phosphate (S1P), to restore endothelial integrity. Platelet CLEC-2 (yellow) acts as backup pathway of vasculoprotective function during inflammation in the absence of GPVI, via binding to podoplanin on perivascular cells (e.g. fibroblasts and macrophages). (B) A lack of both ITAM receptors results in intra-tissue bleeding during inflammation. Adapted from (Ho-Tin-Noe et al., 2018, Boulaftali et al., 2018).

1.8 Potential role of platelet ITAM receptors in skin wound healing

1.8.1 An overview of skin structure

The integumentary system, made up of skin and its appendages, is the largest organ system in the body that function as a protective barrier against external environment (McLafferty et al., 2012). Skin comprises of two layers, including the epidermis (the uppermost part) and the dermis (Figure 1.5 A). Skin epidermis lacks blood vessels. Moreover, it is subdivided into five layers from the deepest to the uppermost layer, including stratum basale, stratum spinosum, stratum granulosum (granular layer), stratum lucidum (only found in the area of thick skin, such as the palms and soles), and stratum corneum, respectively (McLafferty et al., 2012). In mouse skin (Figure 1.5 B, left), the epidermis is thinner than in human (Figure 1.5 B, right) (Wagner et al., 2010, Pasparakis et al., 2014).

Keratinocytes are the most abundant cell population within the skin epidermis. Stratum basale is a basal layer adjacent to dermis, containing columnar keratinocytes, which are capable of dividing (Figure 1.5 A). During homeostasis, keratinocytes regularly multiply and migrate to the upper layers, accompanied by keratin accumulation (keratinised). While moving upward, keratinocytes change their morphology from rounded to flattened shape and finally undergo apoptosis, which become flattened (stratified squamous) dead cells at stratum corneum and are sloughed off overtime (McLafferty et al., 2012).

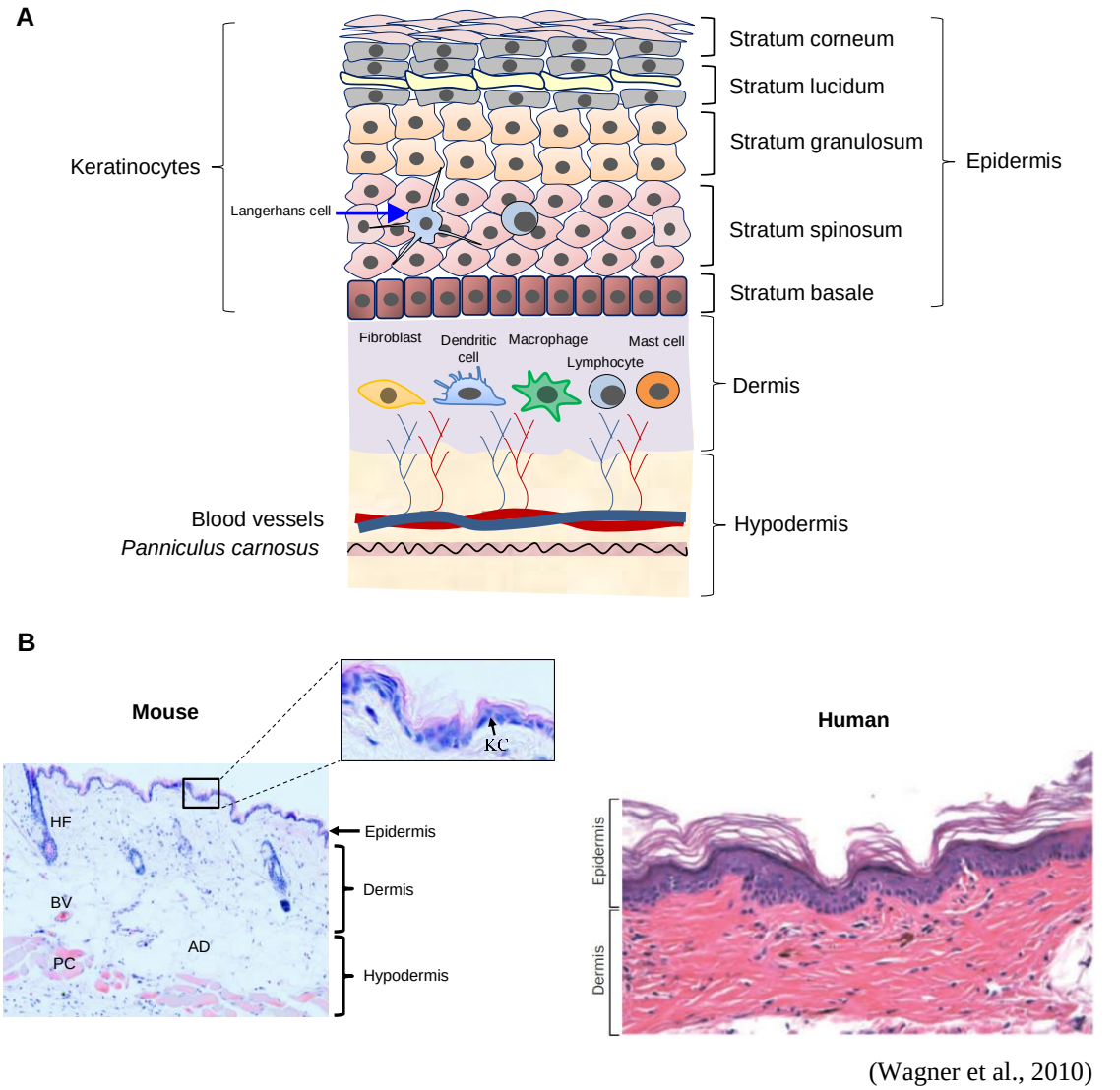

(Wagner et al., 2010)

Figure 1. 5. Structure of murine skin. (A) Schematic illustration of skin structure. Epidermis is the uppermost layer of skin, containing skin epithelium called keratinocytes. Dermis comprises of various structures (e.g. blood and lymphatic vessels), cell types (e.g. fibroblasts and immune cells), and molecules (e.g. collagen and elastic fibres). (B) haematoxylin and eosin (H&E) staining of normal mouse skin (left) and human skin (right). AD = adipocytes, BV = blood vessel, HF = hair follicle, PC = *panniculus carnosus* muscle. KC = keratinocytes. Arrow points to KC.

Dermis contains blood vessels, lymphatic vessels, nerve endings, hair follicles and glands. In addition, fibroblasts in this layer synthesise the collagen and elastic fibres, which constitute a strong connective tissue to mediate tensile strength of skin (Figure 1.5 A). Immune cells, including macrophages, dendritic cells, T-cells, mast cells, mainly reside in dermis, although some of T-cells and Langerhans cells (specific type of dendritic cells) are located in epidermis (Wagner et al., 2010, Pasparakis et al., 2014, McLafferty et al., 2012). In mice, there is a fast-twitch muscle called "*panniculus carnosus"* that lies under the dermis (Figure 1.5 B). This specialised muscle helps twitching a loose skin and regulates body temperature in rodent (Naldaiz-Gastesi et al., 2016, Driskell et al., 2014).

1.8.2 Pathophysiology of skin wound healing

Skin wound repair is a multifactorial process, which comprises of four interdependent phases, including haemostasis, inflammation, proliferation, and remodelling (Figure 1.6) (Shaw and Martin, 2009). Immediately following tissue injury, platelet aggregation and fibrin clot play a haemostatic function to stop bleeding. Circulating neutrophils are the first immune cells recruited into the wound site to eliminate invading microorganisms and cellular debris during the initial inflammatory phase. Monocytes enter shortly after and differentiate into tissue macrophages. By exposing to the inflammatory stimuli in injured tissue, macrophages are directed to M1 pro-inflammatory characteristics, which further contribute to the inflammatory response. In the late inflammatory phase, macrophages switch to a M2 reparative phenotype and initiate the resolution of inflammation (Fadok et al., 1998, Sindrilaru and Scharffetter-Kochanek, 2013). The proliferative phase begins in an overlapping period, where keratinocytes start migration and proliferation to recover skin epithelium; this process is called "re-epithelialisation"

(Shaw and Martin, 2009). In addition, angiogenesis during this stage forms a granular structure, which is termed "granulation tissue" (Flanagan, 1998) in wound area and provides nutrients and oxygen to the tissue. Simultaneously, skin fibroblasts are recruited into the granulation tissue to synthesise extracellular matrix, including collagen, which allows cell migration. Moreover, lymphangiogenesis is stimulated to facilitate draining of inflammatory component. Fibroblasts further differentiate into myofibroblasts and mediate wound contraction in the remodelling (or maturation) phase. The wound turns into healed state during this final phase, represented by the resolution of inflammation, in conjunction with the completion of wound closure and the re-organisation of collagen fibres to restore skin integrity (Shaw and Martin, 2009, Pence and Woods, 2014, Brown et al., 2014, Hur et al., 2014).

1.8.3 Platelets in wound healing

Platelets play additional roles alongside haemostasis during wound healing. Activated platelets secrete growth factors and cytokines/chemokines, which support vessel repair and regulate immune cell recruitment (Shaw and Martin, 2009, Yang et al., 2011). In an animal model of superficial wound, thrombocytopenic and P-selectin-deficient mice show delayed wound healing, in association with a reduction in leucocyte infiltration, following corneal epithelial abrasion (Li et al., 2006). In addition, platelet-rich plasma, which contains growth factors, including PDGF, VEGF, and TGF-β, facilitates skin wound healing in mice (Yang et al., 2011). Moreover, platelet-rich fibrin promotes wound healing in diabetic mice at least by enhancing angiogenesis (Ding et al., 2017). Surprisingly, one report has demonstrated that skin wound healing is not impaired in thrombocytopenic mice (Szpaderska et al., 2003). Although the numbers of macrophages

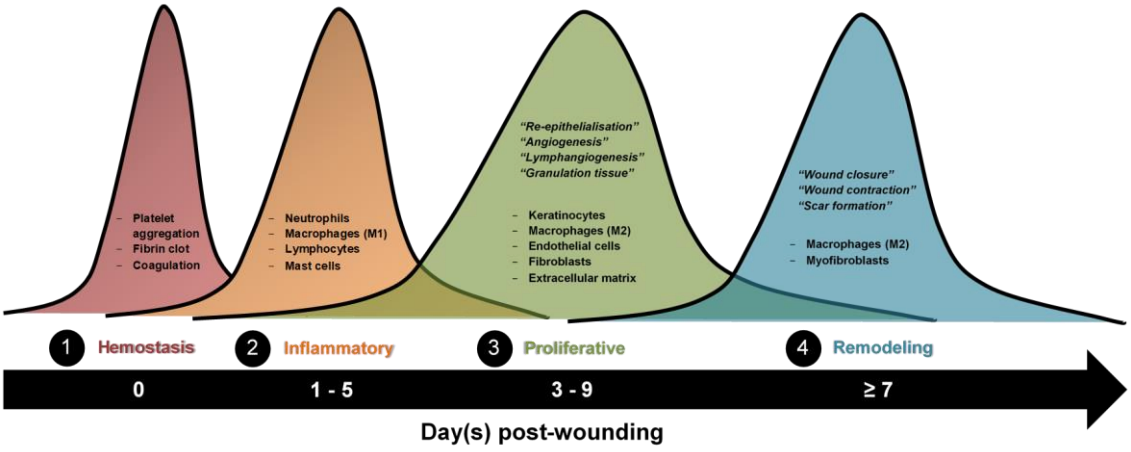

Figure 1. 6. Simplified scheme of skin wound healing phases. Haemostasis (1) immediately begins after injury to terminate blood loss. The influx of leucocytes, particularly neutrophils and macrophages at day 1-5 post-injury drives the inflammatory phase (2). Proliferative phase (3) takes place during day 3-9 post-injury. Re-epithelialisation, a process of keratinocyte migration and proliferation, promotes recovery of skin epidermis. Angiogenesis within the granulation tissue of the wound supplies nutrients and oxygen for cell function. Fibroblasts synthesises extracellular matrix to support cell migration. Lymphangiogenesis aids in draining the inflammatory component. Finally, the remodelling phase (4) occurs approximately at day 7 onwards. Fibroblasts differentiate into myofibroblasts and mediate wound contraction. Complete wound closure and re-organisation of collagen fibres turn the wound into healed state. In each phase, the important events and cellular/molecular contributions are listed. The scheme is depicted based on (Shaw and Martin, 2009, Brown et al., 2014, Pence and Woods, 2014, Hur et al., 2014).

and T-cells are increased in the inflammatory and proliferative phases, respectively, the wound closure, re-epithelialisation, angiogenesis, and collagen synthesis, are unaffected in thrombocytopenic mice (Szpaderska et al., 2003), disclaiming the essential contribution of platelets in wound healing, including in haemotasis. In addition to this controversy, it is unclear which platelet-expressed receptor(s) are required to facilitate wound healing.

1.8.4 Fibrinogen, fibrin, and coagulation cascade in wound healing

During the initial inflammatory phase of wound healing, the increased vascular permeability allows extravasation of plasma proteins, including fibrinogen, coagulation factors, growth factors, cytokines, and chemokines into the site of injury. Tissue factor, expressed on keratinocytes, pericytes, and leucocytes within the wound (Hoffman and Monroe, 2012), can activate clotting factor (F)VII, which mediates thrombin generation. Subsequently, thrombin cleaves fibrinogen into fibrin strands, which stabilise the blood clot. Fibrinogen and fibrin not only initiate haemostatic plug formation but also facilitate wound healing by various mechanisms. Firstly, fibrinogen and fibrin provide a provisional matrix for local cell migration, including endothelial cells, fibroblasts, and keratinocytes (Drew et al., 2001, Brown et al., 1992). Once endothelial cells are recruited from tissue near the wound, they proliferate and migrate over fibrinogen and fibrin matrix, then form a capillary tube, contributing to angiogenesis during wound healing (Chalupowicz et al., 1995, Laurens et al., 2006, Sahni and Francis, 2000). Fibrin is also shown to promote fibroblast proliferation and migration *in vitro* (Cox et al., 2004). Although keratinocytes do not adhere to fibrinogen and fibrin (Kubo et al., 2001), they mediate fibrinolysis, a process of fibrin degradation, and form a tunnel-like structure to

move along this matrix (Ronfard and Barrandon, 2001). In contrast, fibrinogen and fibrin may inhibit the recruitment of neutrophils (Higazi et al., 1994, Hanson and Quinn, 2002) and monocytes/macrophages (Lishko et al., 2007) to the site of injury. Secondly, fibrinogen and fibrin may act as a reservoir for growth factors and cytokines since they bind with high affinity to pro-angiogenic factors, including VEGF and fibroblast growth factor 2 (Drew et al., 2001). Thirdly, fibrinogen and fibrin act as natural suture by stabilising wound field (Drew et al., 2001). Recently, it has also been demonstrated that a fibrin film over surface of the wound protects against bacterial invasion (Macrae et al., 2018).

In mice lacking fibrinogen, abnormal proliferation and migration of keratinocytes are observed, characterised by epithelial hyperplasia and the projection of epithelial tongues away from the centre of the wound. However, the time to complete wound closure is unaltered in these mice (Drew et al., 2001). In diabetic mice, fibrin together with leucocytes and platelets accelerate skin wound healing by promoting angiogenesis (Ding et al., 2017). Moreover, severe impairment in wound healing has been reported in a patient with dysfibrinogenaemia (van Vulpen et al., 2018). In clinical practice, fibrin sealant is used in several surgical procedures, supporting its role in promoting wound healing (Laurens et al., 2006, Alston et al., 2008, Albala, 2003).

Deficiency in FIX (haemophilia B), FVII, and tissue factor also delays wound healing. In haemophilia B mice, an impaired wound healing is associated with the persistent subcutaneous bleeding, due to a defect in fibrin generation, leading to haematoma formation during the course of wound closure (Hoffman et al., 2006). In addition, mice expressing low tissue factor (approximately 1% of normal level) show milder form of

bleeding in the granulation tissue during wound healing (Monroe et al., 2010). Moreover, a reduction in leucocyte recruitment is a proposed mechanism of delayed wound healing in mice with low FVII (less than 1% of normal level), although they display an initial red spot at the centre of the wound, and a subsequent darker wound scab along the healing process, which may indicate certain degree of bleeding within the wound (Xu et al., 2010). FXIII, a transglutaminase, is also important in wound healing. Following fibrin generation and polymerisation by thrombin, FXIIIa (thrombin-activated FXIII) forms a thioester bond with glutamine residue of fibrin. Then, acyl group (R-C=O) in thioester intermediate binds with amine group (R-NH2) of lysine residue from another fibrin molecule and mediates cross-linking of fibrin, which increases the stability and tensile strength of the clot (Ariens et al., 2002). Delayed wound healing is observed in FXIII knockout mice (Dickneite et al., 2015). Therefore, fibrin formation and its stability may promote wound healing by tightening the clot. Moreover, patients with haemophilia and FXIII deficiency demonstrate bleeding, which is related to poor wound healing (Rodriguez-Merchan, 2012). These observations collectively point to an important function of the coagulation cascade in wound healing.

1.8.5 The role of leucocytes in wound healing

During the inflammatory phase, neutrophils are the first inflammatory cells recruited from blood circulation into the wound site, which reach peak level at 24-48 hours. Neutrophil number is maintained at high level until day 3 after injury, and gradually decrease afterwards (Dovi et al., 2003, Kim et al., 2008). Blood monocytes enter the wound later and differentiate into tissue macrophages. The increased number of wound monocytes is observed at day 3 post-injury, and proceeded during the course of wound healing, in

correlation with the number of wound macrophages (Crane et al., 2014). At the early inflammatory phase (day 1-4 post-injury) where wound sterilisation is needed, macrophages mainly express M1 pro-inflammatory phenotype and function with neutrophils to remove invading microorganisms and cellular debris (Sindrilaru and Scharffetter-Kochanek, 2013, Eming et al., 2007). In addition, these cells produce pro-inflammatory cytokines, including TNF-α, IL-1β, and IL-6, which promote inflammation (Eming et al., 2007). In contrast, wound macrophages demonstrate M2 reparative characteristics during the late inflammatory phase (day 5-7 post-injury), which secrete anti-inflammatory cytokines (e.g. IL-10) and growth factors (e.g. TGF-β1), contributing to resolution of inflammation and tissue repair (Sindrilaru and Scharffetter-Kochanek, 2013). The M2 macrophages possibly arise by either a polarisation of M1 macrophages or a direct differentiation of non-classical (murine $Ly6C^{low}$) monocytes within the wound (Crane et al., 2014). In addition, macrophage plasticity is also dependent on its metabolic profiles. For example, M1 macrophages use aerobic glycolysis and pentose phosphate pathway as major metabolism whereas M2 macrophages primarily rely on tricarboxylic acid cycle coupled to oxidative phosphorylation (Van den Bossche et al., 2016, Das et al., 2015, Geeraerts et al., 2017).

Although their role in preventing infections is certain, how inflammatory cells facilitate wound healing is controversial (Martin and Leibovich, 2005). In a model of skin wound healing, neutrophil depletion results in accelerated wound healing, in association with the increase in re-epithelialisation at the early phase (Dovi et al., 2003), suggesting a non-essential function of neutrophils in tissue repair. Moreover, several lines of evidence demonstrate a detrimental activity of neutrophils during wound healing, including the secretion of proteases (Dovi et al., 2003), the production of inflammatory cytokines and

oxidative stress (Wilgus et al., 2013, Slater et al., 2017), and the formation of NETs (e.g. in diabetic wounds, which demonstrate chronic inflammation) (Wong et al., 2015), all of which cause tissue damage and delay wound healing.

Macrophages might also be dispensable for wound healing. In mouse embryos (E11.5-13.5), there is no macrophage recruitment to the wound along the course of repair. In addition, these embryos show absence of scar after wound healing (Hopkinson-Woolley et al., 1994). However, wound macrophages are observed in older foetus (E14.5), which is resemble to adult mice (Hopkinson-Woolley et al., 1994). In PU.1 transcription factor-knockout mouse neonates that lack neutrophils, macrophages, and lymphocytes, the rate of skin wound healing is unaltered and these neonates demonstrate scar-free after healing, similar to that of embryos (Martin et al., 2003). Moreover, it has been reported that deletion of wound macrophages in the early stage (day 1-5 post-injury) does not negatively affect initial wound closure (day 1-4 post-injury) but delays the mid-stage of healing, accompanied by a reduction in M2 macrophages and a defect in re-epithelialisation and granulation tissue formation. However, it leads to a reduction in scar formation at the end (Lucas et al., 2010). Macrophage depletion in mid-stage (day 4-10 post-injury) causes severe haemorrhage within the wound and delays wound closure, suggesting the role of macrophages in regulating vascular stability during tissue repair. Lack of macrophages after this time point does not influence wound healing (Lucas et al., 2010). Therefore, it suggests that M2 macrophages, rather than M1 pro-inflammatory, may be essential for wound healing, especially during the proliferative-to-maturation phases of repair.

Mast cells, derived from blood basophils, have also been illustrated to participate in wound healing. Histamine secreted from mast cells mediates vascular permeability during inflammation and may facilitate wound healing. Mice deficient in mast cells represents a delayed wound closure, especially within the first six days, in association with a decrease in vascular permeability, and neutrophil recruitment (Weller et al., 2006). In addition, histamine promotes wound healing (Numata et al., 2006) whereas anti-histamine mediates the opposite effect in mice (Weller et al., 2006), supporting the role of mast cells and histamine in repair process. In the recent years, a crosstalk between dendritic epithelial T-cells (DETCs) and keratinocytes has been elucidated. In aged mice, a reduction in keratinocyte activation, subsequently lowers the number of recruited DETCs (day 3-7) and decreases re-epithelialisation process, contributing to delayed wound closure compared to young littermates, indicating the role of DETCs in normal wound healing (Keyes et al., 2016).

1.8.6 Other cellular aspects during the wound healing process

As mentioned, keratinocytes at the basal layer are capable of renewing during homeostasis and certainly after skin injury. The activated keratinocytes not only migrate and proliferate during wound healing but also mediate other effects. Keratinocytes release pro-inflammatory cytokines, including IL-1 and TNF-α, which produce paracrine function in fibroblast activation. TGF-β secreted by both keratinocytes and fibroblasts induces differentiation of fibroblasts into myofibroblasts. In addition, keratinocytes express TLRs, which recognises pathogens, providing host defense mechanism during tissue injury. Moreover, stem cell niche within hair follicle has been shown to promote re-epithelialisation process by producing the keratinocyte stem cells (Pastar et al., 2014).

Fibroblasts are resident cells in skin dermis, which turnover ECM under physiological setting. Fibroblasts express vimentin (intermediate filament protein) but not α-smooth muscle actin (α-SMA). Upon tissue injury, fibroblasts at adjacent skin area are activated and differentiate into myofibroblasts in proliferative phase (Li and Wang, 2011). Bone marrow-derived circulating fibrocytes also largely contributes to the source of myofibroblasts during wound healing. It has been reported that 30-50% of wound myofibroblasts are originated from fibrocyte progenitors (Barisic-Dujmovic et al., 2010). Moreover, smooth muscle cells and pericytes are believed as other potential origins of myofibroblasts (Li and Wang, 2011). The main function of myofibroblasts is the ECM synthesis, including collagen and other elastic fibres. In addition, myofibroblasts express α-SMA alongside vimentin, which represent their contractile property to mediate wound contraction. Myofibroblasts generally undergo apoptosis at the final stage of wound healing. However, excessive numbers or activities of myofibroblasts may lead to hypertrophic or keloidal scar formation and a detrimental tissue fibrosis (Li and Wang, 2011).

Pericytes, the cells located nearest to vascular endothelium and have long cytoplasmic processes encircle blood vessel, also participate in tissue repair. Pericytes generally express neuron-glial antigen 2 (NG2) and are further classified into two subsets based on the presence of nestin, including Type 1 ($nestin^-/NG2^+$) and type 2 ($nestin^+/NG2^+$). Type 1 pericytes express α-SMA and are primarily observed around both arterioles and venules, which function in regulating the vessel tone. Type 2 pericytes have mesenchymal stem cells/multipotent stromal cells characteristic, which contribute to angiogenesis (Bodnar et al., 2016). In addition to angiogenesis, pericytes support wound healing by several mechanisms. For example, pericytes enhance vascular permeability and the extravasation

of leucocytes during the inflammatory phase. These perivascular cells also control keratinocyte migration. Moreover, pericytes differentiate into fibroblasts/myofibroblasts, which contribute to late phases of repair (Bodnar et al., 2016, Thomas et al., 2017).

1.8.7 Podoplanin-CLEC-2 axis during skin wound repair

In a murine model of skin wound healing, the increased expression of podoplanin, including in keratinocytes, is observed on day 1 after injury and is prominent on day 3 to day 7 post-injury alongside the progression of re-epithelialisation. At day 10 post-injury, when complete wound closure is achieved; podoplanin is substantially decreased (Asai et al., 2016). Immunostaining of skin wound reveals that platelets are present in the wound and located near podoplanin at day 1 post-injury. In addition, the increase in keratinocyte-expressed E-cadherin is marginally co-localised with podoplanin at day 3 post-injury, suggesting that podoplanin may regulate keratinocyte migration by down-regulating this cell adhesion molecule. This observation is supported by *in vitro* experiments, which demonstrate an elevated expression of E-cadherin in podoplanin-knockdown keratinocytes, in association with reduced keratinocyte migration. In addition, keratinocytes incubated with recombinant human CLEC-2 exhibit complementary results (Asai et al., 2016). Collectively, it is proposed that platelets, via CLEC-2-podoplanin interaction, inhibit keratinocyte migration at the initial phase of repair until the wound bed is completely prepared. During the later phases where platelets do not exist, the upregulation of podoplanin promotes re-epithelialisation process (Asai et al., 2016). However, mice deficient in keratinocyte podoplanin show no significant differences in skin re-epithelialisation and wound closure, compared with controls (Baars et al., 2015). Moreover, there are no defects in cell proliferation, migration, and adhesion in podoplanin

deficient keratinocytes *in vitro*, indicating that keratinocyte podoplanin is dispensable for wound healing (Baars et al., 2015).

The potential function of monocyte-derived podoplanin during wound healing has also been studied. A single intradermal injection of human podoplanin-positive monocytes in combination with platelets around the wound edge significantly accelerates skin wound healing in mice, whereas either platelets or podoplanin-positive monocytes alone does not (Hur et al., 2014). This platelet-monocyte combination enhances lymphangiogenesis in the later phase of wound repair. Anti-podoplanin antibody reverses healing phenotype observed in platelet-monocyte-treated mice, including a reduction in lymphangiogenesis. Although multiple mechanisms may contribute, these data suggest a transdifferentiation of podoplanin-positive monocytes into a lymphatic phenotype, under the interaction with platelets (via CLEC-2), to facilitate tissue repair.

1.9 Aims

Platelets play several roles beyond haemostasis during wound healing as discussed above. Additionally, platelet (hemi)ITAM receptors regulate vascular integrity and inflammatory responses, and this may affect wound repair process. Therefore, the primary aims of my thesis is to investigate the role of CLEC-2 and GPVI in a mouse model of skin wound injury. This is based on the hypothesis that the regulation of vascular integrity and inflammatory responses by GPVI and CLEC-2 may influence wound healing. As part of this, I have also characterised a novel podoplanin cytoplasmic tail-deficient mouse model. The question is how much of the action of podoplanin is by signalling through its tail. Podoplanin is up-regulated on the keratinocytes during wound healing and may influence repair process. Thus, the role of podoplanin cytoplasmic tail in skin wound healing has been studied. I have also studied the effect of CLEC-2-podoplanin on metabolic changes, mainly glycolysis and arginine metabolism, in inflammatory macrophages using metabolomics analysis. This is to understand whether CLEC-2-podoplanin interaction regulates cellular metabolism in inflammatory macrophages.

Chapter 2 Materials and Methods

2.1 Materials

1.2.1 Reagents and antibodies

The reagents and antibodies used in this thesis are described in Table 2.1 and Table 2.2, respectively.

Table 2. 1. List of reagents and chemicals used

Reagents	Company	Cat No.
Martius scarlet blue stain kit	Atom Scientific	RRSK2
Mayer's Haematoxylin	Sigma	MHS32
Eosin Y solution	Sigma	HT110232
Normal goat serum	Vector Lab	S-1000
Histo-clear	Scientific laboratory supplies	NAT1330
Tissue-Tek optimal cutting temperature (O.C.T.) compound	Sakura Finetek	4583
1% Acid alcohol	Atom Scientific	RRSP187-G
DPX mounting medium	Sigma	06522
Rat anti-mouse GPIbα antibody	Emfret Analytics	R300
Anti-podoplanin antibody (for injection)	In-house production	
N-Formyl-Methionyl-Leucyl-Phenylalanine (fMLP)	Sigma	F3506
Collagen type I	Takeda (formerly Nycomed)	
Fibrinogen	Enzyme Research Laboratories	MFg
Thrombin	Sigma	T4648
Factor XIIIa	Zedira	T061

Table 2.1. List of reagents and chemicals used (continued.)

Reagents	Company	Cat No.
LPS (from Escherichia coli 055:B5)	Sigma	L2880
Recombinant dimeric CLEC-2-Fc (rCLEC-2-Fc)	In-house production	
Proteinase K	Thermo Scientific	EO0491
Buffer E 10X Buffer	Promega	R005A
BSA, Acetylated	Promega	R396E
HindIII	Promega	R604A
Orange G dye	Sigma	O3756
Microclean	Labgene Scientific	2MCL-5
BigDye® Terminator v1.1 & v3.1 5X Sequencing Buffer	Life Technologies	4336697

Table 2. 2. List of antibodies used in immunostaining

Reagents	Working dilution	Company	Cat No.
Primary antibodies			
Rat anti-mouse Gr-1 monoclonal antibody	1:200	eBiosciences	14-5931-82
Rat anti-mouse F4/80 monoclonal antibody	1:200 (IHC) 1:100 (IF)	Bio-Rad	MCA497GA
Rabbit anti-mouse CXCL-1 monoclonal antibody	1:200	R&D systems	MAB4532
Syrian hamster anti-mouse podoplanin monoclonal antibody	1:500 (IHC) 1:200 (IF)	eBiosciences	14-5381-85
Rat anti-mouse CD41 monoclonal antibody	1:100	BD Pharmagen	553847

IHC = Immunohistochemistry, IF = Immunofluorescence

Table 2.2. List of antibodies used in immunostaining (continued.)

Reagents	Working dilution	Company	Cat No.
Primary antibodies			
Rabbit anti-CD31 polyclonal antibody	1:100	Abcam	ab28364
Rabbit anti-NG2 polyclonal antibody	1:200	Merk Millipore	AB5320
Rabbit anti-tissue factor monoclonal antibody	1:400	Abcam	ab151748
Rabbit anti-TNF alpha polyclonal antibody	1:200	Abcam	ab9739
Rat anti-mouse Ly6C monoclonal antibody	1:200	Biolegend	128002
Rat anti-mouse CXCL4/PF4 monoclonal antibody	1:200	R&D systems	MAB595-100
Goat anti-mouse fibrinogen polyclonal antibody	1:200	Accurate Chemical & Scientific Corp.	YNGMFBG7S
Rabbit anti-vimentin monoclonal antibody	1:200	R&D systems	MAB2105
Rabbit anti-iNOS polyclonal antibody	1:50	Abcam	ab15323
Rabbit anti-RELM alpha (Fizz-1) polyclonal antibody	1:50	Abcam	ab39626
Rat anti-mouse Ly6G-APC/Cy7-conjugated monoclonal antibody (clone 1A8)	1:100	BD Pharmagen	560600
Rat anti-mouse CLEC-2 monoclonal antibody	1:200	Bio-Rad	MCA5700

Table 2.2. List of antibodies used in immunostaining (continued.)

Reagents	Working dilution	Company	Cat No.
IgG controls			
Rat IgG2b control	1:400	Bio-Rad	MCA1125
Rat IgG1,Ƙ control	1:200	Biolegend	400402
Golden Syrian hamster IgG control	1:500 (IHC) 1:200 (IF)	eBiosciences	14-4914-85
Rabbit IgG control	1: 10,000	Life technologies	10500C
Secondary antibodies			
Goat anti-rat IgG-HRP	1:200 (Gr-1) 1:500 (F4/80, CLEC-2)	Santa Cruz	sc-2032
Goat anti-hamster IgG-HRP	1:500	Santa Cruz	sc-2905
Donkey anti-rabbit IgG-HRP	1:200	GE Healthcare	NA934V
Donkey anti-goat IgG-HRP	1:500	Santa Cruz	Sc-2020
Goat anti-rat IgG-Alexa 568	1:200	Life technologies	A11077
Goat anti-rat IgG-Alexa 488	1:200 (vimentin) 1:100 (F4/80)	Life technologies	A11006
Goat anti-hamster IgG-Alexa 488	1:200	Life technologies	A21110
Goat anti-rabbit IgG-Alexa 647	1:200 1:100 (iNOS, Fizz-1)	Life technologies	A21245
Hoechst	1:10,000	Life technologies	H3570
ImpactDAB substrate	As recommended	Vector Lab	SK-4105

IHC = Immunohistochemistry, IF = Immunofluorescence

2.2 Mice

All animal procedures were performed under the regulation of UK laws (Animal [Scientific Procedures] Act 1986) with approval of local ethics committee and UK Home Office under PPL P0E98D513 and P14D42F37. Transgenic mice used during the course of this thesis are on a C57BL/6 background, which are listed in Table 2.3.

Constitutive GPVI knockout (*Gp6*$^{-/-}$) mice was generated as described previously (Kato et al., 2003). For conditional deletion of CLEC-2, mice that carry the loxP sites flanking exons 3 and 4 of the *Clec1b* gene (*Clec1b*$^{fl/fl}$) were generated. Then *Clec1b*$^{fl/fl}$ mice were bred with either *Pf4-Cre* recombinase-bearing mice (Finney et al., 2012) or *Gp1bα-Cre* mice (Nagy et al., 2019) to delete CLEC-2 on megakaryocyte/platelet lineage. *Gp6*$^{-/-}$ and *Clec1b*$^{fl/fl}$*Pf4-Cre* strains were cross-bred to produce DKO mice. *Clec1b*$^{fl/fl}$ mice were also crossed with *Cd11c-Cre* mice to knockout CLEC-2 on dendritic cells (Finney et al., 2012, Acton et al., 2014). Mice with insertion of the loxP sites to *Pdpn* gene was generated (*Pdpn*$^{fl/fl}$) and bred with *Vav1-Cre* mice for conditional deletion of podoplanin on haematopoietic lineage (Lax et al., 2017b, Rayes et al., 2017). *PdpnCyto* mice was produced by Taconic Biosciences using clustered regularly interspaced palindromic repeats (CRISPR)/CRISPR-associated protein 9 (Cas9) technology. Three stop codons were constitutively inserted immediately before the nucleotide sequence encoding lysine-164 located in exon 5 of *Pdpn* gene. *Clec1b*$^{fl/fl}$ or *Pdpn*$^{fl/fl}$ or WT mice were used as WT controls.

Table 2. 3. List of transgenic mouse strains

Mouse strain	Description
Gp6$^{-/-}$	Constitutive GPVI knockout
Clec1b$^{fl/fl}$*Pf4-Cre*	Platelet-specific CLEC-2 knockout
Clec1b$^{fl/fl}$*Gp1bα-Cre*	Platelet-specific CLEC-2 knockout
Clec1b$^{fl/fl}$*Pf4-Cre/Gp6*$^{-/-}$ (DKO)	Platelet CLEC-2 and GPVI double-knockout
Clec1b$^{fl/fl}$*Cd11c-Cre*	Dendritic cell-specific CLEC-2 knockout
PdpnCyto	Podoplanin cytoplasmic tail deficient
Pdpn$^{fl/fl}$*Vav1-cre*	Haematopoietic cell-specific podoplanin knockout

2.3 DNA extraction and genotyping of *PdpnCyto* colony

Tissue samples from adult mice (ear clipping) or embryos (hind paw) were digested by incubation at 55 ºC overnight in lysis buffer, containing Tris-hydrochloride (100 mM) pH 8.5, EDTA (5 mM), sodium dodecyl sulphate (0.2%), sodium chloride (200 mM), with proteinase K (1.25 mg/ml per sample). Next, tissue samples were vortexed and centrifuged at 16000 g at 4 ºC for 10 minutes, followed by supernatant collection. Isopropanol (1:1 v/v) was added to supernatant with gently mixed and centrifuged at 16000 g at 4 ºC for 20 minutes. The supernatant was discarded. The pellets were left to dry for 20 minutes to allow alcohol evaporation, followed by adding DNase-free water. The DNA samples were incubated at 55 ºC for one hour before adding into the reaction mix for polymerase chain reaction (PCR) amplification with the following primers;

Forwards: GCTTGTGACATGGAATTCAGC

Reverse: CGTATTTCCTCAGCAGAACAGG

Following PCR amplification, the PCR products were added into reaction mix, containing HindIII enzyme, acetylated BSA, and buffer E 10X, and incubated at 37 ºC overnight for DNA restriction digestion. Finally, orange G dye was added followed by running electrophoresis on 1% agarose gel to obtain the bands of digested PCR products for genotype identification.

2.4 DNA Sequencing of *PdpnCyto* colony

Beside HindIII digestion and gel electrophoresis, PCR products were identified using standard Sanger sequencing method (Zimmermann et al., 1988). In brief, the PCR products were cleaned using Microclean, followed by adding into BigDye reaction mix, containing primers shown above, and were subsequently amplified. Next, the PCR products were washed twice with ethanol and denatured with formamide at 94 ºC for two minutes, followed by cooling down to 0 ºC, which were ready to run on an ABI 3730 automated sequencer. The signals of nucleotide sequence were analysed using Chromas 2.6.6 software (Technelysium, AU) based on the reference sequence of murine *Pdpn* (GenBank: AK158855.1).

2.5 Full-thickness excisional skin wound model

Male and female WT, *Clec1b*$^{fl/fl}$*Pf4-Cre*, *Gp6*$^{-/-}$, DKO, and *PdpnCyto*$^{-/-}$ mice at the age of 8-10 weeks were used for skin wound experiments. Analgesic (buprenorphine) was given subcutaneously (s.c.) to all mice at least 30 minutes before procedure, followed by twice daily for two consecutive days. Under general anesthesia using isoflurane inhalation, the flank area of each mouse was shaved and cleaned, followed by a single cut through whole layer of skin using a 4 mm-diameter biopsy punch (Kai Industries, Japan) to generate a

full-thickness excisional skin wound (Figure 2.1). All mice were s.c. injected with 0.5 ml of 5% glucose-saline solution for rehydration after procedure. Wound size was measured using calipers (Moreira et al., 2015) and wound appearance was imaged using a Nikon COOLPIX B500 digital camera every day for up to nine days post-injury. Wound area was calculated as described below (Moreira et al., 2015) and presented as the percentage of initial wound size (Yang et al., 2011).

$$\text{Wound area} = \pi \times (\text{diameter A}/2) \times (\text{diameter B}/2)$$

Where diameter A = larger diameter of the lesion (vertical length),

diameter B = minor diameter of the lesion (horizontal length)

A second set of wound experiments were performed in *Gp6*$^{-/-}$ mice in the presence of a podoplanin-blocking antibody. Two doses of anti-podoplanin antibody (clone 8.1.1, 100 µg) that blocks CLEC-2-podoplanin interaction *in vivo* (Rayes et al., 2018, Rayes et al., 2017, Payne et al., 2017) or Syrian hamster IgG isotype control were intravenously (i.v.) injected into *Gp6*$^{-/-}$ mice at 24 hours prior and after wounding. Wound size was monitored for three days post-injury.

For a pilot wound experiment in platelet depletion model, an anti-GPIbα antibody (1.5 µg/g) was i.v. injected into WT mice 24 hours before biopsy (Rayes et al., 2017). Wound bleeding was monitored every 30 minutes.

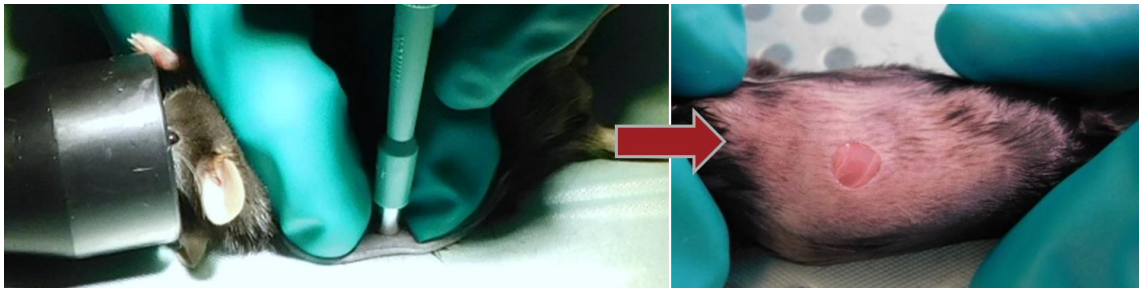

Figure 2. 1. Full-thickness excisional skin wound model in mice. The animal was placed in a lateral position. Then the flank skin was folded. Finally, the punch was gently pressed and slowly screwed on the folded skin to cut the whole layer of skin (*left*). As shown, the muscle underneath the skin was exposed after biopsy (*right*).

2.6 Microscopy

2.6.1 Tissue processing for histology

Tissue samples, including wound tissues, multi-organs from adult mice, and whole embryos (E14.5), were processed using a standard paraffin embedding protocol (Canene-Adams, 2013). In brief, wounds were excised and the inner side was firmly pressed onto a piece of filter paper to hold the tissue, which prevents curling during processing. All tissue samples were fixed in 4% paraformaldehyde for 24 hours. Next, tissues were put into tissue cassettes, followed by dehydration with graded ethanol (70% for 30 minutes, 95% for 30 minutes, two changes in 100% for 30 minutes each) and two changes (one hour each) in Histo-clear at room temperature, respectively. After that, tissues were immersed into two changes (one hour each) of melted paraffin at 65 ºC to allow paraffin infiltration. Finally, tissues were put into the moulds pre-filled with melted paraffin and allowed to cool. Once the paraffin was hardened, tissue blocks were removed from the

moulds. Paraffin-embedded tissues from adult mice were sectioned at 5 µm by microtome (Leica Biosystems, UK) and from embryos at 10 µm. In addition to paraffin-embedding, wound tissues were excised, held with filter paper, and directly embedded in optimal cutting temperature (O.C.T) compound, and frozen at -80 ºC. These O.C.T-embedded tissues were sectioned at 10 µm by Cryostat (Bright instruments, UK).

2.6.2 Morphometric analysis

Paraffin-embedded skin samples and other tissues were stained with haematoxylin and eosin (H&E) and imaged using a ZEISS AxioScan.Z1 slide scanner for microscopic examination. In skin histology (Figure 2.2), the thickening of keratinocytes (hyperplastic epidermis; He) appears at the wound edge within a few days after injury. The formation of granulation tissue, which comprised of newly formed vasculatures, infiltrating cells, and molecules, is also observed. The migration of keratinocytes generates epithelial tongues underneath the scab and above the granulation tissue (red dotted line), which migrate towards the centre of the wound to resurface skin epithelium (Shaw and Martin, 2009, Lucas et al., 2010, Yang et al., 2011).

Morphometric analysis was performed in low power field images of skin histology. All parameters were measured manually using a freehand or straight line tool in Fiji (a distribution of ImageJ software) (Schindelin et al., 2012), and the terms were defined in the following ways;

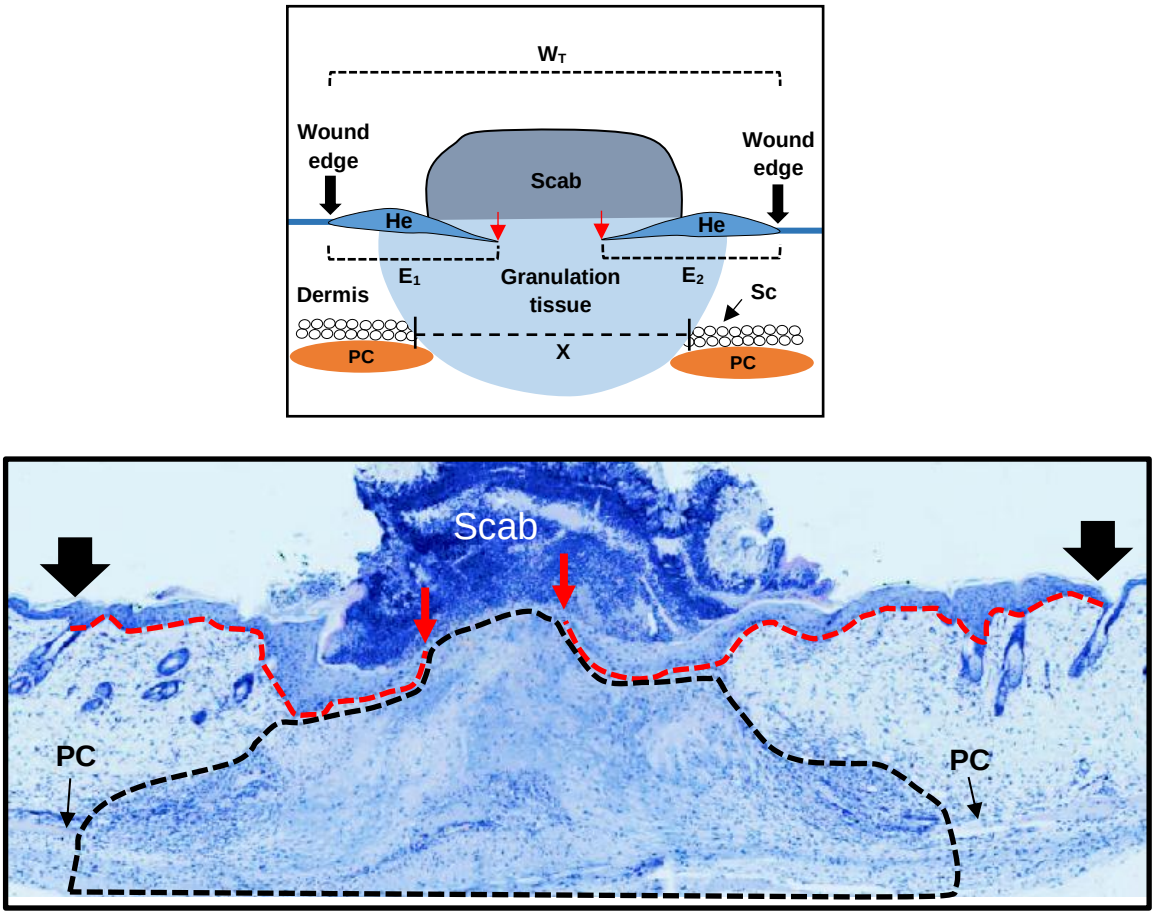

Figure 2. 2. Schematic demonstration for morphometric analysis of skin histology. *Top:* illustration shows morphometric parameters for the assessment of wound healing. Red arrow indicates the tips of epithelial tongue. Black arrow points to wound edge. All abbreviations are described in the text. *Bottom:* representative low power field image of skin histology at day 3 post-injury. Dotted red line indicates migration of keratinocytes from the wound edges toward centre. Dotted black coverage represents the granulation tissue area.

- Re-epithelialisation is the re-generation of skin epidermis, which comprises of proliferation and migration of keratinocytes (Ben Amar and Wu, 2014, Stavrou et

al., 2018). In histology images, the area of thickening of keratinocytes immediately adjacent to the normal skin was considered as the wound edge for measuring re-epithelialisation (Stavrou et al., 2018, Chen et al., 2015, Oda et al., 2017, Sheets et al., 2016, Carretero et al., 2008, Schmidt and Horsley, 2013). Percentage of re-epithelialisation at day 3 post-injury was calculated using the formula (Stavrou et al., 2018, Chen et al., 2015);

$$\% \text{ Re-epithelialisation} = [(E_1+E_2)/W_0] \times 100$$

where E_1 and E_2 = distance of epithelial tongue from each side of wound edge

W_0 = original wound diameter at day 0

- Unlike human, wound contraction significantly affects wound closure in rodents. The specialised muscle *panniculus carnosus* (PC) in deeper layer of murine skin contributes to wound contraction (Davidson et al., 2013). To examine the influence of this effect, closure by contraction at day 3 post-injury was calculated using the formula (Chen et al., 2015);

$$\% \text{ Wound contraction} = [(W_0-W_T)/W_0] \times 100$$

where W_T = distance between the wound edges at indicated time point

- The area of granulation tissue was also measured at day 3 post-injury (Lucas et al., 2010, Yang et al., 2011).
- Scar formation following the complete wound closure was evaluated at day 9 post-injury. This includes the length of hyperplastic epidermis (the remaining thickened keratinocytes) (Yang et al., 2011, Rono et al., 2013) and the distance between intact subcutaneous (Sc) edges at both side of the wound ("X" in Figure 2.2) (Yang et al., 2011), which represents the size of scar at upper and deeper layers, respectively.

2.6.3 Measurement of fibrin and collagen contents

The slides of paraffin-embedded skin sections were dewaxed in two changes of Histo-clear (five and three minutes, respectively), followed by rehydration with graded ethanol (three minutes in 100%, 95%, 70%, 50%, and 30%, respectively) and water (five minutes). Then, Martius scarlet blue staining was performed to detect fibrin and collagen according to the protocol recommended by manufacturer. Tissue slides were dehydrated in graded ethanol (three minutes in 70%, 95%, and 100%) and two steps in Histo-clear (five minutes and overnight, respectively). The tissue slides were mounted with DPX mounting medium and left dry, followed by imaging. For quantitative analysis, high power field (HPF) images were taken from the whole wound area (an example is shown in Figure 2.3).

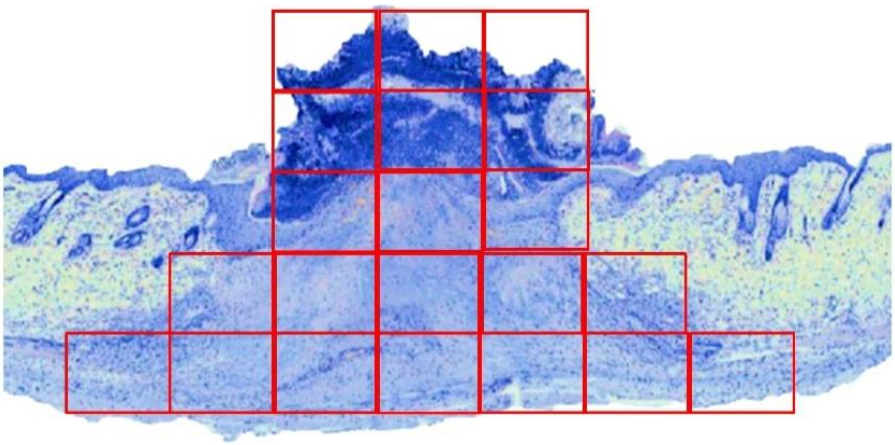

Figure 2. 3. An example histology image demonstrates how to obtain high power field (HPF) images. Each rectangle represents a single HPF image. For consistency of the procedure, HPF images were taken from the bottom (left → right) to the top area of all samples, which covered both granulation tissue and scab area.

A relative quantification of fibrin and collagen contents was performed using Fiji by the following steps;

1) Image colours were isolated using Colour Deconvolution plugin (Masson Trichrome) (Ruifrok and Johnston, 2001) to obtain green, red, and blue colour channel, respectively.

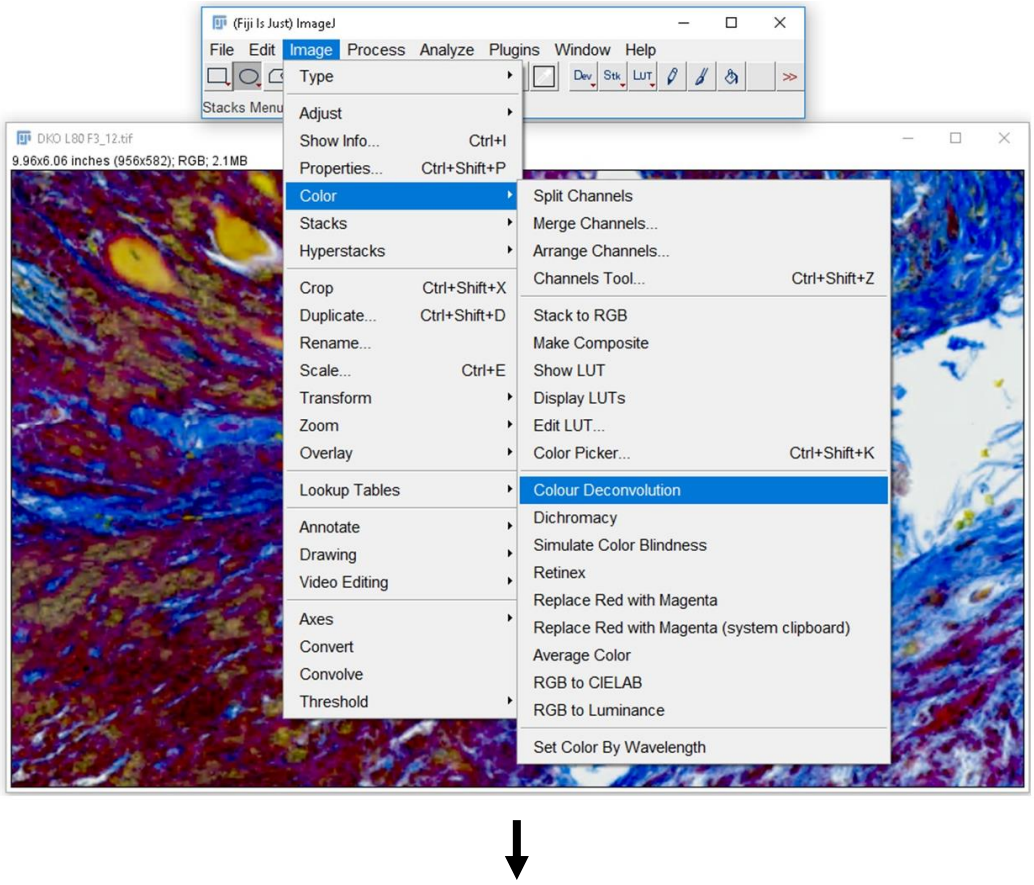

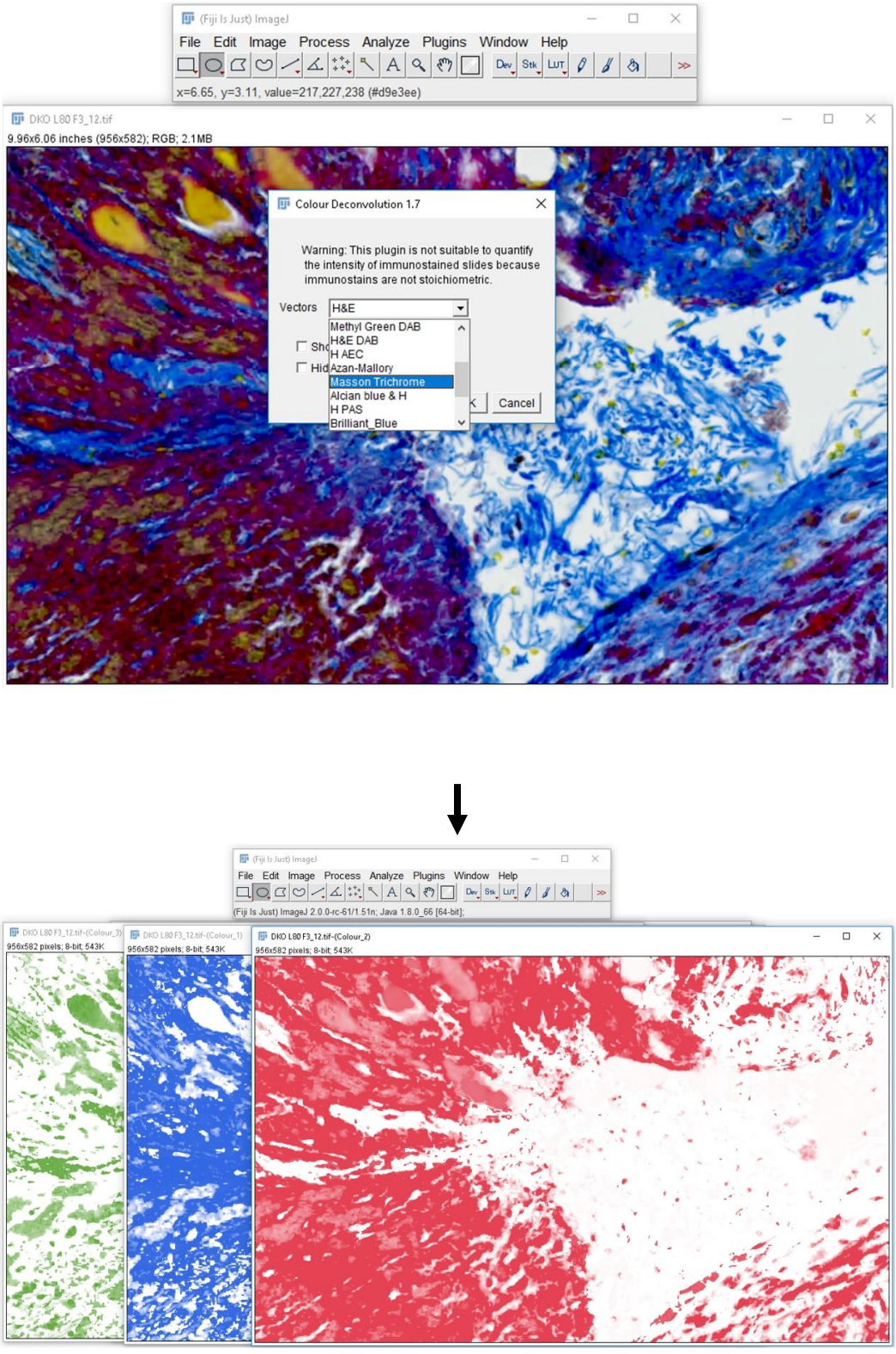
(Fiji Is Just) ImageJ
File Edit Image Process Analyze Plugins Window Help
x=6.65, y=3.11, value=217,227,238 (#d9e3ee)
DKO L80 F3_12.tif
9.96x6.06 inches (956x582); RGB; 2.1MB
Colour Deconvolution 1.7
Warning: This plugin is not suitable to quantify the intensity of immunostained slides because immunostains are not stoichiometric.
Vectors
H&E
Methyl Green DAB
H&E DAB
H AEC
Azan-Mallory
Masson Trichrome
Alcian blue & H
H PAS
Brilliant_Blue
Cancel
(Fiji Is Just) ImageJ
File Edit Image Process Analyze Plugins Window Help
(Fiji Is Just) ImageJ 2.0.0-rc-61/1.51n; Java 1.8.0_66 [64-bit];
DKO L80 F3_12.tif-(Colour_3)
956x582 pixels; 8-bit; 543K
DKO L80 F3_12.tif-(Colour_1)
956x582 pixels; 8-bit; 543K
DKO L80 F3_12.tif-(Colour_2)
956x582 pixels; 8-bit; 543K

2) The red colour (for fibrin) or blue colour (for collagen) channel was converted to binary image (8 bit). Threshold was set using the Otsu method (Luo et al., 2018).

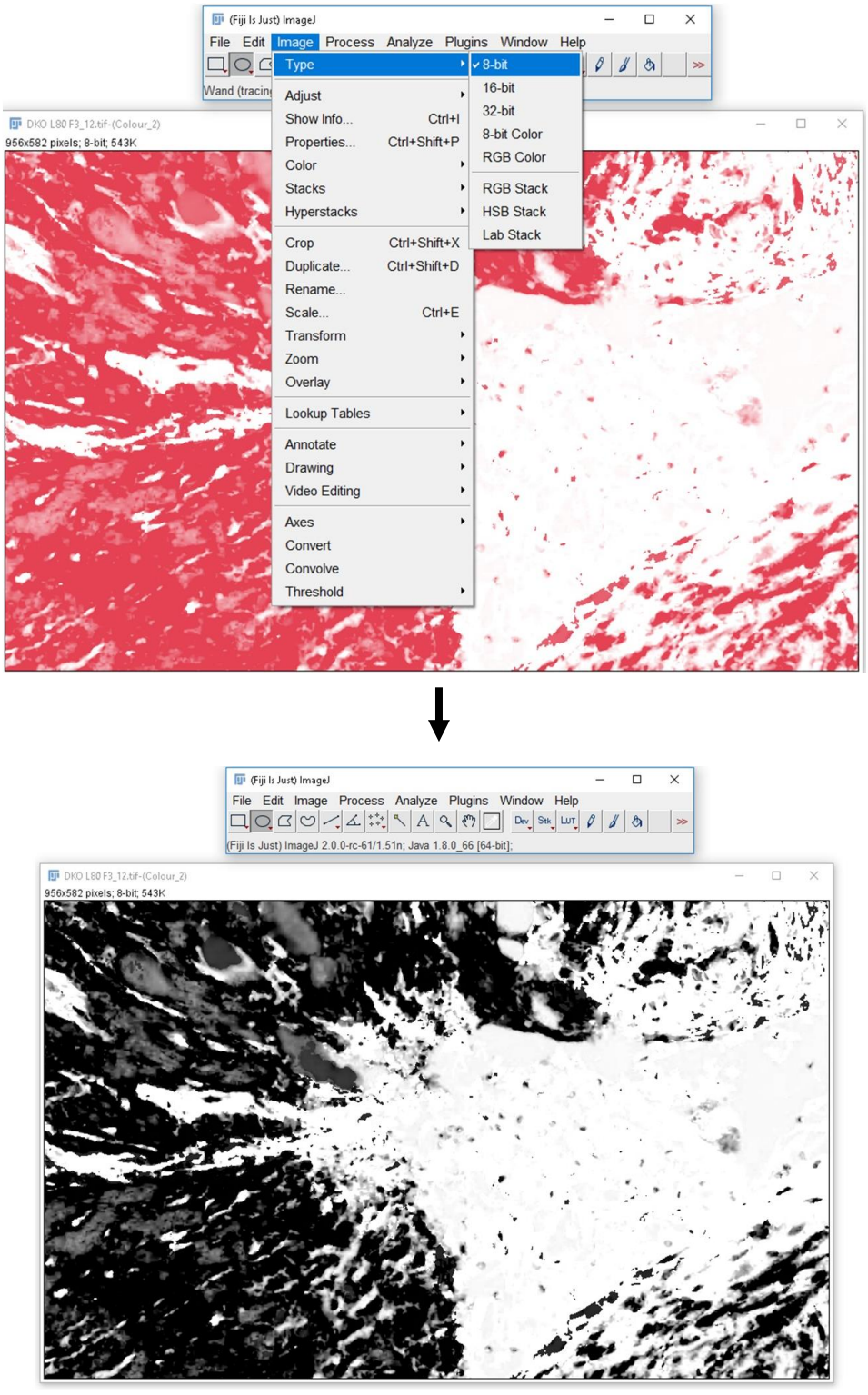

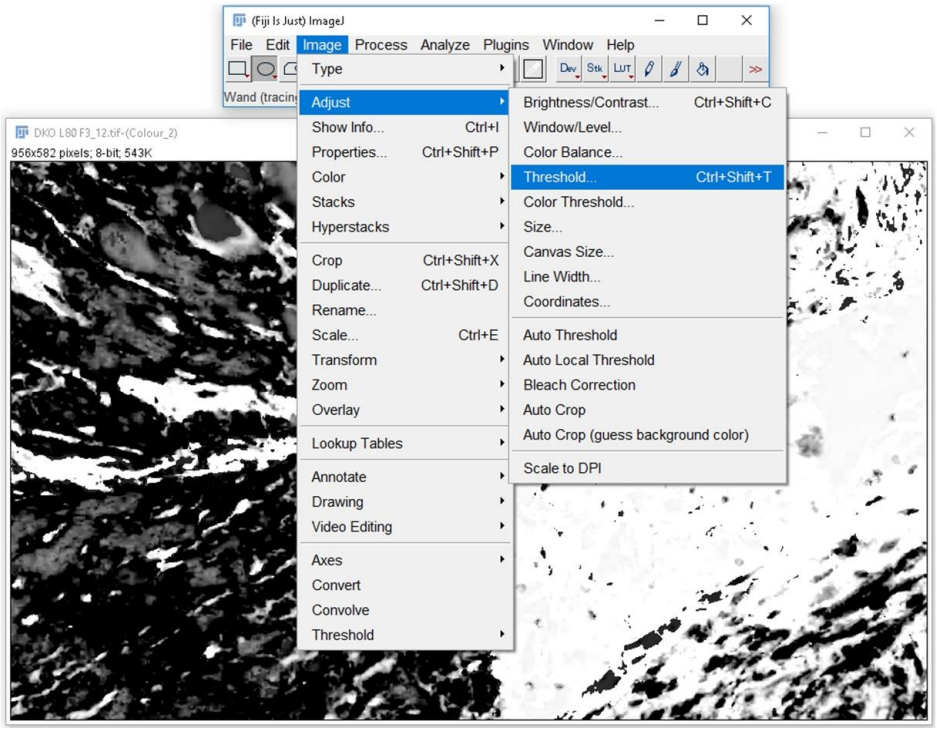
(Fiji Is Just) ImageJ
File Edit Image Process Analyze Plugins Window Help
Type
Adjust
Show Info... Ctrl+I
Properties... Ctrl+Shift+P
Color
Stacks
Hyperstacks
Crop Ctrl+Shift+X
Duplicate... Ctrl+Shift+D
Rename...
Scale... Ctrl+E
Transform
Zoom
Overlay
Lookup Tables
Annotate
Drawing
Video Editing
Axes
Convert
Convolve
Threshold
Brightness/Contrast... Ctrl+Shift+C
Window/Level...
Color Balance...
Threshold... Ctrl+Shift+T
Color Threshold...
Size...
Canvas Size...
Line Width...
Coordinates...
Auto Threshold
Auto Local Threshold
Bleach Correction
Auto Crop
Auto Crop (guess background color)
Scale to DPI
DKO L80 F3_12.tif-(Colour_2)
956x582 pixels; 8-bit; 543K

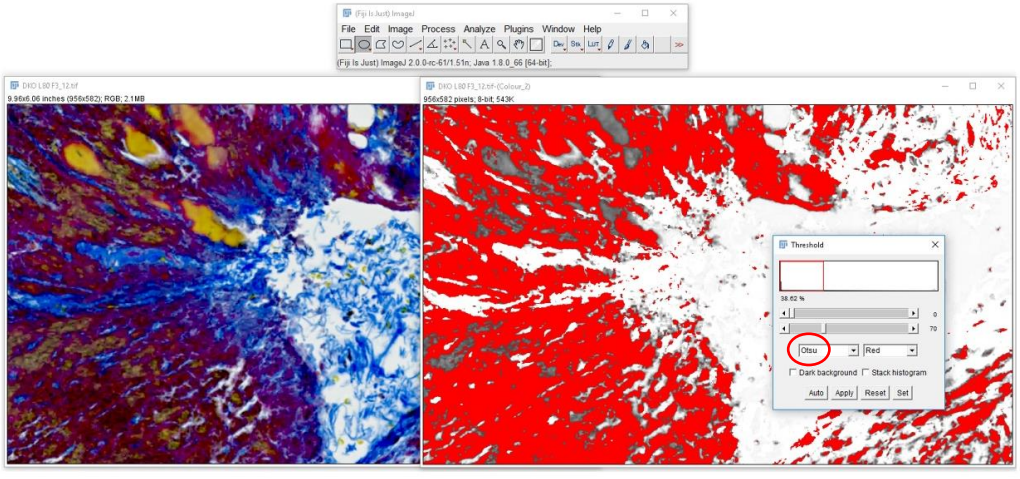
Threshold
Otsu
Red
Dark background
Stack histogram
Auto
Apply
Reset
Set

3) The measurements, including "integrated density" were selected and measured.

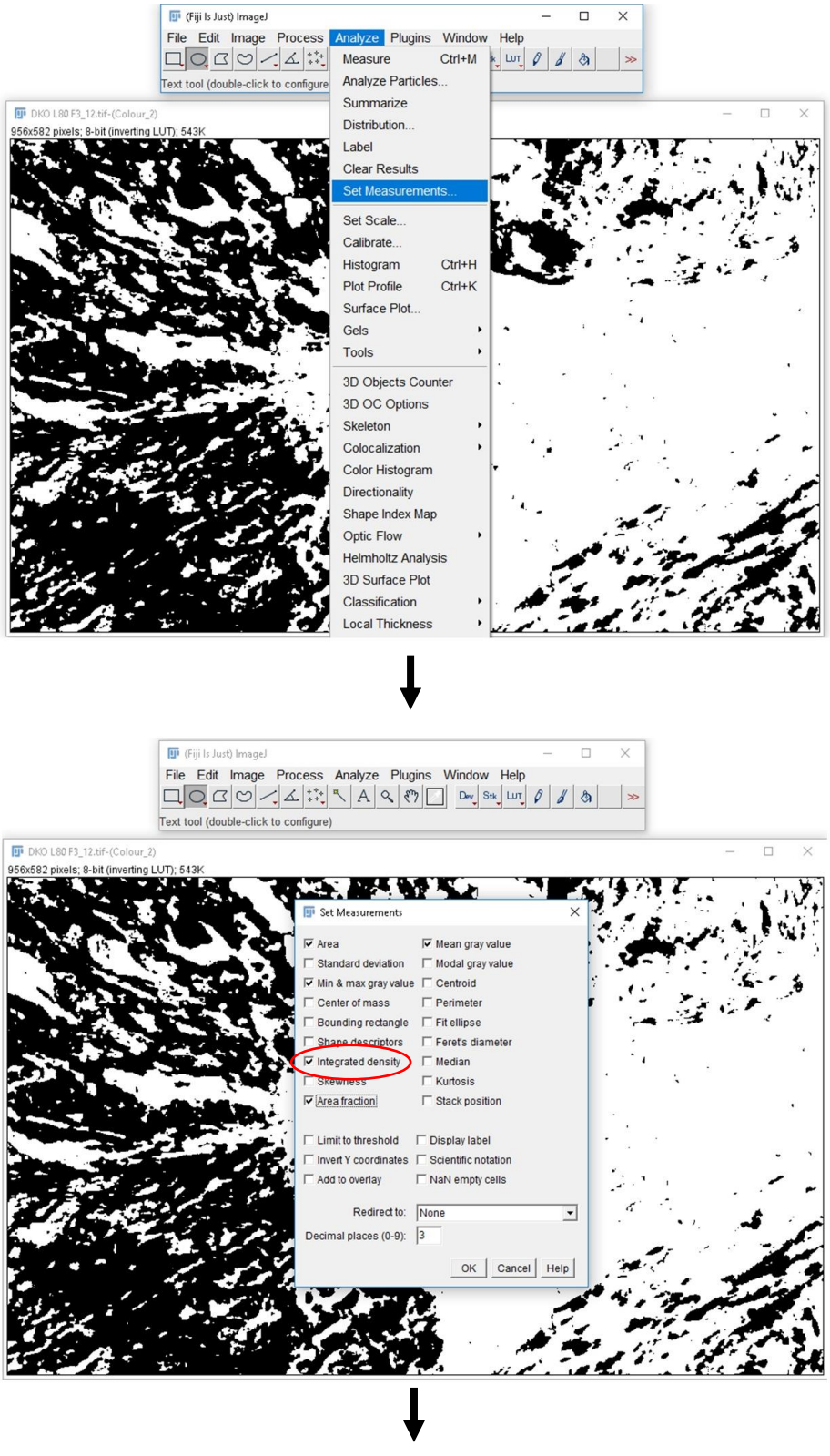

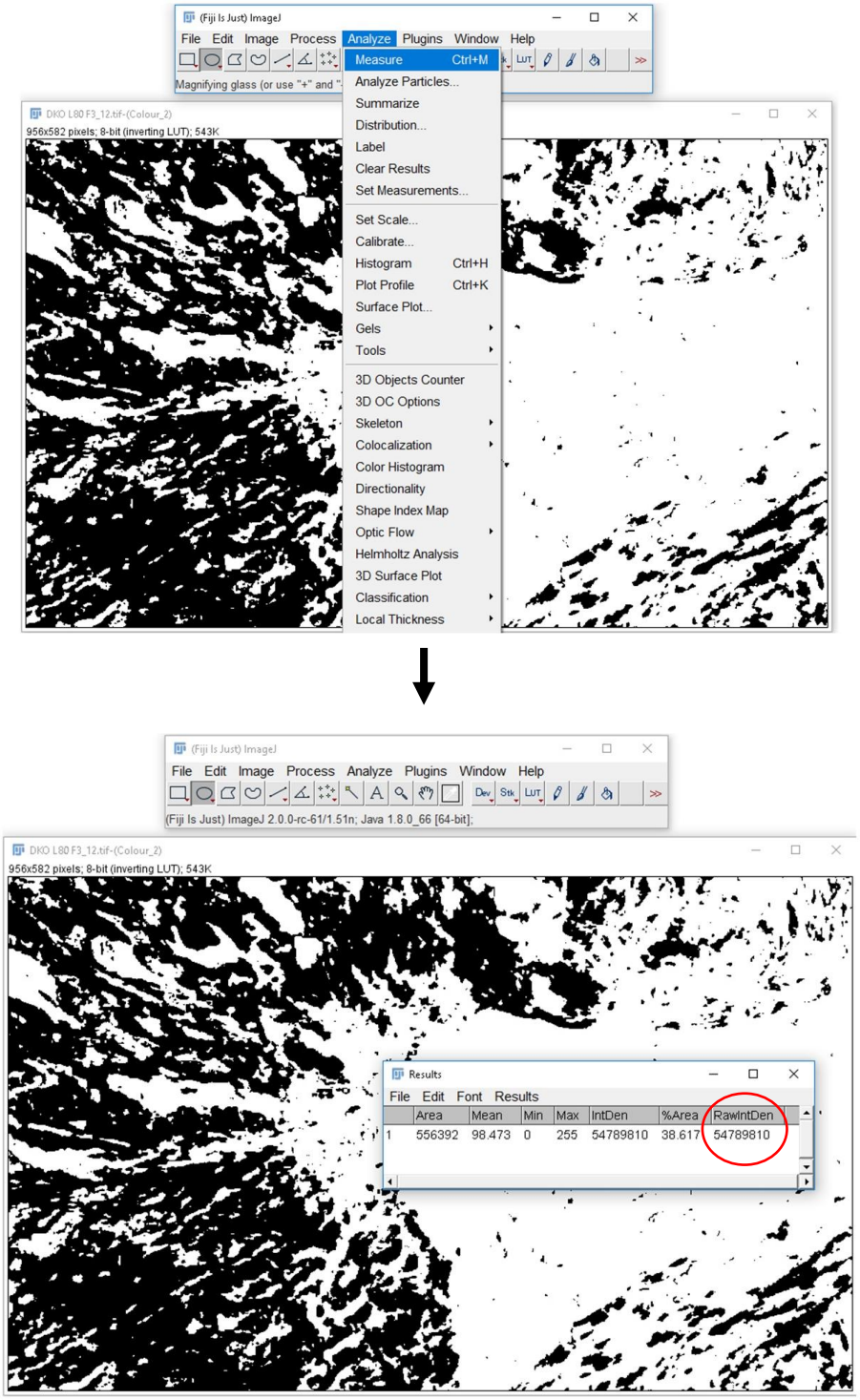

4) A total intensity (RawIntDen) derived from all HPF images was normalised by total measured area (i.e. per HPF), and expressed as fold relative to WT.

2.6.4 Immunohistochemistry

Immunohistochemistry staining for podoplanin, CLEC-2, fibrinogen, tissue factor, Gr-1, Ly6C, F4/80, TNF-α, CXCL-1, and PF4 were performed on paraffin-embedded tissue sections according to a standard protocol (Ramos-Vara, 2017). In brief, the slides of skin sections were dewaxed and rehydrated as stated in the previous section. For antigen retrieval, tissues were incubated in preheated citrate buffer (10 mM citric acid monohydrate+0.5% Tween 20, pH 6.0), and boiled for 15 minutes (skin samples) or 30 minutes (other tissues). After cooling down at room temperature, tissues were washed once (10 minutes) in phosphate buffer saline with 0.1% Tween (PBST) and treated with 3% hydrogen peroxide solution (10 minutes) to block endogenous peroxidase, followed by one hour incubation with blocking buffers, either 5% goat serum + 1% BSA in PBST or 5% BSA in PBST. Next, tissue sections were incubated with primary antibodies at 4 ºC overnight, followed by three washes in PBST (30 minutes each) and one hour incubation with horseradish peroxidase (HRP)-conjugated secondary antibodies. After three washes in PBST (10 minutes each), ImpactDAB substrate were used for signal detection. The tissues were counterstained with haematoxylin (two minutes and wash in water), followed by colour differentiation in 1% acid alcohol (two dips and wash in water), and bluing with Scott's tap water (two minutes and wash in water). Finally, tissue slides were dehydrated and mounted, followed by imaging as described in the previous section. HPF images were taken from the whole wound area for further quantitative analysis.

Gr-1$^+$, Ly6C$^+$, and F4/80$^+$ cells were counted using Fiji, according to a protocol shown below. Then, the total cell count was normalised by total measured area and presented per HPF (Qiang et al., 2017).

1) Brown colour was separated using IHC toolbox in Fiji plugins. H-DAB mode, followed by "color" button, was selected.

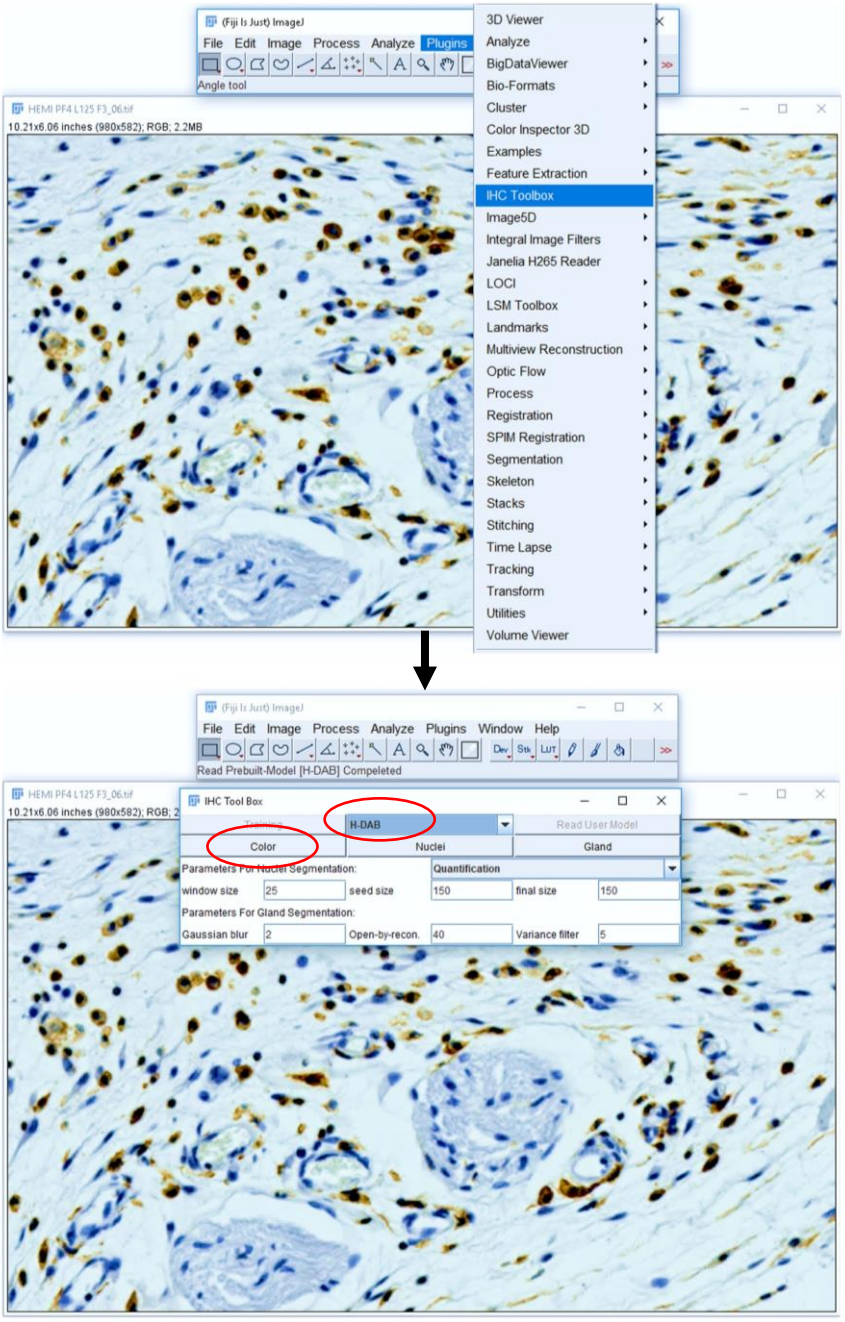

2) Image was converted to binary image (8 bit) and threshold was set using "Ostu" mode to obtain a good signal with minimal background.

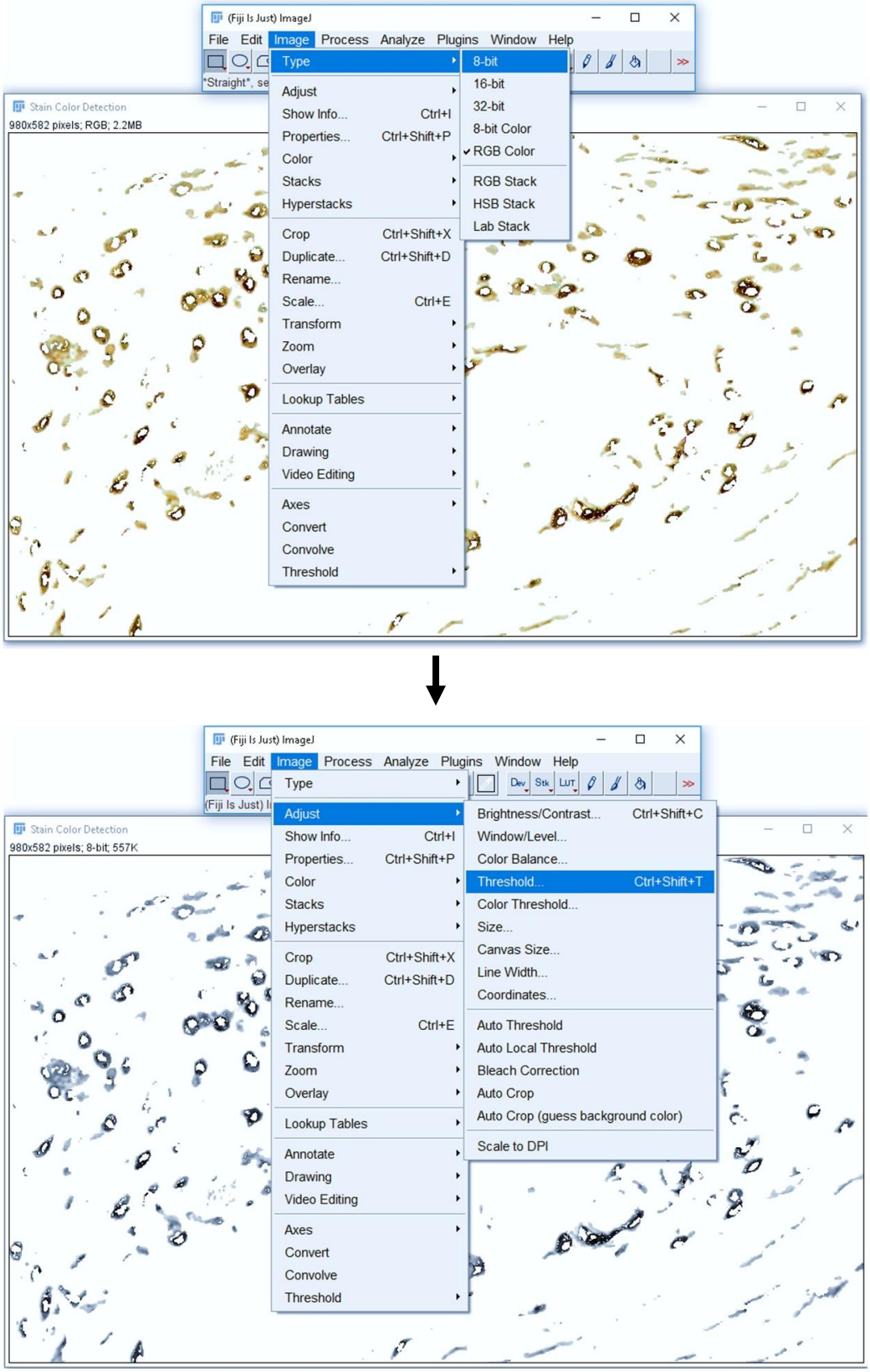

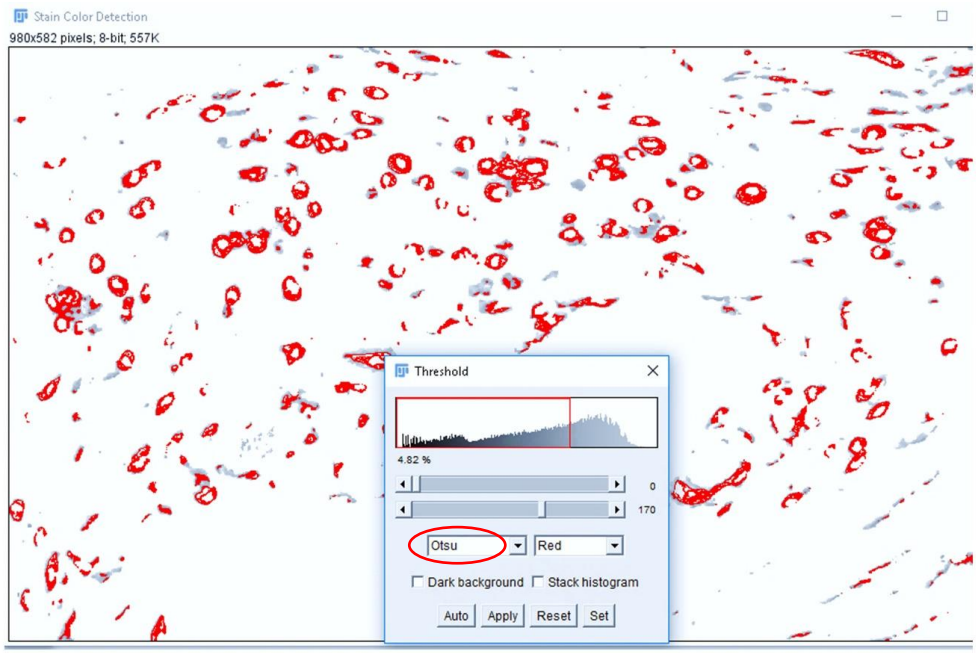

3) Thresholded image was undergone binary process using "fill holes" to fill the possible holes that arose from colour separation process, followed by "watershed" to separate attached particles/cells.

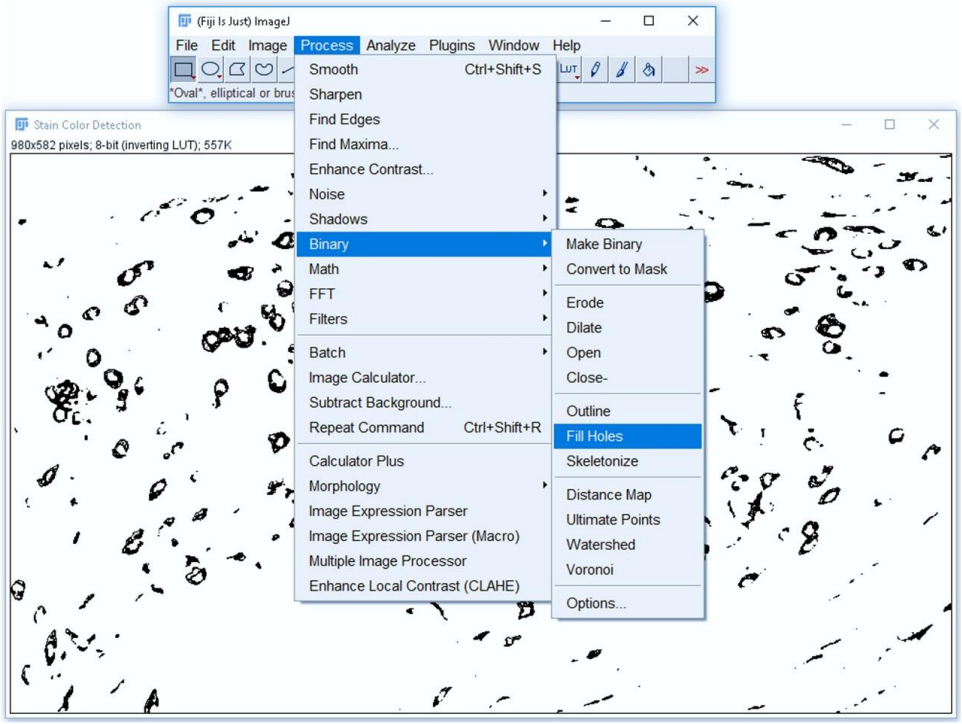

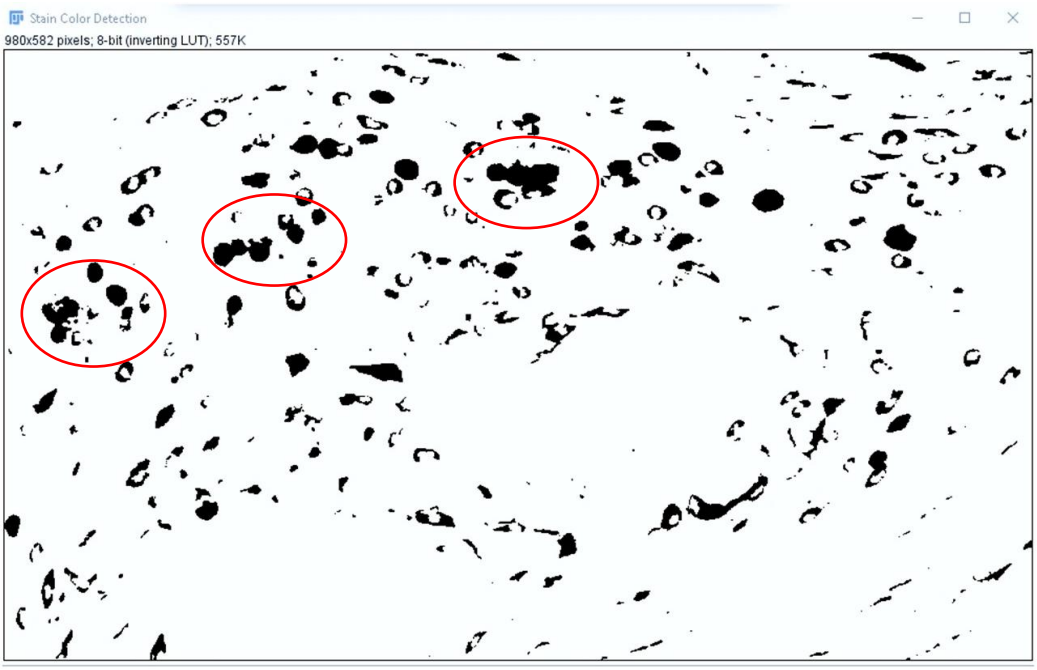
Stain Color Detection
980x582 pixels; 8-bit (inverting LUT); 557K

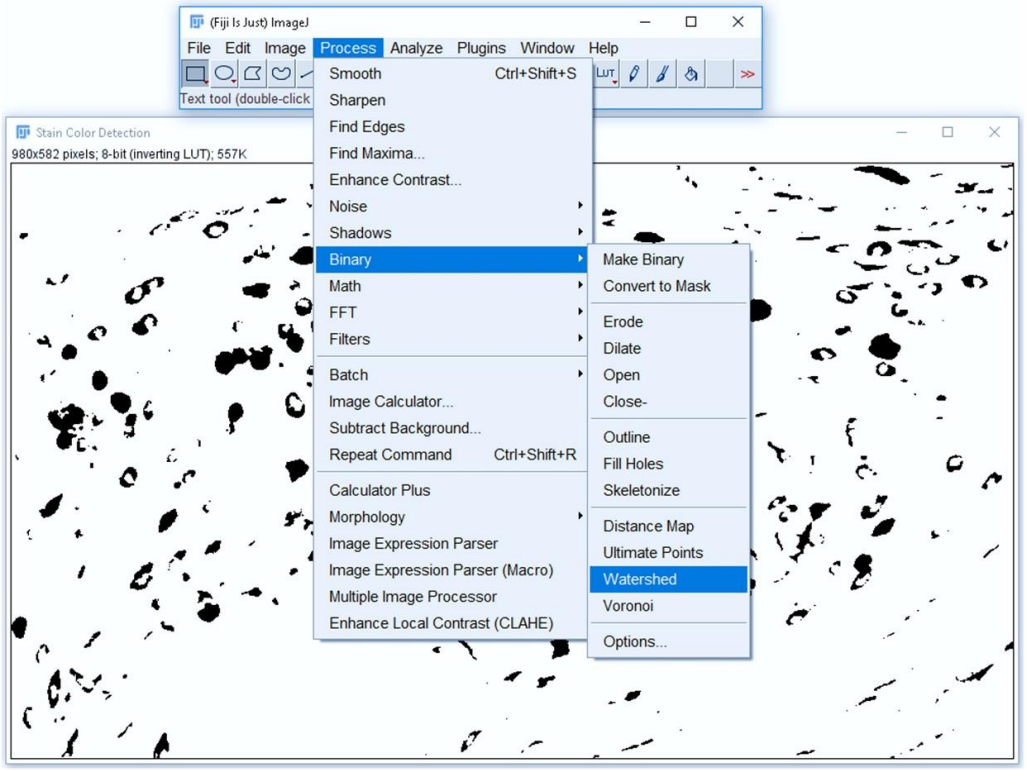
(Fiji Is Just) ImageJ
File Edit Image Process Analyze Plugins Window Help
Text tool (double-click
Stain Color Detection
980x582 pixels; 8-bit (inverting LUT); 557K
Smooth Ctrl+Shift+S
Sharpen
Find Edges
Find Maxima...
Enhance Contrast...
Noise
Shadows
Binary
Math
FFT
Filters
Batch
Image Calculator...
Subtract Background...
Repeat Command Ctrl+Shift+R
Calculator Plus
Morphology
Image Expression Parser
Image Expression Parser (Macro)
Multiple Image Processor
Enhance Local Contrast (CLAHE)
Make Binary
Convert to Mask
Erode
Dilate
Open
Close-
Outline
Fill Holes
Skeletonize
Distance Map
Ultimate Points
Watershed
Voronoi
Options...

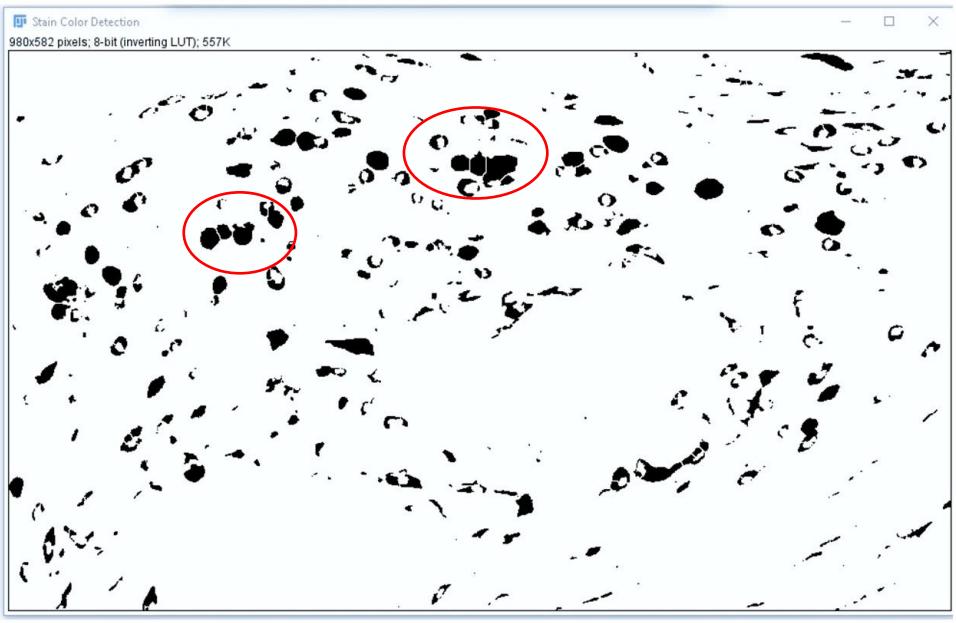

4) The “oval selection tool” was used to select the possible smallest size of signal/particle in the image, followed by “Analyze particles” mode with no any settings. Then, the “Summarize” box, followed by “OK” button, was selected to measure the size of such smallest particle (in a square pixel unit).

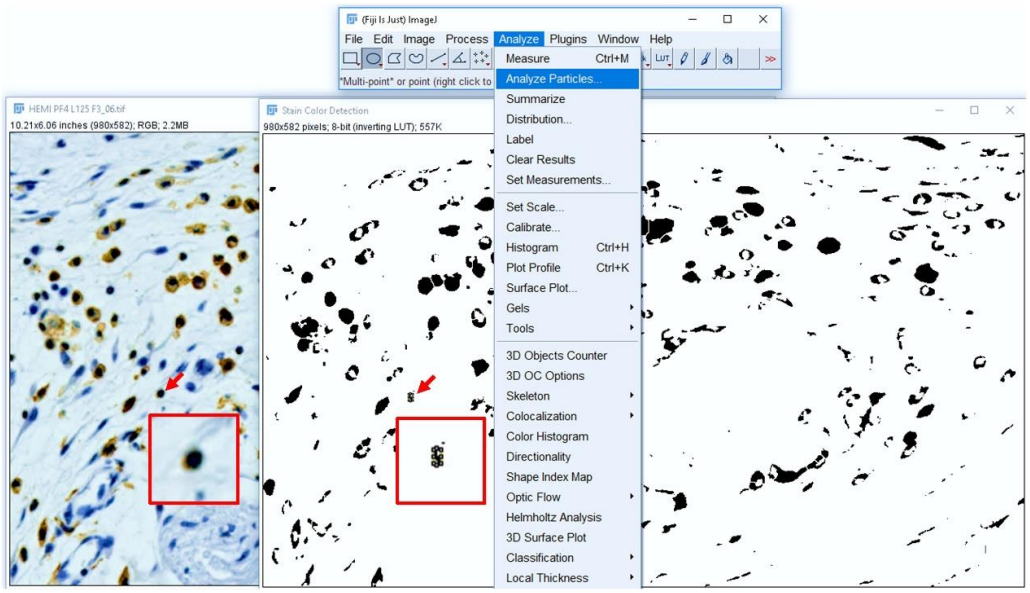

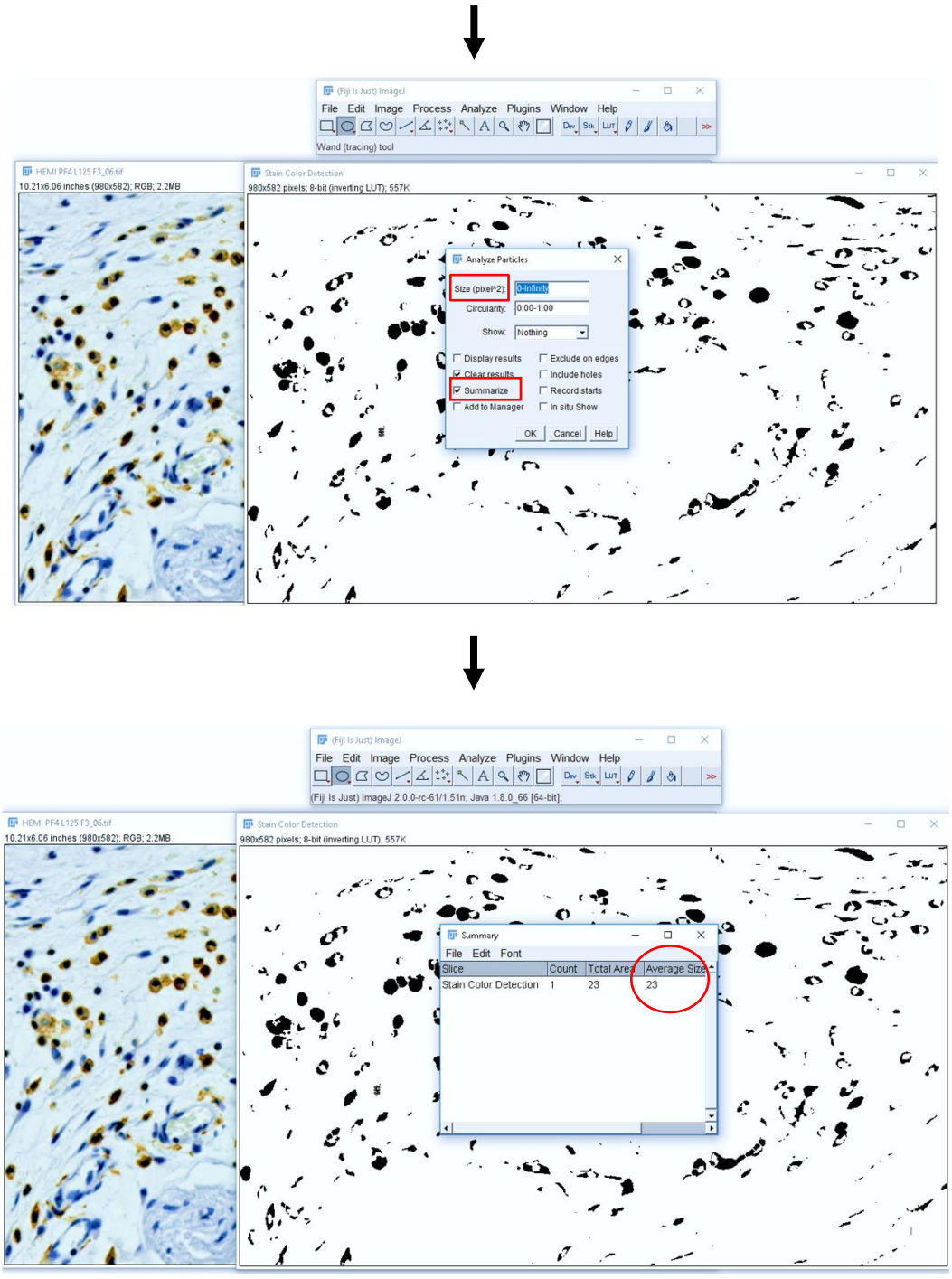

5) The "Analyze particles" mode was used again to set the range of particle size in square pixel unit (e.g. 20-infinity). To count all particles within the image except on edges, "Summarize" and "Exclude on edges" boxes, followed by "OK" button, were selected.

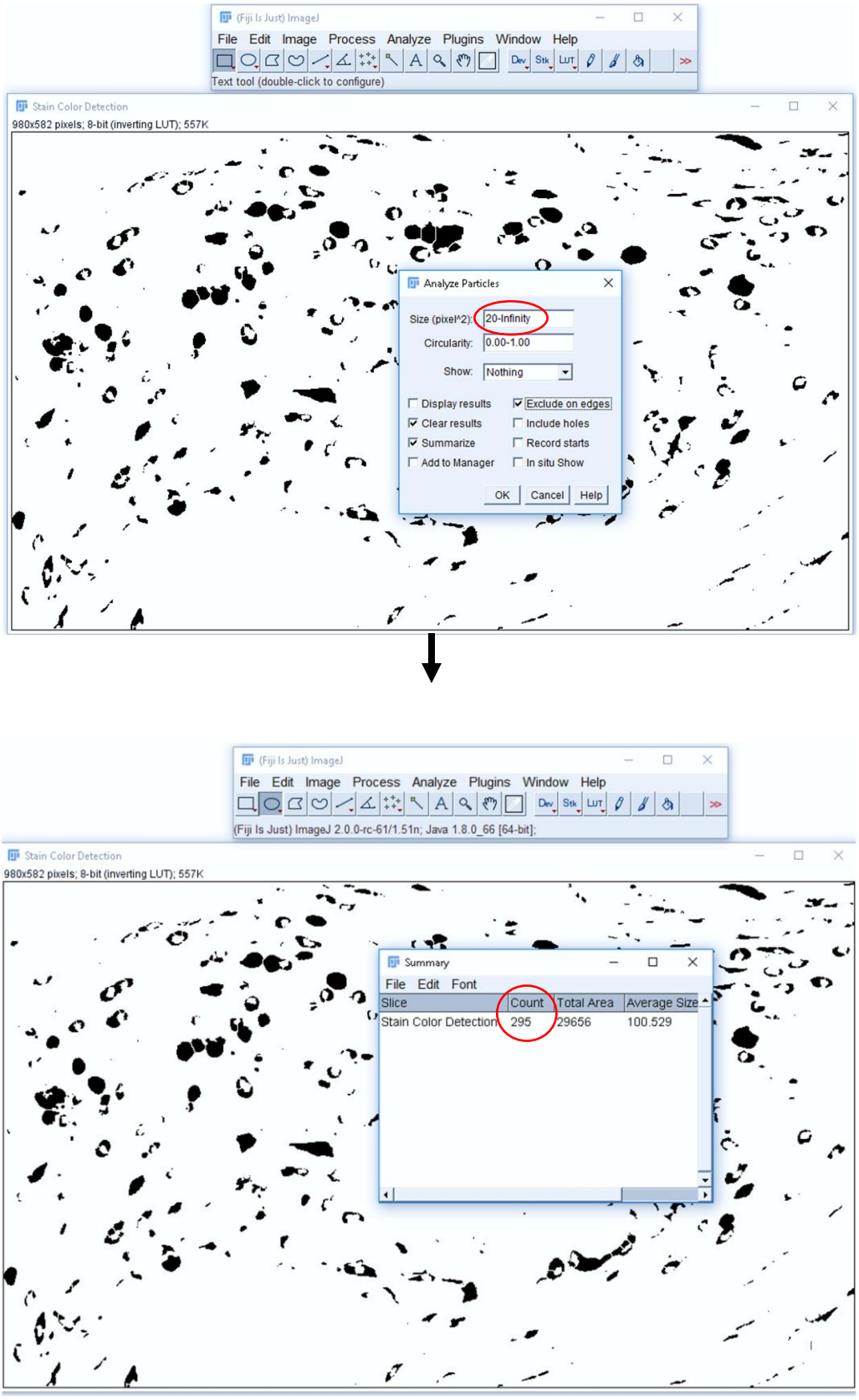
(Fiji Is Just) ImageJ
File Edit Image Process Analyze Plugins Window Help
Text tool (double-click to configure)
Stain Color Detection
980x582 pixels; 8-bit (inverting LUT); 557K
Analyze Particles
Size (pixel^2): 20-Infinity
Circularity: 0.00-1.00
Show: Nothing
Display results
Exclude on edges
Clear results
Include holes
Summarize
Record starts
Add to Manager
In situ Show
OK
Cancel
Help
(Fiji Is Just) ImageJ
File Edit Image Process Analyze Plugins Window Help
(Fiji Is Just) ImageJ 2.0.0-rc-61/1.51n; Java 1.8.0_66 [64-bit];
Stain Color Detection
980x582 pixels; 8-bit (inverting LUT); 557K
Summary
File Edit Font
Slice
Count
Total Area
Average Size
Stain Color Detection
295
29656
100.529

To quantify the intensity of tissue factor (Zhou et al., 2009), TNF-α, PF4, podoplanin, and CXCL-1 (Smith et al., 2010), HPF images were processed using step 1 and 2 shown above, followed by "Measure" mode in "Analyze" menu in Fiji. Then the total intensity (RawIntDen) was normalised by total measured area (i.e. per HPF), and expressed as fold relative to WT.

2.6.5 Immunofluorescence

Immunofluorescence staining for NG2, CD41, podoplanin, vimentin, Ly6C, Ly6G, F4/80, iNOS, Fizz-1, and CD31 were processed in O.C.T-embedded frozen skin sections. In brief, tissue slides were placed at room temperature for 30 minutes to allow O.C.T. melting, and then fixed in iced-cold acetone for 20 minutes, followed by drying at room temperature for 30 minutes and wash once in PBST (five minutes). Next, tissues were permeabilised in 0.5% Triton X-100 (10 minutes) and wash in PBST (five minutes), followed by auto-fluorescence quenching using 20 mM ammonium chloride (15 minutes). After that, tissue slides were incubated with blocking buffer for one hour at room temperature and then primary antibodies at 4 ºC overnight. After three washes in PBST (30 minutes each), tissues were incubated with fluorophore-conjugated secondary antibodies for one hour in the dark at room temperature and washed again with PBST (three times, 30 minutes each). Nuclei were stained with Hoechst (five minutes) and washed three times (five minutes each), followed by mounting and imaging. For subsequent quantification, HPF images were taken from the whole wound area.

To measure $CD31^+$ area (Uchiyama et al., 2014), the single-colour (green) fluorescence images was converted to binary images as shown in the previous section, followed by Otsu thresholding. Then, "Measure" mode from "Analyze" menu was used to measure

area fraction (% area covered by positive signal). Finally, the total % area was normalised by total measured area (i.e. per HPF), and presented as fold relative to WT.

The M1 (iNOS^{+}F4/80^{+} cells) and M2 (Fizz-1^{+}F4/80^{+} cells) macrophages were counted according to the previous protocol (Arqués et al., 2012) with adaptation as presented in the following steps;

1) HPF image was split into a single blue (nuclei), green (F4/80) and red (iNOS or Fizz-1) channel, respectively.

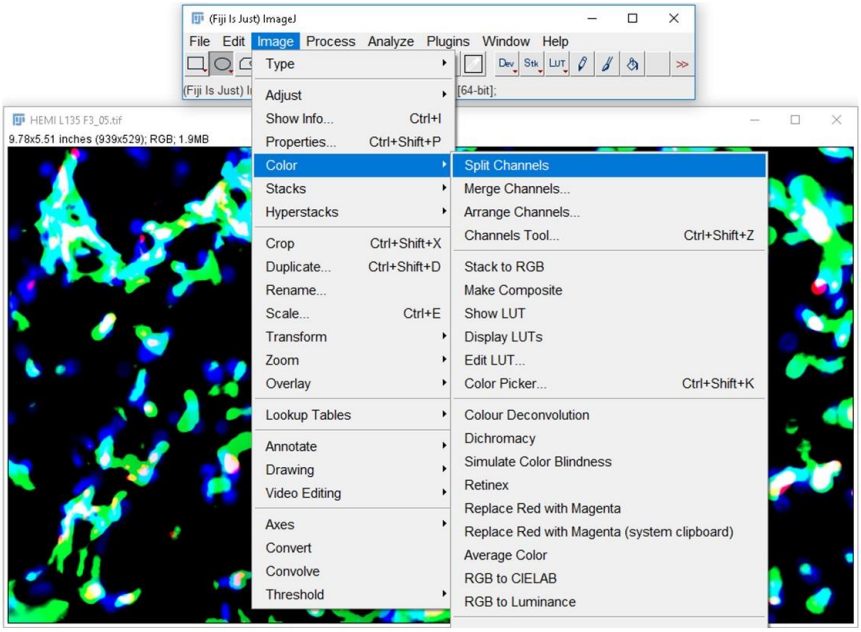

2) The threshold of green fluorescence was set using Otsu model.

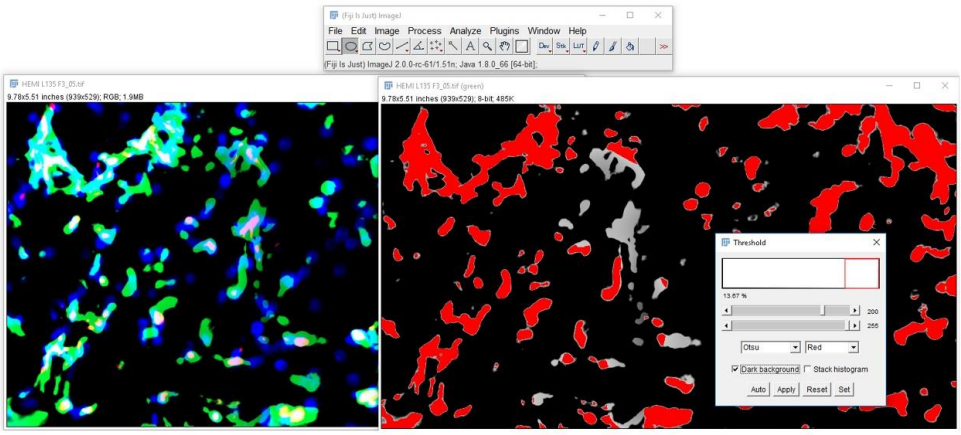

3) Then, the binary images were processed by a "watershed" to separate attached particles.

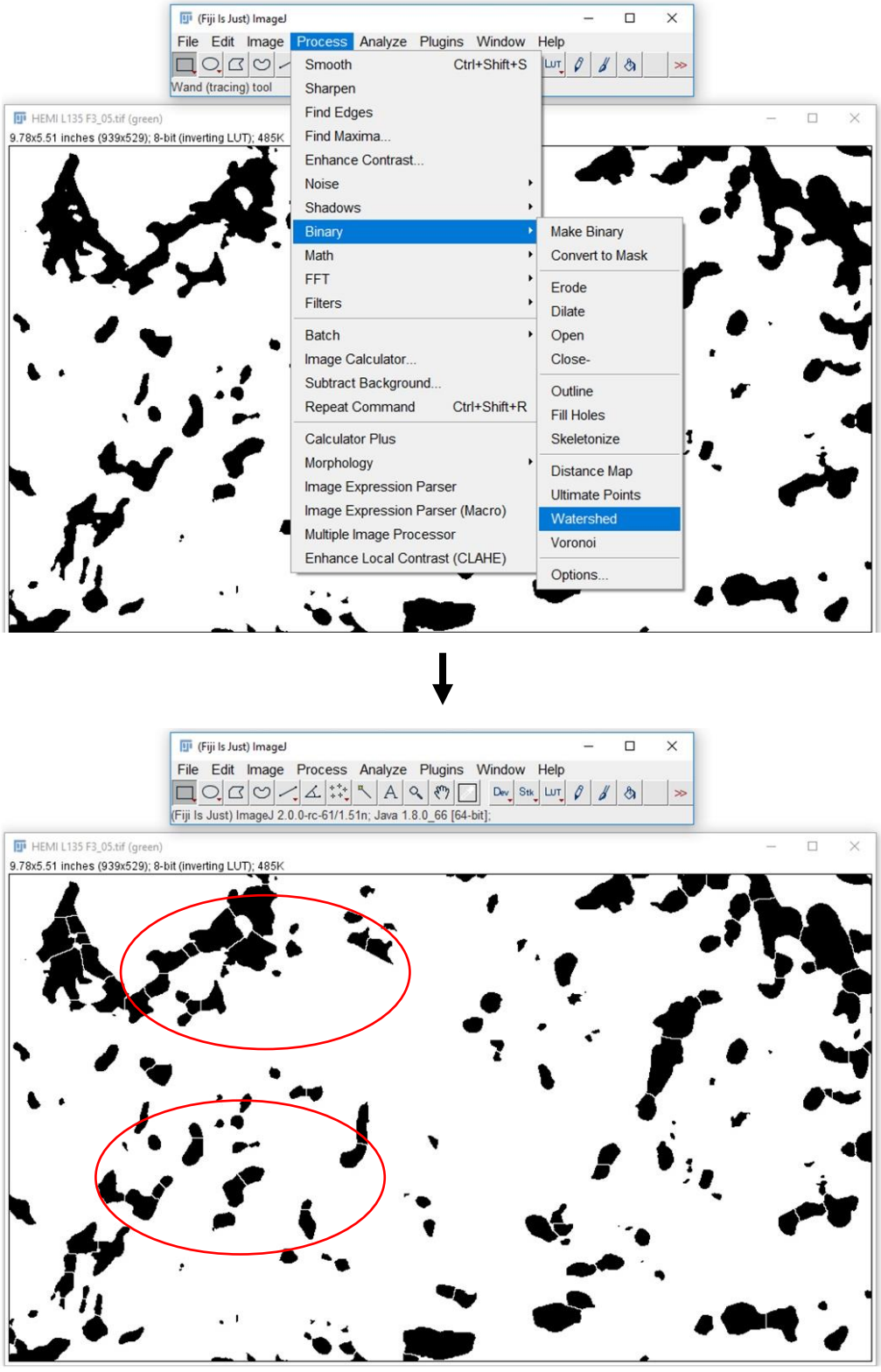

4) The red fluorescence was thresholded without a “watershed” process.

5) To create a merged image of previously processed red and green channels, the “image calculator” mode from “process” menu was used, followed by choosing the operator “AND”.

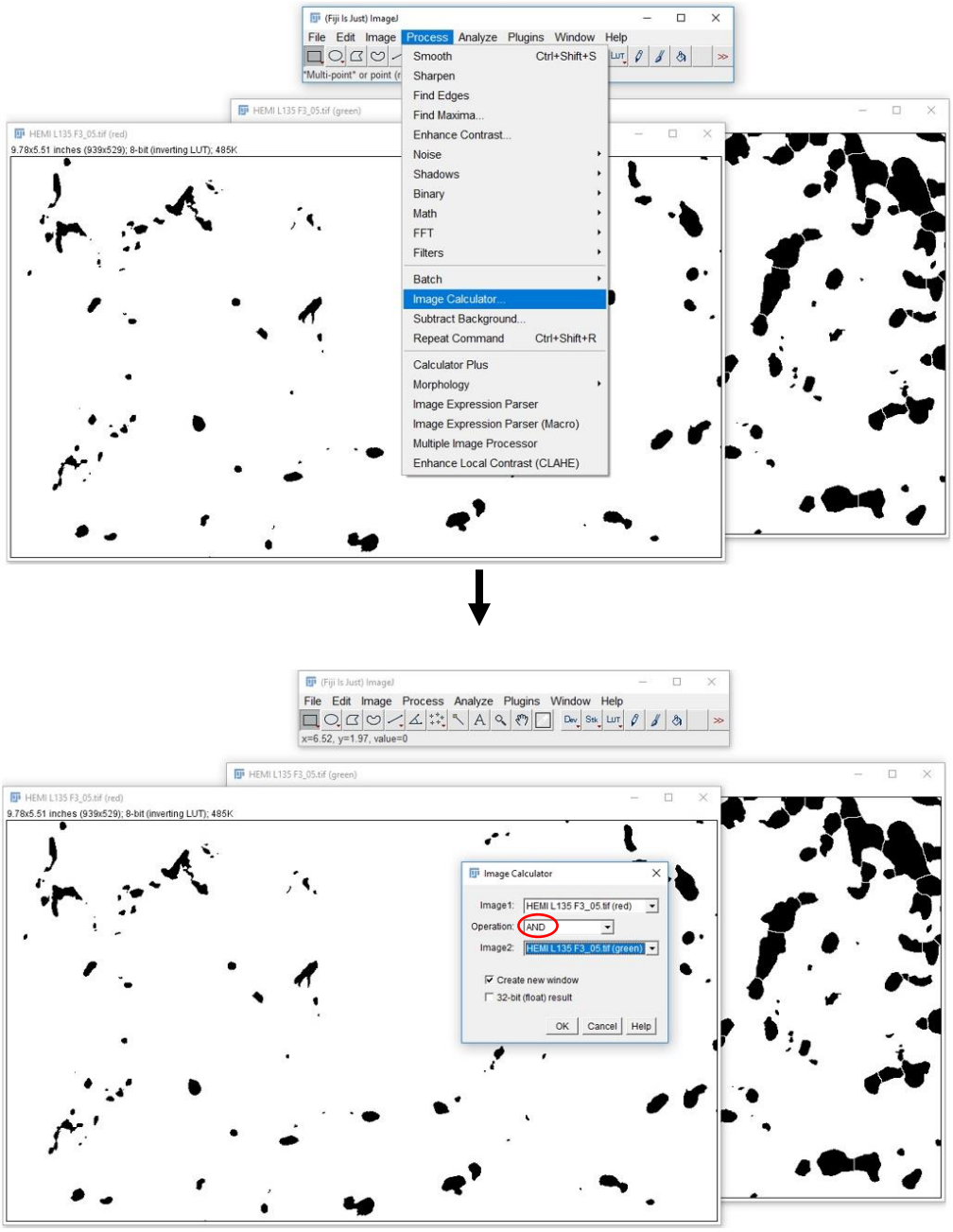

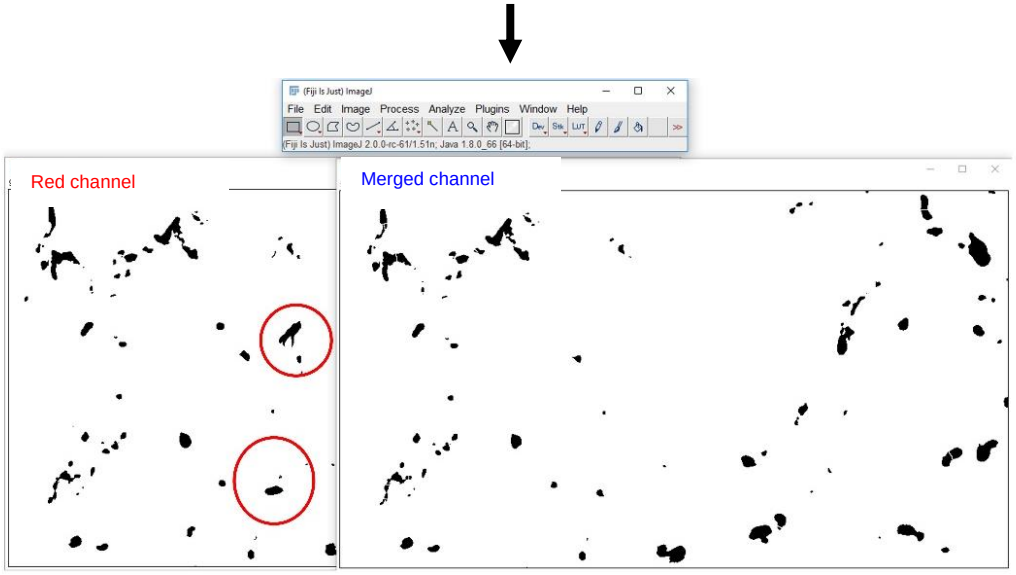

6) All connected areas larger than 20 square pixels were counted using "Analyze particles" mode as shown in the previous section. The total cell count was normalised by total measured area and presented per HPF.

2.7 In vitro neutrophil migration towards fMLP assay

Bone marrow-derived neutrophils from WT and DKO mice were isolated as previously described (Swamydas and Lionakis, 2013). Neutrophils were suspended in Hank's Balanced Salt Solution + 0.5 % BSA. The µ-slides (Ibidi) were pre-coated with either collagen (10 µg/ml) or fibrinogen (100 µg/ml) or cross-linked fibrin (prepared by mixing fibrinogen (1 mg/ml), thrombin (1 U/ml), Ca^{2+} (10 mM), and FXIIIa (7 µg/ml) in PBS and incubated for 1 hour at 37 °C). fMLP (5 µM) was added into lower chamber of µ-slides (Figure 2.4). Next, neutrophils (50,000 cells) were loaded into upper chamber and chemotaxis toward fMLP was assessed for 3 hours.

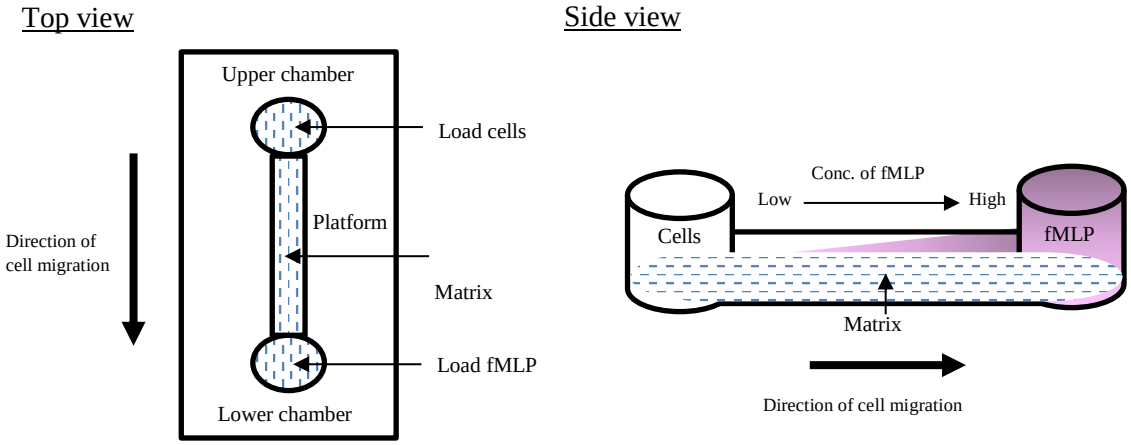

Figure 2. 4. Schematic demonstration of *in vitro* neutrophil migration towards fMLP assay using µ-slides. fMLP slowly diffuses through matrix-filled platform to the cell-containing side (chamber), which spontaneously generates fMLP concentration (Conc.) gradient. Matrix means either collagen or fibrinogen or cross-linked fibrin.

The cells in the loaded and migrated chambers were fixed with formalin and subsequently imaged. The number of cells in five representative areas per sample was quantified using Fiji as shown below.

1) Background was subtracted by setting rolling ball radius at 50 pixels

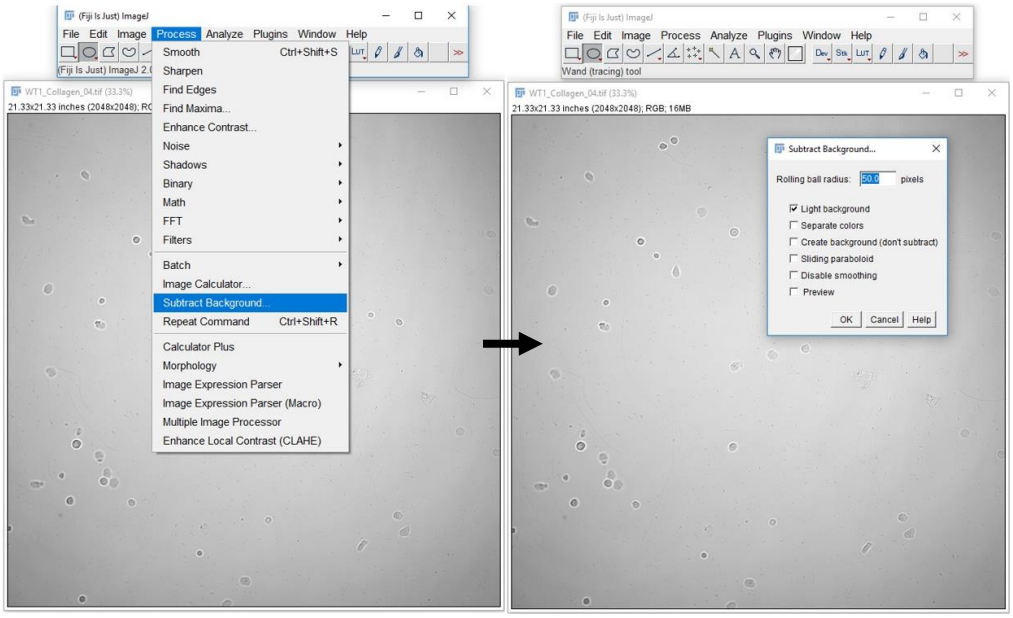

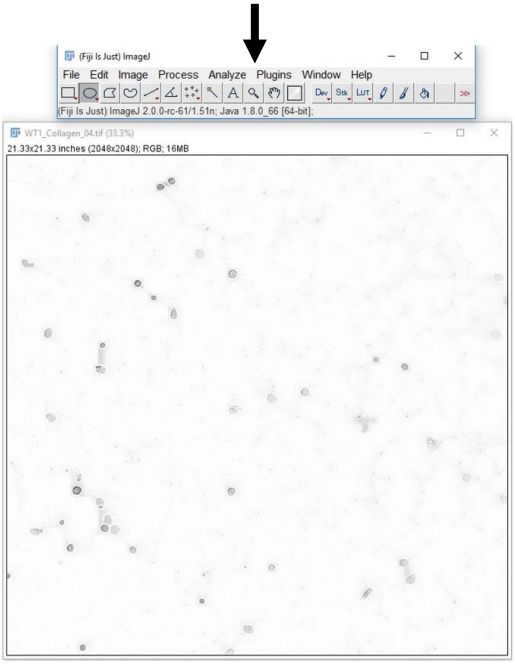

2) Image was converted to 8 bit and the threshold was set using Ostu model.

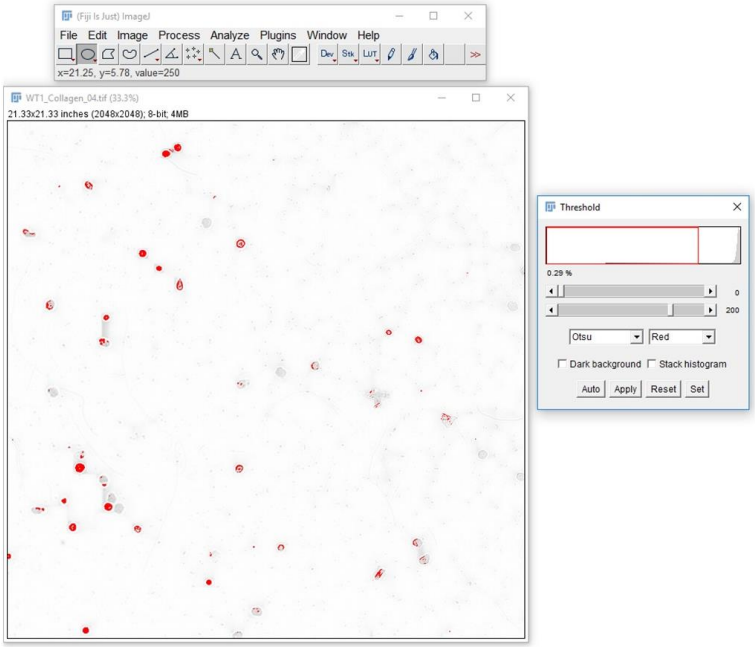

3) Cells were counted using “Analyze particles” mode in “Analyze” menu. The minimal size was estimated according to the previous section and set at 100 square pixels.

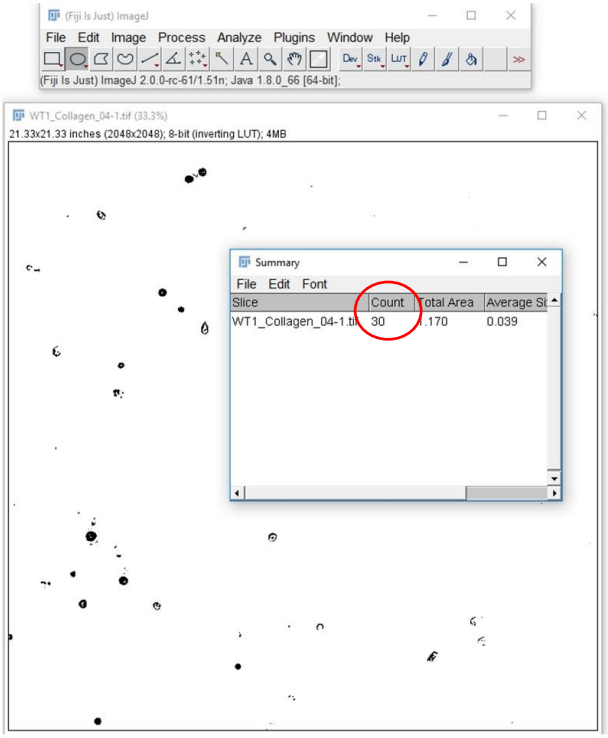

4) Percentage of migrated cells was calculated using the formula;

Percent neutrophil migration = [N1/(N1+N2)] x 100

Where N1 = numbers of migrated cells,

N2 = numbers of remaining cells in loaded chamber

2.8 Haematological analysis

Whole blood was collected from the inferior vena cava using ethylenediaminetetraacetic acid (EDTA)-filled syringe. Blood counts were analysed on an ABX Pentra 60 (Horbia Ltd, UK).

2.9 Untargeted metabolomics analysis

2.9.1 Bone marrow-derived macrophage culture

Hind legs of adult WT and *Pdpn*$^{fl/fl}$*Vav1-cre* mice were cut after cervical dislocation. Then, femur and tibia were taken. To collect progenitor cells, bone marrow cavity was inserted with 25 gauge needle and gently flushed with collection medium (DMEM+10% FBS+1% penicillin/streptomycin/L-glutamine) under the control of 10 ml syringe. Cell suspension was centrifuged at 400 g for 8 minutes at room temperature. After discarding the supernatant, cell pellet was re-suspended in collection medium and filtered through cell strainer. Total cells were counted by haemocytometer and adjusted to 2 x 10^6 cells/ml in macrophage complete medium (DMEM + 20% (v/v) L-929 conditioned medium, which contains M-CSF). Then, cell concentration was diluted to 2 x 10^7 cells/10 ml of macrophage complete medium and transferred to a sterile plastic non-coated 10 cm Petri dish to seed cells in 37 ºC, 5% CO_2 incubator (day 1). At day 4, another 5 ml of macrophage complete medium was added into each Petri dish. At day 7, the culture medium was discarded and replaced by 10 ml of fresh macrophage complete medium (Lee and Hu, 2013).

2.9.2 LPS stimulation

At day 8, macrophages were counted and 3 x 10^5 cells were seeded into 6-well plate. WT macrophages were incubated in three conditions, including no treatment, LPS (1 µg/ml), and LPS plus rCLEC-2-Fc (20 µg/ml) for 24 hours in 37 ºC, 5% CO_2 incubator. *Pdpn*$^{fl/fl}$*Vav1-cre* macrophages were divided into no treatment and LPS-treated groups, respectively.

The rCLEC-2-Fc was kindly provided by Ying Di in Watson laboratory. In brief, this recombinant protein was produced using the following method. The extracellular domain region of mouse CLEC2 was cloned into pFusion-Rabbit FC expression vector (In ViVogen). The construct was used with polyethylenimine to transiently transfect into human embryonic kidney (HEK) 293T cells. The stable clones were selected with Zocin and high expression of mouse rCLEC-2-Fc clone was screened from the cell culture supernatant. Then the recombinant protein was produced from the selected positive stable clone. The cell culture supernatant was collected, filtered by 0.22 μm filter, went through and purified by Protein G column, and therefore eluted by 0.1M pH3 glycine with immediately neutralised by 1M Tris pH 8 buffer. The elutes were pooled and dialysed against PBS. The obtained recombinant protein was characterised by SDS-PAGE and Western blot. The biological activity was verified by specific binding to mouse podoplanin on LPS-stimulated Raw cells via flow cytometry.

2.9.3 Metabolite extraction for metabolomics analysis

After LPS challenge, macrophage extraction was performed as previously described (Fei et al., 2016). In brief, all cells were washed once with ice cold PBS followed by adding 500 μl of cold extraction mixture containing methanol/ethanol/water (2:2:1 v/v) and cells were detached from 6-well plate using a cell lifter. Then, cell suspension was collected into 1.5 ml tube containing two ball bearings (2-mm diameter) (LabTIE B.V., the Netherlands) and vigorously vortexed for 2 minutes, followed by centrifugation at 9500 g for 3 minutes at 4 ºC without bearings. The supernatant was collected. The pellet was re-extracted as above with minimal volume (50 μl) of cold extraction mixture. Cell extract was dried and re-solubilised according to the previous protocol (Fei et al., 2016).

2.9.4 Ultra High Performance Liquid Chromatography-Mass Spectrometry

In collaboration with the Phenome Centre at the University of Birmingham, untargeted metabolomics analysis was performed. In brief, the polar metabolites was examined using the hydrophilic interaction liquid chromatography (HILIC)/mass spectrometry (MS) method (Fei et al., 2016), which run on a Dionex UltiMate 3000 Rapid Separation LC system (Thermo Fisher Scientific, USA) coupled with a heated electrospray Q Exactive Focus mass spectrometer (Thermo Fisher Scientific, USA). The LC-MS spectra were processed, including the conversion to mass spectrometer output file format (mzML) using the open access ProteoWizard software (Kessner et al., 2008) and deconvolution using XCMS software (Smith et al., 2006). The putative metabolites were identified/annotated by matching the mass-to-charge (m/z) and the retention time, which was performed by applying the PUTMEDID-LCMS workflow operating in the Taverna workflow environment (Dunn et al., 2013, Brown et al., 2011, Sumner et al., 2007). The peak area of individual metabolite was used as arbitrary unit of expression. The metabolite of interest from each sample was presented as fold change relative to the mean value in unchallenged WT (Di Guida et al., 2016).

2.10 Statistical analysis

All data are presented as mean ± standard error of mean (SEM). Kinetics of wound closure was compared by two-way ANOVA with Bonferroni's multiple comparison test. Mean differences in other parameters were analysed by either Student's t-test (two-group comparison) or one-way ANOVA with Bonferroni post-hoc test (more than two groups) using GraphPad Prism software. $p<0.05$ was considered as statistically significant.

Chapter 3 Skin Wound Healing in Mice: the Role of Platelet (hemi)ITAM Receptors

3.1 Introduction

Wound healing is a complex mechanism, which involves various cellular and molecular interplays with platelets playing a key role at different stages of the healing process. The role of platelets in wound repair is not limited to the formation of an aggregate to stop bleeding during tissue injury. Several lines of evidence have shown that platelets release growth factors and cytokines, which potentially promote tissue repair in multiple ways (Etulain, 2018, Scully et al., 2018). For example, platelet-rich plasma containing VEGF, PDGF, and fibroblast growth factor 2, facilitates wound closure by enhancing re-epithelialisation, demal regeneration, and angiogenesis in a murine model of full thickness skin wound (Yang et al., 2011). In addition, meta-analysis of animal experiments, including eight rodent and ten non-rodent studies, indicates that platelet-rich plasma provides positive outcomes in the healing of full thickness skin wound, suggesting its use as an adjucntive treatment in veterinary wound care (Tambella et al., 2018). Moreover, platelet-rich fibrin enhances angiogenesis and promotes wound healing in diabetic mice (Ding et al., 2017).

Although the potential advantages of platelets in wound healing have been described, somewhat surprisingly, the results of one study argue against the contribution of platelets in wound healing, including the primary role in haemostasis, by demonstrating that skin wound healing is not impaired in thrombocytopenic mice (Szpaderska et al., 2003). In

this model, rabbit anti-mouse platelet serum was used to deplete platelets. There is no report of uncontrolled bleeding in these thrombocytopenic mice after a full thickness skin biopsy, except the evidence of increased haemorrhage within the wound bed. The number of inflammatory cells, especially macrophages is increased, which is proposed to clear the extravascular red blood cells in thrombocytopenic mice. However, the rate of macroscopic wound closure, re-epithelialisation, angiogenesis, and collagen deposition are normal in these platelet-depleted mice (Szpaderska et al., 2003).

Murine platelets express two (hemi)ITAM receptors, including GPVI and CLEC-2, which signal through a similar Src/Syk-dependent pathway for platelet activation (Watson et al., 2010, Suzuki-Inoue et al., 2011). During dermatitis, GPVI null mice demonstrate vascular leakage following neutrophil diapedesis in the inflamed skin (Gros et al., 2015) whereas the bleeding is not observed in platelet-specific CLEC-2 knockout mice (Rayes et al., 2018). However, lack of both platelet GPVI and CLEC-2 increases intra-skin bleeding in this model (Rayes et al., 2018). In a similar fashion, GPVI-deficient mice treated with antibody against podoplanin, the endogenous ligand for CLEC-2, enhances inflammatory bleeding phenotype (Rayes et al., 2018), suggesting a role for the CLEC-2-podoplanin axis in inflammatory haemostasis in the absence of GPVI. These observations support the primary role of GPVI in inflammatory haemostasis whereas CLEC-2-podoplanin interaction partially compensates this function in the absence of GPVI. This mechanism is independent of classical αIIbβ3-mediated haemostasis (Ho-Tin-Noe et al., 2018).

GPVI has also been reported to mediate pro-inflammatory activity in several disease models, including in skin inflammation. For example, GPVI contributes to neutrophil-mediated tissue damage in cutaneous rpA, an immune complexes-induced inflammation

(Gros et al., 2015). In addition, GPVI knockout mice show an increase in M2 anti-inflammatory macrophages, which contributes to a reduction in pain during paw skin inflammation (Pierre et al., 2017). In contrast, CLEC-2-podoplanin axis demonstrates anti-inflammatory activity, which protects from organ damage and attenuates inflammation during acute lung injury (Lax et al., 2017b) and sepsis (Rayes et al., 2017). In skin wound healing, it is speculated that platelet CLEC-2 also binds podoplanin on keratinocytes, which inhibits keratinocyte migration while the wound bed is being prepared at the initial phase (Asai et al., 2016). Moreover, intradermal injection of human podoplanin-positive monocytes in combination with platelets allows interaction of CLEC-2 to podoplanin, which accelerates skin wound healing by promoting lymphangiogenesis (Hur et al., 2014).

Previous evidences have shown that the leakage of blood vessels may produce potential benefits in wound healing. At the initial phase of skin wound healing, the increase in vascular permeability is generally observed. This extensive vascular leakage allows extravasation of repair-associated plasma components, including fibrinogen and growth factors, into the wound to facilitate healing process (Shaterian et al., 2009, Mendonca et al., 2010). Mast cell-derived histamine, which increases vascular permeability, has also shown to promote skin wound healing in mice (Numata et al., 2006, Weller et al., 2006) whereas anti-histamine attenuates this effect (Weller et al., 2006).

According to their effects in the maintenance of vascular integrity and inflammatory responses during skin inflammation, it is possible that GPVI and CLEC-2 may also influence the wound healing process. The aim of this chapter is to investigate the role of CLEC-2 and GPVI in a mouse model of skin wound injury. A single full-thickness

excisional skin wound (4 mm-diameter) was generated in male and female WT, *Clec1b*$^{fl/fl}$*Pf4-Cre, Gp6*$^{-/-}$, as well as DKO mice. Wound size was monitored on a daily basis for up to 9 days post-injury. Wound tissue was collected at day 1, 3, and 9 post-injury for histological and immunohistochemistry/immunofluorescence analyses. *Clec1b*$^{fl/fl}$*Pf4-cre* and DKO mice display blood/lymphatic mixing and moderate thrombocytopenia (Bender et al., 2013, Rayes et al., 2018). Therefore, wound healing was monitored for 3 days post-injury (the major changes are seen by this time) in *Gp6*$^{-/-}$ mice injected with podoplanin-blocking antibody to recapitulate the DKO setting in the absence of these defects. Moreover, to clarify the haemostatic function of platelets in wound repair, a pilot experiment of skin wound in thrombocytopenic mice was performed.

3.2 Results

3.2.1 The ligands for GPVI and CLEC-2 are present at perivascular area during skin wounding

CLEC-2 and GPVI play a key role in inflammatory haemostasis in the inflamed skin (Rayes et al., 2018), thereby, the presence of GPVI and CLEC-2 ligands in the skin before and after wounding was assessed. In unchallenged WT murine skin, collagen, a GPVI ligand, was highly distributed throughout skin dermis and hypodermis, including the area underneath blood vessels (Figure 3.1 A). Podoplanin was mainly detected on lymphatic endothelial cells and cells around the blood vessels (Figure 3.1 B). At day 3 post-injury, podoplanin was upregulated on migrating keratinocytes, and on stromal and infiltrating cells within the granulation tissue in all mouse strains (Figure 3.1 C). Podoplanin expression was also observed surrounding blood vessels ($NG2^+$) (Figure 3.2 A). Further characterisation of podoplanin-expressing cells at perivascular area in all groups revealed the upregulation of podoplanin on many cell types around the blood vessels, including pericytes ($NG2^+$) (Figure 3.2 A), fibroblasts ($vimentin^+$), infiltrating monocytes ($Ly6C^+$), and macrophages ($F4/80^+$) (Figure 3.2 B). The level of perivascular podoplanin was increased in *Clec1b*$^{fl/fl}$*Pf4-cre* mice compared to WT mice (Figure 3.2 A, B). In DKO mice, podoplanin expression was similar to that observed in WT and *Gp6*$^{-/-}$ mice (Figure 3.2 A, B).

Platelets ($CD41^+$) were observed in proximity to the vessel wall (surrounded by $NG2^+$ pericytes) in WT, *Clec1b*$^{fl/fl}$*Pf4-cre*, and *Gp6*$^{-/-}$ mice (Figure 3.2 A, arrow). There was no notable evidence of extravascular localisation of platelets in these mouse strains. In DKO

mice, platelets were more widely distributed, including at the vessel wall and in the tissue close to blood vessel (Figure 3.2 A, star), supporting the vascular leakage observed in these mice. In WT and *Gp6*$^{-/-}$ mice, the mean platelet count at baseline was 700-800 x 10^3 cell/mm^3 (Figure 3.2 C). The platelet counts prior to injury in *Clec1b*$^{fl/fl}$*Pf4-cre* and DKO mice were 600 and 500 x 10^3 cell/mm^3, which is 25% and 40% lower than in WT, respectively (Figure 3.2 C). However, platelet counts (Figure 3.2 C) and blood haemoglobin (Figure 3.2 D) were not significantly altered during wound healing in all groups.

Overall, these results demonstrate that in mouse skin, platelets are observed in proximity to the vessel wall during the initial wound healing process where the ligands for GPVI and CLEC-2 are also present. Lack of GPVI and CLEC-2 leads to leakage of platelets into perivascular tissue. Deletion of platelet CLEC-2 is associated with the increased infiltration of podoplanin-expressing cells at the perivascular space during inflammatory phase of wound healing while combined deletion with GPVI compromises this phenotype.

3.2.2 Skin wound healing is accelerated in GPVI and CLEC-2 double-deficient mice

The pilot experiment of skin wound generated using 4-mm diameter punch biopsy in WT mice shows that the wound was completely closed by nine days post-injury. Therefore, wound healing between tested mouse strains was compared during this timeframe. Bleeding was mild (not severe) in WT and all transgenic mice after the initial injury (Figure 3.3 A). A wound scab was clearly observed at day 1 post-injury. In addition, oedema occurred during day 1-4 post-injury in all groups (Figure 3.3 A). The skin wound

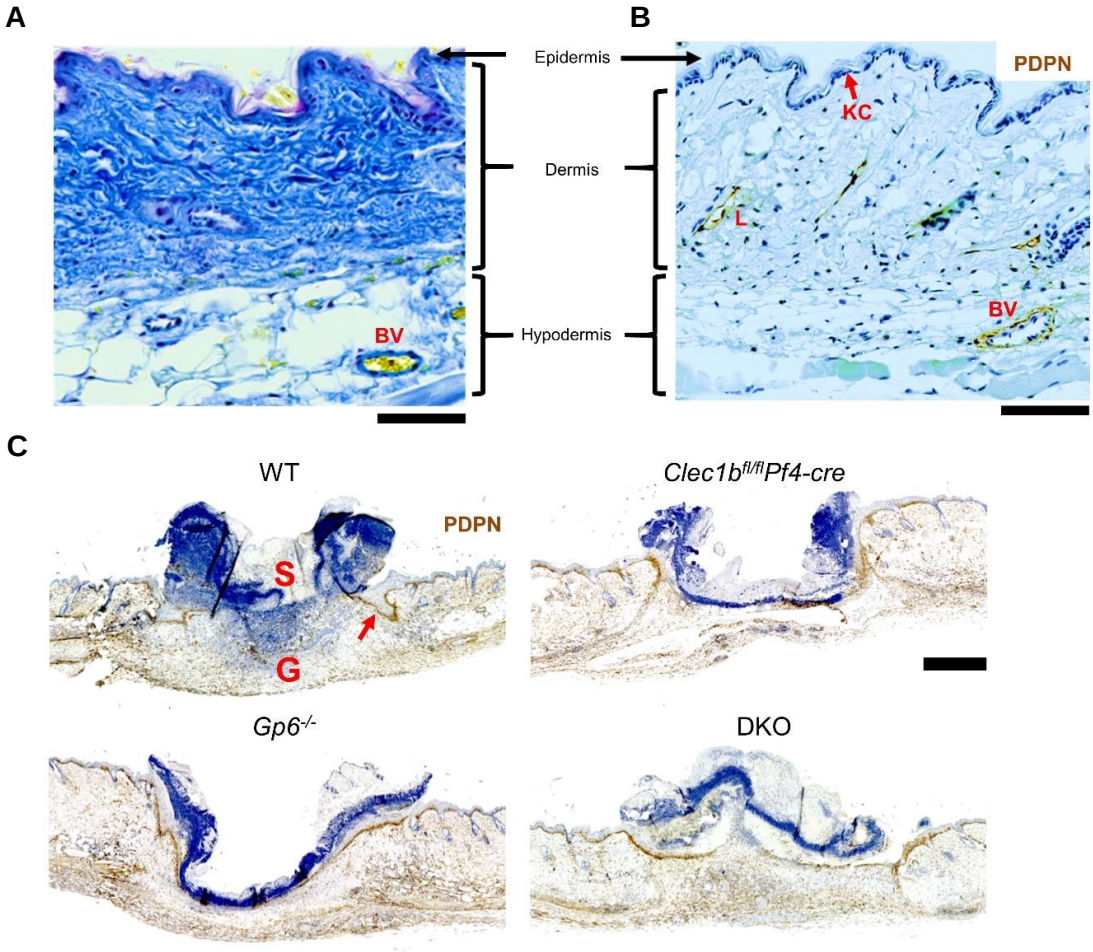

Figure 3. 1. Collagen and podoplanin are present around blood vessels of murine skin. (A) Martius scarlet blue staining shows collagen (blue) in dermis and hypodermis of unchallenged WT mouse skin (n=5). Red = old fibrin, blue = collagen, yellow = red blood cells/fresh fibrin. Scale bar = 100 µm. (B) Immunohistochemistry of podoplanin (brown) in unchallenged WT mouse skin (n=5). L = lymphatic vessel, KC = keratinocyte. PDPN = podoplanin. BV = blood vessel. Scale bar = 100 µm. (C) Representative image of podoplanin immunohistochemistry staining (brown) in all mouse strains at day 3 post-injury (n=6). S = scab, G = granulation tissue. Arrow points to podoplanin on migrating keratinocytes. Scale bar = 500 µm.

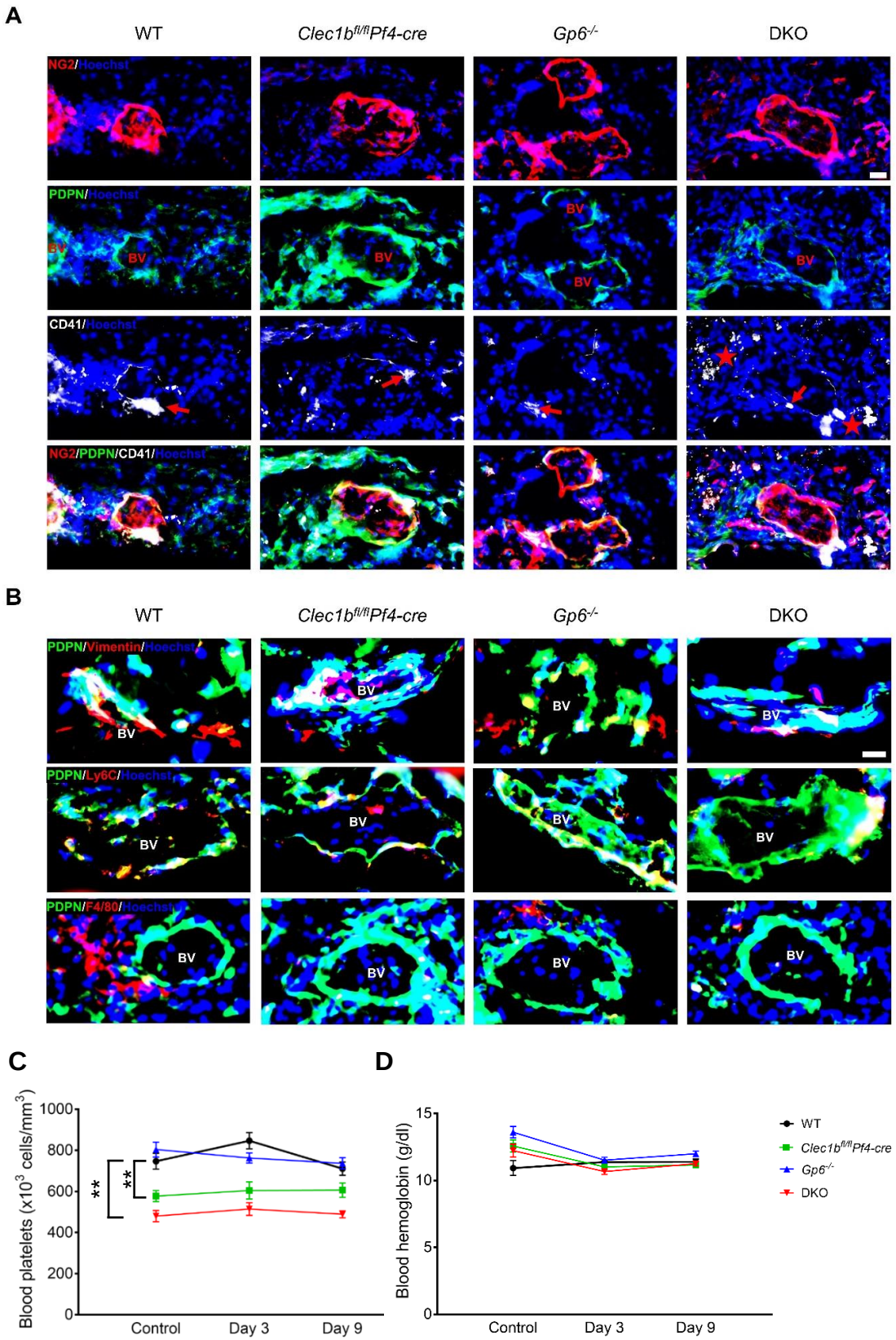
A
WT
Clec1b fl/fl Pf4-cre
Gp6 -/-
DKO
NG2/Hoechst
PDPN/Hoechst
BV
CD41/Hoechst
NG2/PDPN/CD41/Hoechst
B
PDPN/Vimentin/Hoechst
PDPN/Ly6C/Hoechst
PDPN/F4/80/Hoechst
C
Blood platelets (x10^3 cells/mm^3)
1000
800
600
400
200
0
**
**
Control
Day 3
Day 9
D
Blood hemoglobin (g/dl)
15
10
5
0
Control
Day 3
Day 9
WT
Clec1b fl/fl Pf4-cre
Gp6 -/-
DKO

Figure 3.2.

Figure 3. 2. Podoplanin-expressing cells are present at perivascular area in contact with platelets during skin wound repair. (A) Immunofluorescence staining of NG2 (red), podoplanin (green) and CD41 (white) illustrates platelets and podoplanin-expressing pericytes ($NG2^+$) around blood vessel at day 3 after injury (n=5-7). Hoechst counterstains nuclei (blue). BV = blood vessel. Arrow points to platelets at perivascular site. Star indicates extravascular localisation of platelets. Scale bar = 20 µm. (B) Podoplanin (green) was double-stained with either vimentin (white; *top panel*) or Ly6C (white; *middle panel*) or F4/80 (white; *bottom panel*), which are located around blood vessel at day 3 after injury (n=4-5). Scale bar = 20 µm. (C) Platelet counts at baseline (n=10), day 3 post-injury (n=6-9), and day 9 post-injury (n=10-13). (D) Blood haemoglobin at baseline (n=10), day 3 post-injury (n=6-9), and day 9 post-injury (n=10-13). Data are presented as mean ± SEM and analysed by one-way ANOVA with Bonferroni's multiple comparison test. ***p<0.01*.

of DKO mice showed a dark red-to-black colour on scab and increased redness around the wound edge at day 1-3 post-injury compared to other mouse strains (Figure 3.3 A). *Gp6*$^{-/-}$ mice also had a more moderate redness surrounding the wound during this period compared to WT mice. However, the macroscopic wound appearance was identical in all groups at day 4 post-injury and was sustained to the end of experiment (Figure 3.3 A). Although all mouse strains demonstrated full wound closure within nine days post-injury, there was an accelerated rate of healing in DKO mice, represented by a significantly smaller wound size than in WT controls at day 1-5 post-injury, and then single knockout mice at day 2-3 post-injury, respectively (Figure 3.3 B).

Macroscopic measurement using callipers did not differentiate wound size between WT and DKO mice in later phases (day 6-9 post-injury) (Figure 3.3 B). However, histological analysis of wound scar at day 9 post-injury illustrated that these ITAM-receptors double-deficient mice had a faster rate of both epidermal and dermal regeneration than in WT mice (Figure 3.3 C). This was indicated by a shorter length of hyperplastic epidermis in DKO compared to WT and *Clec1b*$^{fl/fl}$*Pf4-cre* mice (Figure 3.3 C, D) and a narrower distance between subcutaneous edges in the deeper dermis layer of DKO skin compared to WT controls (Figure 3.3 C, E). *Gp6*$^{-/-}$ mice did not exhibit significant differences in wound scar at day 9 post-injury compared to DKO mice (Figure 3.3 D, E).

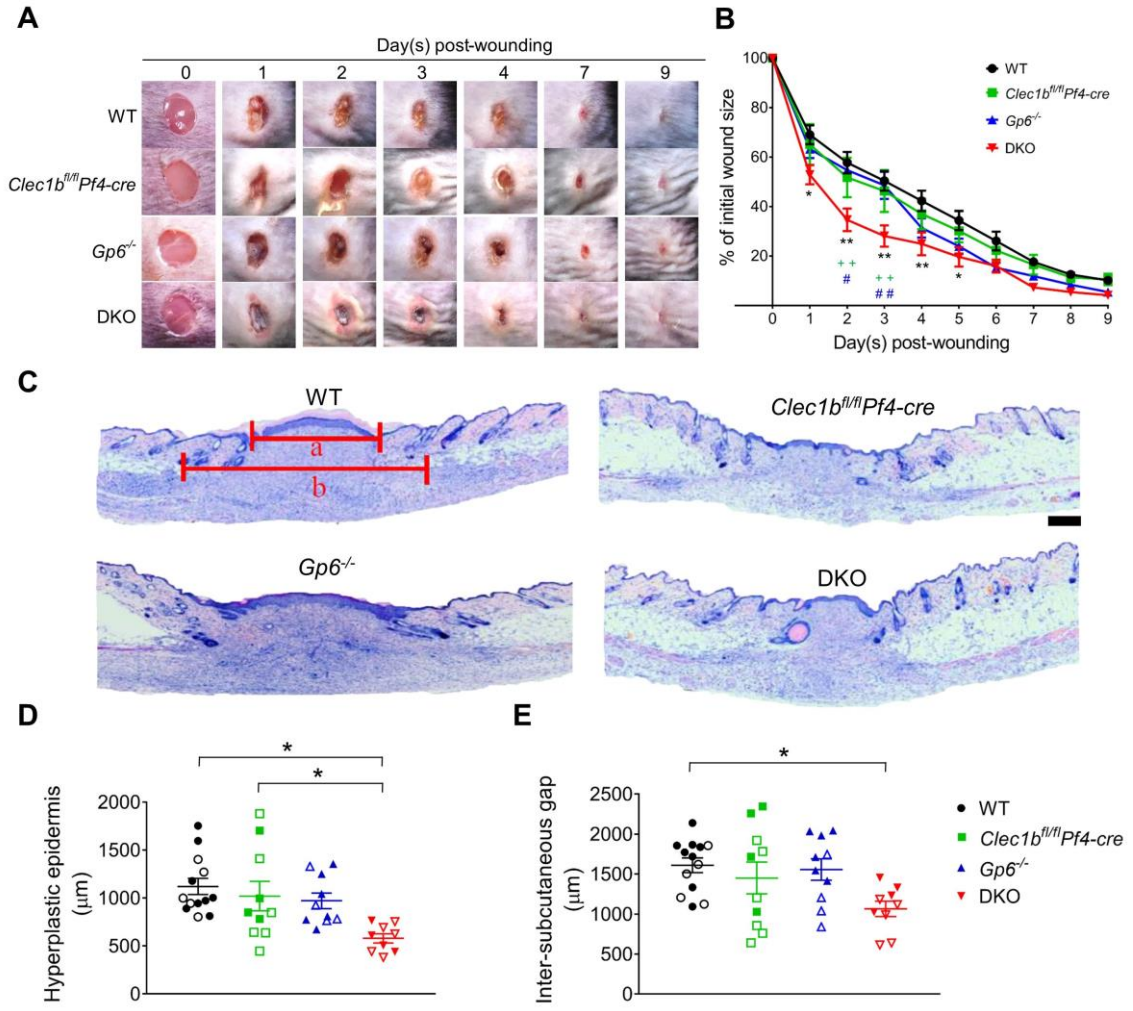

Figure 3. 3. Platelet ITAM-receptors deficiency accelerates skin wound healing. (A) Macroscopic appearance of the wound at indicated time points is shown. (B) Percentage changes in wound size over nine days post-injury (n=10-13). Graphs are presented as mean ± SEM. Kinetics of wound closure are analysed by two-way ANOVA with Bonferroni's multiple comparison test. *$p<0.05$, **$p<0.01$. *WT vs. DKO, $^{+}$*Clec1b$^{fl/fl}$Pf4-cre* vs DKO, $^{\#}$*Gp6$^{-/-}$* vs. DKO. (C) H&E staining of the skin wound tissue at day 9 post-injury (n=9-13). Scale bar = 200 µm. a = length of hyperplastic epidermis, b = inter-subcutaneous distance. (D) Assessment of the length of hyperplastic epidermis. (E) Measurement of inter-subcutaneous distance. Data from females (open symbols) and males (closed symbols) are shown in (E) and (D). Data are presented as mean ± SEM and analysed by one-way ANOVA with Bonferroni's multiple comparison test. *$p<0.05$.

3.2.3 Re-epithelialisation and angiogenesis are enhanced at the early phase of wound healing in DKO mice

In order to investigate the mechanisms involved in the accelerated wound healing in DKO mice, a three-day wound experiment was performed. When wound closure was monitored, there was again a significant reduction in wound size of DKO mice at day 1-3 post-injury, compared to WT mice (Figure 3.4 A), indicating the reproducibility of this model. Histological analysis of skin at day 3 post-injury revealed that re-epithelialisation, a process of epidermal regeneration from the wound edge toward the center of the wound, was observed in all tested groups (Figure 3.4 B). However, DKO mice exhibited a significantly accelerated rate of re-epithelialisation relative to WT and *Clec1b*$^{fl/fl}$*Pf4-cre* mice but not *Gp6*$^{-/-}$ mice (Figure 3.4 B, C) with no differences in wound contraction between all groups (Figure 3.4 B, D). In addition, a greater extent of granulation tissue was observed in DKO mice than WT controls (Figure 3.4 E).

The density of blood vessels (CD31^{+}) (Figure 3.5 A) and lymphatic vessels (podoplanin^{+}) (Figure 3.5 B) in unchallenged skin was similar among all groups. During wound healing, DKO mice had a wide distribution of CD31^{+} cells within the wound at day 3 post-injury (Figure 3.5 C), which was supported by a significant increase in the CD31-labelled area (Figure 3.5 D), compared to all other groups.

Together, these data suggest that DKO mice have an enhanced rate of wound repair, including re-epithelialisation, granulation tissue formation, and angiogenesis, all of which begin at the early stage.

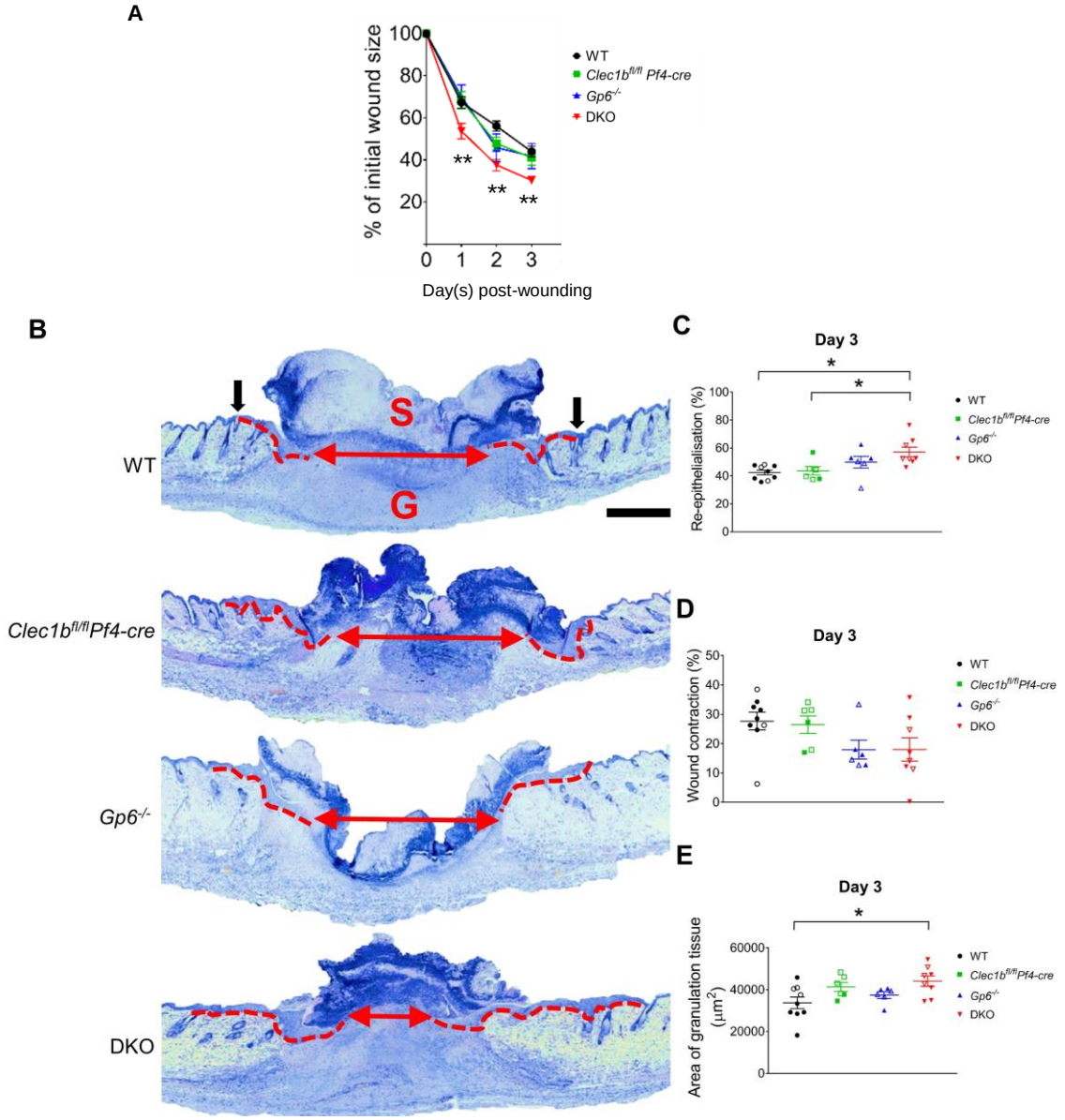
A
% of initial wound size
Day(s) post-wounding
WT
Clec1b fl/fl Pf4-cre
Gp6-/-
DKO
B
WT
Clec1bfl/flPf4-cre
Gp6-/-
DKO
S
G
C
Day 3
Re-epithelialisation (%)
D
Day 3
Wound contraction (%)
E
Day 3
Area of granulation tissue (μm2)

Figure 3.4.

Figure 3. 4. DKO mice demonstrate a faster rate of wound closure, re-epithelialisation, and granulation tissue formation. (A) Kinetics of wound closure over three days post-injury (n=6-9). (B) H&E staining at day 3 post-injury (n=6-9). Dotted red line indicates hyperplastic coverages. Red arrow indicates gap between epithelial tongues. Black arrow points to wound edge. S = scab, G = granulation tissue. Scale bar = 500 µm. (C) Measurement of re-epithelialisation. (D) Assessment of wound contraction. (E) Quantification of granulation tissue area. Data from females (open symbols) and males (closed symbols) are shown in (C-E). All graphs are presented as mean ± SEM. Kinetics of wound closure (A) are analysed by two-way ANOVA with Bonferroni's multiple comparison test. $**p<0.01$ in WT vs. DKO. Other parameters (C-E) are analysed by one-way ANOVA with Bonferroni's multiple comparison test. $*p<0.05$.

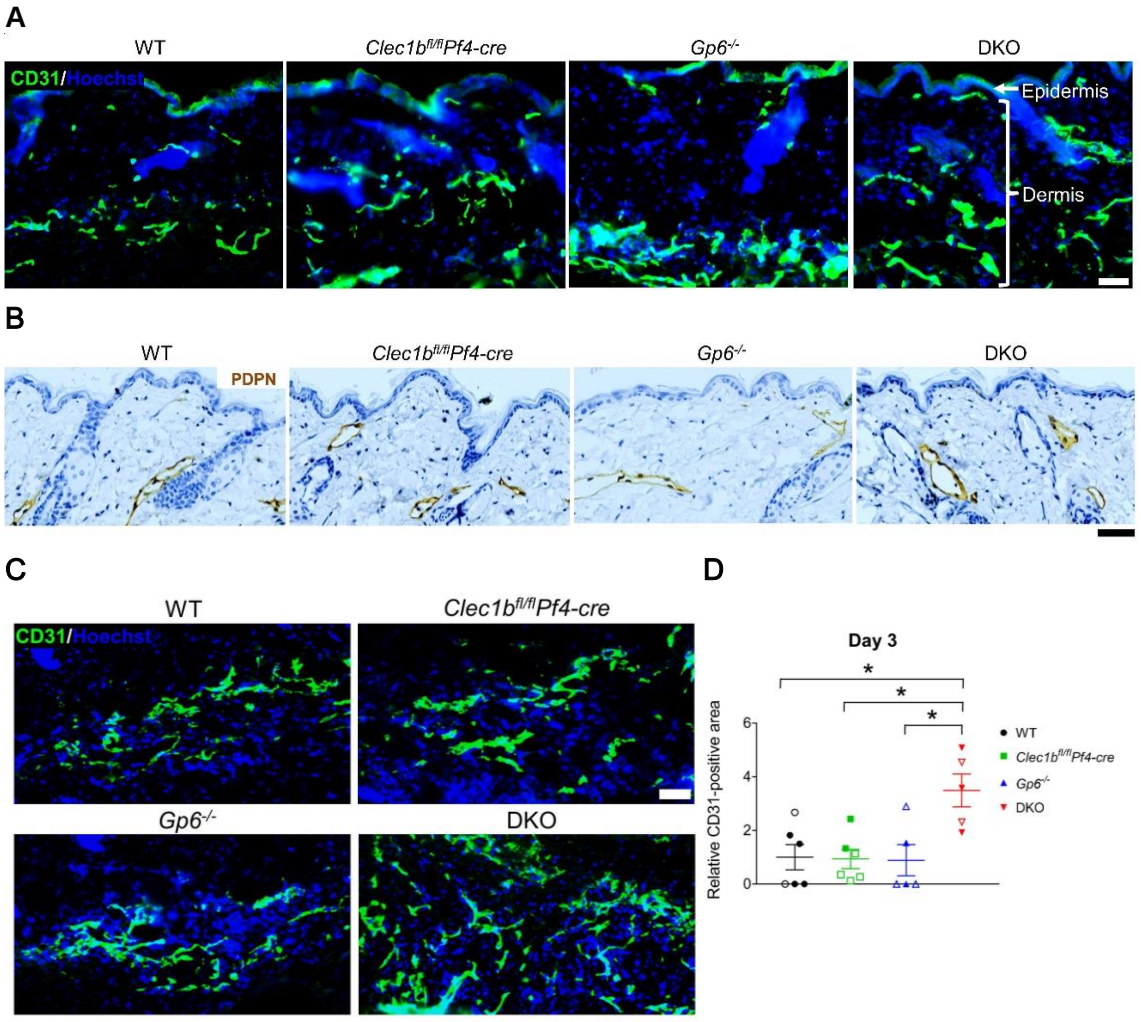

Figure 3. 5. Combined GPVI and CLEC-2 deletion enhances angiogenesis at early phase of wound repair. (A) Immunofluorescence staining of CD31 (green), a marker of endothelial cells, in unchallenged skin of WT and genetically modified mice (n=5). Hoechst counterstains nuclei (blue). (B) Podoplanin staining (brown) on lymphatic vessels in unchallenged skin of WT and genetically modified mice (n=5). PDPN = podoplanin. (C) Detection of endothelial cells ($CD31^+$; green) in wound area at day 3 post-injury. (D) Quantification of $CD31^+$ area within the wound at day 3 post-injury (n=5-6). Data from females (open symbols) and males (closed symbols) are shown in (D). Graphs are presented as mean ± SEM and analysed by one-way ANOVA with Bonferroni's multiple comparison test. *$p<0.05$. Scale bar = 50 µm.

3.2.4 DKO mice demonstrate vascular leakage during the inflammatory phase of repair process

Having observed the redness surrounding the wound in DKO mice, which was pronounced at day 3 post-injury, the inner side of the wound was examined. In the DKO mice, skin wound showed vasodilation and intra-tissue bleeding around the wound area at day 3 post-injury compared to other groups (Figure 3.6 A), indicating a loss of vascular integrity during this time. Vascular leakage was also observed in *Gp6*$^{-/-}$ mice but was less marked (Figure 3.6 A). H&E staining of wound tissue at day 3 post-injury revealed extravasation of Rbcs in skin dermis around the wound edge in DKO mice and to a lesser extent in *Gp6*$^{-/-}$ mice (Figure 3.6 B). This phenotype was not observed in WT and *Clec1b*$^{fl/fl}$*Pf4-cre* mice where Rbcs remained in the skin vasculature (Figure 3.6 B). However, the intra-skin bleeding in DKO and *Gp6*$^{-/-}$ mice did not last throughout the course of healing, especially when the inflammation had ceased. Histological analysis showed no persistent bleeding or haematoma formation within the wound scar at day 9 post-injury in DKO and *Gp6*$^{-/-}$ mice compared to WT and *Clec1b*$^{fl/fl}$*Pf4-cre* mice (Figure 3.6 C), suggesting the complete clearance of extravascular Rbcs from the healing wound in all groups. Due to blood/lymphatic misconnection in DKO mice, with a lesser extent in *Clec1b*$^{fl/fl}$*Pf4-cre* mice, Rbcs were present in both blood and lymphatic vessels (podoplanin^{+}) during this time (Figure 3.6 D).

These data indicate a loss in the maintenance of vascular integrity during the inflammatory phase of wound repair in DKO mice, and a less severe form in *Gp6*$^{-/-}$ mice, which subsequently subsides in later phase.

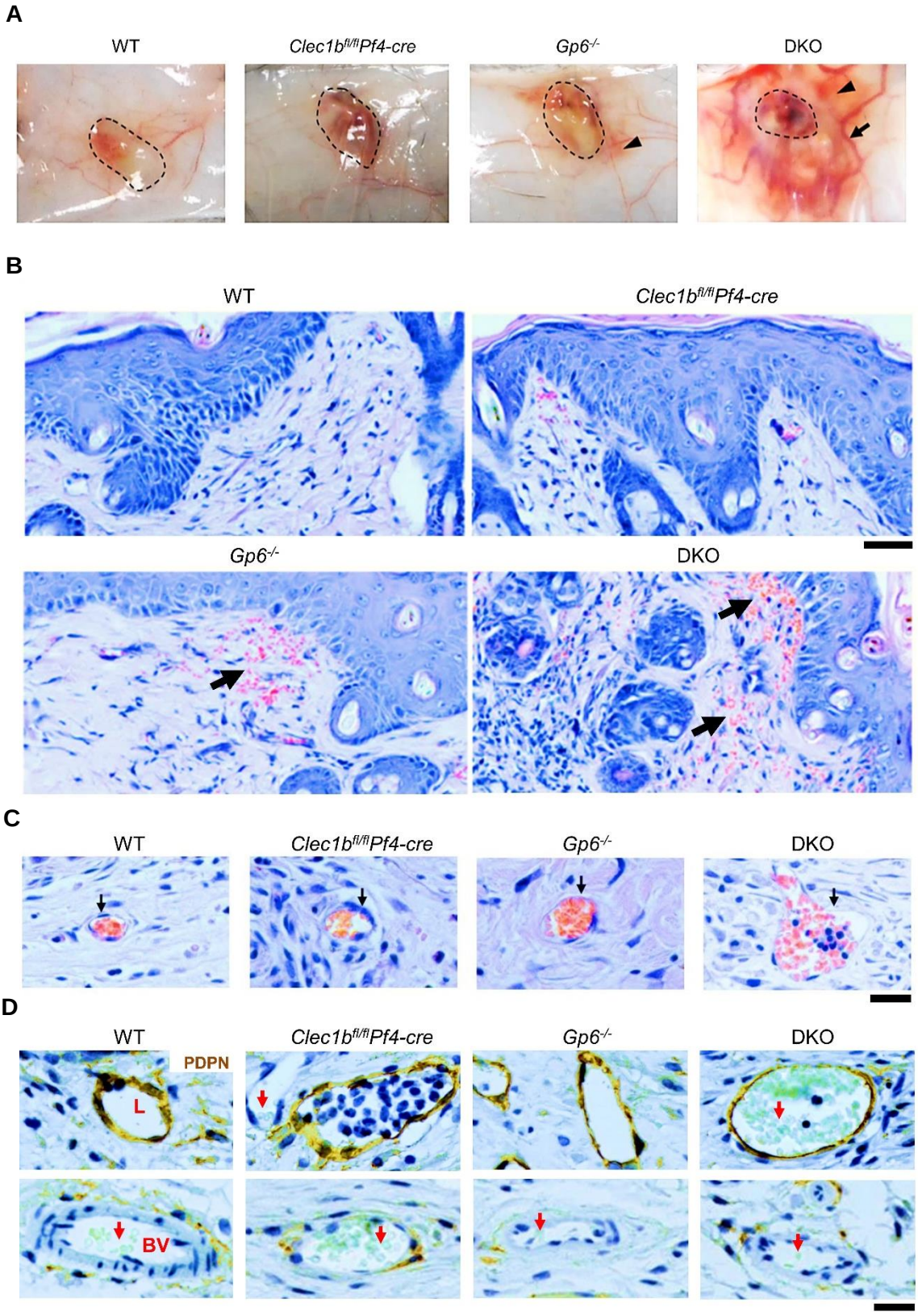
A
WT
Clec1b^fl/fl Pf4-cre
Gp6^-/-
DKO
B
WT
Clec1b^fl/fl Pf4-cre
Gp6^-/-
DKO
C
WT
Clec1b^fl/fl Pf4-cre
Gp6^-/-
DKO
D
WT
Clec1b^fl/fl Pf4-cre
Gp6^-/-
DKO
PDPN
L
BV

Figure 3.6.

Figure 3. 6. Lack of platelet GPVI and CLEC-2 leads to vascular leakage during inflammatory phase of wound repair. (A) Macroscopic images of inner side of skin wound at day 3 post-injury (n=4-6). Dotted circle indicates wound area. Arrow points to dilated vessel. Arrowhead shows bleeding into surrounding skin. (B) H&E staining of the wound at day 3 post-injury (n=6-9). Arrow points to intra-skin bleeding. Scale bar = 50 µm. (C) H&E staining of wound scar at day 9 post-injury (n=10-13). Arrow indicates red blood cells (Rbcs) within the vessel. Scale bar = 20 µm. (D) Immunohistochemistry shows podoplanin on lymphatic endothelium (upper panel) and cells around blood vessel (lower panel). Cells (dark blue nuclei) presented within lymphatic vessel of *Clec1b*$^{fl/fl}$ *Pf4-cre* are leucocytes. L = lymphatic vessel. BV = blood vessel. Arrow points to Rbcs (pale yellow/brown) in both types of vasculature. Scale bar = 20 µm.

3.2.5 The vascular leakage results in fibrinogen deposition and fibrin generation during the inflammatory phase of wound healing in DKO mice

It has been previously demonstrated that the increase in vascular permeability allows entry of blood composition, including fibrinogen, into the wound (Shaterian et al., 2009, Mendonca et al., 2010). Extravascular fibrinogen is subsequently converted to fibrin by tissue factor-mediated pathway within the wound (Hoffman et al., 2006), both of which promote wound healing (Drew et al., 2001). During wound healing in DKO mice, the results of immunohistochemistry showed that wound fibrinogen was identical to that of WT at day 1 post-injury (Figure 3.7 A, B). However, fibrinogen deposition was significantly increased in the granulation tissue area of DKO mice at day 3 post-injury compared to WT (Figure 3.7 C, D). Tissue factor was highly expressed on proliferating/migrating keratinocytes (Figure 3.7 E), with a lower level of expression in the granulation tissue at this time. There was no significant differences in tissue factor level among all strains tested (Figure 3.7 F).

The fibrin content was measured by Martius scarlet blue staining. At day 1 post-injury, fibrin was primarily detected at the wound scab (Figure 3.8 A) and it was similar between WT and DKO mice (Figure 3.8 B). Fibrin content was increased in wound scab of DKO mice at day 3 post-injury (Figure 3.8 C), which was significantly higher than WT and *Clec1b*$^{fl/fl}$*Pf4-cre* mice (Figure 3.8 D) but not *Gp6*$^{-/-}$ mice that presented a certain degree of vascular leakage. At day 9 post-injury, fibrin was mainly observed on the uppermost area of scar in all groups (Figure 3.8 E). The DKO mice had a notably lower level of fibrin than WT and *Gp6*$^{-/-}$ mice (Figure 3.8 F). In addition, *Clec1b*$^{fl/fl}$*Pf4-cre* mice also showed lower levels of fibrin than *Gp6*$^{-/-}$ mice at this time (Figure 3.8 F). During the

course of skin wound healing, DKO mice did not demonstrate significant differences in (myo)fibroblasts (Figure 9 A-C) and collagen content (Figure 9 D, E) compared to WT.

Overall, the loss of vascular integrity may enhance the extravasation of fibrinogen into the wound of DKO mice, leading to increased fibrinogen and fibrin deposition to promote wound healing. This provisional matrix is then removed from the healing wound.

3.2.6 Mice deficient in GPVI and CLEC-2 demonstrate a reduction in wound neutrophils and M1 macrophages during inflammatory phase

The infiltration of inflammatory cells, including neutrophils (Gr-1$^+$), monocytes (Ly6C$^+$), and macrophages (F4/80$^+$), was examined at days 1, 3, and 9 post-injury. At day 1 post-injury, neutrophils were primarily observed in scab area (Figure 3.10 A), with a lower number observed in the granulation tissue. During this time, wound neutrophils were similar between WT and DKO mice (Figure 3.10 B). Monocytes were observed at the sides of the granulation tissue (Figure 3.10 C), indicating an initial entry of this inflammatory cell. In a similar fashion to neutrophils, DKO mice demonstrated equivalent level of wound monocytes compared to WT mice (Figure 3.10 D). Macrophages were also detected at the edge of granulation tissue (Figure 3.10 E). Unlike other leucocytes, a significant decrease in the number of wound macrophages was observed in DKO mice compared to WT mice during this initial phase of wound healing (Figure 3.10 F).

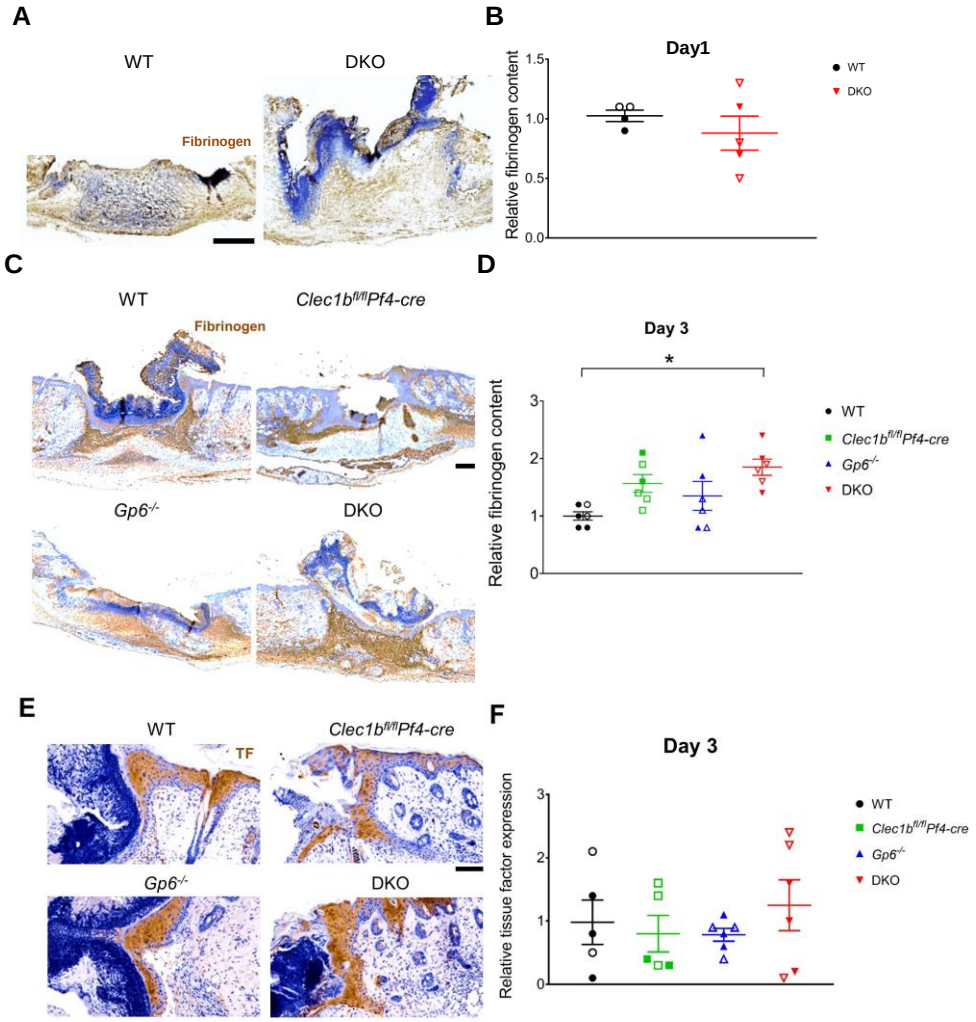

Figure 3. 7. Fibrinogen accumulation within the wound of DKO mice during the inflammatory phase. (A) Fibrinogen staining (brown) of skin wound at day 1 post-injury. Scale bar = 500 µm. (B) Quantification of fibrinogen content at day 1 post-injury (n=4-5). Data are presented as mean ± SEM and analysed by Student's t-test. (C) Fibrinogen staining (brown) of skin wound at day 3 post-injury. Scale bar = 200 µm. (D) Quantification of fibrinogen content at day 3 post-injury (n=6). (E) Staining of tissue factor (TF, brown) at day 3 post-injury. Scale bar = 50 µm. (F) Quantification of tissue factor at day 3 post-injury (n=5-6). Data from females (open symbols) and males (closed symbols) are shown in (B, D, F). Data are presented as mean ± SEM and analysed by one-way ANOVA with Bonferroni's multiple comparison test. *$p<0.05$.

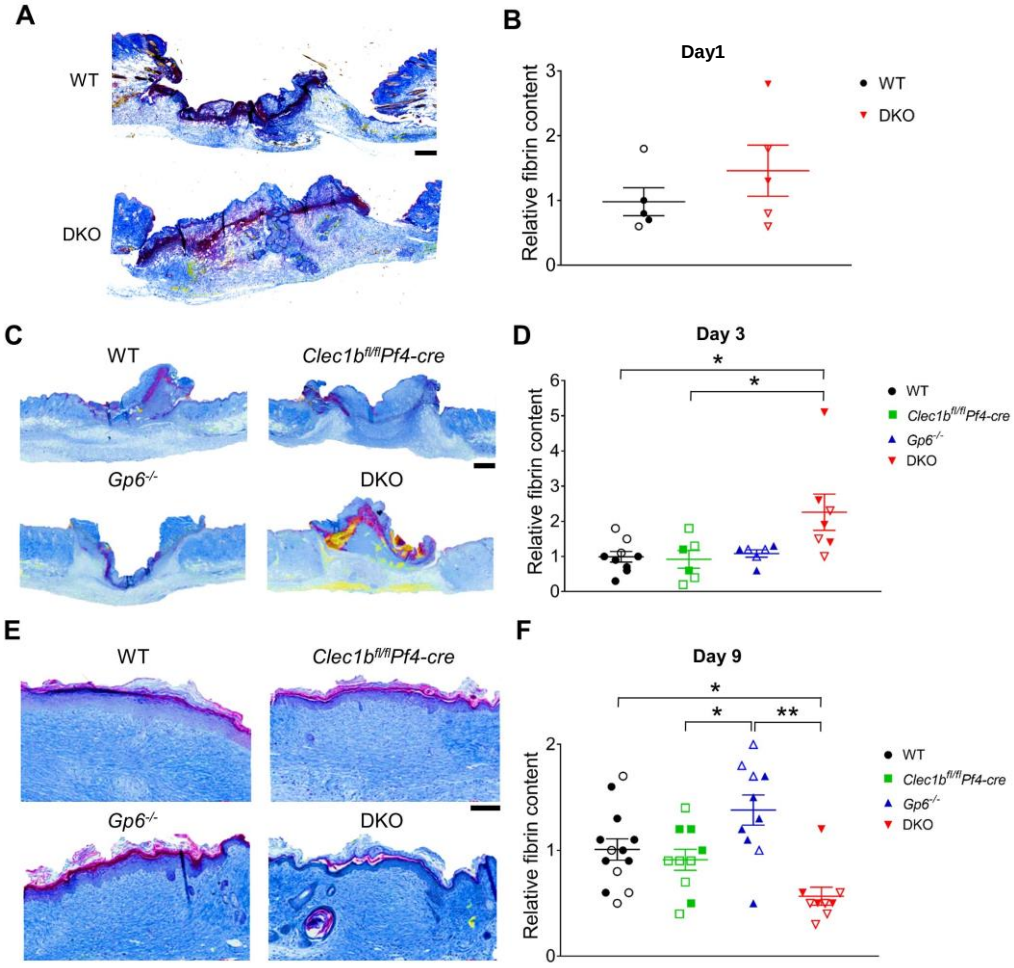

Figure 3. 8. Fibrin generation is enhanced during the inflammatory phase of wound healing in DKO mice. (A) Martius scarlet blue (MSB) staining of skin wound at day 1 post-injury. Red = old fibrin, blue = collagen, yellow = red blood cells/fresh fibrin. Scale bar = 200 µm. (B) Quantification of fibrin content in the wound at day 1 post-injury (n=5). Data are presented as mean ± SEM and analysed by Student's t-test. (C) MSB staining of skin wound at day 3 post-injury. Scale bar = 200 µm. (D) Quantification of fibrin content in the wound at day 3 post-injury (n=6-9). (E) MSB staining of skin wound at day 9 post-injury. Scale bar = 200 µm. (F) Quantification of fibrin content in the scar at day 9 post-injury (n=9-13). Data from females (open symbols) and males (closed symbols) are shown in (B, D, F). Graphs are presented as mean ± SEM and analysed by one-way ANOVA with Bonferroni's multiple comparison test. *$p<0.05$, **$p<0.01$.

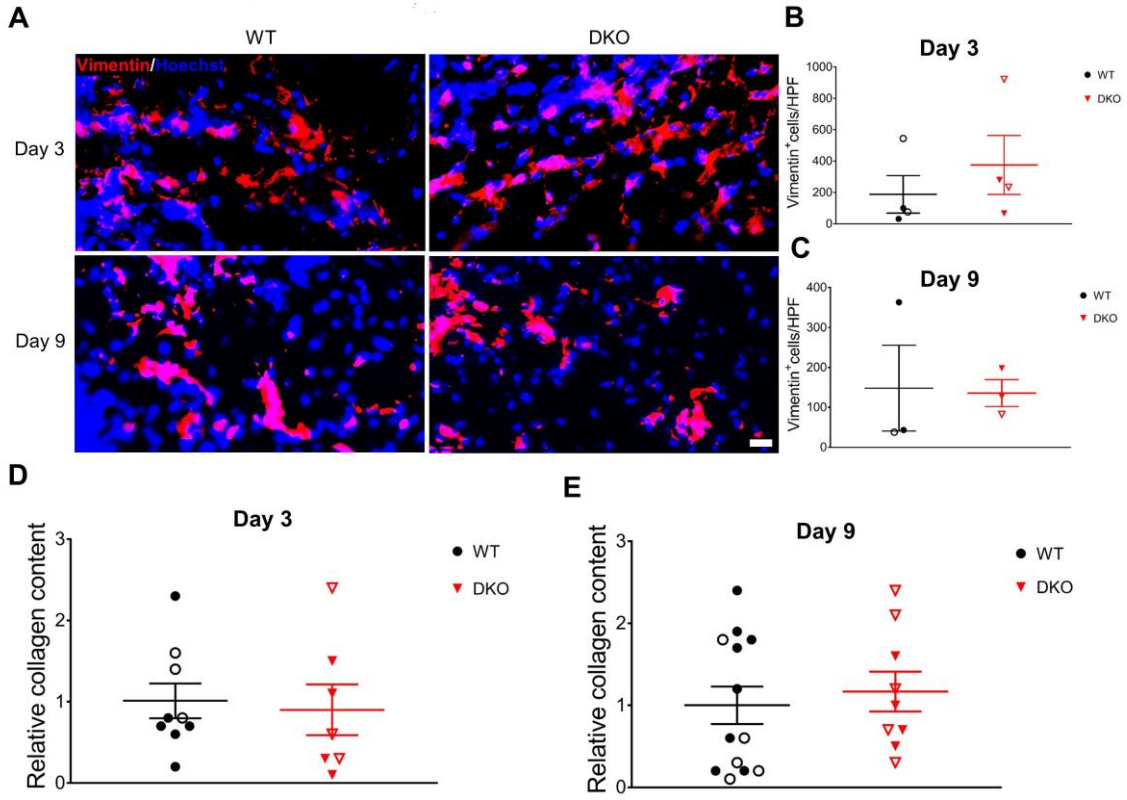

Figure 3. 9. Normal (myo)fibroblasts, and collagen content in DKO mice during the course of skin wound healing. (A) Immunofluorescence staining of (myo)fibroblasts (vimentin$^+$ cells; red) in the wound of WT and DKO mice at day 3 (n=4) and day 9 post-injury (n=3). Hoechst counterstains nuclei (blue). Scale bar = 20 µm. (B) Quantification of (myo)fibroblasts (vimentin$^+$ cells) at day 3 post-injury (n=4). (C) Quantification of (myo)fibroblasts (vimentin$^+$ cells) at day 9 post-injury (n=3). (D) Quantification of collagen content (blue color) in Martius scarlet blue (MSB) staining within the wound at day 3 post-injury (n=7-9). (E) Quantification of collagen content in MSB staining within the scar at day 9 post-injury (n=9-13). Data from females (open symbols) and males (closed symbols) are shown in (B-E). Graphs are presented as mean ± SEM and analysed by Student's t-test.

At day 3 post-injury, neutrophil influx was reduced in DKO mice compared to WT and *Clec1b*$^{fl/fl}$*Pf4-cre* mice (Figure 3.11 A, B). Immunofluorescence staining using anti-Ly6G antibody (clone 1A8) also confirmed a decrease in wound neutrophils in DKO mice at this time (Figure 3.11 C, D). WT mice showed a two-fold increase in neutrophil infiltration at day 3 relative to day 1 post-injury (Figure 3.11 E) whereas a steady level was observed in DKO mice. At day 9 post-injury, wound neutrophils were significantly decreased in both WT and DKO mice relative to the level at initial phase (Figure 3.11 E). However, neutrophils in the wound of DKO mice were higher than in WT at this time (Figure 3.11 F, G). The number of blood neutrophils was equivalent in unchallenged mice in all groups (Figure 3.11 H), and it was significantly decreased only in WT and *Clec1b*$^{fl/fl}$*Pf4-cre* mice at day 3 post-injury (Figure 3.11 H). DKO and *Gp6*$^{-/-}$ mice did not show alteration of blood neutrophils during the time course of wound healing (Figure 3.11 H).

In order to assess a possible defect in neutrophil chemotaxis in the wound of DKO mice, the expression of chemokine CXCL-1 (also known as keratinocyte-derived chemokine), a neutrophil chemoattractant (Devalaraja et al., 2000), was measured. The result demonstrated that CXCL-1 was highly expressed in proliferating/migrating keratinocytes at day 3 post-injury (Figure 3.12 A), although a very low level of expression was observed within the granulation tissue area. There was no alteration in wound CXCL-1 in DKO mice compared to other groups (Figure 3.12 B). PF4 released from activated platelets also contributes to leucocyte chemotaxis (Deuel et al., 1981). At day 3 post-injury, PF4 was detected in the wound in all mouse strains (Figure 3.12 C). However, the lack of platelet GPVI and CLEC-2 did not affect PF4 secretion within the wound area (Figure 3.12 D).

Previous evidences have demonstrated the role of fibrinogen and fibrin in inhibiting neutrophil chemotaxis (Hanson and Quinn, 2002, Higazi et al., 1994). Therefore, *in vitro* migration of bone marrow-derived neutrophils towards fMLP was performed. The results demonstrated that fibrinogen impeded migration of neutrophils from WT mice compared to the migration through collagen matrix (Figure 3.13). Moreover, crosslinked fibrin strongly inhibited migration of WT-derived neutrophils (Figure 3.13). Fibrinogen and fibrin showed a similar degree of potent inhibition for the migration of DKO-derived neutrophils (Figure 3.13).

A significantly higher number of wound monocytes was observed in DKO mice compared to WT and single knockout mice at day 3 post-injury (Figure 3.14 A, B). This was supported by a four-fold increase in wound monocytes relative to day 1 post-injury (Figure 3.14 C). WT mice had low number of wound monocytes during the course of healing (Figure 3.14 C). At day 9 post-injury, a reduction in wound monocytes relative to day 3 post-injury was detected in DKO mice (Figure 3.14 C). However, the level remained higher than in all other groups (Figure 3.14 D, E). Blood monocytes in unchallenged *Clec1b*$^{fl/fl}$*Pf4-cre* mice were increased compared to WT and DKO mice (Figure 3.14 G, *left*). At day 3 and day 9 post-injury, a significant reduction in circulating monocytes was observed in all groups compared to unchallenged controls (Figure 3.14 F). In DKO mice, however, the level of monocytes in blood was significantly greater than *Clec1b*$^{fl/fl}$*Pf4-cre* mice at day 3 post-injury (Figure 3.14 G, *middle*) and all other strains at day 9 post-injury (Figure 3.14 G, *right*).

Wound macrophages in *Clec1b*$^{fl/fl}$*Pf4-cre* mice were significantly increased at day 3 post-injury, relative to other groups (Figure 3.15 A, B). In comparison with day 1, a six-fold

increase in macrophage infiltration was observed in WT mice at day 3 post-injury (Figure 3.15 C). Wound macrophages in DKO mice were decreased compared to WT but not *Gp6*$^{-/-}$ mice at this time (Figure 3.15 B, C). At day 9 post-injury, macrophage numbers were equivalent among DKO, WT, and *Clec1b*$^{fl/fl}$*Pf4-cre* mice (Figure 3.15 D, E). A lower number of macrophages within the wound was observed in *Gp6*$^{-/-}$ mice relative to *Clec1b*$^{fl/fl}$*Pf4-cre* mice at this time (Figure 3.15 E).

To examine whether a reduction of macrophage infiltration in DKO animals affects M1 or M2 phenotype, double immunofluorescence staining was performed. The results showed that iNOS-expressing macrophages (a M1 marker) were decreased (Figure 3.16 A, B) whereas M2 population (Fizz-1-positive) were unaltered relative to WT at day 3 post-injury (Figure 3.16 D, E). At day 9 post-injury, there was no difference in M1 (Figure 3.16 A, C) and M2 macrophages (Figure 3.16 D, F) between WT and DKO mice. During the inflammatory phase of wound healing, the inflammatory cytokines, including IL-1β and TNF-α, are secreted by the inflammatory cells, leading to wound inflammation (Eming et al., 2007). At day 3 post-injury, a significant decrease in TNF-α was observed within the wound tissue of DKO mice compared to WT (Figure 3.16 G, H).

Together, these data suggest that CLEC-2 deficiency promotes leucocyte infiltration to the wound during the inflammatory phase, especially macrophages. A lack of both GPVI and CLEC-2 results in a significant decrease in inflammatory cells (i.e. neutrophils and M1 macrophages) and TNF-α level within the wound at this initial phase.

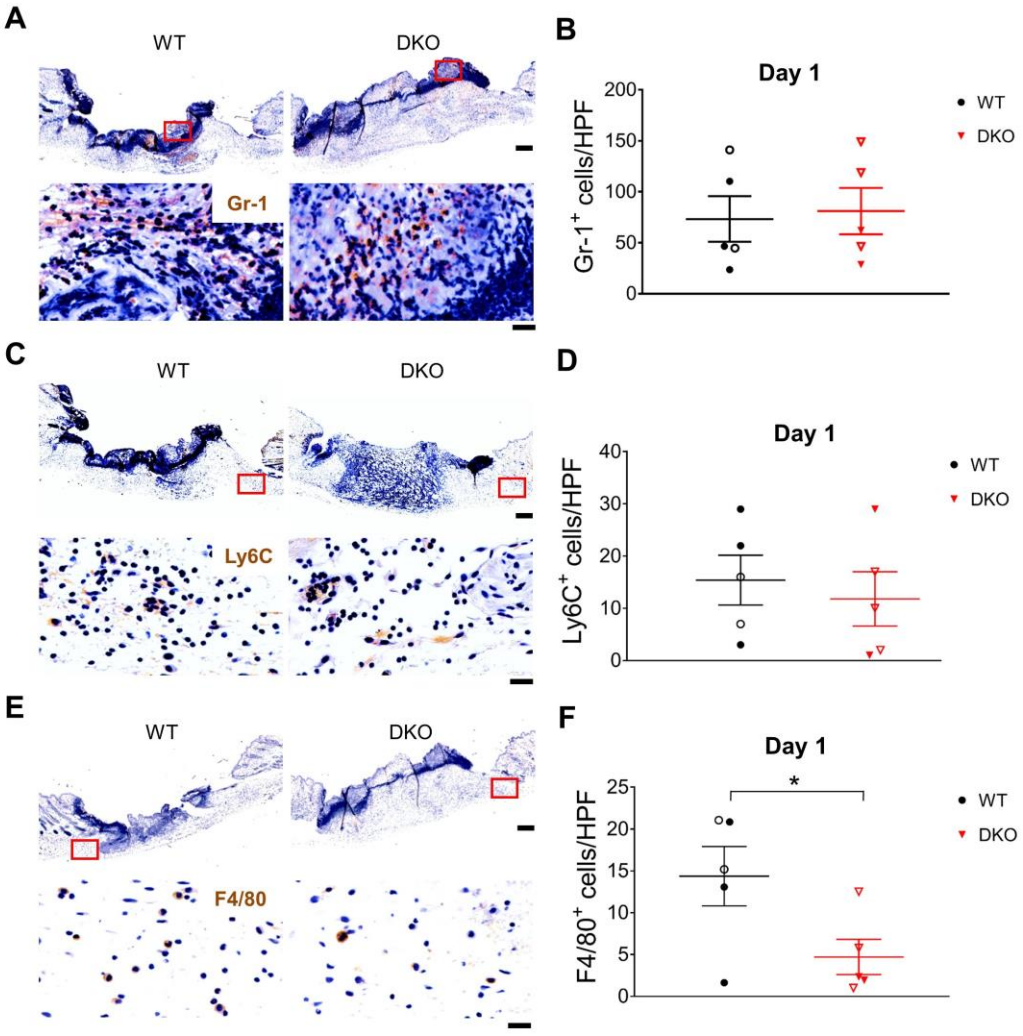

Figure 3. 10. Wound neutrophils, and monocytes (but not macrophages) are unaltered in DKO mice at day 1 post-injury. (A) Staining of neutrophils (Gr-1; brown) in wound area at day 1 post-injury. (B) Quantification of neutrophils (Gr-1$^+$ cells) in wound area at day 1 post-injury (n=5). (C) Staining of monocytes (Ly6C; brown) in wound area at day 1 post-injury. (D) Quantification of monocytes (Ly6C$^+$ cells) in wound area at day 1 post-injury (n=5). (E) Detection of macrophages (F4/80 staining; brown) in wound area at day 1 post-injury. (F) Quantification of macrophages (F4/80$^+$ cells) in wound area at day 1 post-injury (n=5). Data from females (open symbols) and males (closed symbols) are shown in (B, D, F). Graphs are presented as mean ± SEM and analysed by Student's t-test. *$p < 0.05$.

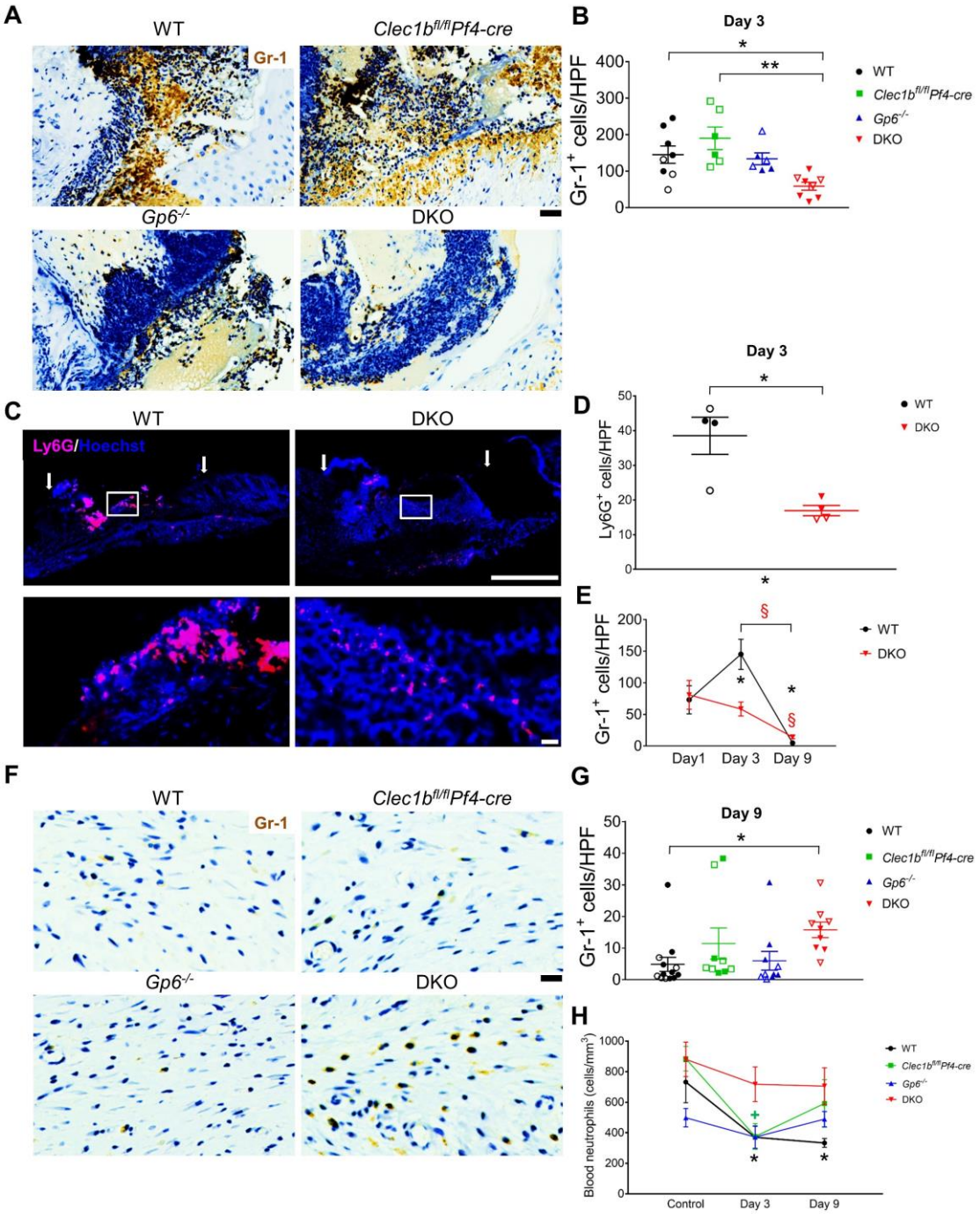
A
WT
Clec1b^fl/fl Pf4-cre
Gr-1
Gp6^-/-
DKO
B
Day 3
Gr-1+ cells/HPF
WT
Clec1b^fl/fl Pf4-cre
Gp6^-/-
DKO
C
WT
DKO
Ly6G/Hoechst
D
Day 3
Ly6G+ cells/HPF
WT
DKO
E
Gr-1+ cells/HPF
WT
DKO
Day1
Day 3
Day 9
F
WT
Clec1b^fl/fl Pf4-cre
Gr-1
Gp6^-/-
DKO
G
Day 9
Gr-1+ cells/HPF
WT
Clec1b^fl/fl Pf4-cre
Gp6^-/-
DKO
H
Blood neutrophils (cells/mm3)
WT
Clec1b^fl/fl Pf4-cre
Gp6^-/-
DKO
Control
Day 3
Day 9

Figure 3.11.

Figure 3. 11. A reduction in neutrophil influx is observed during the inflammatory phase of wound healing in DKO animals. (A) Detection of neutrophils (Gr-1 staining; brown) in wound at day 3 post-injury. Scale bar = 20 µm. (B) Quantification of neutrophils (Gr-1$^+$ cells) in wound at day 3 post-injury. *$p<0.05$, **$p<0.01$. (C) Representative images of neutrophil staining in wound at day 3 post-injury using anti-Ly6G antibody (clone 1A8). Arrow indicates wound edges. Scale bar = 500 µm (upper panel) and 20 µm (lower panel). (D) Quantification of Ly6G$^+$ cells at day 3 post-injury (n=4). *$p<0.05$. (E) Comparison of Gr1$^+$ cells between day 1, day 3, and day 9 post-injury in WT and DKO mice. The symbols * and § indicate $p<0.05$ in WT and DKO mice, compared to the data at day 1 post-injury, respectively. The bracket shows $p<0.05$ for the comparison between day 3 and day 9 post-injury in *WT and §DKO mice, respectively. (F) Detection of neutrophils (Gr-1 staining; brown) in wound at day 9 post-injury. Scale bar = 20 µm. (G) Quantification of neutrophils (Gr-1$^+$ cells) in wound at day 9 post-injury. *$p<0.05$. (H) Comparison of blood neutrophil counts between baseline, day 3, and day 9 post-injury in each mouse strain. The symbols * and + indicate $p<0.05$ in WT and *Clec1b*$^{fl/fl}$*Pf4-cre* mice, compared to their control, respectively. Sample numbers in unchallenged control = 10, day 1 = 5, day 3 = 6-9, and day 9 post-injury = 9-13, respectively. Data from females (open symbols) and males (closed symbols) are shown in (B, D, G). Graphs are presented as mean ± SEM and analysed by either Student's *t*-test (D) or one-way ANOVA with Bonferroni's multiple comparison test (B, E, G, H).

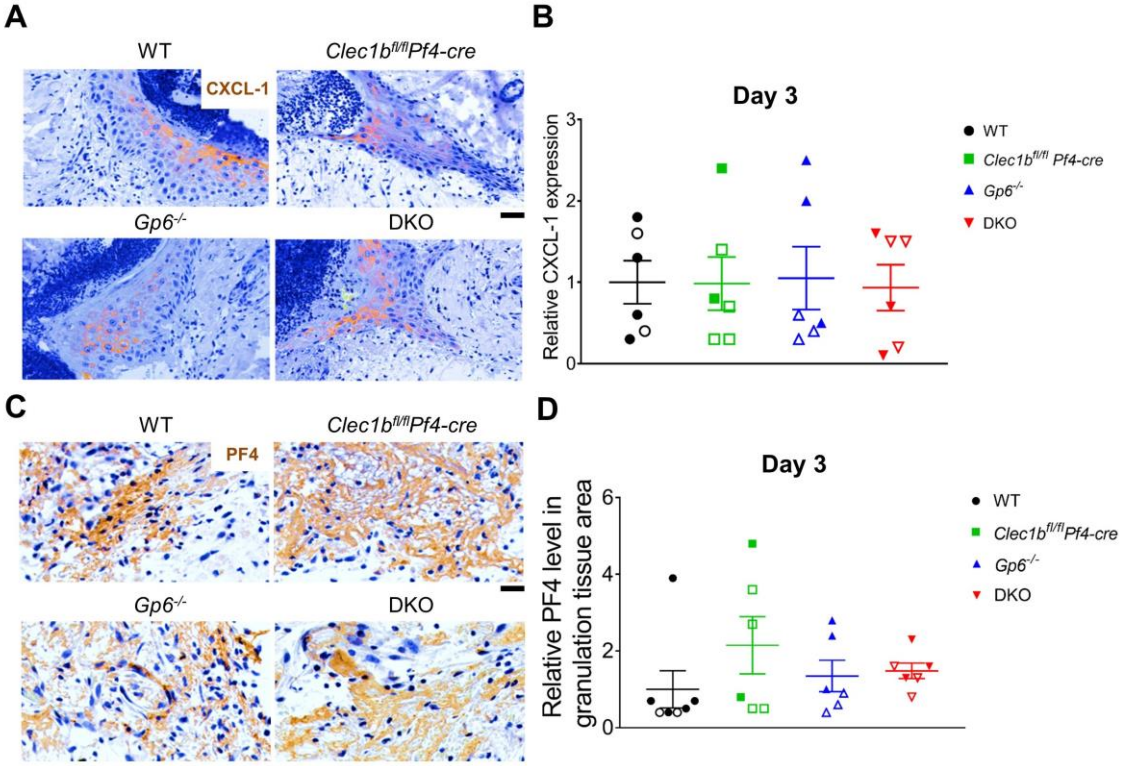

Figure 3. 12. CXCL-1 and PF4 are not impaired during inflammatory phase of wound repair in DKO mice. (A) Detection of CXCL-1 (brown) in wound area at day 3 post-injury. (B) Quantification of keratinocyte-expressed CXCL-1 in wound area at day 3 post-injury (n=6). (C) Detection of PF4 (brown) in wound area at day 3 post-injury. (D) Quantification of PF4 within the granulation tissue in wound area at day 3 post-injury (n=6). Data from females (open symbols) and males (closed symbols) are shown in (B) and (D). Data are presented as mean ± SEM and analysed by one-way ANOVA with Bonferroni's multiple comparison test.

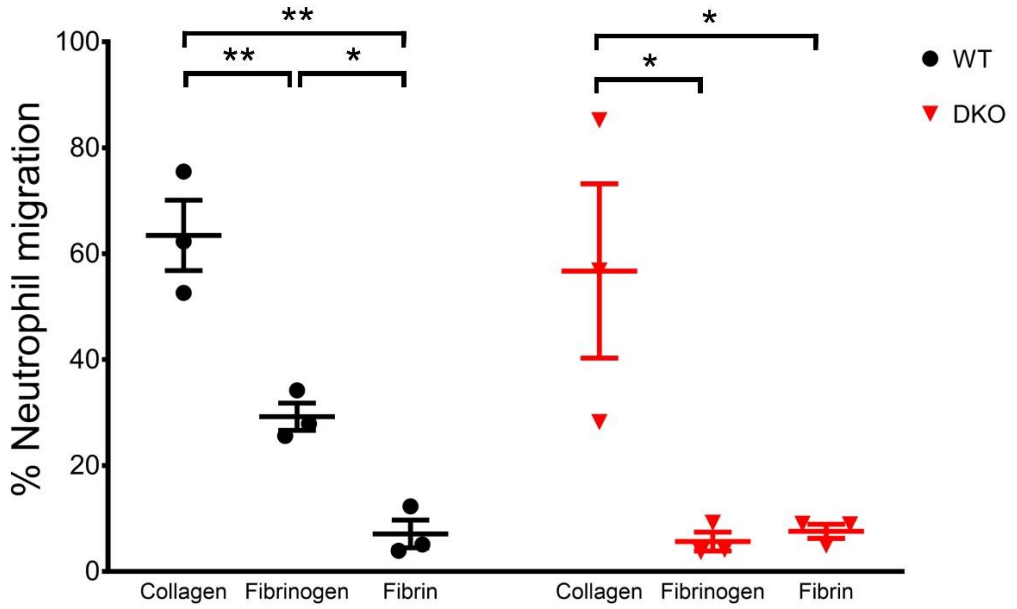

Figure 3. 13. Fibrinogen and fibrin inhibit neutrophil migration towards fMLP *in vitro*. Graphs show percentage of neutrophil migration through collagen, fibrinogen, and fibrin matrix towards fMLP for 3 hours (n=3). Data are presented as mean ± SEM and analysed by one-way ANOVA. *$p<0.05$, **$p<0.01$.

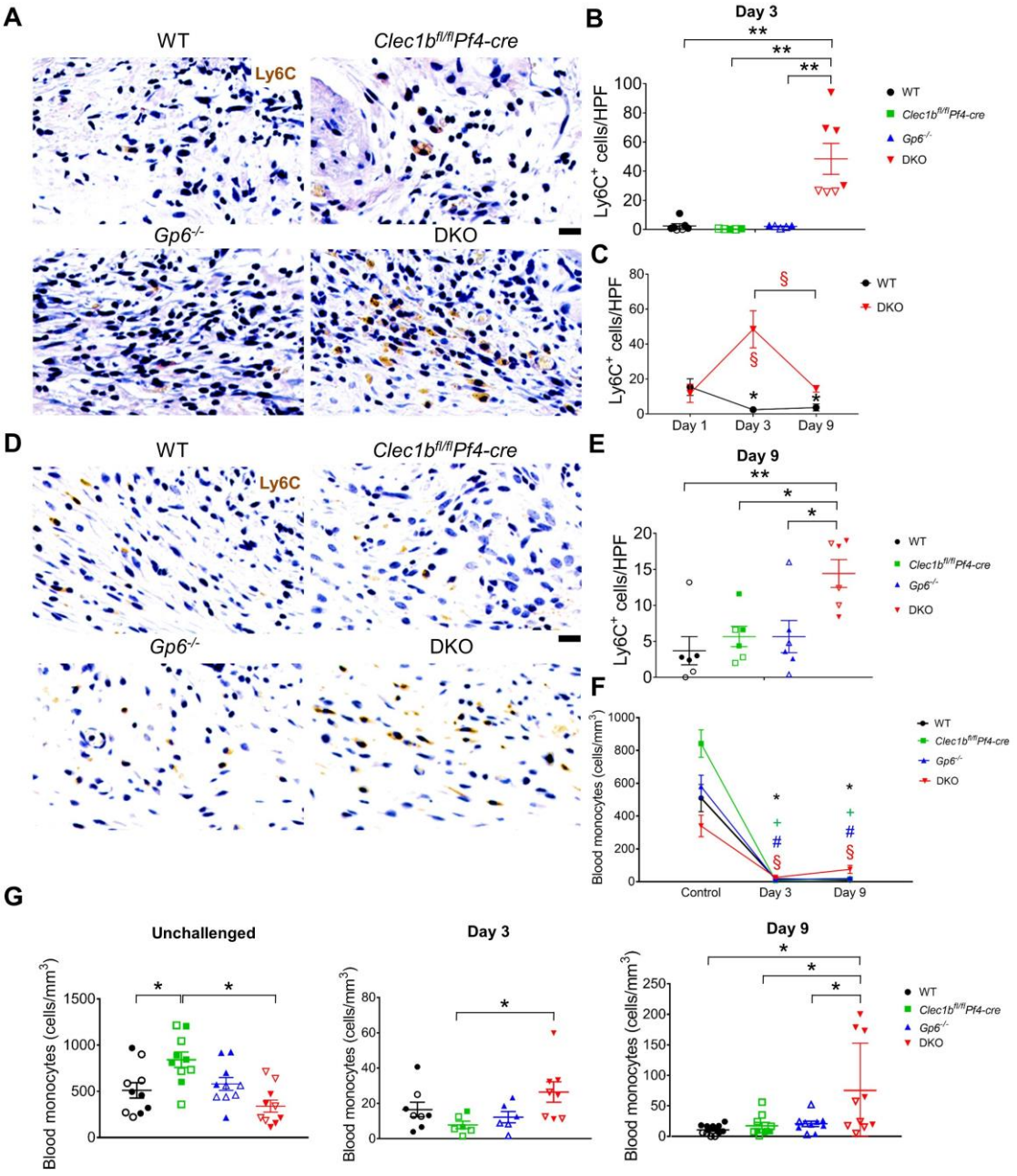
A
WT
Clec1b^fl/fl Pf4-cre
Ly6C
Gp6^-/-
DKO
B
Day 3
Ly6C+ cells/HPF
WT
Clec1b^fl/fl Pf4-cre
Gp6^-/-
DKO
C
Ly6C+ cells/HPF
Day 1
Day 3
Day 9
D
E
Day 9
F
Blood monocytes (cells/mm3)
Control
G
Unchallenged
Day 3
Day 9

Figure 3.14.

Figure 3. 14. Wound monocytes during the inflammatory phase of repair are increased in mice deficient in GPVI and CLEC-2. (A) Detection of monocytes ($Ly6C^+$ cells; brown) in wound at day 3 post-injury. (B) Quantification of $Ly6C^+$ cells in wound at day 3 post-injury (n=5-7). ***p<0.01*. (C) Comparison of $Ly6C^+$ cells between day 1, day 3, and day 9 post-injury in WT and DKO mice. The symbols * and § indicate *p<0.05* in WT and DKO mice, compared to the data at day 1 post-injury, respectively. The bracket shows *p<0.05* for the comparison between day 3 and day 9 post-injury in §DKO mice. (D) Detection of $Ly6C^+$ cells (brown) in wound at day 9 post-injury. (E) Quantification of $Ly6C^+$ cells in wound at day 9 post-injury (n=6). **p<0.05*, ***p<0.01*. (F) Comparison of blood monocyte counts between baseline, day 3, and day 9 post-injury in each mouse strain. The symbols *, +, #, and § indicate *p<0.05* in WT, *Clec1b*$^{fl/fl}$*Pf4-cre*, *Gp6*$^{-/-}$, and DKO mice, compared to their control, respectively. (G) Comparison of blood monocytes between all groups at baseline (left), day 3 (middle), and day 9 post-injury (right). Sample numbers in unchallenged control = 10, day 1 = 5, day 3 = 6-9, and day 9 post-injury = 10-13, respectively. Data from females (open symbols) and males (closed symbols) are shown in (B, E, G). Graphs are presented as mean ± SEM and analysed by one-way ANOVA with Bonferroni's multiple comparison test. Scale bar = 20 µm.

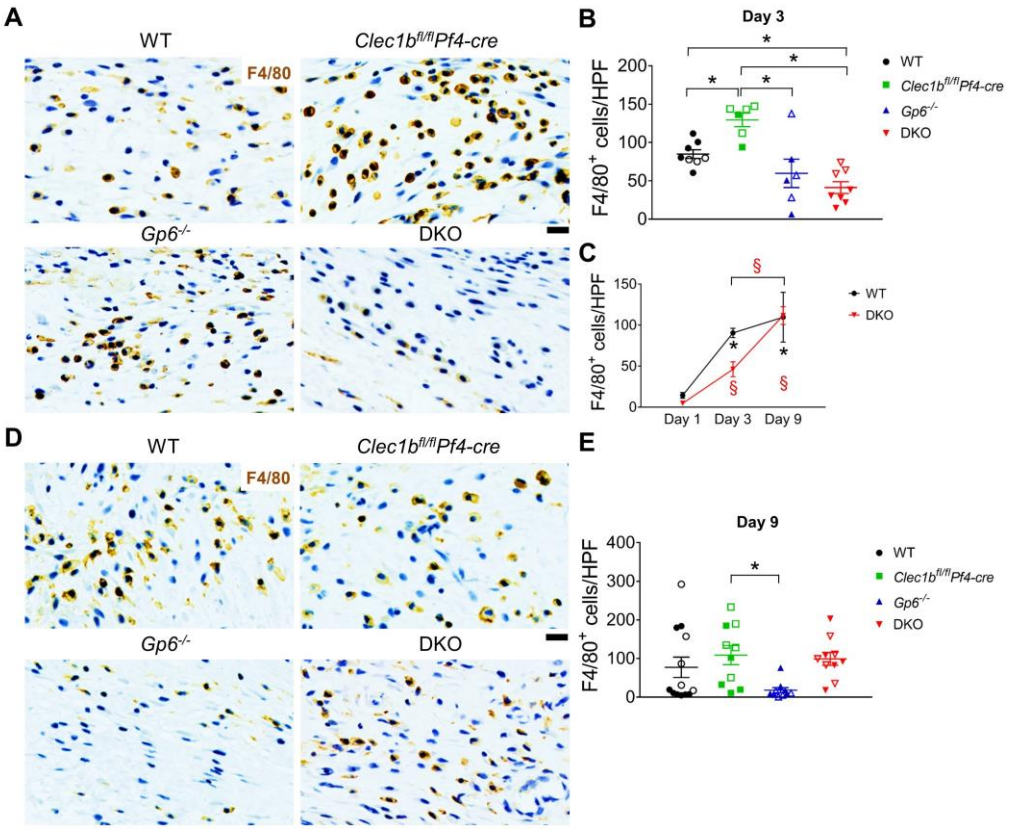

Figure 3. 15. Wound Macrophages are reduced during the inflammatory phase of wound healing in ITAM receptors-deficient mice. (A) Detection of macrophages ($F4/80^+$ cells; brown) in wound at day 3 post-injury. (B) Quantification of $F4/80^+$ cells in wound at day 3 post-injury (n=6-8). *$p<0.05$. (C) Comparison of $F4/80^+$ cells between day 1, day 3, and day 9 post-injury in WT and DKO mice. The symbols * and § indicate $p<0.05$ in WT and DKO mice, compared to the data at day 1 post-injury, respectively. The bracket shows $p<0.05$ for the comparison between day 3 and day 9 post-injury in §DKO mice. Sample numbers at day 1 = 5, day 3 = 6-9, and day 9 post-injury = 10-13, respectively. (D) Detection of macrophages ($F4/80^+$ cells; brown) in wound at day 9 post-injury. (E) Quantification of $F4/80^+$ cells in wound at day 9 post-injury (n=10-13). *$p<0.05$. Data from females (open symbols) and males (closed symbols) are shown in (B) and (E). Graphs are presented as mean ± SEM and analysed by one-way ANOVA with Bonferroni's multiple comparison test. Scale bar = 20 µm.

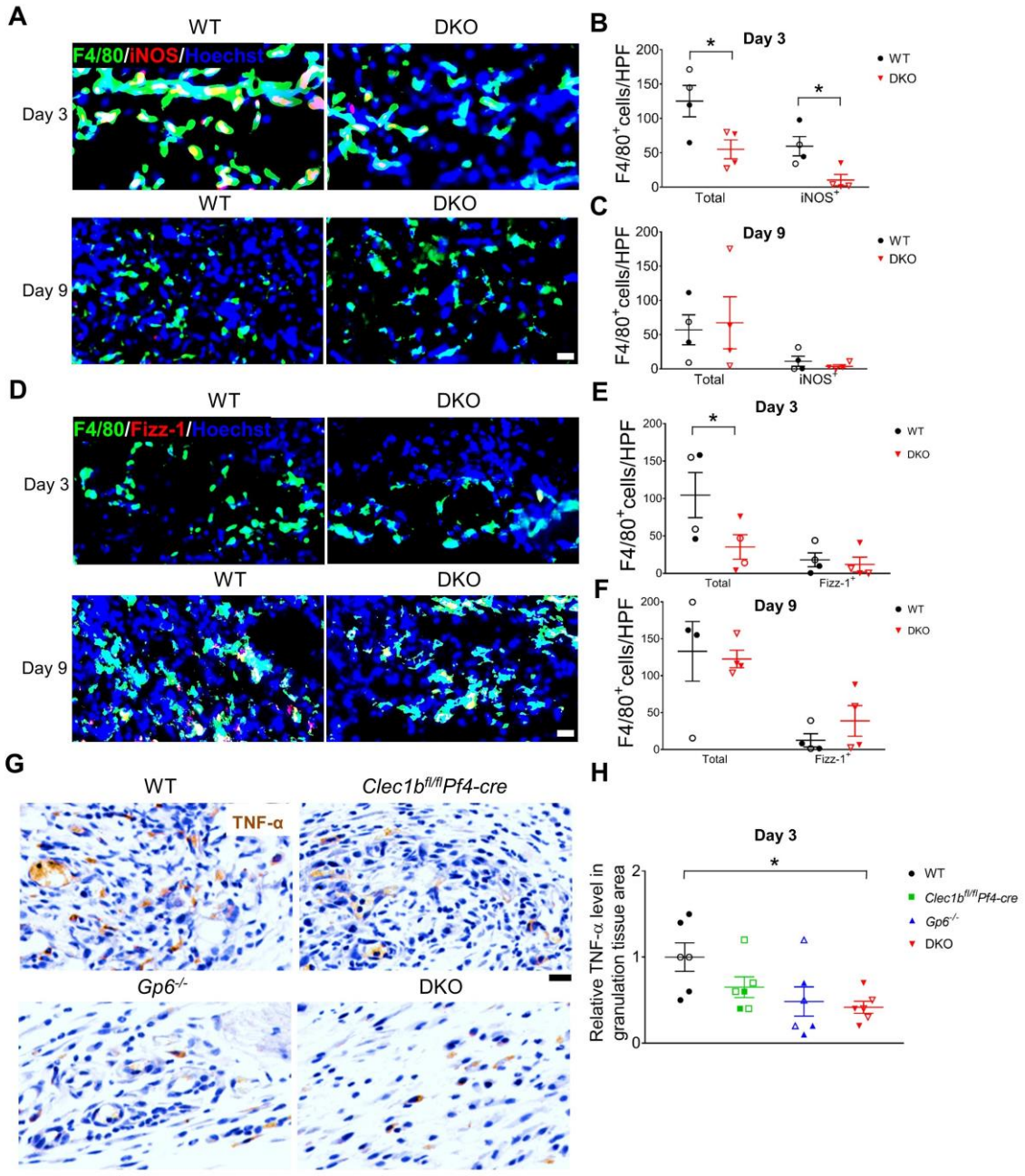
A
WT
DKO
F4/80/iNOS/Hoechst
Day 3
Day 9
B
Day 3
F4/80+cells/HPF
Total
iNOS+
WT
DKO
C
Day 9
D
F4/80/Fizz-1/Hoechst
E
Fizz-1+
F
G
Clec1bfl/flPf4-cre
TNF-α
Gp6-/-
H
Relative TNF-α level in granulation tissue area

Figure 3.16.

Figure 3. 16. M1 pro-inflammatory macrophages and TNF-α level are decreased during the inflammatory phase of repair in DKO mice. (A) Immunofluorescence double staining of iNOS (red) and F4/80 (green) in the wound of WT and DKO mice at day 3 (n=4) and day 9 post-injury (n=4). Hoechst counterstains nuclei (blue). (B) Quantification of M1 macrophages ($iNOS^+F4/80^+$ cells; yellow) at day 3 post-injury (n=4). (C) Quantification of M1 macrophages ($iNOS^+F4/80^+$ cells; yellow) at day 9 post-injury (n=4). (D) Immunofluorescence double staining of Fizz-1 (red) and F4/80 (green) in the wound of WT and DKO mice at day 3 (n=4) and day 9 post-injury (n=4). (E) Quantification of M2 macrophages ($Fizz\text{-}1^+F4/80^+$ cells; yellow) at day 3 post-injury (n=4). (F) Quantification of M2 macrophages ($Fizz\text{-}1^+F4/80^+$ cells; yellow) at day 9 post-injury (n=4). (G) Immunohistochemistry staining of TNF-α (brown) in the wound at day 3 post-injury. (H) Quantification of TNF-α level in granulation tissue area at day 3 post-injury (n=6). Data from females (open symbols) and males (closed symbols) are shown in (B, C, E, F, H). Graphs are presented as mean ± SEM and analysed by either Student's t-test (B, C, E, F) or one-way ANOVA with Bonferroni's multiple comparison test (H). *$p<0.05$. Scale bar = 20 μm.

3.2.7 Blocking CLEC-2-podoplanin axis promotes skin wound healing in GPVI deficient mice

Deletion of both CLEC-2 and GPVI accelerated wound healing in a murine model of full-thickness excisional skin wound, which was associated with inflammatory bleeding (i.e. a loss of vascular integrity), fibrinogen and fibrin matrix deposition, a reduction in inflammation (i.e. decreased wound neutrophils, M1 macrophages, and TNF-α level), and enhanced re-epithelialisation and angiogenesis during the initial phase of repair process. However, DKO mice had blood-filled lymphatics and a moderate degree of thrombocytopenia, which may influence the repair process. To generate DKO setting in the absence of these limitations, *Gp6*$^{-/-}$ mice, which have a normal platelet count and no blood/lymphatic mixing phenotype, were treated with an anti-podoplanin antibody that blocks CLEC-2-podoplanin interaction. This antibody has previously been shown to increase vascular leakage in *Gp6*$^{-/-}$ mice during a model of skin inflammation (Rayes et al., 2018).

During the period of wound monitoring for up to 3 days post-injury, *Gp6*$^{-/-}$ mice treated with anti-podoplanin antibody (*Gp6*$^{-/-}$ + anti-podoplanin) displayed redness around the wound edge (Figure 3.17 A), although a mild degree of redness was also observed in IgG isotype-treated *Gp6*$^{-/-}$ mice. However, there was no significant vasodilation in this setting, which possibly contributes to a lower extent of redness compared to the transgenic DKO mice. Wound closure was significantly accelerated in *Gp6*$^{-/-}$ + anti-podoplanin at day 2 and 3 post-injury compared to *Gp6*$^{-/-}$ controls (Figure 3.17 A, B). Macroscopic observation of the inner side of skin wound at day 3 post-injury indicated an increase in vascular leakage (Figure 3.17 A, *arrow*). Histological analysis of wound tissue showed

an increase in the extravasation of Rbcs into the skin dermis at the wound edge of *Gp6*$^{-/-}$ + anti-podoplanin mice relative to *Gp6*$^{-/-}$ controls (Figure 3.17 C, *arrow*).

3.2.8 Co-localisation of anti-podoplanin antibody on podoplanin-positive cells in the skin wounding in GPVI deficient mice

To validate the anti-podoplanin antibody on podoplanin-positive cells in the skin tissue, immunofluorescence staining was performed using a secondary antibody against syrian hamster IgG. The results showed that the antibody was highly detected at perivascular area in *Gp6*$^{-/-}$ + anti-podoplanin mice whereas it was absent in *Gp6*$^{-/-}$ + IgG controls (Figure 3.18) at day 3 post-injury. In addition, the leakage of platelets into perivascular tissue was observed in *Gp6*$^{-/-}$ + anti-podoplanin mice, confirming the impairment of vascular integrity during this time (Figure 3.18).

In support of previous reports, these data indicate that injection of anti-podoplanin antibody blocks the binding of CLEC-2 to its ligand podoplanin in *Gp6*$^{-/-}$ mice, especially at perivascular area, which recapitulates GPVI and CLEC-2 double deficient setting, leading to an increase in vascular leakage during the inflammatory phase of wound healing. In addition, this experimental setting provides further evidence that the accelerated wound healing in DKO mice is not due to developmental defects or thrombocytopenia, but it is due to a combined loss of the interaction of platelet CLEC-2 and GPVI with their respective ligands.

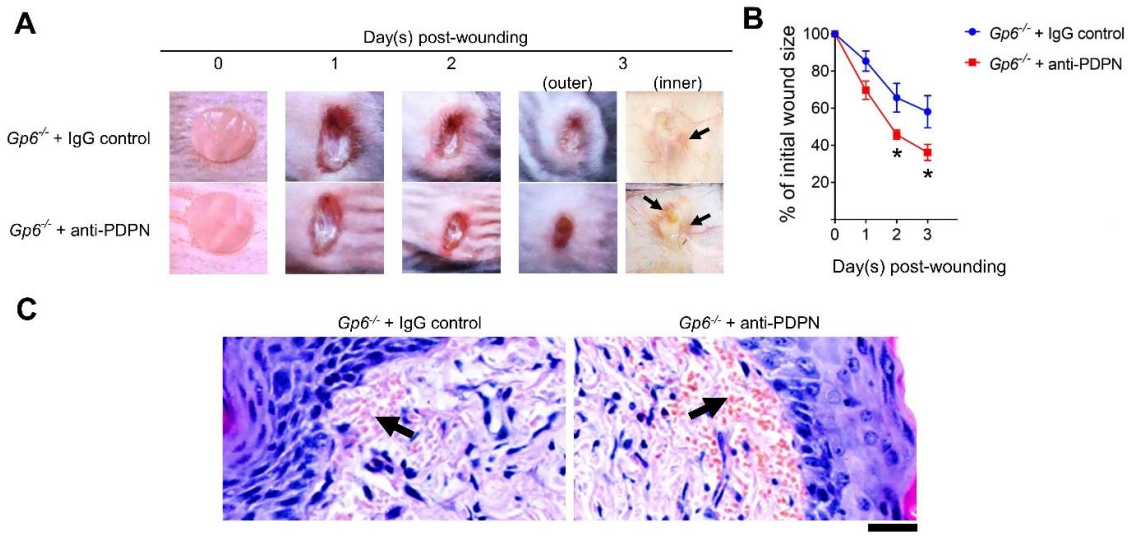

Figure 3. 17. Anti-podoplanin antibody injection in *Gp6*$^{-/-}$ mice (*Gp6*$^{-/-}$ + anti-PDPN) recapitulates the accelerated wound healing observed in DKO mice. (A) Macroscopic appearance of wound at indicated time points is shown. Arrow points to intra-skin bleeding around the wound at day 3 post-injury. (B) Percentage changes of wound size over 3 days post-injury (n=5). (C) H&E staining at day 3 post-injury (n=5). Arrow points the bleeding into surrounding skin. Scale bar = 20 µm. Graphs are presented as mean ± SEM. Kinetics of wound closure are analysed by two-way ANOVA with Bonferroni's multiple comparison test. *$p<0.05$.

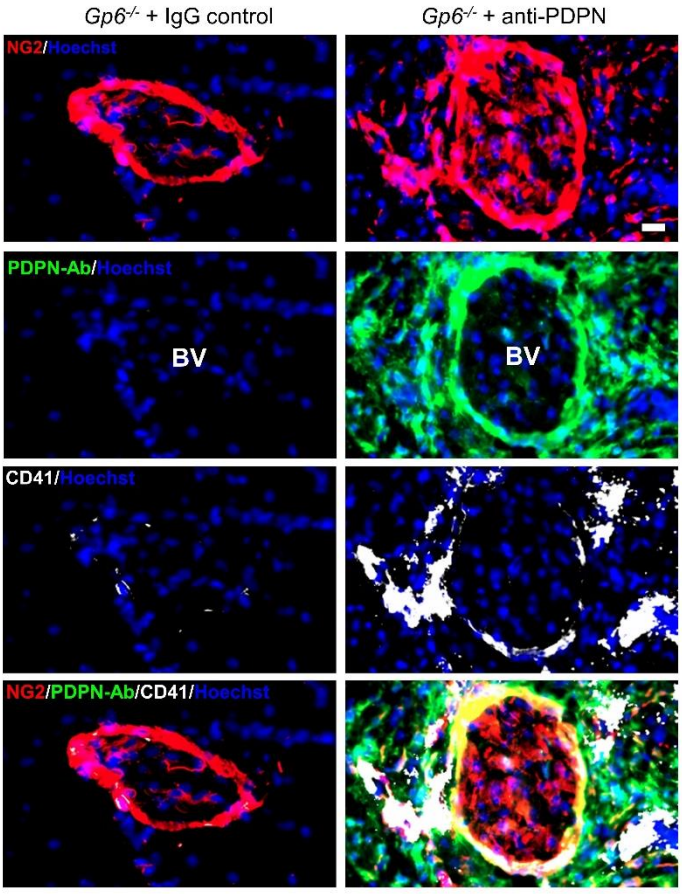

Figure 3. 18. Anti-podoplanin antibody (PDPN-Ab) is detected together with extravascular platelets at perivascular area in *Gp6*$^{-/-}$ mice treated with this antibody. Immunofluorescence staining of NG2 (red), PDPN-Ab (green) and CD41 (white) illustrates extravasation of platelets and the presence of PDPN-Ab on pericytes (NG2^{+}) and other cells around blood vessel at day 3 after injury (n=4-5). Alexa 488-conjugated goat anti-hamster IgG secondary antibody was used in immunofluorescence to detect PDPN-Ab (clone 8.1.1.). Hoechst counterstains nuclei (blue). BV = blood vessel. Scale bar = 20 µm.

3.2.9 Treatment of GPVI deficient mice with anti-podoplanin antibody enhances re-epithelialisation and angiogenesis during the inflammatory phase of wound healing

In association with the accelerated wound closure, histological analysis of skin wound at day 3 post-injury revealed that *Gp6*$^{-/-}$ treated with anti-podoplanin mice had a longer distance of re-epithelialisation arising from the wound edges toward the center of the wound (Figure 3.19 A, B) with no alteration in wound contraction (Figure 3.19 C). A larger area of granulation tissue was also observed in the antibody-treated mice (Figure 3.19 A, D).

Examination of angiogenesis using immunofluorescence staining illustrated that *Gp6*$^{-/-}$ + anti-podoplanin mice had an increased expansion of endothelial cells (CD31^{+}) within the wound at day 3 post-injury (Figure 3.19 E), and the quantitative analysis confirmed a signigficant increase in CD31^{+} area (Figure 3.19 F), compared to *Gp6*$^{-/-}$ controls.

These data indicate that blocking CLEC-2-podoplanin axis in GPVI deficient mice phenocopies the wound repair process observed in DKO mice, including enhanced re-epithelialisation, granulation tissue formation, and angiogenesis, all of which begin at the early stage, rejecting the influence of blood/lymphatic mixing or a low platelet counts in wound healing of DKO animals.

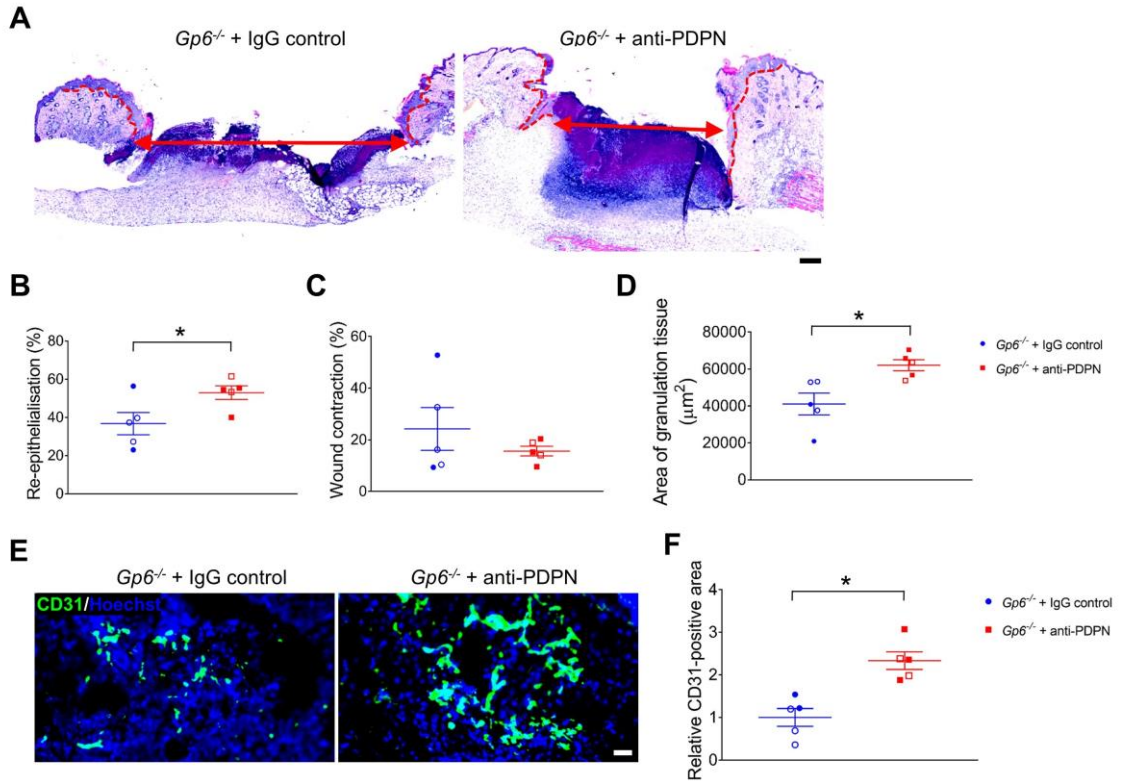

Figure 3. 19. Enhanced re-epithelialisation, granulation tissue formation, and angiogenesis in *Gp6*$^{-/-}$ mice treated with anti-podoplanin antibody. (A) H&E staining at day 3 post-injury. Dotted line indicates hyperplastic coverages. Arrow indicates gap between epithelial tongues. Scale bar = 500 µm. (B) Measurement of re-epithelialisation (n=5). (C) Assessment of wound contration (n=5). (D) Quantification of granulation tissue area (n=5). (E) Immunofluorescence staining of endothelial cells (CD31^{+} cells; green) in wound area at day 3 post-injury. Hoechst counterstains nuclei (blue). Scale bar = 50 µm. (F) Quantification of CD31^{+} area within the wound at day 3 post-injury (n=5). Data from females (open symbols) and males (closed symbols) are shown in (B, C, D, F). All graphs are presented as mean ± SEM and analysed by Student's t-test. *$p<0.05$.

3.2.10 Fibrin accumulation during the inflammatory phase of wound healing is increased in GPVI deficient mice treated with podoplanin-blocking antibody

Due to the increase in vascular leakage during the inflammatory phase of repair in *Gp6*$^{-/-}$ + anti-podoplanin mice, the extravasation of fibrinogen and the formation of fibrin were further investigated. Immunohistochemistry staining of fibrinogen showed that fibrinogen was accumulated in the granulation tissue area (Figure 3.20 A), although no significant increase in *Gp6*$^{-/-}$ + anti-podoplanin mice was observed at day 3 post-injury relative to *Gp6*$^{-/-}$ controls (Figure 3.20 B). Tissue factor was abundantly expressed on proliferating/migrating keratinocytes (Figure 3.20 C), with a lower level was detected in the granulation tissue. There was no significant difference in tissue factor expression in the tissue between two groups (Figure 3.20 D). However, the fibrin content in the wound scab of *Gp6*$^{-/-}$ + anti-podoplanin mice was significantly higher than IgG-treated *Gp6*$^{-/-}$ mice at day 3 post-injury (Figure 3.20 E, F).

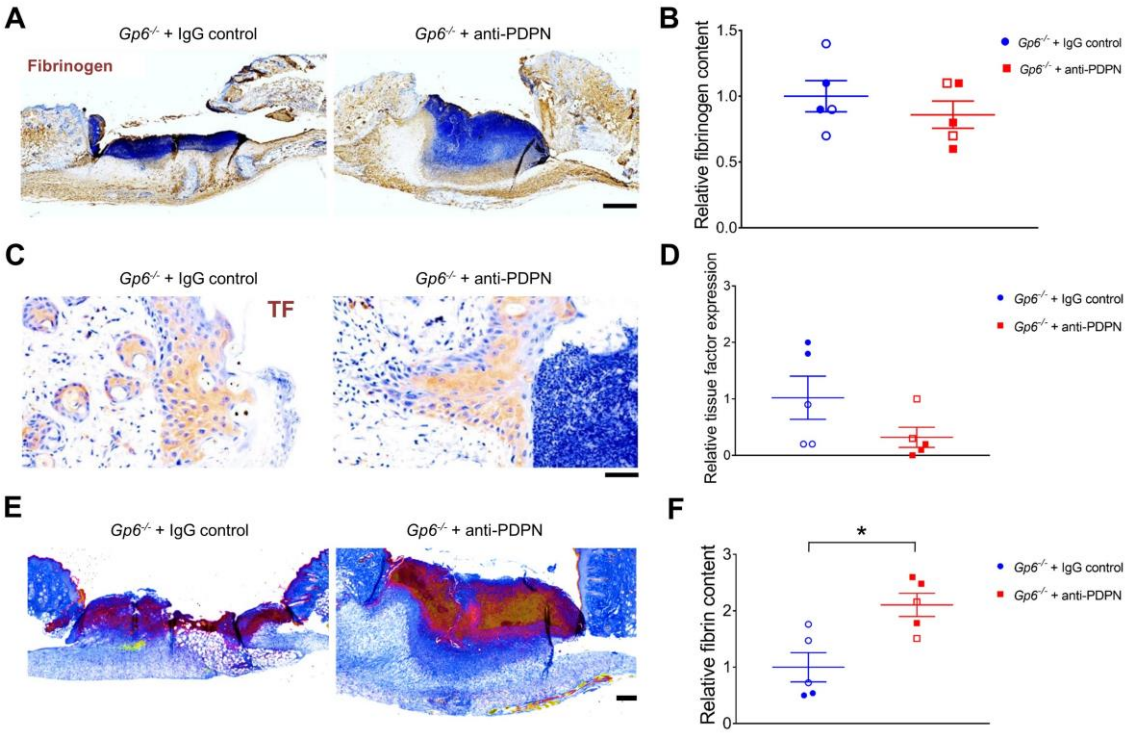

Figure 3. 20. Wound fibrin is increased during the inflammatory phase in *Gp6*$^{-/-}$ mice treated with anti-podoplanin antibody. (A) Fibrinogen staining (brown) of skin wound at day 3 post-injury. Scale bar = 500 µm. (B) Quantification of fibrinogen content at day 3 post-injury (n=5). (C) Immunohistochemistry staining of tissue factor (brown) at day 3 post-injury. TF = tissue factor. Scale bar = 50 µm. (D) Quantification of tissue factor at day 3 post-injury (n=5). (E) Martius scarlet blue staining of skin wound at day 3 post-injury. Red = old fibrin, blue = collagen, yellow = red blood cells/fresh fibrin. Scale bar = 200 µm. (F) Quantification of fibrin content in the wound at day 3 post-injury (n=5). Data from females (open symbols) and males (closed symbols) are shown in (B, D, F). Graphs are presented as mean ± SEM and analysed by Student's t-test.

3.2.11 Injection of podoplanin-blocking antibody in GPVI deficient mice reduced neutrophils and macrophages in the wound during the inflammatory phase

At day 3 post-injury, wound neutrophils was abundantly present at the border between the scab and granulation tissue (Figure 3.21 A), which was significantly reduced in the *Gp6*$^{-/-}$ + anti-podoplanin mice compared to *Gp6*$^{-/-}$ controls (Figure 3.21 B). Monocytes and macrophages were primarily localised in the granulation tissue (Figure 3.21 C, E) at day 3 post-injury. The number of wound monocytes in *Gp6*$^{-/-}$ + anti-podoplanin mice was significantly higher than IgG-treated *Gp6*$^{-/-}$ controls (Figure 3.21 D). In contrast, a reduction in wound macrophages was observed in *Gp6*$^{-/-}$ + anti-podoplanin mice (Figure 3.21 F).

Moreover, CXCL-1, which highly expressed in proliferating/migrating keratinocytes (Figure 3.22 A), was unaltered in *Gp6*$^{-/-}$ + anti-podoplanin mice relative to controls (Figure 3.22 B). There was also no significant reduction in TNF-α level in the granulation tissue area in *Gp6*$^{-/-}$ + anti-podoplanin mice compared to IgG-treated *Gp6*$^{-/-}$ controls (Figure 3.22 C, D) possibly because of the pre-existing pro-inflammatory activity of GPVI (Pierre et al., 2017).

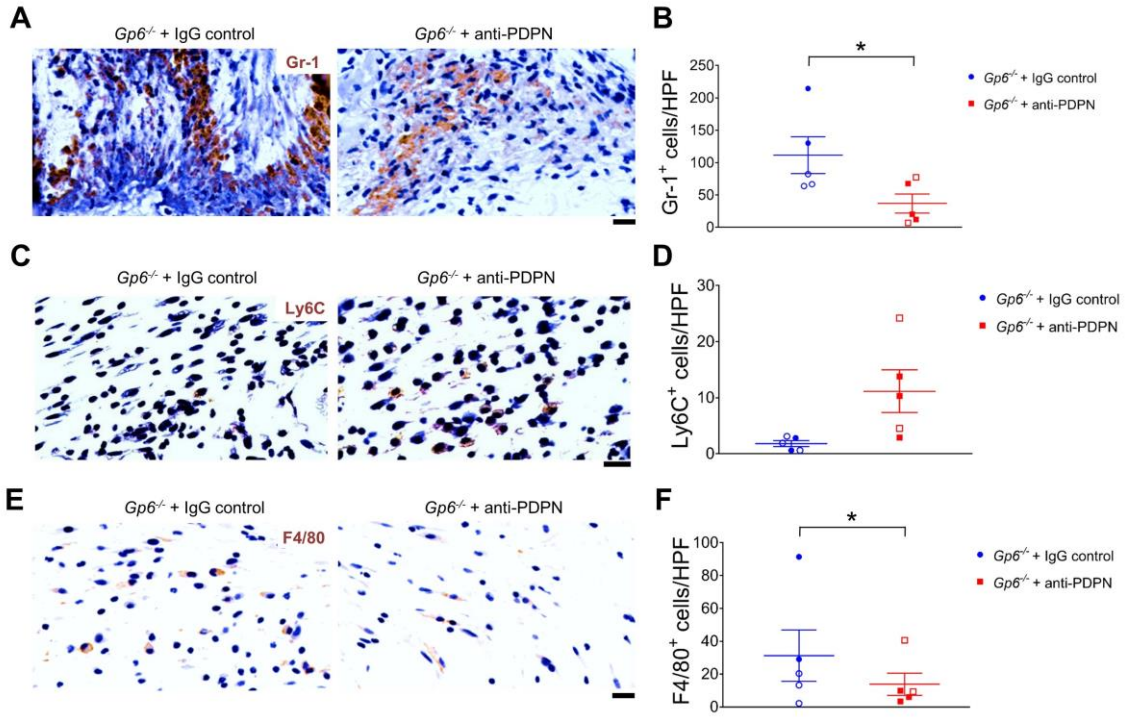

Figure 3. 21. Treating *Gp6*$^{-/-}$ mice with podoplanin-blocking antibody leads to a reduction in wound neutrophils and macrophages (but increase in monocytes) during the inflammatory phase. (A) Staining of neutrophils (Gr-1; brown) in wound area at day 3 post-injury. (B) Quantification of neutrophils (Gr-1^{+} cells) in wound area at day 3 post-injury (n=5). (C) Detection of Ly6C^{+} cells (brown) in wound at day 3 post-injury. (D) Quantification of Ly6C^{+} cells in wound at day 3 post-injury (n=5). (E) Detection of macrophages (F4/80 staining; brown) in wound area at day 3 post-injury. (F) Quantification of macrophages (F4/80^{+} cells) in wound area at day 3 post-injury (n=5). Data from females (open symbols) and males (closed symbols) are shown in (B, D, F). All graphs are presented as mean ± SEM and analysed by Student's t-test. *$p<0.05$. Scale bar = 20 µm.

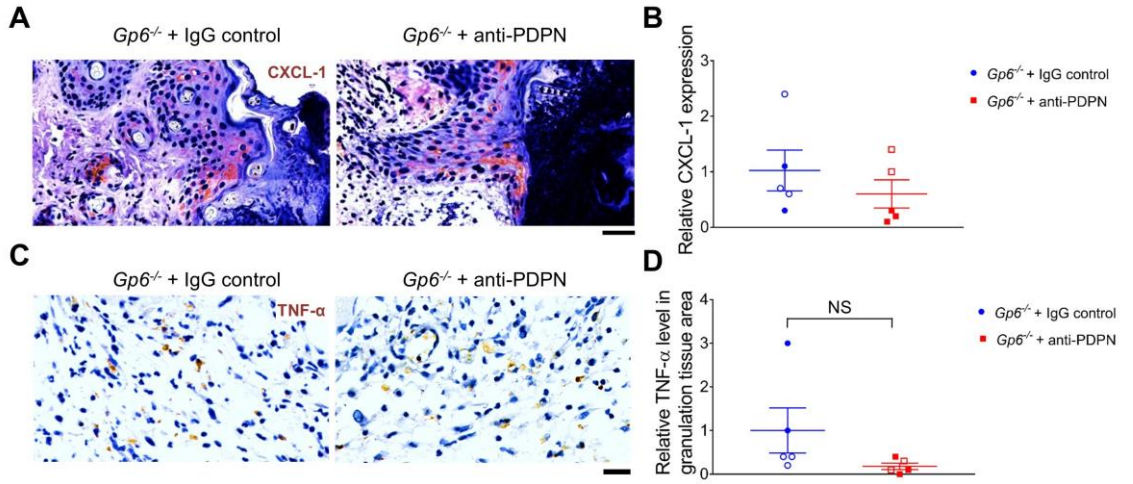

Figure 3. 22. Wound CXCL-1 and TNF-α are similar between *Gp6*$^{-/-}$ mice with and without anti-podoplanin antibody injection. (A) Detection of CXCL-1 (brown) in wound area at day 3 post-injury. Scale bar = 50 µm. (B) Quantification of keratinocyte-expressed CXCL-1 in wound at day 3 post-injury (n=5). (C) Immunohistochemistry staining of TNF-α (brown) in the wound at day 3 post-injury. Scale bar = 20 µm. (D) Quantification of TNF-α level in granulation tissue area (n=5). Data from females (open symbols) and males (closed symbols) are shown in (B) and (D). All graphs are presented as mean ± SEM and analysed by Student's t-test. NS = non-significant.

3.2.12 Platelet depletion results in severe haemorrhage following skin injury

It has previously been demonstrated that thrombocytopenia does not affect skin wound healing in mice (Szpaderska et al., 2003). To assess the haemostatic function of platelets, a pilot wound experiment in thrombocytopenic mice was investigated. Platelet depetion was performed by intravenous injection of anti-GPIb antibody 24 hours before skin biopsy. According to small sample numbers, a subjective interpretation was presented here. Immediately after biopsy where the mice were under general anesthesia, wound bleeding was minor (Figure 3.23). Once the mice started moving, the wound of severe thrombocytopenic mice (platelet count was lower than 70 x 10^3 cell/mm^3) showed persistent bleeding and had a severe haemorrhage, accompanied with impaired movement at 2 hours post-injury (Figure 3.23) whereas moderate thrombocytopenia had normal blood clot formation. The severe phenotype prevented further experimentation in this setting.

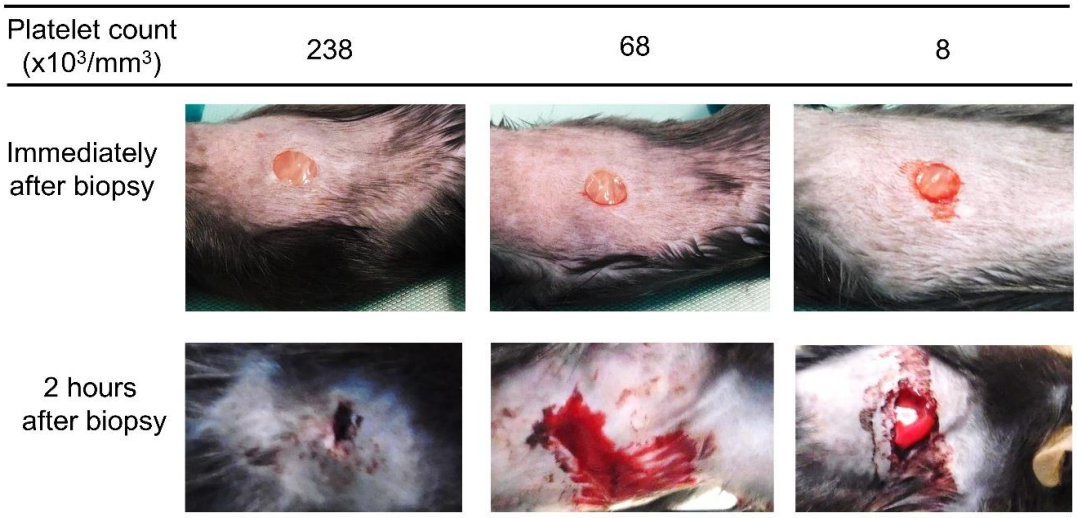

Figure 3. 23. Severe bleeding following skin injury in thrombocytopenic mice. All mice were intravenously injected with anti-GPIb antibody at 24 hours prior to skin biopsy. Platelet counts were measured before skin biopsy. The severity of platelet depletion depended on the extent of antibody that entered systemic circulation. Immediately after biopsy, minor bleeding at the wound site was observed in mice with platelet count lower than 70 x 10^3 cells/mm^3 (n=2). At 2 hours after biopsy, severe haemorrhage was observed in severe thrombocytopenic mice whereas normal blood clot was generated in moderate thrombocytopenia, which has platelet count higher than 200 x 10^3 cells/mm^3 (n=1).

3.3 Discussion

In this chapter, the data show that platelet CLEC-2 and GPVI double deficiency facilitates skin wound healing in mice, resulting in a smaller wound scar at the end. The accelerated wound closure is associated with a temporal and self-limited vascular leakage during the inflammatory phase, which promotes the deposition of fibrinogen and fibrin, accompanied by a reduced infiltration of leucocytes and enhanced re-epithelialisation and angiogenesis. A proposed model for multistep contribution of the accelerated wound healing in the absence of CLEC-2 and GPVI is summarised in Figure 3.24.

Skin wound healing requires multiple cellular and molecular contributions, including haemostasis (Drew et al., 2001, Shaw and Martin, 2009), vascular permeability that allows extravasation of plasma-derived solutes (Shaterian et al., 2009, Mendonca et al., 2010), the recruitment of inflammatory cells to remove invading microbes and cellular debris (Martin and Leibovich, 2005), the proliferation and migration of skin epithelial and stromal cells to regenerate skin tissue (Shaw and Martin, 2009, Pastar et al., 2014), and the synthesis of connective tissue to recover skin elasticity (Shaw and Martin, 2009). Combined deletion of CLEC-2 and GPVI in platelets does not affect classical haemostasis but results in transient bleeding into the wound during the inflammatory phase, which reflects the role of GPVI and CLEC-2 in rescuing vascular integrity in the skin at sites of inflammation (Gros et al., 2015, Rayes et al., 2018). The presence of collagen and podoplanin (i.e. on pericytes, fibroblasts, infiltrating monocytes, and macrophages), in contact with platelets, at perivascular area of skin also supports this function of the two (hemi)ITAM receptors.

A

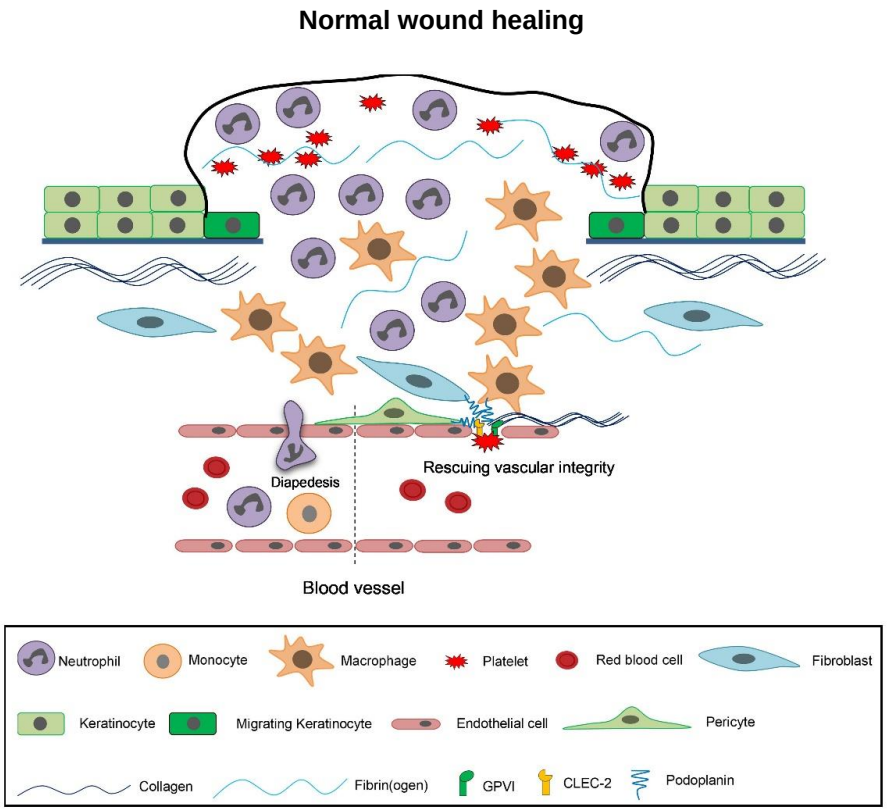

B

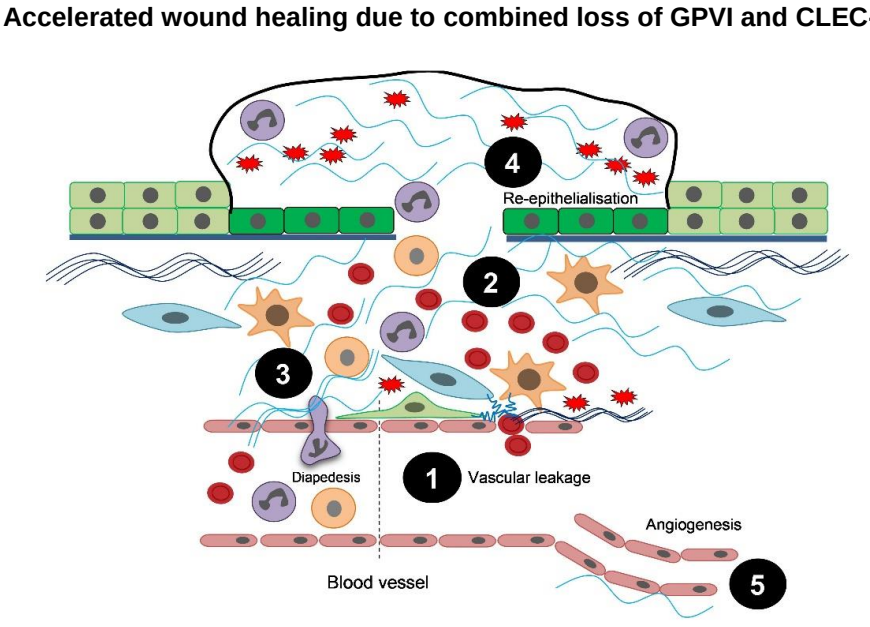

Figure 3.24.

Figure 3. 24. Proposed model for the multiple regulation of accelerated wound healing in the absence of GPVI and CLEC-2. (A) During the inflammatory phase of normal wound healing, GPVI binds collagen in subendothelial matrix underneath the vessel wall to safeguard vascular integrity following leucocyte diapedesis. CLEC-2 provides a backup function by binding to podoplanin that expressed on cells in proximity to the vessel wall, including pericytes, fibroblasts, infiltrating monocytes, and macrophages. (B) A lack of GPVI and CLEC-2 causes local and transient vascular leakage (1), which allows increased extravasation of fibrinogen into the wound (2) during the inflammatory phase of wound healing. In addition, other plasma-derived macromolecules (e.g. clotting factors, growth factors, and cytokines) may also entry into the wound. Tissue factor-expressing cells in wound area promote the conversion of fibrinogen to fibrin through extrinsic pathway of coagulation, which in turn facilitates wound healing. Moreover, a reduction in wound leucocytes during inflammatory phase is observed under ITAM-receptors deficiency, likely because of physical obstruction by fibrinogen and fibrin (3), which subsequently attenuates inflammation and tissue damage. Together, an increased vascular leakage-mediated accumulation of fibrinogen/fibrin matrix and a decrease in inflammation contribute to an accelerated skin wound healing, at least by promoting re-epithelialisation (4) and angiogenesis (5).

Several animal studies have previously demonstrated the benefits of increased vascular permeability, a less severe form of vascular leakage, in facilitating cutaneous wound healing. For example, histamine released from mast cells enhances vascular permeability during the inflammatory phase, which promotes wound healing (Weller et al., 2006). In addition, accelerated wound healing is observed in mice directly treated with histamine (Numata et al., 2006), VEGF (Howdieshell et al., 2001), and serum fraction of the natural latex from rubber tree (Mendonca et al., 2010), all of which increase vascular permeability. In contrast, antihistamine delays wound healing (Weller et al., 2006). Therefore, impairment of vascular integrity and enhanced vascular permeability caused by various mechanisms result in leakage of plasma-derived growth factors, cytokines, and proteins into the tissue, which potentially facilitates wound healing.

It is important to note that the cause of increase in vascular leakage was not due to a defect in coagulation. On one hand, continuous intra-tissue bleeding due to a defect in blood coagulation impairs wound healing. In hemophilia B mice (lack of FIX) (Hoffman et al., 2006) or mice expressing low tissue factor (Monroe et al., 2010), persistent subcutaneous bleeding arises, in association with a reduction in fibrin generation, which leads to haematoma formation within the wound, contributing to delayed wound healing. On the other hand, the increased bleeding into the wound in the context of GPVI and CLEC-2 deficiency arises only at initial stage and it is ceased in later phase of repair when the inflammation subsides. In addition, there is an increase in fibrinogen accumulation and fibrin generation, in the presence of an intact tissue factor within the wound, under platelet CLEC-2 and GPVI double deficient setting. Therefore, it is likely that the mechanism and characteristics of bleeding direct its consequences in wound healing. Indeed, the temporal and self-limited intra-skin bleeding following GPVI and CLEC-2 deficiency is associated

with accelerated wound healing. A similar result of wound healing is observed in *Gp6*$^{-/-}$ mice treated with a podoplanin-blocking antibody, which negates the influences of blood/lymphatic mixing and the reduced platelet counts in wound healing of DKO mice. By using this antibody, it also demonstrates the contribution of CLEC-2-podoplanin interaction, especially in the regulation of vascular integrity during skin wound healing, in addition to GPVI. Moreover, it has been already demonstrated that anti-podoplanin antibody inhibits CLEC-2 interaction to podoplanin *in vivo*, including in dermatitis (Rayes et al., 2018), deep vein thrombosis (Payne et al., 2017) and sepsis (Rayes et al., 2017). In a murine model of dermatitis, anti-podoplanin antibody also enhances vascular leakage in *Gp6*$^{-/-}$ mice (Rayes et al., 2018). These results support that treatment of *Gp6*$^{-/-}$ mice with anti-podoplanin antibody blocks CLEC-2 interaction to podoplanin, which mimics the GPVI and CLEC-2 double deficient setting during skin wound healing.

Fibrinogen and fibrin not only function for clot formation, but also act as provisional matrix for cell migration, a reservoir for accumulation of growth factors and cytokines, and a natural suture/sealant during wound healing (Brown et al., 1992, Drew et al., 2001). In DKO setting, deposition of fibrinogen and fibrin in the inflammatory phase may enhance migration of keratinocytes (Ronfard and Barrandon, 2001) and endothelial cells (Chalupowicz et al., 1995, Sahni and Francis, 2000), contributing to the accelerated progression of re-epithelialisation and angiogenesis during wound healing.

However, fibrinogen/fibrin matrix appears to inhibit neutrophil and monocyte recruitment. Fibrinogen (Higazi et al., 1994) and a high concentration of fibrin (Hanson and Quinn, 2002) have been reported to inhibit neutrophil chemotaxis, which is similar to the results of *in vitro* neutrophil chemotaxis presented in this chapter. In addition,

fibrinogen shows *in vitro* anti-adhesive effect against monocytes (Lishko et al., 2007). In agreement with the finding in DKO animals, wound neutrophils and monocytes are not altered at day 1 post-injury where the fibrinogen/fibrin content is identical to WT controls. Rather, a decrease in wound neutrophils and M1 macrophages is present in the inflammatory phase of wound repair where fibrinogen/fibrin content is increased in DKO mice. Moreover, the higher number of wound monocytes is detected, which may further suggest a reduction in monocyte-to-M1 macrophage differentiation in DKO animals. Previous studies have shown that TNF-α secretion is elevated during monocyte-to-macrophage differentiation (Francke et al., 2011, Crane et al., 2014, Vasamsetti et al., 2015). Therefore, a reduction in TNF-α level, in association with increased fibrinogen/fibrin deposition, during the inflammatory phase may explain a decrease in monocyte-to-M1 macrophage transition in DKO mice.

It is no doubt that leucocytes are important for pathogen killing during wound healing (Kim et al., 2008, Chen et al., 2018). However, several lines of evidence demonstrate that inflammatory cells may not be essential in wound healing as long as the wound is kept sterile (Hopkinson-Woolley et al., 1994, Dovi et al., 2003, Martin et al., 2003). Indeed, improved wound healing is observed in neutrophil-depleted conditions (Dovi et al., 2003, Mori et al., 2002, Wong et al., 2015). Neutrophil can cause tissue damage and delay wound healing through several mechanisms, including a production of proteases (Dovi et al., 2003), inflammatory cytokines and oxidative radicals (Wilgus et al., 2013), and NETs (Wong et al., 2015). In addition, macrophage depletion model in mice demonstrates that a lack of macrophages within the first five days does not significantly affect wound closure during the inflammatory phase (day 1-3) but rather delays the later stages of wound closure (Lucas et al., 2010), which is related to a decrease in M2 macrophages. In

DKO mice, there was no alteration in M2 macrophages during the course of wound healing, but a decrease in M1 macrophages in the early phase may contribute to a reduction in scar formation, which is resemble to the finding in previous study (Lucas et al., 2010).

A prolonged/excessive accumulation of extravascular fibrin can induce skin fibrosis (de Giorgio-Miller et al., 2005). Therefore, fibrinolysis and fibrin degradation are also important for repair process, which have been previously demonstrated to promote wound healing (Romer et al., 1996, Chan et al., 2001). Macrophages have also been reported to mediate clearance of extravascular fibrin (Motley et al., 2016) and Rbcs (Yin et al., 2015). During wound healing in DKO mice, extravascular fibrin and Rbcs were completely removed in the later phases, suggesting no risk of skin fibrosis.

A reduction in leucocyte infiltration might raise the concern of wound contamination. However, a recent study has shown that a rapid fibrin film formation over the surface of the wound plays a protective function against bacterial invasion (Macrae et al., 2018). This mechanism might also limit the need for leucocyte infiltration to eliminate pathogens. Although it has previously been reported that *Staphylococcus aureus* infection leads to a two-fold increase in wound neutrophils (Kim et al., 2008), this has not yet been investigated in DKO mice. Further studies are required to test whether targeting GPVI and CLEC-2 might increase the risk of wound infection.

Taken together, this study demonstrates that a local and self-limited intra-skin bleeding caused by loss of GPVI and CLEC-2 provides potential benefits in wound healing. Unlike the persistent bleeding due to a lack of fibrin generation in coagulation-deficient mice, the increased vascular leakage following platelet GPVI and CLEC-2 deficiency results in fibrinogen/fibrin deposition and reduced leucocyte infiltration, which promotes wound healing. Therefore, these findings may present the potential implication of targeting platelet CLEC-2 and GPVI to facilitate wound healing and reduce scar formation.

Chapter 4 Characterisation of the CRISPR/Cas9-generated Podoplanin Cytoplasmic Tail Deficient Mouse Model

4.1 Introduction

Podoplanin is the only known endogenous ligand for CLEC-2 (Pan and Xia, 2015). This mucin type transmembrane glycoprotein comprises of 172 and 162 amino acids in mice and humans, respectively (Pan and Xia, 2015), which is expressed on podocytes, LECs, and type I lung epithelial cells, and is upregulated on inflammatory macrophages, fibroblasts, T cells and many cancer cells (Kerrigan et al., 2012, Peters et al., 2015, Nylander et al., 2017, Retzbach et al., 2018). The extracellular domain of podoplanin contains repeat regions known as PLAG domains, a heavily O-glycosylated stalk, and a short cytoplasmic tail of 10 amino acids (Figure 4.1). The binding of podoplanin to CLEC-2 requires the electrostatic interaction between a conserved EDXXXT/S sequence in PLAG and four arginine residues in CLEC-2 to mediate platelet aggregation (Kaneko et al., 2006, Nagae et al., 2014). The cytoplasmic tail of podoplanin contains three basic residues crucial for the binding of ERM proteins, which further activate downstream signals to regulate cell migration and function (Pan and Xia, 2015, Astarita et al., 2012).

The vast majority of experimental studies demonstrate the role of the extracellular domains of podoplanin for the activation of CLEC-2. For example, podoplanin has been shown to activate CLEC-2 on platelets and mediate platelet aggregation, preventing

backfilling of blood into lymphatic (Bertozzi et al., 2010, Hess et al., 2014). Podoplanin can also interact with several lateral membrane proteins to mediate cellular function, including (1) the binding with CD44 on tumour cells, which promotes cell migration (Martin-Villar et al., 2010), (2) the association with galectin-8 on LECs, subsequently regulates LEC adhesion to the surrounding ECM during lymphvasculogenesis (Cueni and Detmar, 2009), and (3) the interaction with tetraspanin family member CD9 to inhibit podoplanin-induced platelet aggregation, attenuating cancer metastasis (Nakazawa et al., 2008). CLEC-2 is also proposed to inhibit lateral interaction of podoplanin in mediating fibroblastic reticular cell (FRC) contraction, leading to lymph node expansion during immunisation (Astarita et al., 2015).

Moreover, soluble factors physically bind to podoplanin and modulate biological function. For example, CCL21, a leucocyte chemoattractant found in secondary lymphoid organs and tumour microenvironment, has been reported to bind podoplanin on LECs, FRCs, and cancer-associated fibroblasts. This interaction promotes the binding of CCL21 to its receptor, the CCR7, on leucocytes and tumour cells, contributing to leucocyte trafficking and tumour cell migration (Astarita et al., 2012, Tejchman et al., 2017). Heat shock protein A9 secreted from cancer cells also binds podoplanin, promoting cancer cell growth and invasion (Tsuneki et al., 2013). In addition, nerve growth factor has been shown to interact with podoplanin on hippocampal neurons, which promotes neuritogenesis, facilitating learning and memory (Cicvaric et al., 2016).

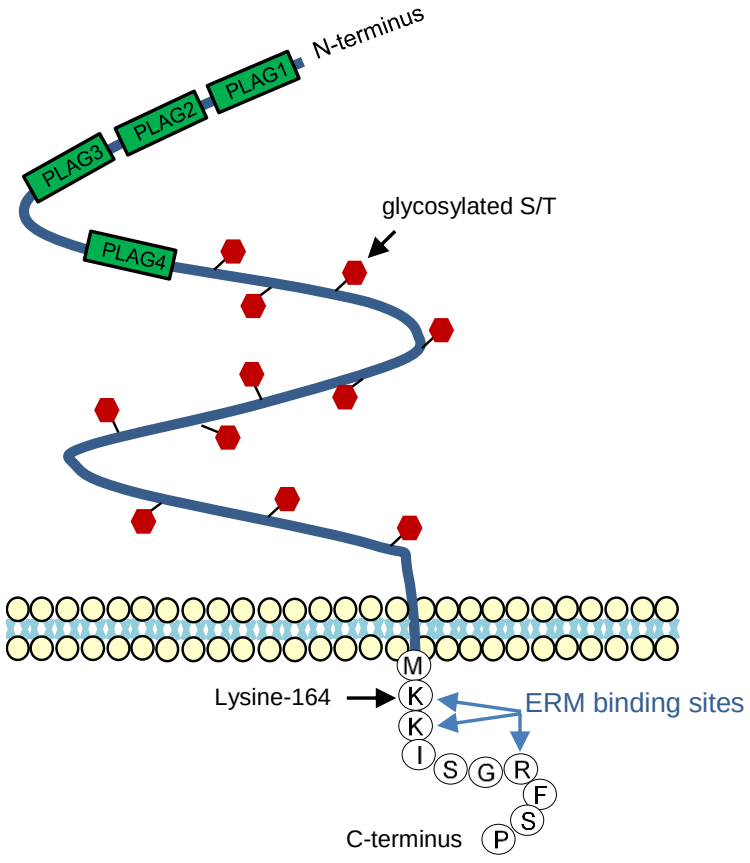

Figure 4. 1. Schematic representation of murine podoplanin structure. Serine (S) and threonine (T) residues in extracellular region of podoplanin are extensively glycosylated. The conserved EDXXXT/S sequence within platelet aggregation-stimulating (PLAG) domain is a potential binding site for CLEC-2. Three basic residues, comprising lysine (K) and arginine (R), in cytoplasmic tail of podoplanin act as binding sites for ERM proteins. Podoplanin can signal through ERM phosphorylation, which subsequently mediate cellular function (e.g. cell migration). Adapted from (Pan and Xia, 2015, Astarita et al., 2012, Kaneko et al., 2006, Nagae et al., 2014).

Interestingly, the interaction of CLEC-2 with podoplanin under (patho)physiological conditions is primarily associated with the upregulation of podoplanin, although it is unclear whether these effects are mediated through podoplanin signalling in the intracellular tail or the changes of its interaction with other lateral membrane proteins. A previous model of podoplanin cytoplasmic tail deficiency, called 'Δcyto', has been generated (Astarita et al., 2015) by inserting three STOP codons immediately after the sequence encoding lysine-164 (K164) within exon 5 of *Pdpn* (slightly different locus to the model in this thesis). These mice did not show physical abnormalities although it was noted that podoplanin expression was reduced in FRCs. In addition, the phosphorylated ezrin/radixin/moesin (ERM) level in FRCs of Δcyto mice was unaltered whereas it was reduced in FRCs of constitutive podoplanin knockout ($Pdpn^{-/-}$) mice. Moreover, there was no clear evidence of blood-filled lymphatics in these mice (Astarita et al., 2015), arguing against the roles of podoplanin cytoplasmic tail in inhibiting LEC migration during blood-lymphatic separation (Pollitt et al., 2014).

During skin wound healing, podoplanin is upregulated in various cell types, including in the proliferating/migrating keratinocytes, and it is recovered when the wound is completely healed. A previous report has demonstrated that the increased expression of keratinocyte podoplanin is related to the progression of re-epithelialisation to resurface skin epidermis (Asai et al., 2016). In this model, platelets are present in proximity to podoplanin-expressing cells at day 1 post-injury, which may function in limiting keratinocyte migration at initial period while waiting the preparation of wound bed. In the absence of platelets, podoplanin is speculated to mediate keratinocyte migration in later phases of wound healing (Asai et al., 2016). However, keratinocyte-specific

podoplanin knockout mice display a normal skin wound closure, suggesting non-essential function of keratinocyte-derived podoplanin in skin wound healing (Baars et al., 2015). Another aspect of CLEC-2-podoplanin interaction in wound healing is illustrated by a significant acceleration in skin wound healing following a single intradermal injection of human podoplanin-positive monocytes in combination with platelets around the wound edge in mice (Hur et al., 2014). A proposed mechanism of improved wound healing underlying this model is the observation of enhanced lymphangiogenesis at day 7 post-injury, which may help draining the inflammatory component (Hur et al., 2014). However, the accelerated wound closure begins at the early phase (day 3 post-injury), suggesting other potential mechanisms that may have promoted wound healing in this setting.

The global deletion of podoplanin in mice leads to perinatal death (Uhrin et al., 2010), limiting its uses for investigating podoplanin function in adulthood. To examine the significance of podoplanin signalling through its cytoplasmic tail *in vivo*, a novel *PdpnCyto* mouse model was generated and characterised. This model of mutated podoplanin was produced by Taconic Biosciences using CRISPR/Cas9 technology, which constitutively inserts three stop codons immediately before the nucleotide sequence encoding K164 located in exon 5 of *Pdpn* gene (Figure 4.1 and 4.2 A). Mice were monitored for viability and inheritance, haematological parameters, the evidence of blood-lymphatic mixing and leucocyte infiltrates within specific organs alongside WT and CELC-2 deficient animals. In addition, skin wound experiment was performed to examine the contribution of podoplanin cytoplasmic tail in wound repair.

4.2 Results

4.2.1 Identification of the podoplanin cytoplasmic tail deficient mice

In addition to the insertion of three stop codons, the nucleotide sequence containing A to C mutation (A AGATT→A AGCTT) designed as a site for HindIII restriction enzyme (Loenen, Dryden et al. 2014) was introduced during CRISPR/Cas9-mediated gene editing (Figure 4.2 B). Therefore, mutated *Pdpn* alleles can be cleaved into two fragments by HindIII enzyme. Genotyping using PCR that amplifies the sequences encoding cytoplasmic domain of podoplanin, followed by HindIII digestion revealed that in WT mice that lack HindIII restriction site, a single PCR product was present at 496 base pair (bp) on agarose gel following gel electrophoresis (Figure 4.2 C). The DNA samples derived from homozygous podoplanin cytoplasmic tail deficient (*PdpnCyto*$^{-/-}$) animals was digested by HindIII and gave rise to two bands of nucleotide fragments at the size of 327 bp and 176 bp (Figure 4.2 C). The heterozygous littermates (*PdpnCyto*$^{+/-}$) that had both intact and mutated *Pdpn* alleles demonstrated three PCR bands at 496, 327, and 176 bp, respectively (Figure 4.2 C). The incomplete HindIII digestion may cause false negative results during genotyping, in which three PCR bands might also be detected from *PdpnCyto*$^{-/-}$ samples.

Moreover, in order to confirm whether the samples are classified in correct genotypes, PCR products were further amplified and identified using the Sanger method of DNA sequencing. The results showed there was no stop codons detected in the exon 5 of *Pdpn* gene in WT mice (Figure 4.3, upper). In *PdpnCyto*$^{-/-}$ mice, three stop codons were observed, accompanied with the A to C mutation for HindIII restriction site (Figure 4.3,

middle). The *PdpnCyto*$^{+/-}$ mice exhibited a mixed nucleotide sequence that indicated stop codons and A to C mutation in overlap with the sequence identical to WT controls (Figure 4.3, lower).

4.2.2 Podoplanin cytoplasmic tail deficient colony shows Mendelian inheritance

To set up the *PdpnCyto* colony, *PdpnCyto*$^{-/-}$ females were bred out with WT C57BL/6 males to generate *PdpnCyto*$^{+/-}$ offspring. Then, the breeding pairs of *PdpnCyto*$^{+/-}$ parents were set to maintain the colony that was expected to give approximately 25 % of either WT or *PdpnCyto*$^{-/-}$ mice and 50% of *PdpnCyto*$^{+/-}$ mice, according to Mendelian genetics (Figure 4.4). In total, 22 litters were monitored. The analysis showed that 47 pups (25%) died during pre-wean (age less than 3 weeks). The total number of mice that survived was 138 animals, which comprised of 18% of WT, 57% of *PdpnCyto*$^{+/-}$, and 25% of *PdpnCyto*$^{-/-}$ mice, respectively (Figure 4.5 A), suggesting that the *PdpnCyto* colony was born at Mendelian frequency. There was no significant difference between the expected numbers and the actual numbers as assessed using Chi-squared test. However, the *PdpnCyto*$^{-/-}$ females were more prevalent than males (Figure 4.5 B).

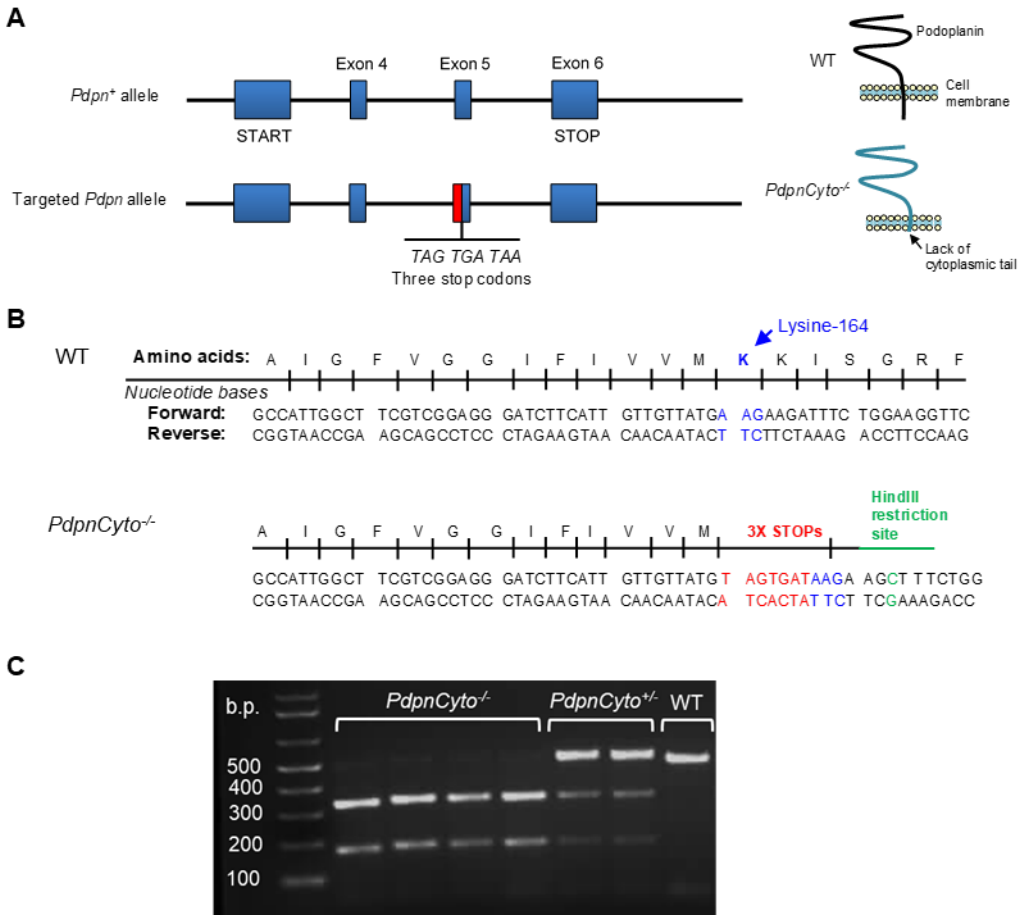

Figure 4. 2. Generation and identification of podoplanin cytoplasmic tail deficient mice. (A) Schematic demonstration of CRISPR/Cas9-mediated podoplanin cytoplasmic tail deficiency. Three STOP codons are constitutively inserted immediately before the sequence encoding lysine-164 located in exon 5 of *Pdpn*. (B) Representative nucleotide sequence within exon 5 of *Pdpn* in WT mice (upper) and *PdpnCyto*$^{-/-}$ mice (lower), which comprises of three stop codons and A to C mutation for HindIII restriction site. (C) PCR bands on agarose gel indicating the genotyping results to identify WT, *PdpnCyto*$^{+/-}$, and *PdpnCyto*$^{-/-}$ mice. WT mice show a single PCR band at 496 bp. *PdpnCyto*$^{+/-}$ mice exhibit three bands at 496, 327, and 176 bp whereas there are two PCR bands at 327 and 176 bp in *PdpnCyto*$^{-/-}$ mice.

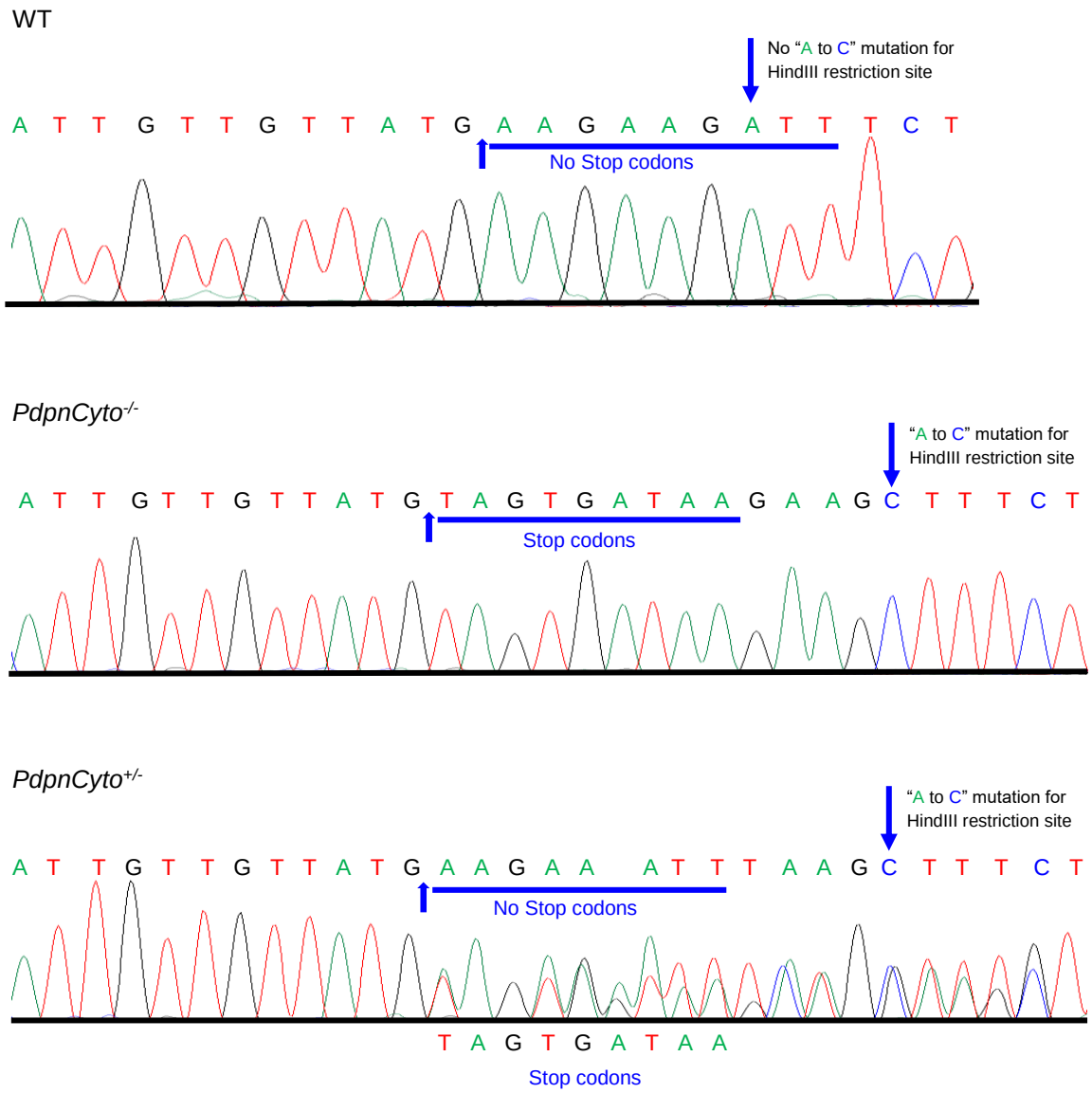

Figure 4. 3. DNA Sequencing of the podoplanin cytoplasmic tail deficient mice. Sequence of PCR fragments amplified from DNA of WT mice (upper) shows no stop codons in exon 5 of *Pdpn*. The *PdpnCyto*$^{-/-}$ mice (middle) have three stop codons and the A to C mutation for HindIII restriction site. In *PdpnCyto*$^{+/-}$ mice (lower), the nucleotide sequence consisting stop codons and A to C mutation similar to *PdpnCyto*$^{-/-}$ mice are detected in combination with the normal sequences identical to WT mice.

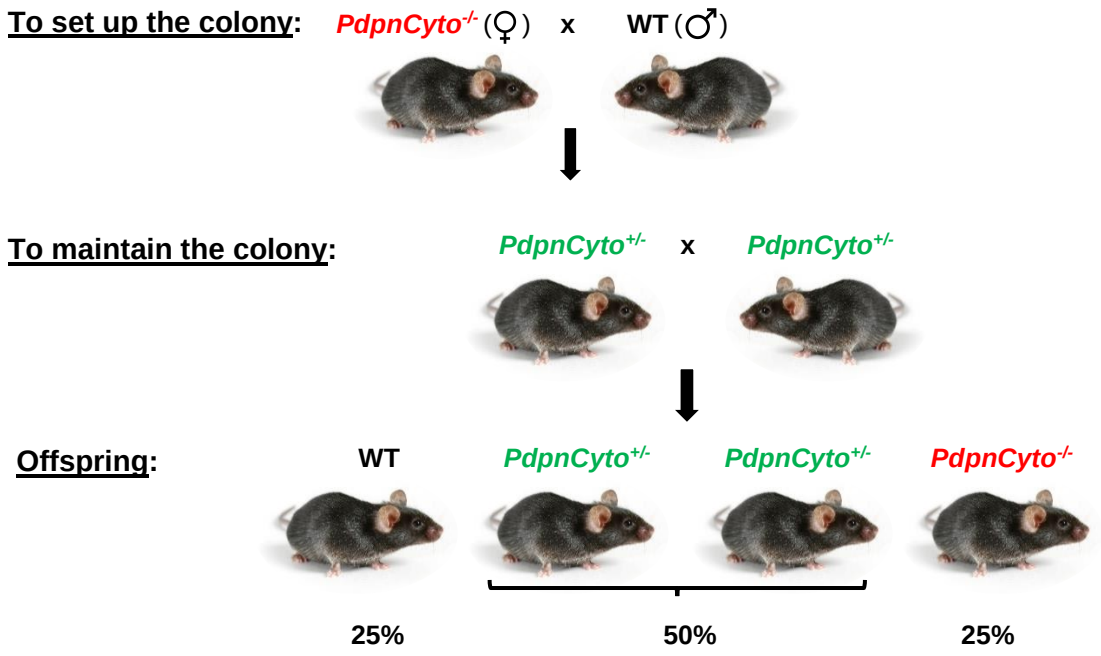

Figure 4. 4. Generation and maintenance of podoplanin cytoplasmic tail deficient colony. Homozygous podoplanin cytoplasmic tail deficient (*PdpnCyto*$^{-/-}$) females were bred with WT C57BL/6 males to produce the first generation containing all heterozygous podoplanin cytoplasmic tail deficient (*PdpnCyto*$^{+/-}$) mice. Then, the breeding pairs of *PdpnCyto*$^{+/-}$ parents were set to maintain the colony. The excepted offspring is according to Mendelian inheritance, which includes 25% of either WT or *PdpnCyto*$^{-/-}$ and 50% of *PdpnCyto*$^{+/-}$ mice.

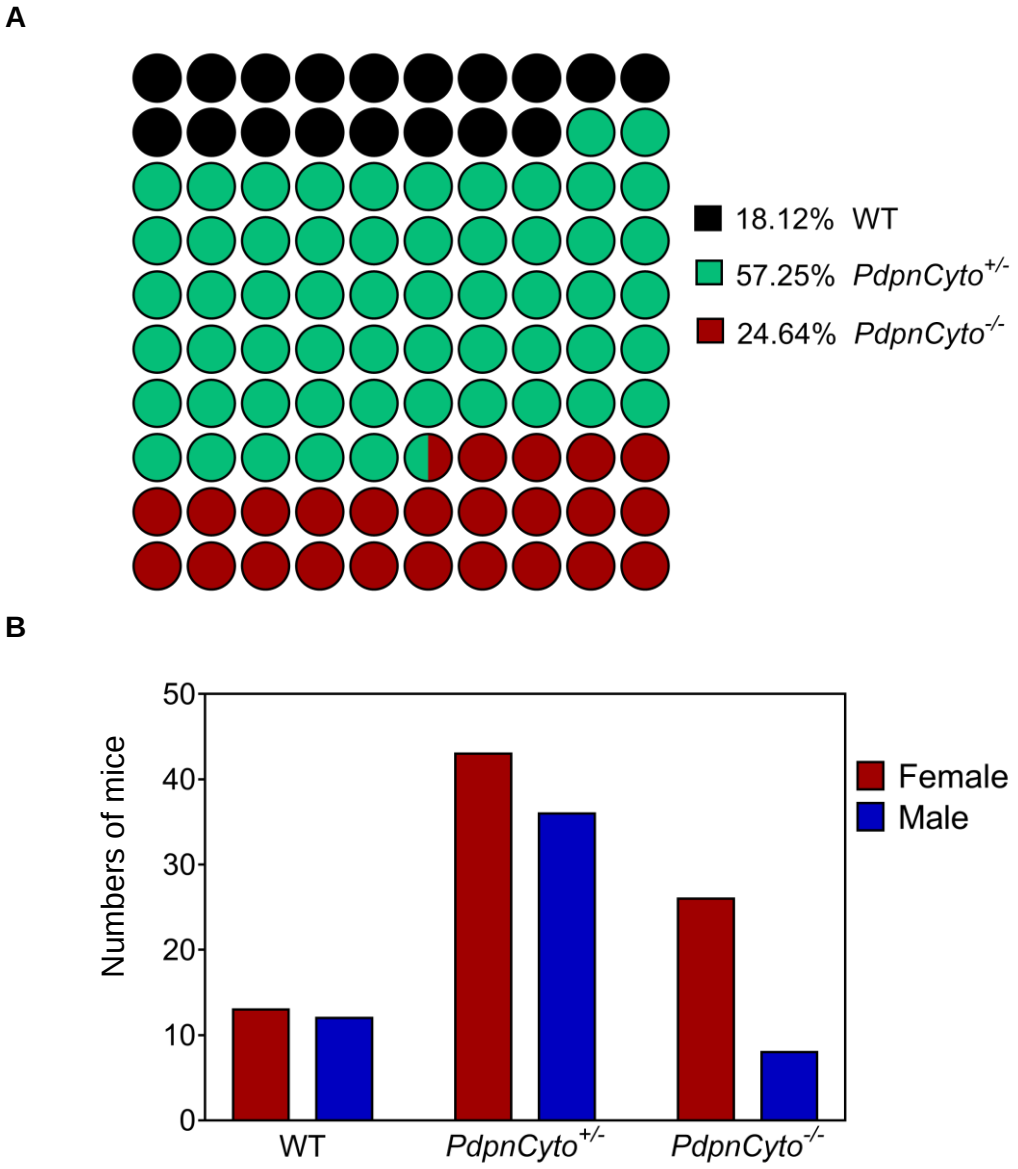

Figure 4. 5. Viability and inheritance of the podoplanin cytoplasmic tail deficient mice. (A) Frequency of genotypes observed in podoplanin cytoplasmic tail deficient colony suggests Mendelian inheritance. The offspring born from heterozygous podoplanin mutant parents (total 138 mice) include 18% of WT, 57% of *PdpnCyto*$^{+/-}$, and 25% of *PdpnCyto*$^{-/-}$ mice, respectively, which are not significantly different from the expected amounts. Data are analysed by Chi-squared test. (B) Numbers of male and female mice in each genotype from podoplanin cytoplasmic tail deficient colony.

4.2.3 Podoplanin cytoplasmic tail deficient embryos demonstrate an increased vasodilation and occasionally develop a mild degree of blood-filled skin vessels

Previous studies have reported that global podoplanin knockout embryos show blood-filled cutaneous vessels and extravasation of blood, indicating blood-lymphatic misconnection and the impairment of vascular integrity, respectively. The severity of the phenotype increased with age (E12.5-E16.5) (Bertozzi, Schmaier et al. 2010, Uhrin, Zaujec et al. 2010, Lowe, Finney et al. 2015). To examine the contribution of podoplanin cytoplasmic tail in the development of blood and lymphatic separation, embryos were taken from *PdpnCyto*$^{+/-}$ mothers at E14.5. Macroscopic observation revealed normal skin appearance in WT embryos (Figure 4.6 A). High proportion of both heterozygous (70%) and homozygous (90%) podoplanin mutant embryos displayed an increased vasodilation without vascular leakage around the head and face areas (Figure 4.6 B). Only a few number of *PdpnCyto*$^{-/-}$ embryos (25%) showed a limited degree of blood-filled cutaneous vessels during this stage, compared to WT (Figure 4.6 C).

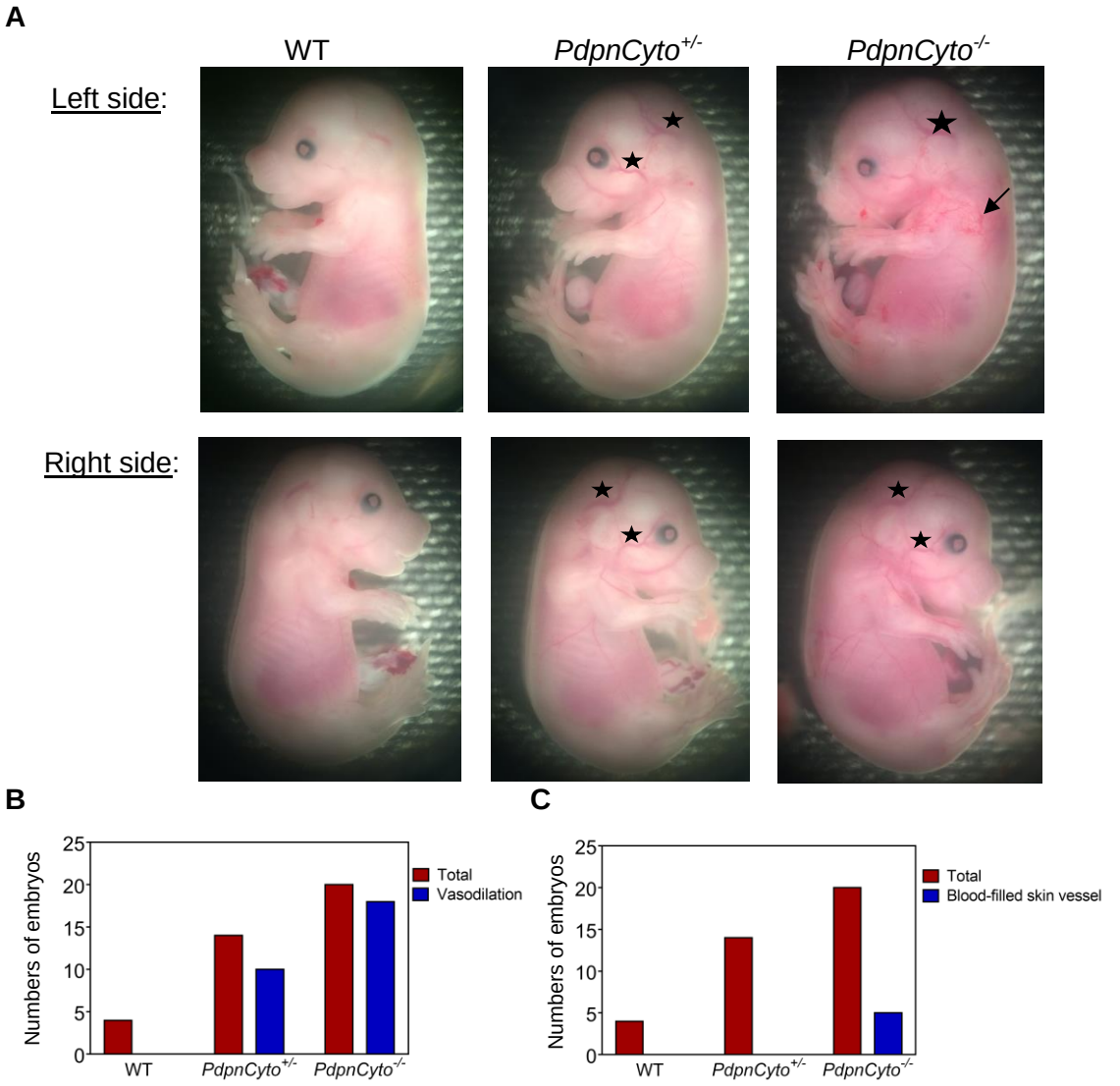

Figure 4. 6. Embryos taken from podoplanin cytoplasmic tail deficient colony at E14.5 show minor degree of gross abnormalities. (A) Macroscopic appearance of E14.5 embryos. There were no gross abnormalities in WT embryos. The increased vasodilation is observed (star) around the head and face areas in *PdpnCyto*$^{+/-}$ and *PdpnCyto*$^{-/-}$ embryos. The mild form of blood-filled cutaneous vessels (arrow) is also detected in a small number of *PdpnCyto*$^{-/-}$ embryos. The prevalence of increased vasodilation and blood-filled cutaneous vessels in embryos are shown in (B) and (C), respectively.

4.2.4 Normal podoplanin expression is detected at E14.5 in podoplanin cytoplasmic tail deficient embryos

To examine whether the novel model of podoplanin cytoplasmic tail deficiency affects global podoplanin expression, immunohistochemistry staining of podoplanin was performed in E14.5 embryos. It has previously been reported in mice that podoplanin is present at choroid plexus in the brain (Kaji et al., 2012) and the developing alveolar epithelial cells (Millien et al., 2006). In *PdpnCyto*$^{-/-}$ embryos, the result showed no apparent alteration in podoplanin expression at choroid plexus and surrounding neuroepithelium of the developing brain relative to WT embryos (Figure 4.7 A). In a similar manner, podoplanin expression in the developing lung of *PdpnCyto*$^{-/-}$ embryos was equivalent to that of WT controls (Figure 4.7 B), suggesting it is no defect in surface expression of the podoplanin extracellular domain during embryonic development in this mouse model.

4.2.5 Homozygous podoplanin cytoplasmic tail deficient mice show a reduction in blood monocytes but an increase in lymphocytes

In contrast to global podoplanin knockout mice that generally die before or immediately at birth (Uhrin et al., 2010), the *PdpnCyto*$^{-/-}$ animals are viable after birth in the absence of any detectable gross abnormalities, which allow studying the role of podoplanin, especially its cytoplasmic tail, in adulthood. *PdpnCyto*$^{-/-}$ mice were further characterised in comparison to their littermate control alongside with platelet CLEC-2 deficient mice. Blood cell counts in adult *PdpnCyto*$^{-/-}$ mice demonstrated a small increase in red blood cells (Figure 4.8 A), and a normal platelets count (Figure 4.8 B), compared to WT mice.

Although total white blood cell counts (Figure 4.8 C) and neutrophils (Figure 4.8 D) in the blood were not altered, the percentage of monocytes from total leucocytes (Figure 4.8 E) was significantly reduced in *PdpnCyto*$^{-/-}$ mice. In contrast, the percentage of circulating lymphocytes were increased in *PdpnCyto*$^{-/-}$ mice relative to WT littermates (Figure 4.8 F).

4.2.6 A reduction in cardiac-to-body weight ratio is observed in mice that lack podoplanin cytoplasmic tail

The change in organ-to-body weight ratio is one of an important indicator for organ toxicity, such as hypertrophy and hyperplasia (Michael et al., 2007, Mubbunu et al., 2018). The lack of podoplanin has also been reported to affect cellularity of many internal organs, including the lung, liver, and spleen (Peters et al., 2015). In comparison to WT littermates, no significant changes in the organ-to-body weight ratio of multiple organs, including the liver (Figure 4.9 A), kidney (Figure 4.9 B), spleen (Figure 4.9 C), and lung (Figure 4.9 D) were observed in *PdpnCyto*$^{-/-}$ animals. However, the heart-to-body weight ratio was decreased in the *PdpnCyto*$^{-/-}$ mice compared to WT mice (Figure 4.9 E).

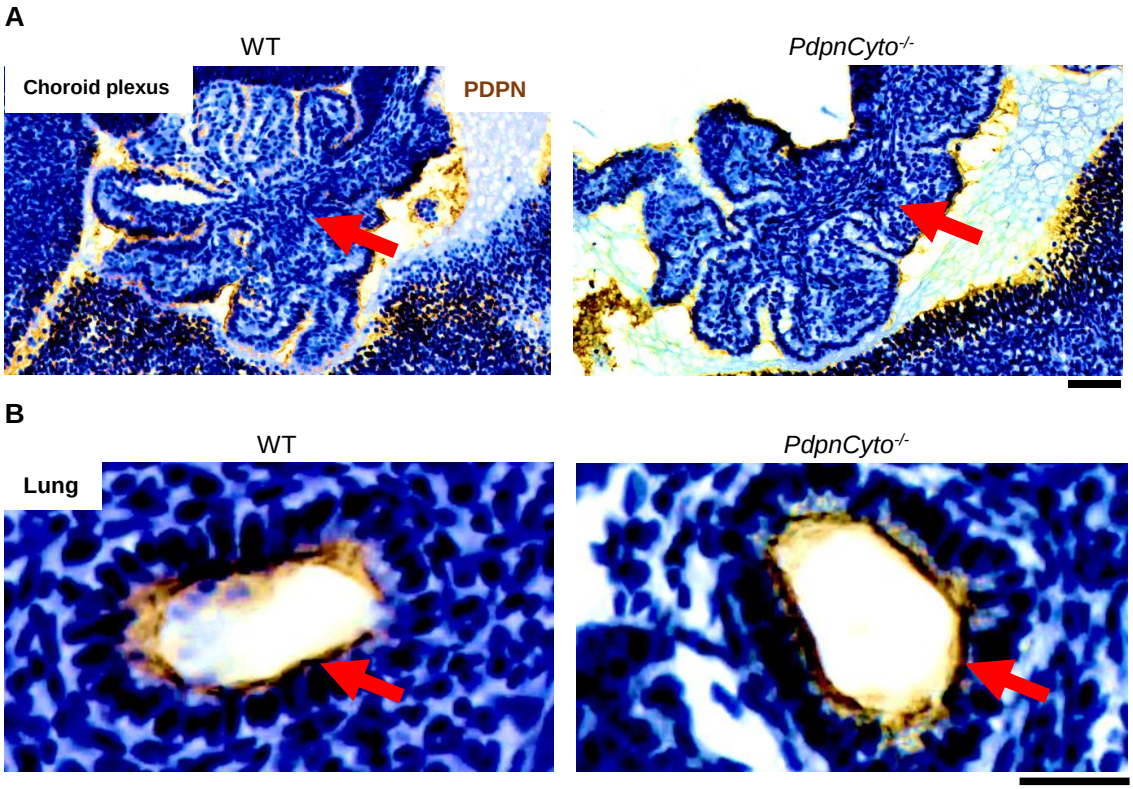

Figure 4. 7. Extracellular domain of podoplanin is normally detected in podoplanin cytoplamic tail deficient embryos at E14.5. (A) Immunohistochemistry shows podoplanin expression (brown) at choroid plexus and surrounding neuroepithelium in the developing brain (n=3). Arrow points to choroid plexus. Scale bar = 50 µm. (B) Immunohistochemistry of podoplanin (brown) in the developing lung (n=3). Arrow indicates developing alveolar epithelial cells. Scale bar = 20 µm.

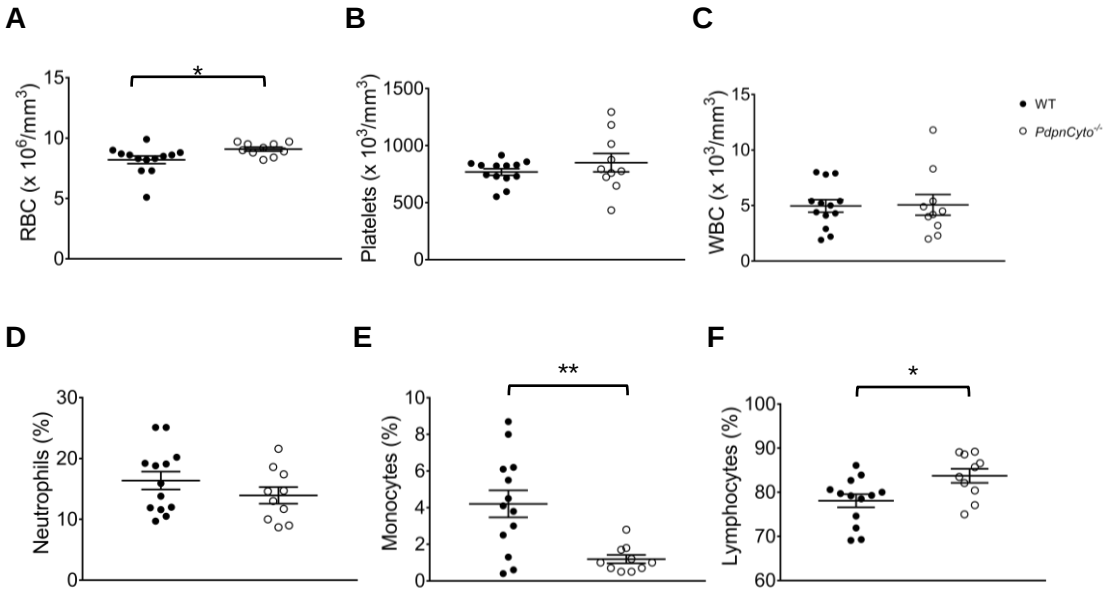

Figure 4. 8. A reduction in circulating monocytes and an increase in lymphocytes are observed in homozygous podoplanin cytoplasmic tail deficient mice. Complete blood counts of WT (n=13) and *PdpnCyto*$^{-/-}$ mice (n=10) are presented as mean ± SEM, including (A) red blood cells (RBC), (B) platelets, (C) white blood cells (WBC), (D) neutrophils, (E) monocytes, and (F) lymphocytes. Data are analysed by Student's t-test. **p*<0.05, ***p*<0.01.

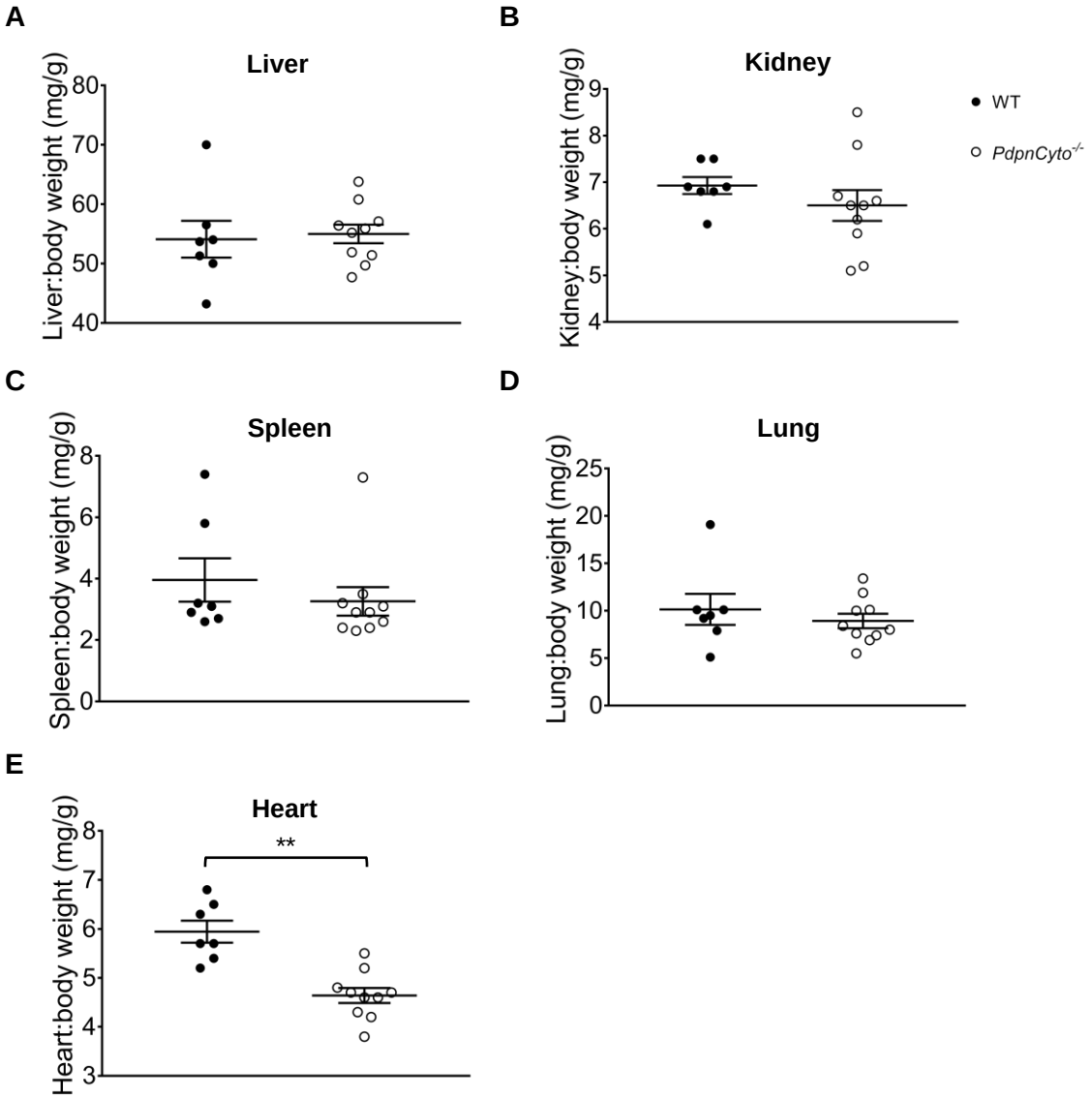

Figure 4. 9. Cardiac-to-body weight ratio is reduced in podoplanin cytoplasmic tail deficient mice. The mean ± SEM of organ-to-body weight ratios are presented, including (A) liver, (B) kidney, (C) spleen, (D) lung, and (E) heart, respectively. Data are analysed by Student's t-test. $^{**}p<0.01$.

4.2.7 Podoplanin expression is downregulated in multiple organs of the adult podoplanin cytoplasmic tail deficient mice

In the previous study using a murine model of podoplanin cytoplasmic tail deficiency, it has been stated that podoplanin expression in FRCs is normal. However, the data of both surface and total podoplanin expression in FRCs derived from these podoplanin mutated mice indicate partial loss of podoplanin expression (Astarita et al., 2015). To determine the expression of podoplanin in different organs, an anti-podoplanin antibody that recognises the extracellular domain of podoplanin (clone 8.1.1) was used and podoplanin expression was assessed using immunohistochemistry (Pan et al., 2014). In WT lung, podoplanin was highly expressed, especially on type I alveolar epithelial cells. Podoplanin was also detected on LECs and possibly other stromal cells in the lung (Figure 4.10 A). In *PdpnCyto*$^{-/-}$ mice, the expression of podoplanin in the lung was decreased, accompanied with increased leucocyte infiltrates around the blood vessels and respiratory tract (Figure 4.10 A, star). In the kidney, podoplanin was primarily observed on glomerulus and LECs in WT mice, and it was significantly decreased in *PdpnCyto*$^{-/-}$ mice (Figure 4.10 B). Podoplanin was mainly located at bile duct and LECs in the liver, which was also downregulated in *PdpnCyto*$^{-/-}$ mice, compared to WT controls (Figure 4.10 C). In the heart, podoplanin was only found on LECs, and the level of expression in *PdpnCyto*$^{-/-}$ animals was almost undetectable using this method (Figure 4.10 D). In red pulp of the spleen, LECs were the major podoplanin-positive area (Figure 4.10 E, upper) whereas there was periarteriolar podoplanin-expressing cells within the splenic white pulp (Figure 4.10 E, lower) of WT mice. In a similar fashion, a reduction in podoplanin expression was observed in the spleen of *PdpnCyto*$^{-/-}$ mice (Figure 4.10 E).

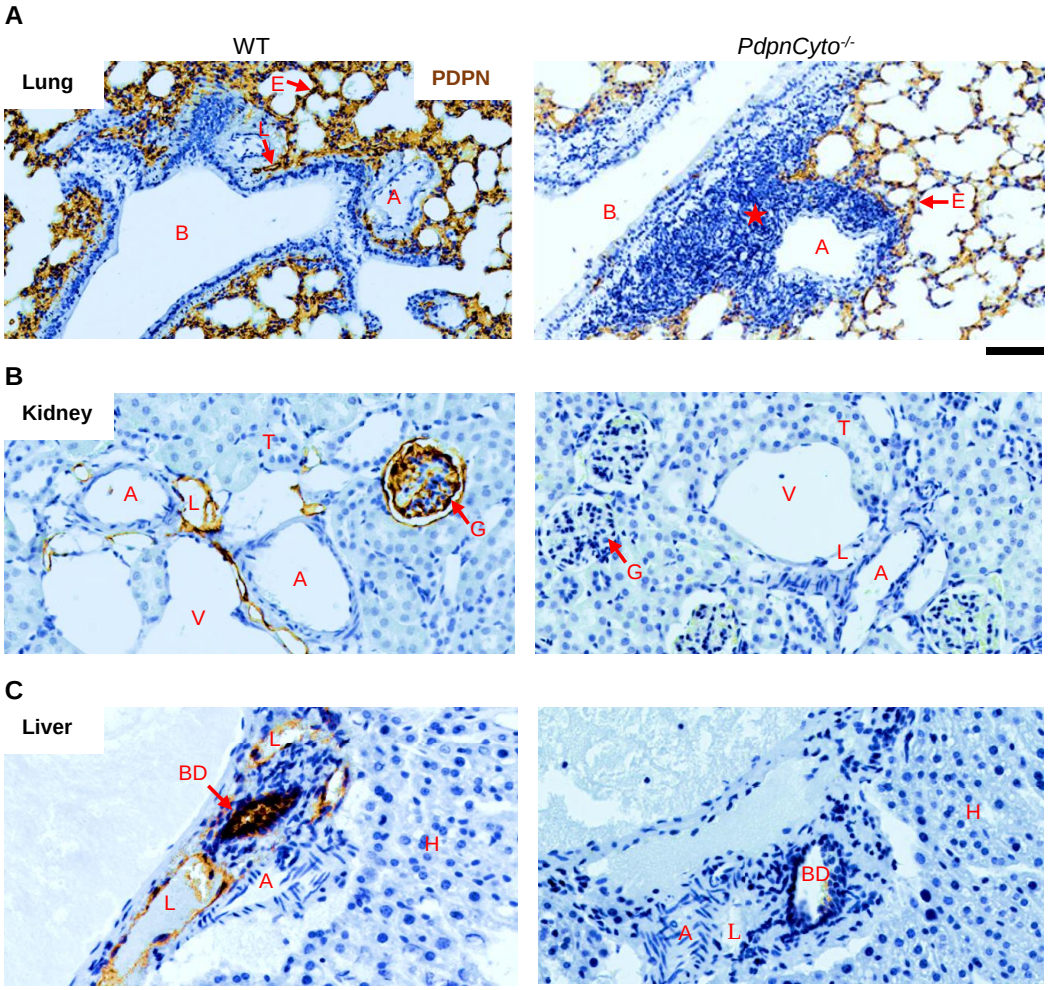

Figure 4. 10. (A-C) Adult podoplanin cytoplasmic tail deficient mice demonstrate downregulation of the basal podoplanin level in multiple organs. Immunohistochemistry of podoplanin (brown) is performed in the internal organs (n =3-4), including (A) lung, (B) kidney, (C) liver, (D) heart, and (E) splenic red pulp (upper) and white pulp (lower). Star in (A) indicates leucocyte infiltrates. Arrow in (E) points to periarteriolar podoplanin-expressing cells. PDPN = podoplanin, A = arteriole, V = vein, L = lymphatic vessel, E = lung epithelium, containing podoplanin-expressing type I lung alveolar cells, B = bronchi/bronchiole, G = glomerulus, T = renal tubule, BD = bile duct, H = hepatocyte, M = cardiac myocyte. Scale bar = 50 µm.

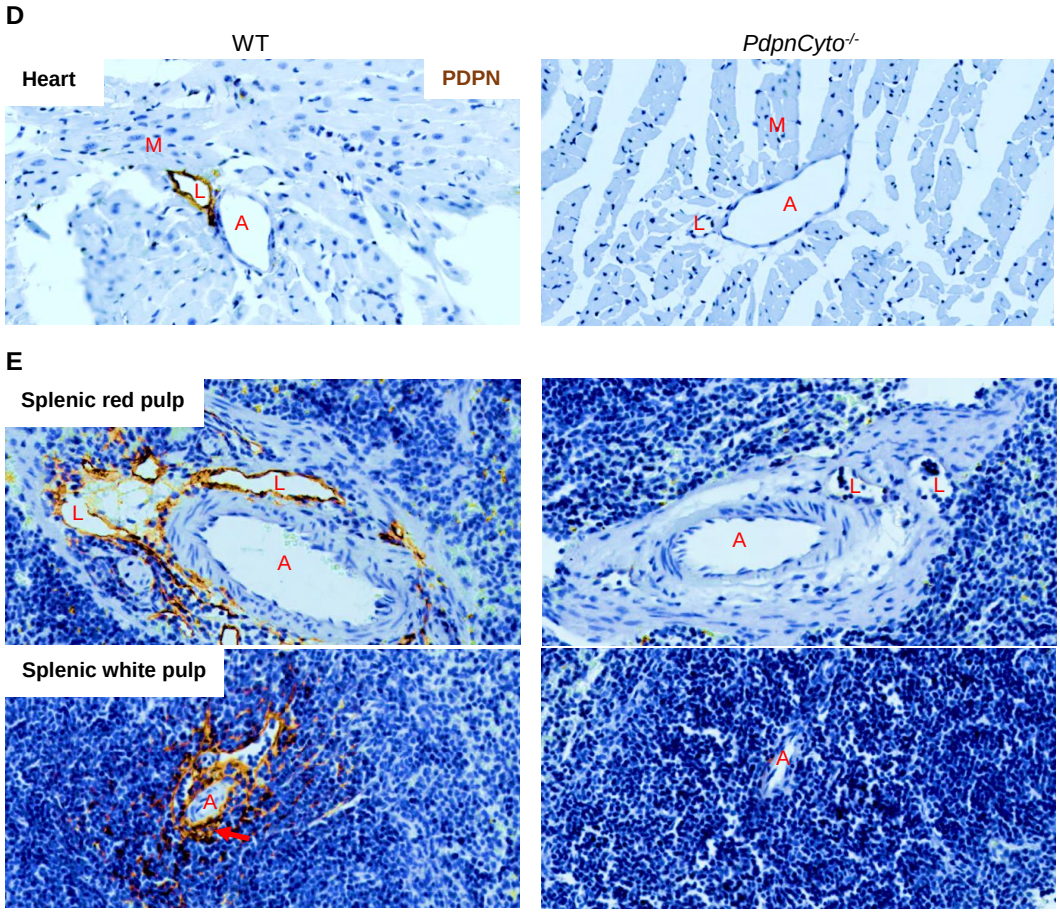

Figure 4.10. (D-E) Adult podoplanin cytoplasmic tail deficient mice demonstrate downregulation of the basal podoplanin level in multiple organs. Immunohistochemistry of podoplanin (brown) is performed in the internal organs (n =3-4), including (A) lung, (B) kidney, (C) liver, (D) heart, and (E) splenic red pulp (upper) and white pulp (lower). Star in (A) indicates leucocyte infiltrates. Arrow in (E) points to periarteriolar podoplanin-expressing cells. PDPN = podoplanin, A = arteriole, V = vein, L = lymphatic vessel, E = lung epithelium, containing podoplanin-expressing type I lung alveolar cells, B = bronchi/bronchiole, G = glomerulus, T = renal tubule, BD = bile duct, H = hepatocyte, M = cardiac myocyte. Scale bar = 50 μm.

4.2.8 Absence of significant blood-filled lymphatics in multiple internal organs of adult podoplanin cytoplasmic tail deficient mice

A defect in blood and lymphatic vessel separation during embryonic development is speculated to cause blood-filled lymphatic vessels observed in post-natal period in mice (Bertozzi et al., 2010). In addition, it has been reported that podoplanin maintains this function during late gestation and in adulthood by mediating platelet aggregation to prevent backflow of blood through lymphovenous junction into lymphatic vessels (Hess et al., 2014). The observation for blood-filled lymphatics in several organs of adult *PdpnCyto*$^{-/-}$ mice revealed that there was no apparent evidence of this phenotype in the lung, liver, kidney, heart, and spleen (Figure 4.10) whereas the *Clec1b*$^{fl/fl}$*Pf4-cre* mice clearly demonstrated blood/lymphatic mixing in the lung, heart, and spleen but not in the liver and kidney (Figure 4.11).

4.2.9 Podoplanin cytoplasmic tail deficient and *Pf4-cre*-driven CLEC-2 knockout mice exhibit infiltrates of immune cells in the lung and liver tissues

Previous study has shown that inflammatory infiltrates are observed in multiple organs of transgenic mice with constitutive podoplanin deletion (Peters et al., 2015). The histological examination demonstrated that there was inflammatory cell infiltration around blood vessels within lung tissue of *PdpnCyto*$^{-/-}$ and *Clec1b*$^{fl/fl}$*Pf4-cre* mice (Figure 4.12, star) but not in WT and *Clec1b*$^{fl/fl}$*Gp1ba-cre* mice (another platelet-specific CLEC-2 knockout model). In addition, CLEC-2 deletion on dendritic cells (*Clec1b*$^{fl/fl}$*Cd11c-cre*) did not show this ectopic lymphoid structure within the lung (Figure 4.12). A similar fashion of leucocyte infiltration was observed in the liver of *PdpnCyto*$^{-/-}$ and

Clec1b$^{fl/fl}$*Pf4-cre* mice (Figure 4.13). However, it was not detected in the kidney and cardiac tissues of *PdpnCyto*$^{-/-}$ (Figure 4.10) and *Clec1b*$^{fl/fl}$*Pf4-cre* mice (Figure 4.11).

4.2.10 CELC-2 is expressed on nucleated cells within the dermis of the skin in *Pf4-cre*-driven platelet-specific CLEC-2 knockout mice

Although CLEC-2 is primarily expressed on platelets, CLEC-2 expression was also shown on myeloid cells, especially on dendritic cells (Acton et al., 2012, de Winde et al., 2018), and contributes to function of dendritic cells (Acton et al., 2014). To examine whether the expression of *cre* recombinase driven by *Pf4* promoter (*Pf4-cre*) could delete *Clec1b*$^{fl/fl}$ on myeloid cells, the immunohistochemistry was performed to detect CLEC-2 in unchallenged mouse skin. The results showed that CLEC-2 was still present on extravascular nucleated cells, indicating the resident myeloid cells rather than anucleated platelets within the skin dermis of *Clec1b*$^{fl/fl}$*Pf4-cre* mice, which was identical to WT and *PdpnCyto*$^{-/-}$ mice (Figure 4.14).

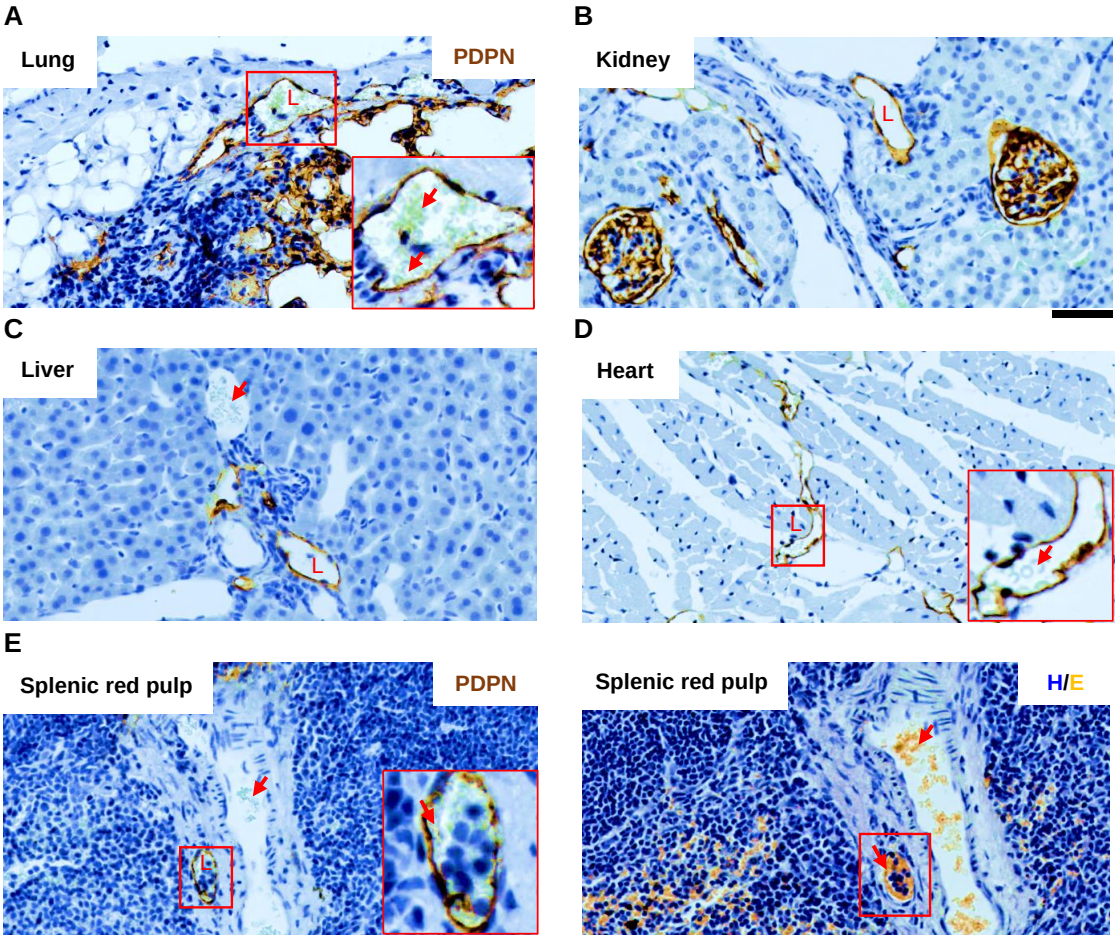

Figure 4. 11. Mice with platelet CLEC-2 deficiency display blood/lymphatic mixing in the lung, heart, and spleen. Immunohistochemistry of podoplanin (brown) in the internal organs of *Clec1b*$^{fl/fl}$*Pf4-cre* mice (n =3), including (A) lung, (B) kidney, (C) liver, (D) heart, and (E, left) spleen. Areas covered by rectangle are magnified to emphasise blood-filled lymphatic vessel in the organs. Arrow points to red blood cells. L = lymphatic vessel. (E, right) shows H&E staining of spleen that confirms blood-filled lymphatic vessels (rectangle) at the same red pulp area observed in podoplanin staining. Red/orange colour indicates red blood cells. Scale bar = 50 µm.

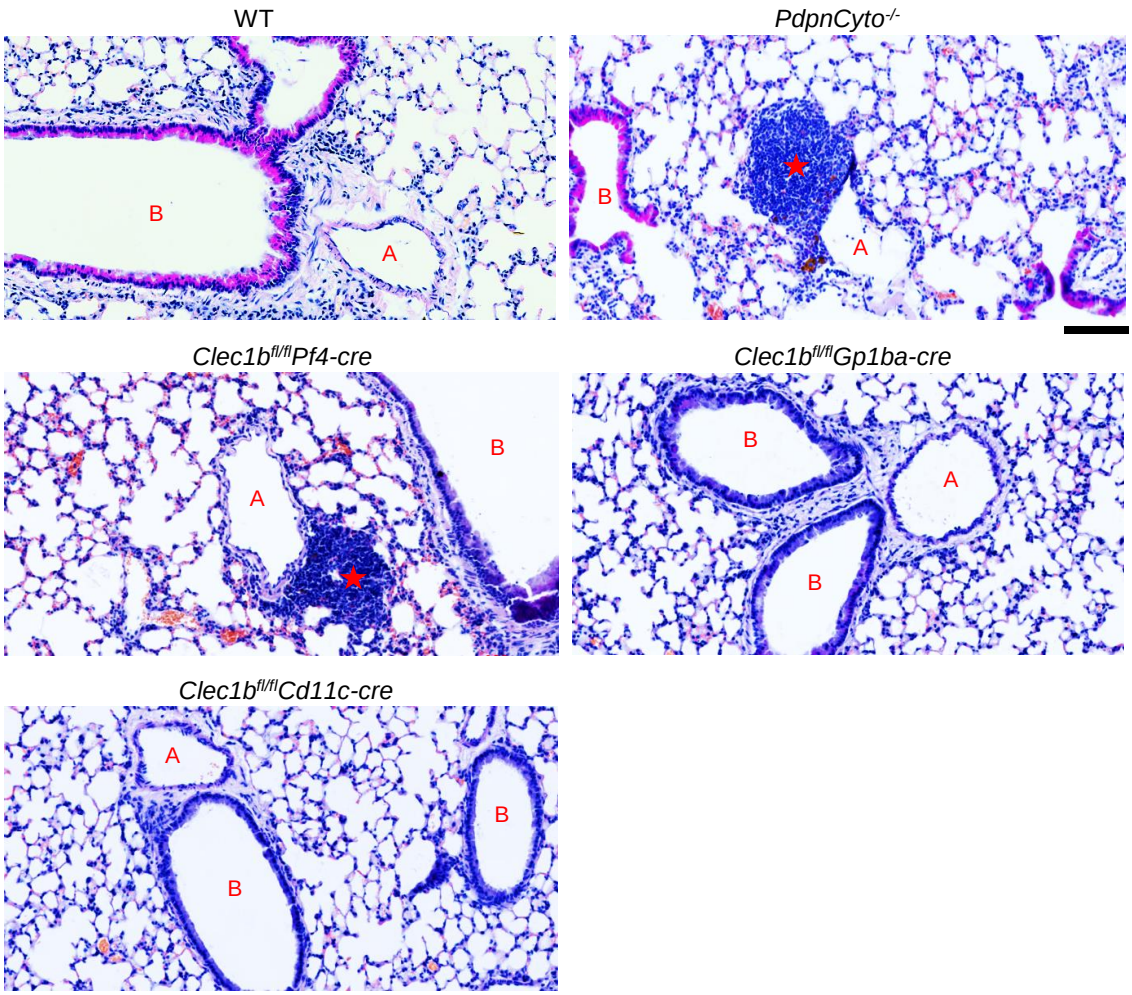

Figure 4. 12. Infiltration of leucocytes are observed in the lung of podoplanin cytoplasmic tail deficient and *Pf4-cre*-driven platelet-specific CLEC-2 knockout mice. H&E staining of lung tissues from WT, *PdpnCyto*$^{-/-}$, two platelet-specific CLEC-2 deficient models (i.e. *Clec1b*$^{fl/fl}$*Pf4-cre* and *Clec1b*$^{fl/fl}$*Gp1ba-cre*), and dendritic cell-specific CLEC-2 knockout (*Clec1b*$^{fl/fl}$*Cd11c-cre*) mice (n=3). Star indicates leucocyte infiltrates. A = arteriole, B = bronchi/bronchiole. Scale bar = 100 µm.

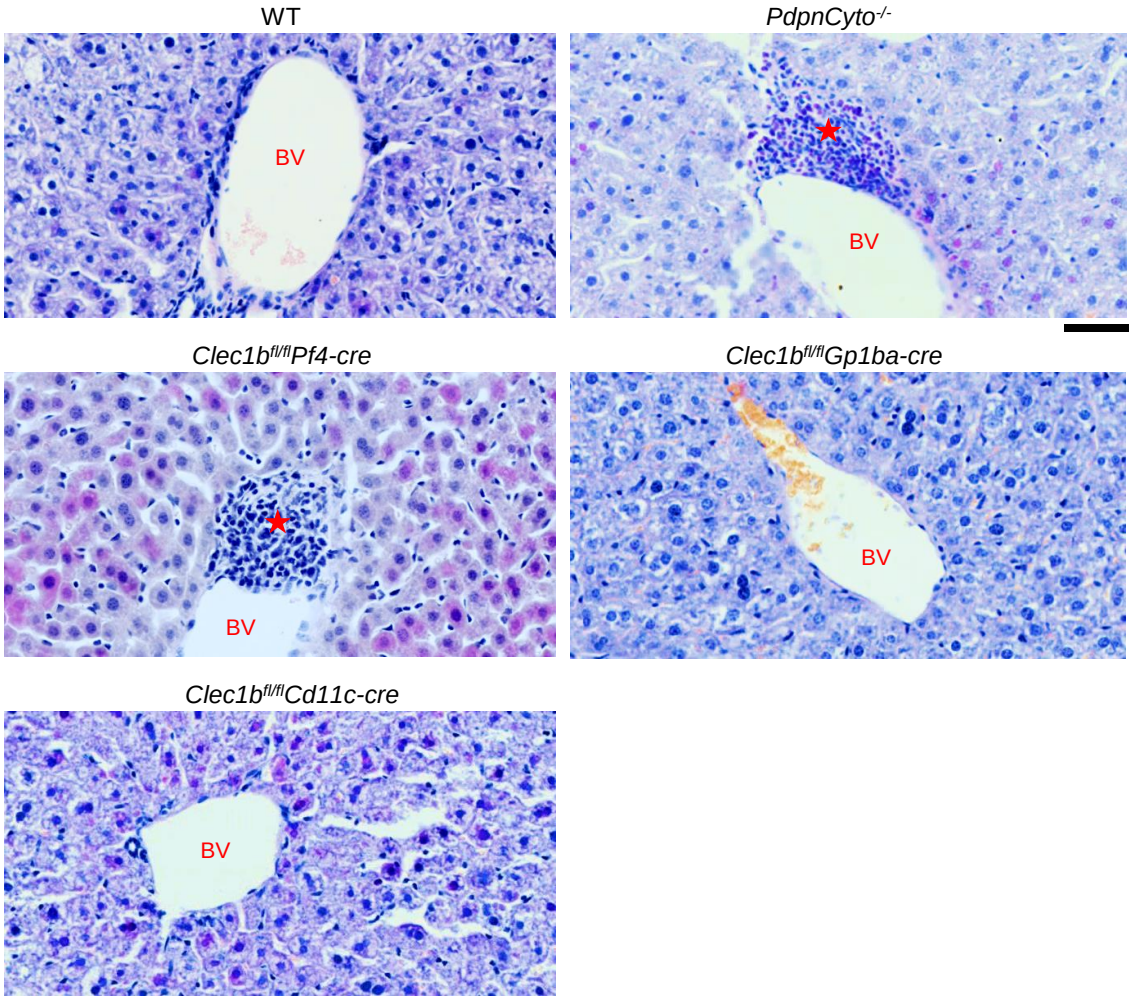

Figure 4. 13. Leucocyte infiltrates are present in the liver of podoplanin cytoplasmic tail deficient and *Pf4-cre*-driven platelet-specific CLEC-2 knockout mice. H&E staining of liver tissues from WT, *PdpnCyto*$^{-/-}$, two platelet-specific CLEC-2 deficient models (i.e. *Clec1b*$^{fl/fl}$*Pf4-cre* and *Clec1b*$^{fl/fl}$*Gp1ba-cre*), and dendritic cell-specific CLEC-2 knockout (*Clec1b*$^{fl/fl}$*Cd11c-cre*) mice (n=3). Star indicates leucocyte infiltrates. BV = Blood vessel. Scale bar = 50 µm.

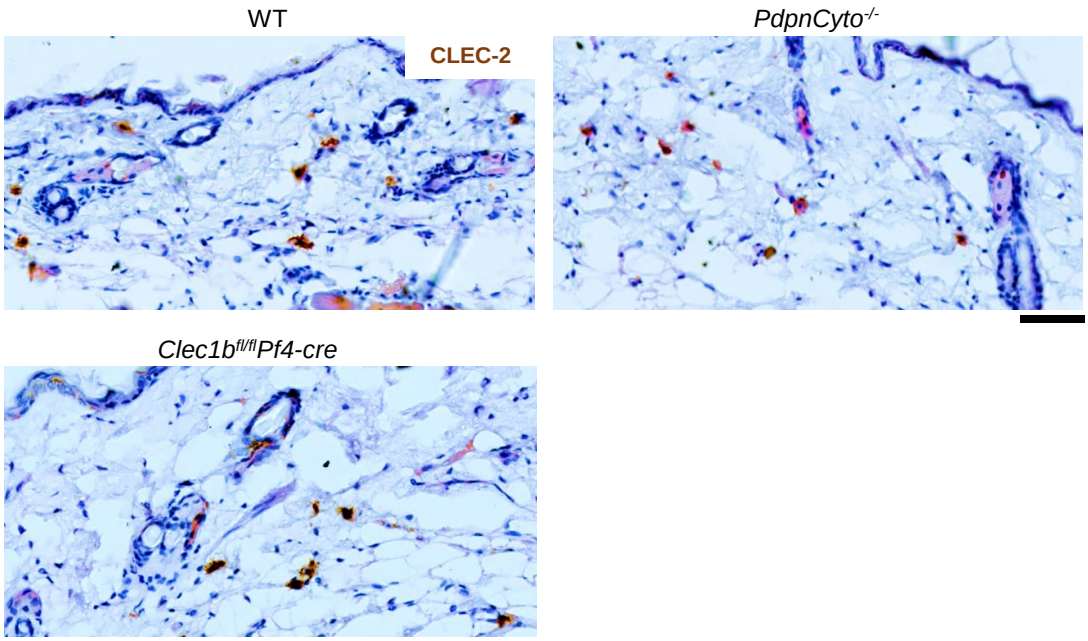

Figure 4. 14. *Pf4-cre*-driven platelet-specific CLEC-2 knockout strategy does not delete CLEC-2 on myeloid cells in murine skin dermis. Immunohistochemistry of CLEC-2 (brown) in the unchallenged skin of WT, *PdpnCyto*$^{-/-}$, and *Clec1b*$^{fl/fl}$*Pf4-cre* mice (n=3). Scale bar = 50 µm.

4.2.11 Lack of podoplanin cytoplasmic tail has no impact on skin wound healing

As shown in chapter 3, podoplanin was primarily expressed on LECs and cells that encircle blood vessels in unchallenged murine skin whereas it was upregulated during skin wound healing, including in proliferating/migrating keratinocytes, stromal cells, and other infiltrating cells. In *PdpnCyto*$^{-/-}$ mice, the results showed a reduction in basal podoplanin expression in multiple organs. However, it is unknown whether the lack of cytoplasmic tail affects podoplanin expression and its physiological function in challenged conditions, such as during skin wounding. Following a full-thickness excisional skin wound injury, *PdpnCyto*$^{-/-}$ mice demonstrated a comparable wound appearance to that of WT mice throughout the course of wound monitoring for up to nine days post-injury (Figure 4.15 A). In addition, there was no difference in wound closure between *PdpnCyto*$^{-/-}$ mice and WT controls at any time points of a daily observation, both of which showed complete wound closure at day 9 post-injury (Figure 4.15 B).

Although podoplanin on LECs was significantly decreased in unchallenged skin of *PdpnCyto*$^{-/-}$ mice relative to WT mice (Figure 4.16 A, B), there was no evidence of blood-filled lymphatic vessels in the skin of this mouse strain (Figure 4.16 A). Moreover, immunohistochemistry using antibody (clone 8.1.1) that recognises the extracellular domain of podoplanin (Pan et al., 2014) demonstrated that podoplanin was upregulated on the cells within wound area of *PdpnCyto*$^{-/-}$ mice at day 9 post-injury (Figure 4.16 C) and it was not significantly different to that of WT mice (Figure 4.16 D). These data suggest that in case of podoplanin upregulation is required, cell surface expression of podoplanin is not deficient in the *PdpnCyto*$^{-/-}$ mice.

A

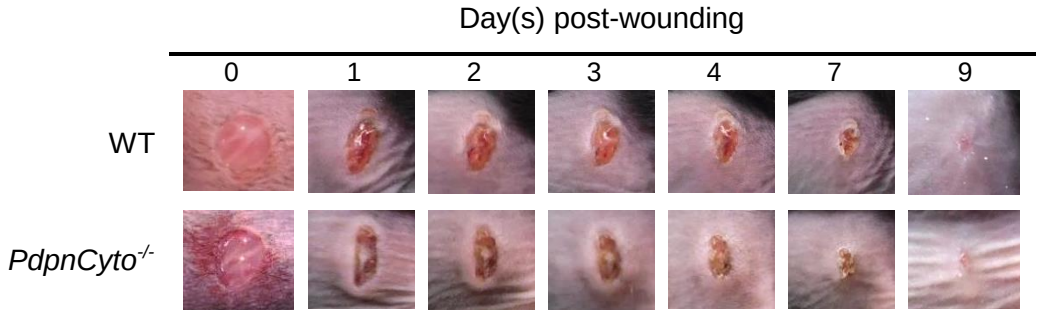

B

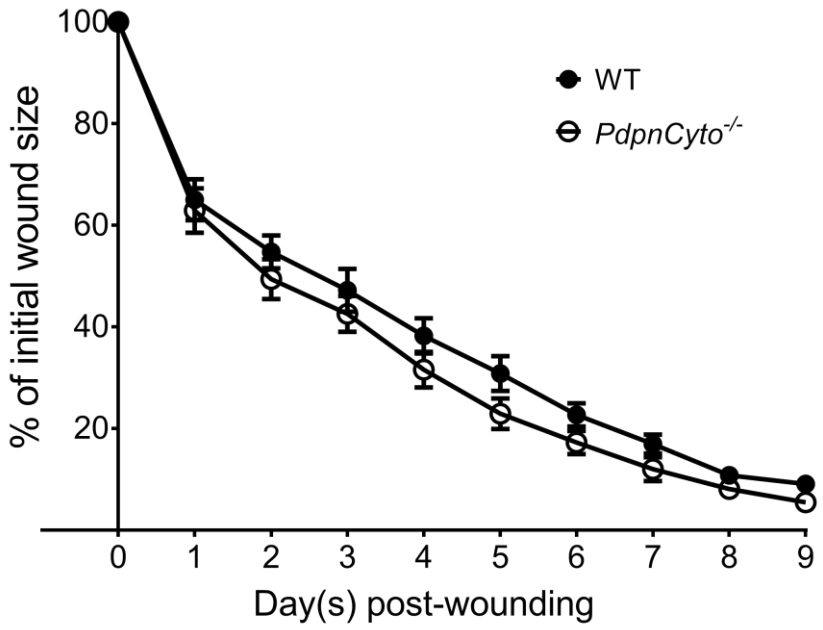

Figure 4. 15. Podoplanin cytoplasmic tail deficiency does not influence skin wound healing. (A) Macroscopic appearance of wound at indicated time points. (B) Changes of wound size over 9 days post-injury (n=10). Graphs are presented as mean ± SEM. Kinetics of wound closure are analysed by two-way ANOVA with Bonferroni's multiple comparison test.

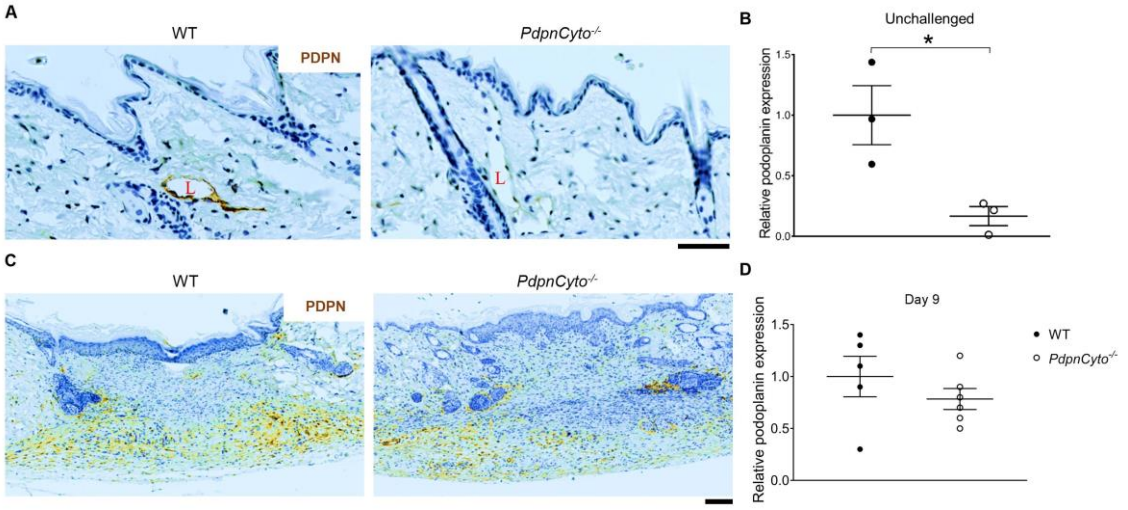

Figure 4. 16. Expression of podoplanin is upregulated during skin wound healing in both WT and podoplanin cytoplasmic tail deficient mice. (A) Detection of podoplanin expression (brown) in unchallenged murine skin. PDPN = podoplanin. Scale bar = 50 µm. (B) Quantification of podoplanin expression in unchallenged skin (n=3). Average intensity from five representative lymphatic vessel-containing (podoplanin-positive) HPF images per skin sample were taken. (C) Detection of podoplanin expression (brown) in wound area at day 9 post-injury. Scale bar = 100 µm. (E) Quantification of podoplanin expression within the wound at day 9 post-injury (n=5-6). Data are presented as mean ± SEM and analysed by Student's t-test.*$p < 0.05$.

4.2.12 Normal wound macrophage numbers are observed in the podoplanin cytoplasmic tail deficient animals

Previous evidence has demonstrated an important function of podoplanin in cell migration (Martin-Villar et al., 2006, Suchanski et al., 2017). In addition, podoplanin is expressed on macrophages (Kerrigan et al., 2012) and it is upregulated during inflammatory conditions, including in arthritis, lung injury, and sepsis (Rayes et al., 2017, Croft et al., 2016, Lax et al., 2017b). However, the contribution of podoplanin in macrophage migration is unknown. Although the time course of macrophage infiltration during skin wound healing has not been investigated, the result of immunohistochemistry staining at day 9 post-injury revealed that macrophages were present within the wound scar of *PdpnCyto*$^{-/-}$ mice (Figure 4.17 A). In addition, the quantitative analysis demonstrated there was no significant difference in macrophage numbers between *PdpnCyto*$^{-/-}$ mice and WT controls at this time (Figure 4.17 B). In support of the intact upregulation of podoplanin in *PdpnCyto*$^{-/-}$ mice at day 9 post-injury (Figure 4.16 C), these results may suggest that macrophage turnover during skin wound healing in mice does not require podoplanin cytoplasmic tail.

4.2.13 The absence of podoplanin cytoplasmic tail does not alter scar formation during skin wound healing

The measurement of wound size using callipers showed a similar wound area between WT and *PdpnCyto*$^{-/-}$ mice at the end of experiment (day 9 post-injury) (Figure 4.15 B). To ensure this is not due to limitation of the technique used to assess macroscopic wound closure, the histological analyses of wound scar were performed. At day 9 post-injury,

PdpnCyto$^{-/-}$ mice had complete epithelial regeneration, which was comparable to the WT controls (Figure 4.18 A). In addition, these mice exhibited the same length of hyperplastic epidermis (Figure 4.18 B) and distance between subcutaneous gaps (Figure 4.18 C) to that observed in WT mice at this time.

The function of podoplanin on skin fibroblasts (Nazari et al., 2016) has also never been reported in skin wound healing whereas there is evidence demonstrating its role in fibroblast migration in cancers (Suchanski et al., 2017). In the present model of skin wound, Martius scarlet blue staining illustrated that in addition to the normal dermis around the wound edges, collagen was observed within the scar of both *PdpnCyto*$^{-/-}$ and WT mice at day 9 post-injury (Figure 4.19 A). The results of quantification demonstrated an identical collagen content within the scar area between *PdpnCyto*$^{-/-}$ and WT mice (Figure 4.19 B), suggesting there is no defect in fibroblast/myofibroblast function in relation to collagen synthesis.

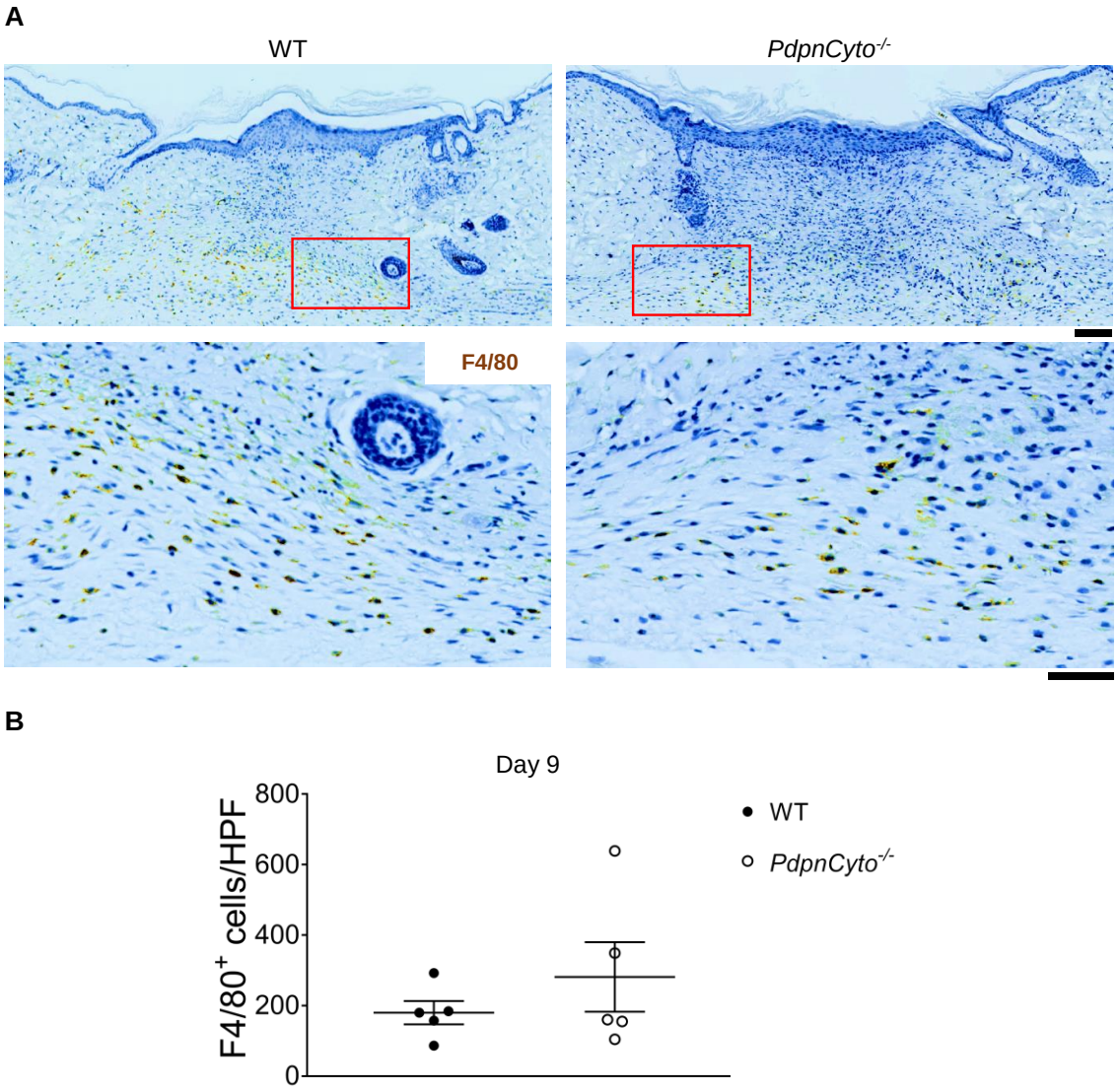

Figure 4. 17. Macrophage numbers in the wound of podoplanin cytoplasmic tail deficient mice are normal. (A) Detection of macrophages (F4/80 staining; brown) in wound area at day 9 post-injury. The areas covered by rectangle are magnified as shown in the lower panel. Scale bars = 100 µm (upper panel) and 50 µm (lower panel), respectively. (B) Quantification of macrophages ($F4/80^+$ cells) in wound area at day 9 post-injury (n=5). Graphs are presented as mean ± SEM and analysed by Student's t-test.

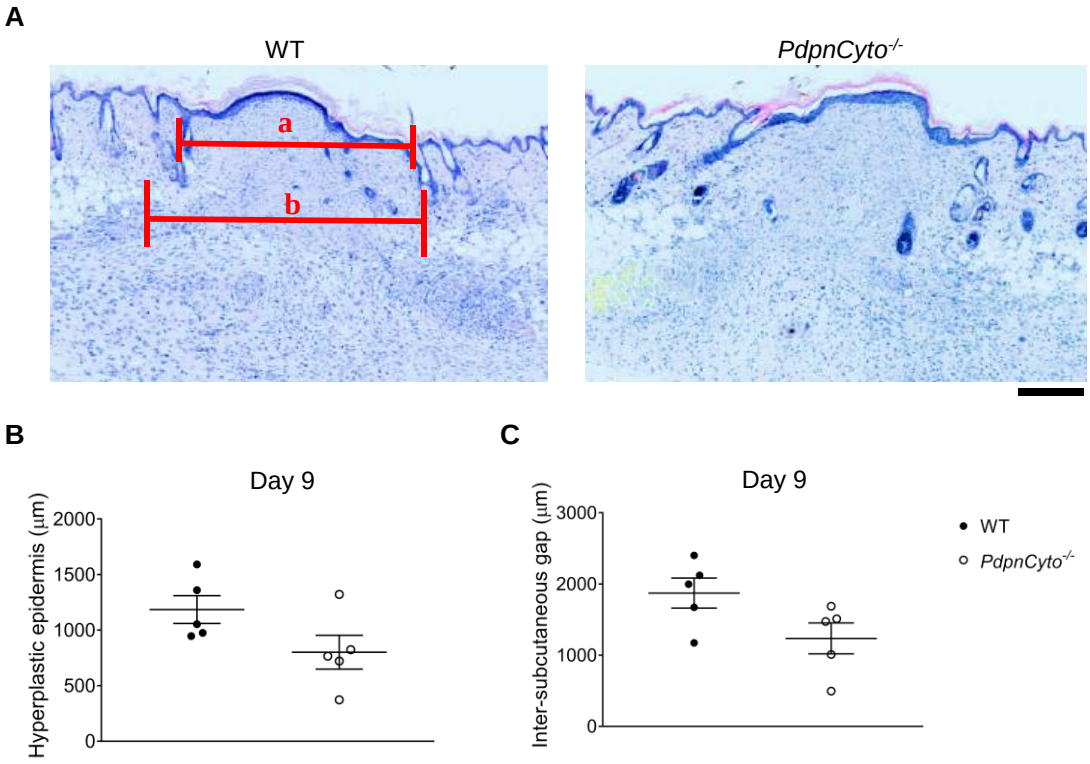

Figure 4. 18. Normal scar formation during skin wound healing in podoplanin cytoplasmic tail deficient mice. (A) H&E staining of the skin wound tissue at day 9 post-injury (n=5). a = length of hyperplastic epidermis, b = inter-subcutaneous distance. (B) Assessment of the length of hyperplastic epidermis. (C) Measurement of inter-subcutaneous distance. Scale bar = 200 µm. Data are presented as mean ± SEM and analysed by Student's t-test.

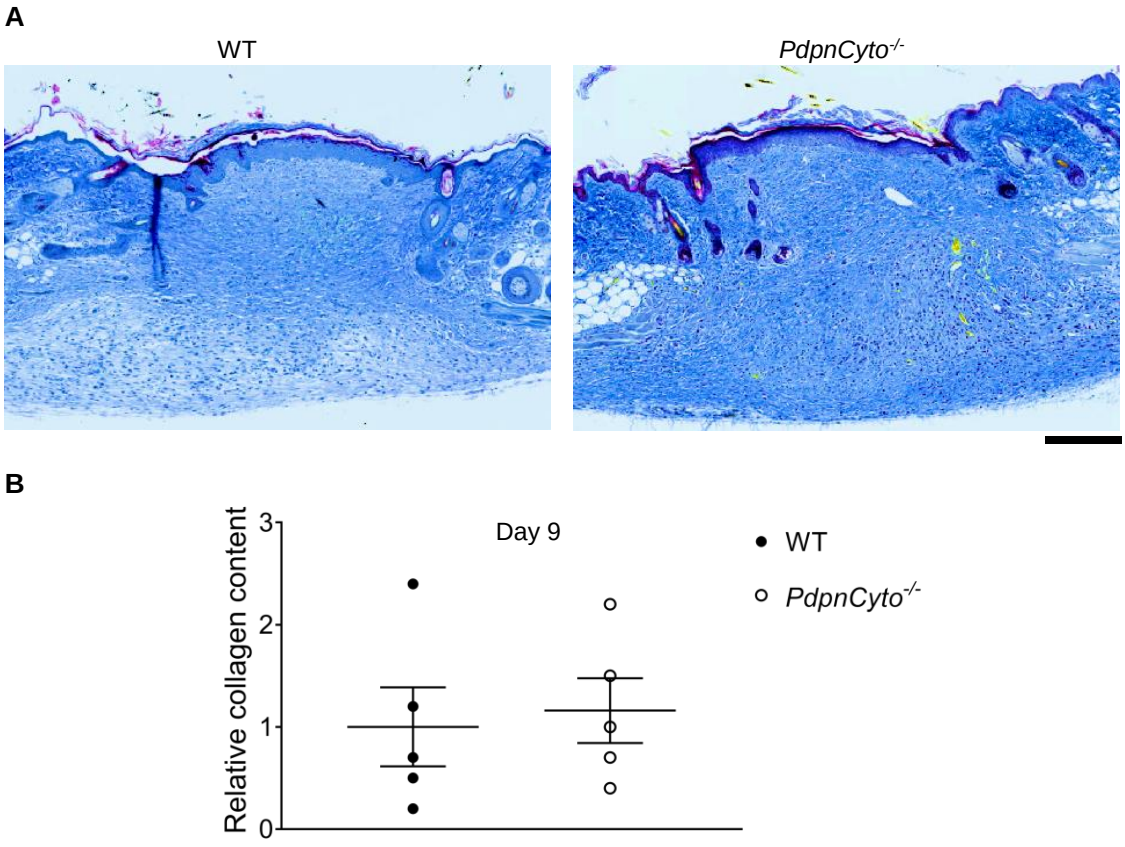

Figure 4. 19. Collagen deposition in wound scar is unaltered in podoplanin cytoplasmic tail deficient mice. (A) Martius scarlet blue staining of skin wound at day 9 post-injury. Red = old fibrin, blue = collagen, yellow = red blood cells/fresh fibrin. Scale bar = 200 µm. (B) Quantification of collagen content in the wound at day 9 post-injury (n=5). Data are presented as mean ± SEM and analysed by Student's t-test.

4.3 Discussion

On one hand, podoplanin contributes to physiological functions through its extracellular domain that acts as CLEC-2-activating ligand to induce platelet activation and aggregation (Hess et al., 2014, Rayes et al., 2018). On the other hand, the cytoplasmic tail of podoplanin modulates downstream signalling in regulating the function of podoplanin-expressing cells (Astarita et al., 2015). Moreover, podoplanin also interacts with lateral integral proteins (e.g. galectin-8) (Martin-Villar et al., 2010, Cueni and Detmar, 2009) and some soluble molecules (e.g. CCL21), which subsequently produce biological effects (Tejchman et al., 2017, Cicvaric et al., 2016). In this chapter, the (patho)physiological contribution of podoplanin cytoplasmic tail is described through the characterisation of podoplanin cytoplasmic tail deficient mice, which were generated using CRISPR/Cas9 technology to knock-in three stop codons before the nucleotide sequence encoding lysine-164 in exon 5 of *Pdpn*. These mice are viable, fertile, and have no evidence of severe abnormalities. Pre-wean mortality rate of this mouse colony is also normal (Weber et al., 2013). In support of previous evidences demonstrating the role of podoplanin in various settings, the characterisation data suggests that podoplanin cytoplasmic tail might provide potential function in (1) the development of cerebral blood vessel and (2) the regulation of lymphocyte response. However, the results indicate that cytoplasmic tail of podoplanin might not be required for (1) the prevention of blood-filled lymphatics, especially during adulthood, (2) safeguarding cerebral vascular integrity, (3) bone marrow-derived platelet production, (4) lung development, and (5) the turnover and/or function of various podoplanin-expressing cells, including keratinocytes, macrophages, and

(myo)fibroblasts, during skin wound healing. The observed physiological settings that may or may not require podoplanin cytoplasmic tail are shown in Figure 4.20.

In the present model of podoplanin cytoplasmic tail deficiency, the expression of podoplanin at E14.5 was relatively comparable to that of WT embryos. In adult podoplanin cytoplasmic tail deficient animals, the basal podoplanin expression was downregulated in several organs. However, the mutated podoplanin was present on cell surface at the equivalent amounts observed in WT during skin wound healing, a challenged condition that shows the upregulation of podoplanin. Based on these data, it is likely that during the initial period of podoplanin expression/upregulation, the extracellular domain of mutated podoplanin might be presented normally on cell surface. As an abnormal protein, podoplanin that lacks its cytoplasmic region might be degraded overtime, leading to the observed downregulation of podoplanin during basal/unchallenged setting in adult podoplanin cytoplasmic tail deficient mice. In agreement with this, it is well recognised that in eukaryotic cells, several membrane proteins are regulated by internalisation followed by lysosomal degradation inside the cells (Lecker et al., 2006, Hicke and Dunn, 2003).

During murine embryonic development, previous studies also suggest that the separation of blood and lymphatic vessels via CLEC-2-podoplanin interaction is completed in a short period. At E11.5, where podoplanin is initially expressed in cardinal vein and primary lymph sac (Schacht et al., 2003), platelet aggregation allows (Bertozzi et al., 2010) to separate lymphatic vessel from cardinal vein. These evidences suggest that podoplanin is essential at critical period of blood and lymphatic vessel separation. The persistence of podoplanin on LECs until adulthood may be important for other functions, including the

migration of dendritic cells, which requires CLEC-2-podoplanin interaction (Acton et al., 2012). Although *in vitro* model speculates the contribution of podoplanin cytoplasmic tail for the separation of blood and lymphatic vessels via inhibiting LEC migration (Pollitt et al., 2014), blood-filled cutaneous vessels rarely occurred (25%) at E14.5 in podoplanin cytoplasmic tail deficient embryos and it is entirely mild compared to what has been previously reported in the podoplanin null embryos (Bertozzi et al., 2010, Uhrin et al., 2010). In addition, blood/lymphatic mixing was not detected in all tested organs in adult mice that lack podoplanin cytoplasmic tail. A slightly different *in vivo* model of podoplanin cytoplasmic tail deficiency, which inserts three stop codons immediately after the sequence encoding lysine-164, also reports no any detectable gross abnormalities in adult mice (Astarita et al., 2015). In addition, the phosphorylation of ERM in FRCs from these mice is not affected (Astarita et al., 2015).

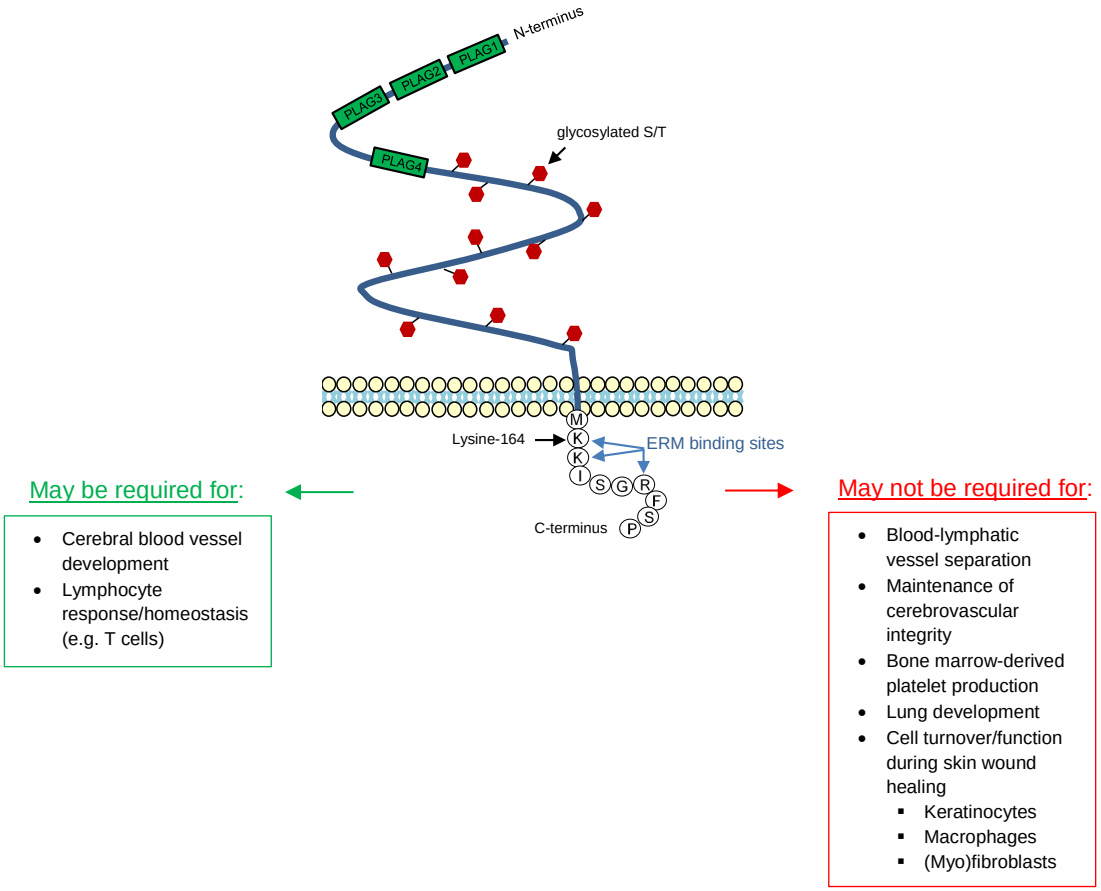

Figure 4. 20. Diagram shows the physiological conditions that may or may not require the podoplanin cytoplasmic tail. The known functions of podoplanin are listed based on the literatures and further classified in relation to the contribution of its cytoplasmic tail according to the present data of characterisation. On one hand, podoplanin cytoplasmic tail might be required (green box) for (1) development of cerebral blood vessel and (2) the regulation of lymphocyte homeostasis. On the other hand, cytoplasmic tail of podoplanin might not be required (red box) for (1) blood/lymphatic separation, especially during adulthood, (2) maintaining cerebral vascular integrity, (3) bone marrow-derived platelet production, (4) lung development, and (5) cell turnover/function during skin wound healing, including keratinocytes, macrophages, and (myo)fibroblasts.

Upon CLEC-2 interaction, podoplanin on neuroepithelial cells may induce secretion of pro-angiogenic factors that contribute to the recruitment of endothelial and mural cells for cerebral blood vessel development in mouse embryos, suggesting a functional role of the cytoplasmic tail. Simultaneously, podoplanin activates platelet CLEC-2 to maintain cerebrovascular integrity (Lowe et al., 2015a). Unlike CLEC-2 null and neuroepithelium-specific podoplanin knockout embryos (Lowe et al., 2015a), the podoplanin cytoplasmic tail deficient embryos have no macroscopic appearance of cerebral haemorrhage at E14.5, supporting the role of podoplanin extracellular domain in stimulating CLEC-2 to safeguard vascular integrity during brain development. However, embryos that lack podoplanin cytoplasmic tail demonstrated an increased vasodilation around head area at E14.5, which possibly indicates a certain degree of impairment of cerebrovascular development. In CLEC-2 null and neuroepithelium-specific podoplanin knockout embryos, a larger vascular lumen relative to WT controls has been observed, in addition to a reduction in pericyte recruitment, contributing to tortuous/disorganised vascular network within the brain (Lowe et al., 2015a). Therefore, it is likely that podoplanin cytoplasmic tail in neuroepithelial cells participates in normal development of cerebral blood vessel but not its integrity.

Previous studies have shown the role of podoplanin for normal development of the lung (Ramirez et al., 2003, Tsukiji et al., 2018a) and the heart (Mahtab et al., 2008). Global podoplanin deletion leads to death of new-born shortly after birth due to non-inflated lung (Ramirez et al., 2003). In addition, CLEC-2 knockout and LEC-specific podoplanin deficient mice, but not either lung epithelial cell-specific or mesothelial cell-specific podoplanin knockout mice, exhibit this phenotype (Tsukiji et al., 2018a). Thus, it is

proposed that extracellular domain of podoplanin on lung LECs activates platelet CLEC-2 leading to secretion of TGF-β, which regulates differentiation of lung mesothelial cells into myofibroblast to synthesise ECM that support alveolar structure (Tsukiji et al., 2018a). This is in line with the observation of normal viability without any signs of breathing difficulty in adult mice that lack podoplanin cytoplasmic tail. In terms of cardiac development, it has been shown that murine embryos deficient in podoplanin exhibit cardiac malformations, represented by severe hypoplasia in several areas, including the myocardium, cardiac conduction system, and coronary artery (Mahtab et al., 2008). These defects are due to the absence of podoplanin in epicardium, which leads to impaired migration of epicardium-derived cells to the developing heart, contributing to embryonic/neonatal death (Mahtab et al., 2008). It is unclear whether a reduction in heart-to-body weight ratio in podoplanin cytoplasmic tail deficient mouse strain reflects a contribution of podoplanin cytoplasmic tail in normal cardiac development. In addition, these mice are alive and develop normally until adulthood.

In the context of platelet production, it has been demonstrated that megakaryocyte CLEC-2 activates podoplanin-expressing stromal cells around arterioles within bone marrow to secrete CCL5, which regulates megakaryocyte expansion and a subsequent proplatelet formation (Tamura et al., 2016). However, a normal platelet count is observed in mice with podoplanin cytoplasmic tail deficiency. Moreover, unlike a reduction in circulating platelets in *Pf4-cre* driven CLEC-2 knockout model (Tamura et al., 2016), CLEC-2 deletion in adult mice using tamoxifen-inducible Cre/loxP strategy does not cause thrombocytopenia (Lowe et al., 2015b). Therefore, it is controversial whether CLEC-2-

podoplanin axis mediates platelet production. Indeed, the present data suggest that podoplanin cytoplasmic tail has no role in this physiological process.

Recently, the role of podoplanin in immune regulation has been described. Podoplanin expression is detected in non-pathogenic T cells whereas it is downregulated/absence in pathogenic pro-inflammatory Th17 cells (Peters et al., 2015, Nylander et al., 2017). In addition, CLEC-2 enhances anti-inflammatory/immunosuppressive regulatory T cell population *in vitro* (Agrawal et al., 2015). These data suggest that CLEC-2-podoplanin negatively regulates T cell response. Moreover, transgenic mice with podoplanin overexpression demonstrate severe lymphopaenia and this phenotype is rescued by crossing with CLEC-2 null mice (Peters et al., 2015). In contrast, the podoplanin cytoplasmic tail deficient mice showed increased percentage of circulating lymphocytes. In a similar fashion to podoplanin cytoplasmic tail deficient and *Pf4-cre* driven CLEC-2 knockout mice, the inflammatory infiltrates comprising macrophages, dendritic cells, B-cells, and substantial amounts of T-cells, are observed within the lung, liver, and intestine, but not in the heart and brain among constitutive podoplanin knockout animals (Peters et al., 2015). Therefore, podoplanin cytoplasmic tail (upon platelet CELC-2 interaction) may reduce T cell survival and response, which subsequently attenuate tissue inflammation (Peters et al., 2015, Nylander et al., 2017, Agrawal et al., 2015). However, the effects of lymphatic abnormality on lymphocyte homeostasis cannot be excluded since the lymphocyte infiltration is also observed in various organs, accompanied with chylothorax, in α9 integrin knockout mice that have defect in lymphatic valve formation without blood-lymphatic mixing (Huang et al., 2000, Hess et al., 2014).

The absence of inflammatory foci in *Gp1ba-cre*-driven CLEC-2 knockout mice raises concern of non-specific cre recombination under the control of *Pf4* promoter (Pertuy et al., 2015), which may delete CLEC-2 on immune cells. However, cre recombination does not occur in dendritic cells following *Pf4* promoter-driven (Pertuy et al., 2015). The result of CLEC-2 immunohistochemistry also indicates the presence of CLEC-2 on nucleated cells within the skin of *Pf4-cre*-driven CLEC-2 knockout mice, which is similar to WT mice. Further investigations of *Gp1ba-cre*-driven CLEC-2 knockout colony may provide more information whether *Pf4-cre* or *Gp1ba-cre* is more specific for deletion of CLEC-2 on megakaryocyte/platelet lineage. A lack of inflammatory infiltrates in *Clec1b*$^{fl/fl}$*Cd11c-cre* animals refuses the association of dendritic CLEC-2 to this phenotype.

A non-essential function of podoplanin cytoplasmic tail was revealed in many aspects during skin wound healing. Firstly, mice that lack podoplanin cytoplasmic tail displayed comparable level of podoplanin upregulation during skin wound healing and had normal wound closure, accompanied with the complete re-epithelialisation. In agreement with this data, previous study has also shown that keratinocyte-specific podoplanin deletion does not affect skin wound healing in mice (Baars et al., 2015). Secondly, macrophage numbers were not altered in the wound of podoplanin cytoplasmic tail deficient mice, suggesting that it is no relevant function of podoplanin cytoplasmic tail in macrophage turnover/recruitment, although the upregulation of podoplanin has been reported in inflammatory macrophages (Kerrigan et al., 2012, Rayes et al., 2017). Thirdly, the absence of podoplanin cytoplasmic tail had no impact on scar formation and collagen synthesis during skin wound healing. In agreement with this, podoplanin on lung epithelial and mesothelial cells is not required for myofibroblast differentiation during

lung development. Rather, the extracellular region of podoplanin on LECs (but not fibroblast lineage) activates platelet CLEC-2 to release TGF-β, which promotes mesothelial-to-myofibroblast transition. This leads to subsequent synthesis of ECM, including collagen, to support alveolar structure and function (Tsukiji et al., 2018a). Therefore, it might also imply that podoplanin, especially its cytoplasmic tail, that expressed on skin myofibroblasts (Nazari et al., 2016) is not necessary for cell migration and collagen synthesis.

In conclusion, characterisation of podoplanin cytoplasmic tail deficient mice provides the evidence that suggests indispensable roles of podoplanin cytoplasmic tail in various developmental and biological settings, including the prevention of blood-filled lymphatics, cerebrovascular integrity, platelet production, lung development, and skin wound healing. However, podoplanin cytoplasmic tail may regulate cerebrovascular development and lymphocyte homeostasis. Overall, this novel mouse model of mutated podoplanin may serve as a useful tool to discover or to further understand the role of podoplanin cytoplasmic tail, particularly in various pathophysiological conditions.

Chapter 5 The Association of Podoplanin Expression and Metabolic Changes in Macrophages

5.1 Introduction

5.1.1 An overview of metabolomics

In systems biology, there are hierarchical links between biomolecules, starting from genes that are transcribed into RNAs, subsequently translated into proteins, and finally metabolised into a low molecular weight metabolites (Tolstikov, 2016). Metabolomics is the study that provides collective information of metabolite expression in a biological system (Kim et al., 2016, Rochfort, 2005). This is one of the new "omics" that can support other omics data, including genomics, transcriptomics, and proteomics, to understand the connection between metabolite profiles and the expression and function of genes, proteins, and other biomolecules under certain phenotype (Rochfort, 2005, Kim et al., 2016). Emerging evidences demonstrate that metabolomics may provide benefits for biomedical research in multiple ways, including the finding of metabolite(s) that act as biomarkers for disease diagnosis (Zhang et al., 2016, Ussher et al., 2016) or targets for drug discovery, development, and monitoring (Tolstikov, 2016).

Nuclear magnetic resonance (NMR) spectroscopy and MS are commonly used techniques in metabolomics (Tolstikov, 2016). In NMR, metabolomics data are generated based on atomic nuclei, which differently absorb and re-emit energy following the applied magnetic field (Alonso et al., 2015). NMR is highly selective and is beneficial for structural determination of metabolites. However, the sensitivity is relatively low

(Tolstikov, 2016). MS is generally coupled with a separation technique, such as chromatography. Different metabolites take different times to pass through chromatographic column, allowing separation of biomolecules to reduce the complexity of sample. Chromatography also separates isomers, such as glucose, fructose, mannose, and galactose. Following separation, the sample is ionised by mass spectrometer to generate peaks that define the fingerprint of metabolite (Alonso et al., 2015, Tolstikov, 2016). MS provides high specificity and sensitivity, allowing detection of metabolites in various classes and concentrations (Tolstikov, 2016).

Metabolomics can be applied to various types of biological samples (e.g. blood, urine, cell or tissue extract, and other biofluids), which is manipulated either by untargeted or targeted approach (Schrimpe-Rutledge et al., 2016, Alonso et al., 2015). Untargeted metabolomics is a discovery-based study to examine the initial comprehensive information of putative metabolites by matching data with reference compounds in databases or libraries. A relative quantification can be performed in this approach (Schrimpe-Rutledge et al., 2016, Vinayavekhin and Saghatelian, 2010). Targeted metabolomics is generally a validation-based analysis to measure well-known metabolites. In this approach, the data derived from exact concentrations of standard compounds are used as reference for absolute quantification of metabolites from biological samples (Schrimpe-Rutledge et al., 2016, Roberts et al., 2012).

5.1.2 Cellular metabolism of glucose in macrophages

Glucose metabolism is essential for energy production and cellular function in macrophages (Langston et al., 2017, Blagih and Jones, 2012). Glucose can be metabolised by a pathway, namely glycolysis with or without a subsequent tricarboxylic acid (TCA)

cycle. Glucose undergoes glycolysis to produce pyruvate and two molecules of ATP, and in turn, under low oxygen conditions, pyruvate is metabolised into lactate. The rapid generation of ATP through glycolysis fuels the inflammatory response and anti-bacterial defence (Geeraerts et al., 2017). Under a sufficient oxygen supply, pyruvate is transported into mitochondria and further transformed to acetyl coenzyme A, which enters the TCA cycle to yield two additional ATPs. The reducing intermediates (electron donors), including nicotinamide adenine dinucleotide (NADH) from glycolysis and TCA cycle, and flavin adenine dinucleotide ($FADH_2$) generated in the TCA cycle, serve as fuels for electron transport chain (also called oxidative phosphorylation (OXPHOS) or mitochondrial respiration), which produces the majority of ATP (32-34 ATPs per glucose molecule) (Langston et al., 2017, Domblides et al., 2018). In addition, succinate donates electrons to complex II of the electron transport chain, which gives rise to fumarate (Figure 5.1), demonstrating the link between TCA cycle-derived intermediates and OXPHOS (Galvan-Pena and O'Neill, 2014, Diskin and Palsson-McDermott, 2018). The OXPHOS provides support for the anti-inflammatory function of macrophages (Geeraerts et al., 2017).

As mentioned previously, macrophages are classified into two main subtypes, including M1 pro-inflammatory and M2 anti-inflammatory/reparative phenotypes (Sindrilaru and Scharffetter-Kochanek, 2013). Macrophage plasticity is driven by the metabolic profile. M1 macrophages primarily rely on glycolysis (Figure 5.1 A). Previous reports have shown that in response to M1 activators (LPS and/or IFN-γ), the intracellular levels of pyruvate and lactate are elevated in macrophages (Baseler et al., 2016, Jha et al., 2015). This is associated with the secretion of pro-inflammatory cytokines and phagocytosis (Nishizawa et al., 2014, Rodriguez-Prados et al., 2010, Baseler et al., 2016, Jha et al.,

2015, Galvan-Pena and O'Neill, 2014, Diskin and Palsson-McDermott, 2018, Ussher et al., 2016). Macrophages from patients with coronary artery disease also demonstrate increased glycolysis, which contributes to the enhanced secretion of pro-inflammatory cytokines and the pathogenesis of vascular inflammation (Watanabe et al., 2018). A truncated TCA cycle has been described in M1 macrophages with two major breaks occurring at isocitrate dehydrogenase (IDH) and succinate dehydrogenase (SDH) enzymes (Figure 5.1 A). A reduced activity of IDH and SDH results in accumulation of citrate and succinate, respectively, in macrophages treated with LPS plus IFN-γ (Jha et al., 2015). The increase in succinate release from M1 macrophages also acts in an autocrine manner by binding to its surface receptor, which promotes inflammatory responses (Littlewood-Evans et al., 2016). Moreover, LPS and IFN-γ have been reported to inhibit OXPHOS in macrophages (Jha et al., 2015, Van den Bossche et al., 2016).

M2 macrophages are predominantly dependent on mitochondrial function, including the TCA cycle and OXPHOS (Figure 5.1 B) (Van den Bossche et al., 2016, Das et al., 2015, Geeraerts et al., 2017, Galvan-Pena and O'Neill, 2014). In contrast to accumulated succinate, fumarate is a TCA cycle intermediate that has been shown to promote M2 polarisation of macrophages, represented by a reduction in pro-inflammatory mediators (e.g. iNOS and TNF-α) but an increase in anti-inflammatory mediators (e.g. arginase-1 and IL-10) (Han et al., 2016, Bomprezzi, 2015). Previous evidence has also illustrated that M2 activators (e.g. IL-4 and IL-13) show increased activity of the TCA cycle (Rodriguez-Prados et al., 2010) and OXPHOS in macrophages (Jha et al., 2015, Van den Bossche et al., 2016, Binger et al., 2015). The glucose metabolism is therefore a key regulator of immune cell functions.

5.1.3 Arginine metabolism in macrophage polarisation

In addition to glucose, the amino acid arginine is important for macrophage function (Rath et al., 2014, Comalada et al., 2012). M1 macrophage increases uptake of arginine, which is metabolised by iNOS to produce nitric oxide and citrulline following activation with LPS plus IFN-γ (Figure 5.1 A) (Yeramian et al., 2006a). This metabolic pathway involves reactive oxygen species production and pathogen killing (Galvan-Pena and O'Neill, 2014, Sosroseno et al., 2004, Comalada et al., 2012). In contrast, arginase-1 activity and ornithine level are increased in macrophages treated with anti-inflammatory cytokines (IL4/IL10) (Figure 5.1 B) (Yeramian et al., 2006a), indicating alternative arginine catabolism, which supports tissue repair, characteristic of the M2 phenotype (Galvan-Pena and O'Neill, 2014, Comalada et al., 2012). Moreover, amino acid glutamine acts as a precursor for glutamate and α-ketoglutarate, which bypasses citrate to replenish the TCA cycle. This process can be driven by IL-4 (Langston et al., 2017).

5.1.4 Macrophage-expressed podoplanin in inflammation

Podoplanin is expressed at low level or not at all on macrophages and is upregulated during inflammatory conditions *in vitro* (Kerrigan et al., 2012) and *in vivo*, including in lung injury (Lax et al., 2017b), sepsis (Rayes et al., 2017), and skin wound healing. It is currently unknown whether the upregulation of podoplanin on inflammatory macrophages regulates their function. To study the function of podoplanin in macrophages, the haematopoietic cell-specific podoplanin-deficient mouse model (*Pdpn*$^{fl/fl}$*Vav1-cre*) has been generated. Previous evidence has demonstrated that cultured alveolar macrophages derived from this model show a 50% reduction in baseline podoplanin expression compared to macrophages derived from WT mice (Lax et al.,

2017a). These *Pdpn*$^{fl/fl}$*Vav1-cre* macrophages produce increased levels of pro-inflammatory cytokines in response to low-dose LPS (0.1 µg/ml) without an upregulation of podoplanin (Lax et al., 2017a), suggesting that podoplanin-deficient macrophages are hypersensitive to LPS/inflammatory challenge. On the other hand, in a sepsis model, a reduction in macrophage recruitment is observed in *Pdpn*$^{fl/fl}$*Vav1-cre* mice relative to controls, suggesting a role for podoplanin in macrophage migration (Rayes et al., 2017). A recent study also reports that the interaction of platelet CLEC-2 with podoplanin on alveolar macrophages stimulates matrix metalloproteinase-12 secretion to inactivate chemokines, which reduces inflammation and tissue damage during LPS-induced lung injury (Lax et al., 2017b), demonstrating the anti-inflammatory activity of the CLEC-2-podoplanin axis. However, there is no known association between podoplanin and the metabolic profile of macrophages.

In this chapter, the alteration of macrophage metabolism, focusing on glycolysis, TCA cycle coupled to OXPHOS, and arginine catabolism, were investigated in bone marrow-derived macrophages from WT and *Pdpn*$^{fl/fl}$*Vav1-cre* mice using HILIC/MS-based untargeted metabolomics. In addition, the metabolic changes during stimulation by LPS in the absence and presence of rCLEC-2-Fc were examined.

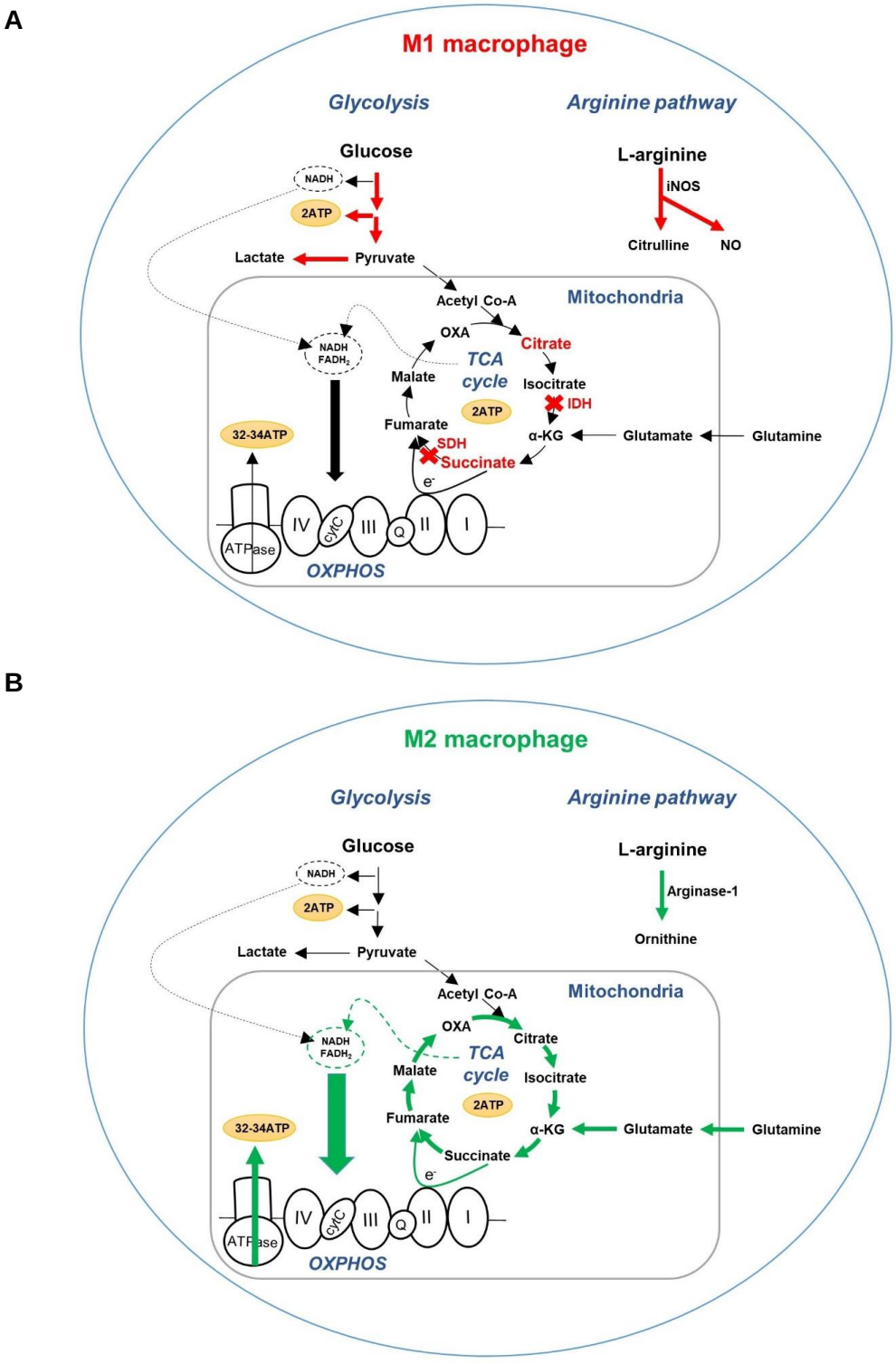
A
M1 macrophage
Glycolysis
Arginine pathway
Glucose
NADH
2ATP
Lactate
Pyruvate
L-arginine
iNOS
Citrulline
NO
Acetyl Co-A
Mitochondria
OXA
Citrate
NADH
FADH2
TCA
cycle
Malate
Isocitrate
IDH
2ATP
Fumarate
SDH
Succinate
α-KG
Glutamate
Glutamine
32-34ATP
e-
IV
cytC
III
Q
II
I
ATPase
OXPHOS
B
M2 macrophage
Glycolysis
Arginine pathway
Glucose
NADH
2ATP
Lactate
Pyruvate
L-arginine
Arginase-1
Ornithine
Acetyl Co-A
Mitochondria
OXA
Citrate
NADH
FADH2
TCA
cycle
Malate
Isocitrate
2ATP
Fumarate
α-KG
Glutamate
Glutamine
32-34ATP
Succinate
e-
IV
cytC
III
Q
II
I
ATPase
OXPHOS

Figure 5.1.

Figure 5. 1. Immunometabolic profile of M1 and M2 macrophages. (A) Glycolysis is the primary pathway of metabolism of M1 macrophages. In addition, arginine is metabolised by inducible nitric oxide synthase (iNOS) to produce nitric oxide (NO) that promotes M1 pro-inflammatory phenotype. The red arrows represent the metabolic pathways that are mainly used by M1 macrophages. Red cross mark indicates breakage of the TCA cycle in M1 macrophages. (B) The tricarboxylic acid (TCA) cycle coupled to oxidative phosphorylation (OXPHOS) is the major metabolic pathway in M2 macrophages. In contrast to M1 macrophages, arginase-1 metabolises arginine and gives rise to ornithine, which induces the M2 anti-inflammatory/reparative phenotype. The green arrows represent the metabolic pathways that are primarily used by M2 macrophages. I, II, III, and IV = complex I, II, III, and IV of electron transport chain, Co-A = coenzyme-A, Q = ubiquinone, Cyt C = cytochrome C, α-KG = α-ketoglutarate, OXA = oxaloacetate, IDH = isocitrate dehydrogenase, SDH = succinate dehydrogenase, NADH = nicotinamide adenine dinucleotide, $FADH_2$ = flavin adenine dinucleotide, ATP = adenosine triphosphate (Galvan-Pena and O'Neill, 2014, Geeraerts et al., 2017, Jha et al., 2015).

5.2 Results

5.2.1 Macrophages deficient in podoplanin show an increase in glycolytic metabolites

In this preliminary study, two metabolites in glycolysis, glucose and pyruvate were detected in bone marrow-derived WT macrophages (Figure 5.2 A, B). LPS treatment (1 µg/ml) of bone marrow-derived macrophages for 24 hours, a concentration known to induce the M1 phenotype and upregulation of podoplanin *in vitro* (Rayes et al., 2017, Kerrigan et al., 2012) had no effect on the glucose content (Figure 5.2 A). A 1.7-fold increase in pyruvate was observed in LPS-treated WT macrophages, which is in agreement with a previous study (Baseler et al., 2016) (Figure 5.2 A); however, a two-group comparison between LPS-treated and unchallenged WT macrophages demonstrated statistical significance for the increase in pyruvate following LPS (Figure 5.2 B). To examine the influence of the CLEC-2-podoplanin interaction on metabolic changes, LPS-treated WT macrophages were also incubated with rCLEC-2-Fc (20 µg/ml). The results showed that rCLEC-2-Fc did not affect the level of glucose and pyruvate in LPS-treated macrophages (Figure 5.2 A).

A significant increase in glucose and pyruvate levels was observed in *Pdpn$^{fl/fl}$Vav1-cre* macrophages relative to WT cells (7-fold and 3-fold respectively, Figure 5.2 A). There was no further alteration of glucose and pyruvate upon LPS stimulation in *Pdpn$^{fl/fl}$Vav1-cre* macrophages (Figure 5.2 A). These preliminary data indicate a negative association of podoplanin expression and glycolysis in macrophages.

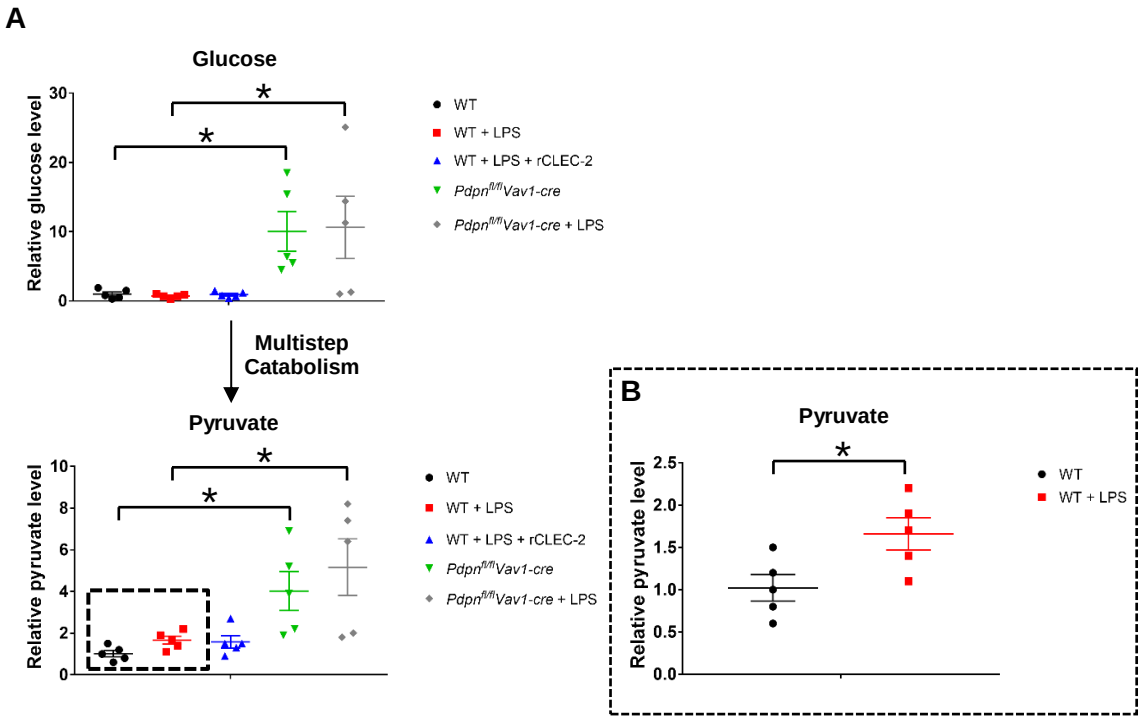

Figure 5. 2. Glycolytic metabolites are increased in podoplanin-deficient macrophages. (A) Relative quantification of glucose and pyruvate level in macrophages (n=5). Rectangle indicates a certain change of pyruvate in LPS-treated WT macrophages. (B) A subsequent two-group analysis of pyruvate level between unchallenged and LPS-treated WT macrophages revealed statistical significance (n=5). Bone marrow-derived macrophages from WT and haematopoietic cell-specific podoplanin deficient (*Pdpn*$^{fl/fl}$*Vav1-cre*) mice were incubated with LPS (1 µg/ml) for 24 hours. In addition, macrophages from WT mice were treated with LPS plus recombinant CLEC-2-Fc (rCLEC-2-Fc, 20 µg/ml). Cell extracts were collected for LC/MS-based untargeted metabolomics analysis. The peak area of individual metabolite was used as arbitrary unit of metabolite expression. The metabolite of interest from each sample was presented as fold change relative to the mean value in unchallenged WT. Data are presented as mean ± SEM, and analysed by either one-way ANOVA with Bonferroni's post-hoc test (A) or Student's t-test (B). *p<0.05.

5.2.2 A reduction of podoplanin does not alter the TCA cycle and/or OXPHOS in macrophages

Only a few metabolites related to the TCA cycle and OXPHOS were detected in this work. Fumarate was observed in unchallenged WT macrophages and there was no alteration following LPS treatment with or without rCLEC-2-Fc (Figure 5.3 A). Macrophages derived from *Pdpn*$^{fl/fl}$*Vav1-cre* mice did not exhibit differences in the baseline level of fumarate compared to WT (Figure 5.3 A). In a similar manner, LPS did not affect fumarate expression in *Pdpn*$^{fl/fl}$*Vav1-cre* macrophages (Figure 5.3 A). Glutamine was also detected but was not significantly different between all groups (Figure 5.3 B). These preliminary results suggest that a decrease in podoplanin does not affect the TCA cycle and OXPHOS in macrophages.

A

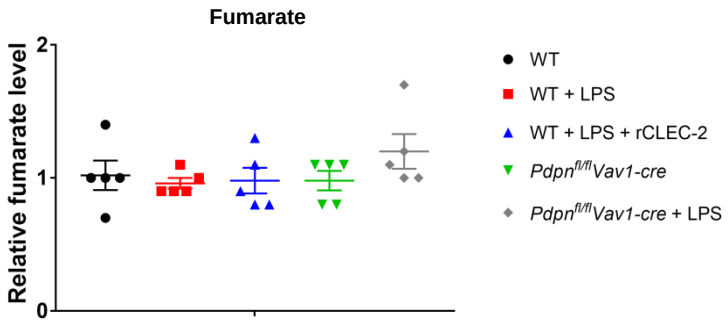

B

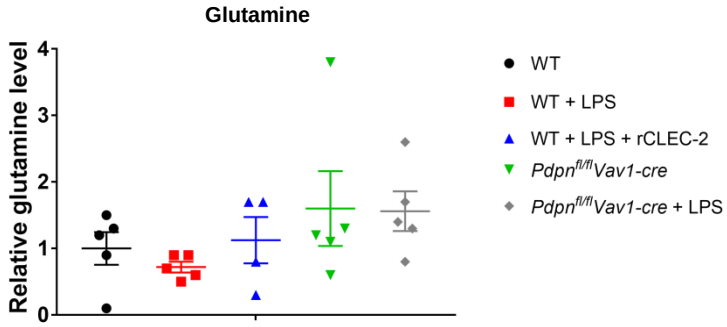

Figure 5. 3. Expression of fumarate and glutamine are unaltered in podoplanin-deficient macrophages. (A) Relative quantification of fumarate level in macrophages (n=5). (B) Relative quantification of glutamine level in macrophages (n=5). Bone marrow-derived macrophages from WT and haematopoietic cell-specific podoplanin deficient (*Pdpn$^{fl/fl}$Vav1-cre*) mice were incubated with LPS (1 µg/ml) for 24 hours. In addition, macrophages from WT mice were treated with LPS plus recombinant CLEC-2-Fc (rCLEC-2-Fc, 20 µg/ml). Cell extracts were collected for LC/MS-based untargeted metabolomics analysis. The peak area of individual metabolite was used as arbitrary unit of metabolite expression. The metabolite of interest from each sample was presented as fold change relative to the mean value in unchallenged WT. Data are presented as mean ± SEM, and analysed by one-way ANOVA with Bonferroni's post-hoc test.

5.2.3 Podoplanin deficiency leads to increased expression of metabolites in arginine metabolism, particularly iNOS-mediated pathway, in macrophages

In unchallenged WT macrophages, several metabolites in arginine pathway were detected, including arginine, citrulline, and ornithine (Figure 5.4 A). LPS did not cause significant changes of these metabolites in WT macrophages (Figure 5.4 A), which is in agreement with a previous study (Yeramian et al., 2006b). The metabolites were also unaltered in the presence of rCLEC-2-Fc (Figure 5.4 A). The *Pdpn*$^{fl/fl}$*Vav1-cre* macrophages exhibited a 30-fold increase in baseline arginine compared to WT macrophages and there was no further alteration following LPS treatment (Figure 5.4 A). In addition, citrulline and ornithine were upregulated (25-fold and 13-fold, respectively) in *Pdpn*$^{fl/fl}$*Vav1-cre* macrophages compared to WT, irrespective of LPS challenge (Figure 5.4 A). Moreover, a sub-analysis of the data revealed that *Pdpn*$^{fl/fl}$*Vav1-cre* macrophages had significantly higher levels of citrulline (approximately 2-fold) than ornithine (Figure 5.4 B). Together, these results show that arginine catabolism, the iNOS-mediated pathway in particular, is enhanced in podoplanin-deficient macrophages.

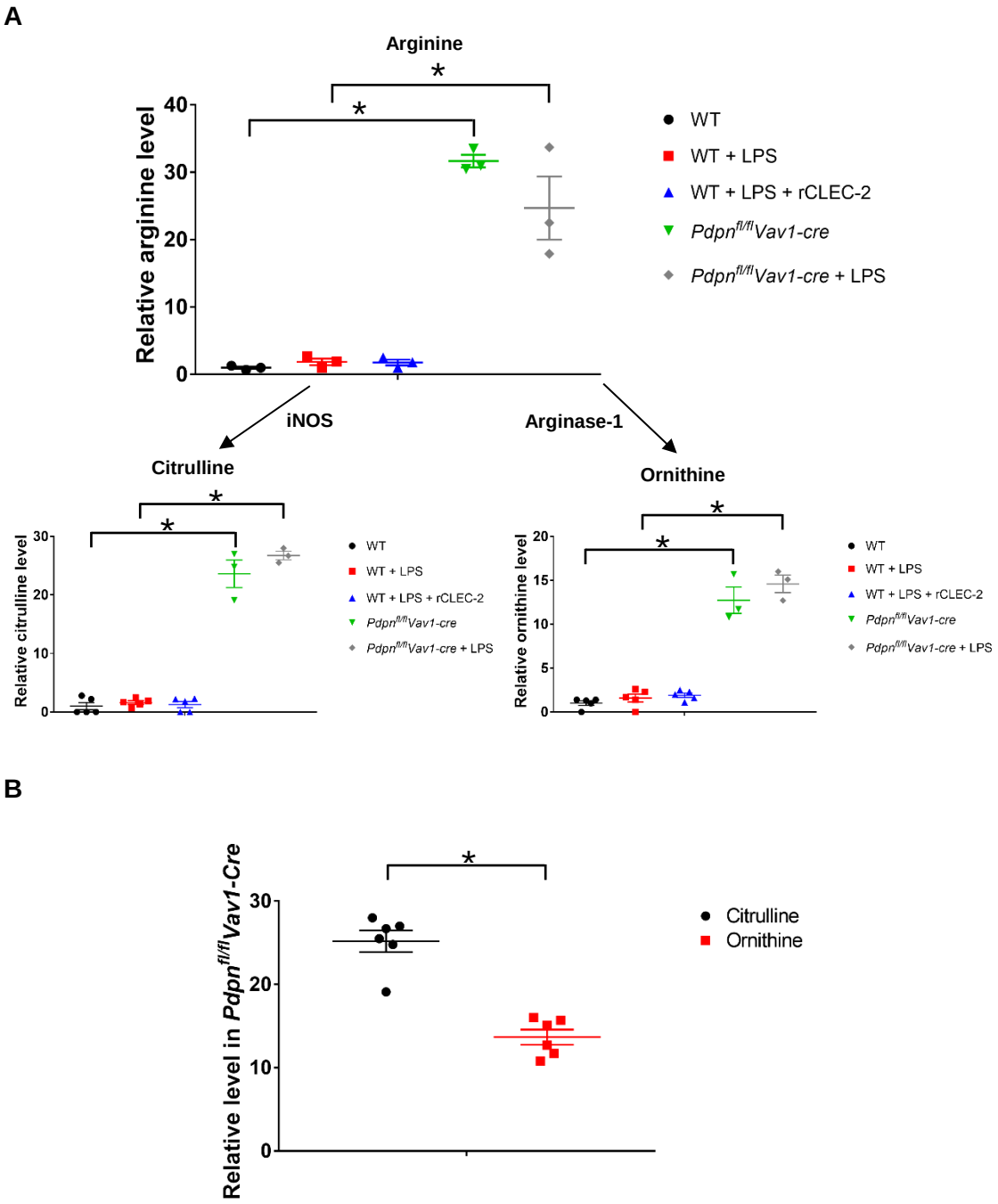
A
Arginine
Relative arginine level
WT
WT + LPS
WT + LPS + rCLEC-2
Pdpn fl/fl Vav1-cre
Pdpn fl/fl Vav1-cre + LPS
iNOS
Arginase-1
Citrulline
Ornithine
Relative citrulline level
Relative ornithine level
B
Relative level in Pdpn fl/fl Vav1-Cre
Citrulline
Ornithine

Figure 5.4.

Figure 5. 4. Metabolites in arginine catabolism, especially iNOS-mediated pathway, are upregulated in podoplanin-deficient macrophages. (A) Relative quantification of arginine, citrulline, and ornithine level in macrophages (n=3-5). (B) Comparison between the level of citrulline and ornithine in haematopoietic cell-specific podoplanin deficient (*Pdpn*$^{fl/fl}$*Vav1-cre*) macrophages. Data from unchallenged and LPS-treated *Pdpn*$^{fl/fl}$*Vav1-cre* mice are combined (n=6). Bone marrow-derived macrophages from WT and *Pdpn*$^{fl/fl}$*Vav1-cre* mice were incubated with LPS (1 μg/ml) for 24 hours. In addition, macrophages from WT mice were treated with LPS plus recombinant CLEC-2-Fc (rCLEC-2-Fc, 20 μg/ml). Cell extracts were collected for LC/MS-based untargeted metabolomics analysis. The peak area of individual metabolite was used as arbitrary unit of metabolite expression. The metabolite of interest from each sample was presented as fold change relative to the mean value in unchallenged WT. Data are presented as mean ± SEM, and analysed by either one-way ANOVA with Bonferroni's post-hoc test (A) or Student's t-test (B). *p<0.05.

5.3 Discussion

In response to stimuli, macrophages change their metabolic profile to support their numerous biological functions (Diskin and Palsson-McDermott, 2018, Galvan-Pena and O'Neill, 2014). In this chapter, the alteration of metabolic pathways has been examined in cultured bone marrow-derived macrophages from WT and podoplanin-deficient mice in order to investigate whether the anti-inflammation action of podoplanin is mediated by alteration of metabolism. Although limited numbers of metabolites were detected in this work, the preliminary results show that macrophages deficient in podoplanin had a significant increase in the expression of key metabolites in glycolysis and arginine catabolism but not in TCA cycle and/or OXPHOS, suggesting a negative regulatory role of podoplanin in glycolysis and arginine metabolism. Moreover, the metabolic profile in LPS-treated WT macrophages was not affected by rCLEC-2-Fc, indicating that the alteration of these two metabolic pathways in macrophages is independent of CLEC-2-podoplanin interaction. Alternatively, this might be due to the limited binding of this recombinant protein to macrophage podoplanin in the studied condition (unpublished data in Watson laboratory). The summary of metabolic status of podoplanin-deficient macrophages is shown in Figure 5.5.

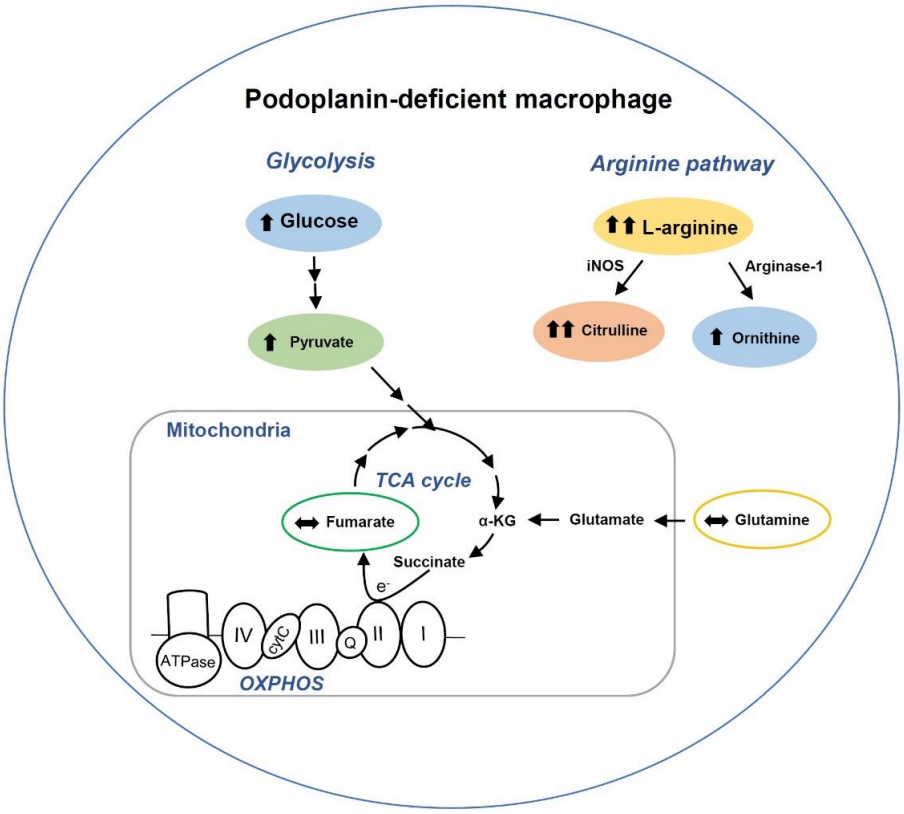

Figure 5. 5. An alteration of tested metabolic pathways in podoplanin-deficient macrophages. Metabolic intermediates in glycolysis (i.e. glucose and pyruvate), a primary pathway used by M1 macrophages, are increased in podoplanin-deficient macrophages. Podoplanin deficiency does not affect the TCA cycle and/or OXPHOS-related metabolites (i.e. fumarate and glutamine), an important metabolism found in M2 macrophages. Baseline arginine is also increased in podoplanin-deficient macrophages. However, the increase in iNOS-mediated metabolite (i.e. citrulline) is greater than arginase-1-mediated metabolite (i.e. ornithine) in podoplanin-deficient macrophages. Together, these metabolic data support the pro-inflammatory activity of podoplanin-deficient macrophages. ↑↑ = highly increased level, ↑ = increased level, ↔ = unchanged level. Metabolites with no coloured circle are not measured in this study. I, II, III, and IV = complex I, II, III, and IV of electron transport chain, Q = Ubiquinone, Cyt C = cytochrome C, α-KG = α-ketoglutarate.

As previously described, *Pdpn*$^{fl/fl}$*Vav1-cre* model of podoplanin deficiency does not completely delete podoplanin in macrophages. However, an approximately 50% reduction in podoplanin is sufficient to produce significant phenotypic changes in macrophages (Lax et al., 2017a). Treatment with 0.1 µg/ml LPS causes the upregulation of pro-inflammatory cytokines, including TNF-α, IL-6, and CXCL2 in *Pdpn*$^{fl/fl}$*Vav1-cre* macrophages, suggesting they are more sensitive to LPS in mediating inflammation. In accordance with this, basal glycolysis was upregulated in podoplanin-deficient bone marrow-derived macrophages whereas the TCA cycle and/or OXPHOS-associated metabolites (i.e. fumarate and glutamine) were unaltered. In addition, the iNOS-mediated metabolite citrulline was increase to a higher degree than the arginase-1-driven metabolite ornithine. Although a previous study has reported a normal level of iNOS in *Pdpn*$^{fl/fl}$*Vav1-cre* alveolar macrophages (Lax et al., 2017a), the enzymatic activity of either iNOS or arginase-1 was not tested. More recently, it has been shown in another model of podoplanin-deficient macrophages that mRNA expression of arginase-1 (*Arg-1*), but not iNOS (*NOS2*), is reduced when co-cultured with cancer cells (i.e. glioma), contributing to an increase in inflammation (Eisemann et al., 2019). These *in vitro* data support the negative association between podoplanin expression and M1 pro-inflammatory phenotype of macrophages independent of CLEC-2.

In agreement with the metabolic data, it has been shown *in vivo* that podoplanin-positive macrophages are increased during the resolution phase (72 hours post-injection) of zymosan-induced peritonitis (Hou et al., 2010). In addition, enhanced phagocytic activity is observed in this macrophage population *in vitro*. Thus, it is speculated that podoplanin-positive macrophages facilitate the resolution of inflammation by mediating clearance of pro-inflammatory components (e.g. leucocytes) through phagocytosis (Hou et al., 2010).

Following intra-tracheal LPS infiltration in mice, macrophages collected from bronchoalveolar lavage fluid of *Pdpn*$^{fl/fl}$*Vav1-cre* mice exhibit a 50% reduction in podoplanin expression relative to WT, which contributes to the worsening of lung injury (Lax et al., 2017b). In a model of glioma, podoplanin on macrophages has been shown to suppress immune response, contributing to cancer progression (Eisemann et al., 2019). These observations support the role of podoplanin in limiting macrophage-induced inflammation *in vivo*.

In conclusion, the results of preliminary metabolomics analysis reveal the potential function of podoplanin in limiting glycolysis and arginine metabolism in macrophages, which possibly attenuates inflammatory response following activation. This metabolic profile provides additional evidence that may explain why podoplanin-deficient macrophages are more prone to mediate inflammatory responses during inflammation.

Chapter 6 General Discussion

6.1 Summary of results

This thesis has shown that inflammatory bleeding caused by deficiency in platelet (hemi)ITAM receptors enhances the rate of cutaneous wound healing. During the inflammatory phase of repair process, it is postulated that a lack of interaction between platelet GPVI and CLEC-2 with their ligands in the injured vessel (i.e. collagen and podoplanin, respectively) leading to transient vascular leakage that allows extravasation of plasma-derived molecules, including fibrinogen, into the wound. The accumulation of fibrinogen and fibrin promotes wound healing in multiple ways as shown by the accompanied increase in re-epithelialisation and angiogenesis. Simultaneously, fibrinogen and fibrin may physically impede leucocyte infiltration, resulting in a reduction in inflammation and tissue damage, which also facilitate wound healing. This is the first insight into how a different form of bleeding dictates its beneficial or detrimental role in wound repair.

The (patho)physiological contribution of the podoplanin cytoplasmic tail has also been described. The loss of the cytoplasmic region however caused a reduction in basal podoplanin expression in various organs making it unclear whether a phenotype was mediated by the reduced and/or the loss of the tail. As such, the use of the mouse is limited. Nevertheless, in contrast to constitutive loss of podoplanin, the mice are viable demonstrating that at least part of the physiological role of podoplanin is independent of the tail region possibly because part of action of podoplanin is through activation of CLEC-2. The demonstration of normal development of the lymphatics and unchanged

wound healing times provides evidence that the cytoplasmic tail is dispensable for these two processes.

In addition, this study has provided preliminary evidence that podoplanin regulates macrophage metabolism. Glycolysis and iNOS-mediated arginine catabolism, the metabolic pathways that are primarily used in M1 pro-inflammatory macrophages, were increased in podoplanin-deficient macrophages. The underlying mechanism is not known.

6.2 The cause of intra-tissue bleeding determines its beneficial or detrimental role in wound healing

The association of platelets and vascular integrity has been known for more than a half century (Majno and Palade, 1961, Cotran, 1965). More recently, the role of platelets in preventing vascular leakage during inflammation, including in skin, was shown in thrombocytopenic (Goerge et al., 2008) and (hemi)ITAM-deficient animals (Boulaftali et al., 2013). Several previous studies have shown devastating effects of inflammation-induced bleeding, particularly in the major organs (Ho-Tin-Noe et al., 2009, Goerge et al., 2008, Hillgruber et al., 2015). For example, in the model of LPS-induced lung inflammation, the intra-alveolar bleeding spreads throughout the lung in thrombocytopenic mice (Goerge et al., 2008, Hillgruber et al., 2015). These mice demonstrate breathing difficulty, anaemia, and restricted activity, indicating severe illness (Goerge et al., 2008). Following skin rPA, there are no reports of adverse effects directly related to intra-tissue bleeding (Rayes et al., 2018, Gros et al., 2015), but the severity of inflammation itself may lead to skin necrosis and systemic immune complex diseases

(Movat, 1979). Interestingly, this thesis presents the positive effect of inflammatory bleeding for the first time in skin wound healing. The short-term intra-wound bleeding due to a lack of platelet (hemi)ITAM receptors, GPVI and CLEC-2, resulted in accumulation of fibrinogen and fibrin in the wound and accelerated wound healing at an early phase, providing a new paradigm for medical impact of intra-tissue bleeding. This is in contrast to the delay in wound healing in haemophilia B mice that lack FIX and exhibit reduced fibrin generation in association with leakiness of newly-formed blood vessel and dysregulated angiogenesis (Hoffman et al., 2006). This thereby emphasises the causal link between bleeding characteristics and its consequences.

6.3 Targeting vascular integrity and platelet (hemi)ITAM in wound healing

Wounds have a global impact in medical and economical aspects (Lindholm and Searle, 2016, Meier and Nanney, 2006). Millions of people over the world suffer from various types of wound injury (Lindholm and Searle, 2016, Meier and Nanney, 2006). The shortened healing duration provides effective wound management by reducing the cost of care and the risk of complications (e.g. infections and disabilities) (Lindholm and Searle, 2016). However, while current therapeutic interventions partially improve the healing process, a single agent/method may not be applicable to all cases (Meier and Nanney, 2006, Zielins et al., 2015). Therefore, new therapeutic modalities are emerging (Boateng and Catanzano, 2015, Park et al., 2013). Platelet and fibrin preparations, such as autologous platelet-rich plasma (Chicharro-Alcantara et al., 2018, Lacci and Dardik, 2010, Carter et al., 2011) and platelet-rich fibrin (Naik et al., 2013, Pinto et al., 2018) demonstrate a promising outcome in facilitating skin wound healing, most likely because

of growth factors and cytokines released from activated platelets. However, these treatments require blood from patients, which is invasive, and the efficacy may vary depending on the preparation techniques (Chicharro-Alcantara et al., 2018, Lacci and Dardik, 2010, Carter et al., 2011). Intriguingly, this thesis provides a possible way for non-invasive therapeutic intervention that allows self-operated release of plasma components, including platelets and fibrinogen, into the wound to promote repair process. Indeed, the temporal intra-wound bleeding suggests that the degree of vascular leakage in platelet (hemi)ITAM receptor deficiency is greater than the increased vascular permeability during inflammation (Ono et al., 2017, Park-Windhol and D'Amore, 2016), which also shown to enhance wound healing (Mendonca et al., 2010, Cipriani Frade et al., 2004, Shaterian et al., 2009, Seo et al., 2007). However, this inflammatory bleeding did not cause discernible adverse effects, thereby paving the way for its potential use in wound management. Future studies should investigate the impact of this method on wound healing in comparison with platelet/fibrin preparations or enhanced vascular permeability.

It has been previously shown that inhibition of kinases of GPVI and CLEC-2, such as Syk (Long et al., 2016) or Src kinases (Apperley et al., 2009) disrupts vascular integrity, but there is no formal study conducting the impact of tyrosine kinase inhibitors on wound healing (Shah et al., 2014). In the future, it will be interesting to investigate whether topical inhibition of the two (hemi)ITAM receptors or their downstream tyrosine kinases might provide benefits in skin wound healing. In human, a low level of podoplanin is only observed around blood vessel during skin inflammation, such as in eczema and psoriasis, but not in normal skin (Groger et al., 2007), raising the question of the clinical implications of targeting platelet (hemi)ITAM and vascular integrity in human skin

wound. Moreover, the repair process in murine skin does not fully represent wound healing in human, partly because of a significant contribution of wound contraction to the healing process in loose-skin animals (Davidson et al., 2013, Chen et al., 2015). This factor should also be considered in order to apply the findings in animal experiments for human studies.

6.4 Filling the gaps in the multifaceted role of podoplanin

Podoplanin has diverse patterns of expression, interaction, and biological function (Schacht et al., 2005, Astarita et al., 2012, Quintanilla et al., 2019). Until recently, many aspects of podoplanin biology were elusive. Firstly, it has never been clearly defined how platelet CLEC-2 interacts with podoplanin to aid GPVI in maintaining vascular integrity during skin inflammation (Ho-Tin-Noe et al., 2018, Boulaftali et al., 2018). This thesis reports that podoplanin-positive cells encircled the microvasculature in unchallenged murine skin and that this is preserved during wound healing, thereby providing the potential to bind to platelet CLEC-2 during vascular endothelial disruption or activation. The podoplanin-expressing cells at the perivascular area of skin were shown to include pericytes, fibroblasts, infiltrating monocytes, and inflammatory macrophages (*Section 3.2.1*). However, podoplanin was not detected in the vicinity of blood vessels in other tissues, such as the lungs, liver, and kidneys (*Section 4.2.6*), supporting previous evidence of organ-specific roles of platelet GPVI and CLEC-2 in maintaining vascular integrity (Rayes et al., 2018, Ho-Tin-Noe et al., 2018) Secondly, although podoplanin is upregulated on keratinocytes during skin wound healing (*Section 3.2.1*) (Asai et al., 2016), it is unlikely to affect the healing process as shown by a normal wound closure in mice that lack podoplanin on keratinocytes (Baars et al., 2015), arguing against the role

of CLEC-2-podoplanin in keratinocyte migration demonstrated *in vitro* (Asai et al., 2016). Thirdly, the significance of signalling through podoplanin cytoplasmic tail is controversial. Although it is not conclusive, the work in this thesis hints that certain developmental and (patho)physiological functions of podoplanin are unlikely to be mediated by its cytoplasmic region. For example, the finding of normal blood-lymphatic separation in mice that lack the podoplanin cytoplasmic tail (*Section 4.2.7*) may emphasise the crucial role of its ectodomain in activating CLEC-2, leading to platelet aggregation to prevent blood-lymphatic vessel mixing (Bertozzi et al., 2010, Hess et al., 2014). This also suggests that a small amount of podoplanin ectodomain is required for blood-lymphatic separation. Future studies should rule out additional interactions of its ectodomain and/or transmembrane region in regulating this function e.g. the lateral interaction between podoplanin and galectin-8 on cell surface of LECs has been proposed to regulate lymphvasculogenesis (Cueni and Detmar, 2009). Further, podoplanin has been shown to produce either pro-inflammatory or anti-inflammatory activity depending on pathological conditions (Croft et al., 2016, Takakubo et al., 2017, Peters et al., 2015). The present metabolic findings in macrophages reveal a negative association of podoplanin in glycolysis and iNOS-mediated arginine metabolism (*Section 5.2.1*), the two metabolic pathways found in M1 pro-inflammatory macrophages (Diskin and Palsson-McDermott, 2018), providing a metabolic contribution for the anti-inflammatory function of podoplanin in macrophages (Lax et al., 2017b, Hou et al., 2010). Future studies should examine the connection between these metabolites and the biological/functional responses, particularly *in vivo*, to fully understand the role of podoplanin in inflammation.

6.5 Final conclusions

Many emerging roles of platelet CLEC-2 and podoplanin have been investigated, with the urgent need for a viable animal model of podoplanin deficiency that allows an understanding of podoplanin biology in health and disease. Overall, the newly discovered acceleration of skin wound healing in mice deficient in platelet GPVI and CLEC-2 provides an important insight into a positive regulatory role of intra-tissue haemorrhage in repair process. Although there are detailed differences in skin wound healing between mice and humans, which require further studies, this new understanding of the benefit of targeting platelet (hemi)ITAM and vascular integrity in wound repair may lead to the discovery of novel therapeutic innovations.

References

ABTAHIAN, F., GUERRIERO, A., SEBZDA, E., LU, M. M., ZHOU, R., MOCSAI, A., MYERS, E. E., HUANG, B., JACKSON, D. G., FERRARI, V. A., TYBULEWICZ, V., LOWELL, C. A., LEPORE, J. J., KORETZKY, G. A. & KAHN, M. L. 2003. Regulation of blood and lymphatic vascular separation by signaling proteins SLP-76 and Syk. Science, 299**,** 247-51.

ACTON, S. E., ASTARITA, J. L., MALHOTRA, D., LUKACS-KORNEK, V., FRANZ, B., HESS, P. R., JAKUS, Z., KULIGOWSKI, M., FLETCHER, A. L., ELPEK, K. G., BELLEMARE-PELLETIER, A., SCEATS, L., REYNOSO, E. D., GONZALEZ, S. F., GRAHAM, D. B., CHANG, J., PETERS, A., WOODRUFF, M., KIM, Y. A., SWAT, W., MORITA, T., KUCHROO, V., CARROLL, M. C., KAHN, M. L., WUCHERPFENNIG, K. W. & TURLEY, S. J. 2012. Podoplanin-rich stromal networks induce dendritic cell motility via activation of the C-type lectin receptor CLEC-2. Immunity, 37**,** 276-89.

ACTON, S. E., FARRUGIA, A. J., ASTARITA, J. L., MOURAO-SA, D., JENKINS, R. P., NYE, E., HOOPER, S., VAN BLIJSWIJK, J., ROGERS, N. C., SNELGROVE, K. J., ROSEWELL, I., MOITA, L. F., STAMP, G., TURLEY, S. J., SAHAI, E. & REIS E SOUSA, C. 2014. Dendritic cells control fibroblastic reticular network tension and lymph node expansion. Nature, 514**,** 498-502.

AGRAWAL, S., GANGULY, S., HAJIAN, P., CAO, J. N. & AGRAWAL, A. 2015. PDGF upregulates CLEC-2 to induce T regulatory cells. Oncotarget, 6**,** 28621-32.

AL-TAMIMI, M., GARDINER, E. E., THOM, J. Y., SHEN, Y., COOPER, M. N., HANKEY, G. J., BERNDT, M. C., BAKER, R. I. & ANDREWS, R. K. 2011. Soluble glycoprotein VI is raised in the plasma of patients with acute ischemic stroke. Stroke, 42**,** 498-500.

ALBALA, D. M. 2003. Fibrin sealants in clinical practice. Cardiovasc Surg, 11 Suppl 1**,** 5-11.

ALONSO, A., MARSAL, S. & JULIA, A. 2015. Analytical methods in untargeted metabolomics: state of the art in 2015. Front Bioeng Biotechnol, 3**,** 23.

ALSHEHRI, O. M., HUGHES, C. E., MONTAGUE, S., WATSON, S. K., FRAMPTON, J., BENDER, M. & WATSON, S. P. 2015. Fibrin activates GPVI in human and mouse platelets. Blood, 126**,** 1601-8.

ALSTON, S. M., SOLEN, K. A., SUKAVANESHVAR, S. & MOHAMMAD, S. F. 2008. In vivo efficacy of a new autologous fibrin sealant. J Surg Res, 146**,** 143-8.

APPERLEY, J. F., CORTES, J. E., KIM, D. W., ROY, L., ROBOZ, G. J., ROSTI, G., BULLORSKY, E. O., ABRUZZESE, E., HOCHHAUS, A., HEIM, D., DE SOUZA, C. A., LARSON, R. A., LIPTON, J. H., KHOURY, H. J., KIM, H. J., SILLABER, C., HUGHES, T. P., ERBEN, P., VAN TORNOUT, J. & STONE, R. M. 2009. Dasatinib in the treatment of chronic myeloid leukemia in accelerated phase after imatinib failure: the START a trial. J Clin Oncol, 27**,** 3472-9.

ARIENS, R. A., LAI, T. S., WEISEL, J. W., GREENBERG, C. S. & GRANT, P. J. 2002. Role of factor XIII in fibrin clot formation and effects of genetic polymorphisms. Blood, 100**,** 743-54.

ARQUÉS, O., CHICOTE, I., TENBAUM, S., PUIG, I. & PALMER, H. G. 2012. Standardized Relative Quantification of Immunofluorescence Tissue Staining. Protocol Exchange

ARTHUR, J. F., DUNKLEY, S. & ANDREWS, R. K. 2007. Platelet glycoprotein VI-related clinical defects. Br J Haematol, 139**,** 363-72.

ASAI, J., HIRAKAWA, S., SAKABE, J., KISHIDA, T., WADA, M., NAKAMURA, N., TAKENAKA, H., MAZDA, O., URANO, T., SUZUKI-INOUE, K., TOKURA, Y. & KATOH, N. 2016. Platelets Regulate the Migration of Keratinocytes via Podoplanin/CLEC-2 Signaling during Cutaneous Wound Healing in Mice. Am J Pathol, 186**,** 101-8.

ASTARITA, J. L., ACTON, S. E. & TURLEY, S. J. 2012. Podoplanin: emerging functions in development, the immune system, and cancer. Front Immunol, 3**,** 283.

ASTARITA, J. L., CREMASCO, V., FU, J., DARNELL, M. C., PECK, J. R., NIEVES-BONILLA, J. M., SONG, K., KONDO, Y., WOODRUFF, M. C., GOGINENI, A., ONDER, L., LUDEWIG, B., WEIMER, R. M., CARROLL, M. C., MOONEY, D. J., XIA, L. & TURLEY, S. J. 2015. The CLEC-2-podoplanin axis controls the contractility of fibroblastic reticular cells and lymph node microarchitecture. Nat Immunol, 16**,** 75-84.

BAARS, S., BAUER, C., SZABOWSKI, S., HARTENSTEIN, B. & ANGEL, P. 2015. Epithelial deletion of podoplanin is dispensable for re-epithelialization of skin wounds. Exp Dermatol, 24**,** 785-7.

BARISIC-DUJMOVIC, T., BOBAN, I. & CLARK, S. H. 2010. Fibroblasts/myofibroblasts that participate in cutaneous wound healing are not derived from circulating progenitor cells. J Cell Physiol, 222**,** 703-12.

BASELER, W. A., DAVIES, L. C., QUIGLEY, L., RIDNOUR, L. A., WEISS, J. M., HUSSAIN, S. P., WINK, D. A. & MCVICAR, D. W. 2016. Autocrine IL-10 functions as a rheostat for M1 macrophage glycolytic commitment by tuning nitric oxide production. Redox Biol, 10**,** 12-23.

BAUTCH, V. L. & CARON, K. M. 2015. Blood and lymphatic vessel formation. Cold Spring Harb Perspect Biol, 7**,** a008268.

BEN AMAR, M. & WU, M. 2014. Re-epithelialization: advancing epithelium frontier during wound healing. J R Soc Interface, 11**,** 20131038.

BENDER, M., MAY, F., LORENZ, V., THIELMANN, I., HAGEDORN, I., FINNEY, B. A., VOGTLE, T., REMER, K., BRAUN, A., BOSL, M., WATSON, S. P. & NIESWANDT, B. 2013. Combined in vivo depletion of glycoprotein VI and C-type lectin-like receptor 2 severely compromises hemostasis and abrogates arterial thrombosis in mice. Arterioscler Thromb Vasc Biol, 33**,** 926-34.

BERTOZZI, C. C., SCHMAIER, A. A., MERICKO, P., HESS, P. R., ZOU, Z., CHEN, M., CHEN, C. Y., XU, B., LU, M. M., ZHOU, D., SEBZDA, E., SANTORE, M. T., MERIANOS, D. J., STADTFELD, M., FLAKE, A. W., GRAF, T., SKODA, R., MALTZMAN, J. S., KORETZKY, G. A. & KAHN, M. L. 2010. Platelets regulate lymphatic vascular development through CLEC-2-SLP-76 signaling. Blood, 116**,** 661-70.

BEST, D., SENIS, Y. A., JARVIS, G. E., EAGLETON, H. J., ROBERTS, D. J., SAITO, T., JUNG, S. M., MOROI, M., HARRISON, P., GREEN, F. R. & WATSON, S. P. 2003. GPVI levels in platelets: relationship to platelet function at high shear. Blood, 102**,** 2811-8.

BIGALKE, B., HAAP, M., STELLOS, K., GEISLER, T., SEIZER, P., KREMMER, E., OVERKAMP, D. & GAWAZ, M. 2010a. Platelet glycoprotein VI (GPVI) for early identification of acute coronary syndrome in patients with chest pain. Thromb Res, 125**,** e184-9.

BIGALKE, B., STELLOS, K., GEISLER, T., KREMMER, E., SEIZER, P., MAY, A. E., LINDEMANN, S., MELMS, A., LUFT, A. & GAWAZ, M. 2010b. Expression of platelet glycoprotein VI is associated with transient ischemic attack and stroke. Eur J Neurol, 17**,** 111-7.

BIGALKE, B., STELLOS, K., GEISLER, T., LINDEMANN, S., MAY, A. E. & GAWAZ, M. 2010c. Glycoprotein VI as a prognostic biomarker for cardiovascular death in patients with symptomatic coronary artery disease. Clin Res Cardiol, 99**,** 227-33.

BINGER, K. J., GEBHARDT, M., HEINIG, M., RINTISCH, C., SCHROEDER, A., NEUHOFER, W., HILGERS, K., MANZEL, A., SCHWARTZ, C., KLEINEWIETFELD, M., VOELKL, J., SCHATZ, V., LINKER, R. A., LANG, F., VOEHRINGER, D., WRIGHT, M. D., HUBNER, N., DECHEND, R., JANTSCH, J., TITZE, J. & MULLER, D. N. 2015. High salt reduces the activation of IL-4- and IL-13-stimulated macrophages. J Clin Invest, 125**,** 4223-38.

BIRD, J. E., WANG, X., SMITH, P. L., BARBERA, F., HUANG, C. & SCHUMACHER, W. A. 2012. A platelet target for venous thrombosis? P2Y1 deletion or antagonism protects mice from vena cava thrombosis. J Thromb Thrombolysis, 34**,** 199-207.

BLAGIH, J. & JONES, R. G. 2012. Polarizing macrophages through reprogramming of glucose metabolism. Cell Metab, 15**,** 793-5.

BOATENG, J. & CATANZANO, O. 2015. Advanced Therapeutic Dressings for Effective Wound Healing--A Review. J Pharm Sci, 104**,** 3653-80.

BODNAR, R. J., SATISH, L., YATES, C. C. & WELLS, A. 2016. Pericytes: A newly recognized player in wound healing. Wound Repair Regen, 24**,** 204-14.

BOILARD, E., NIGROVIC, P. A., LARABEE, K., WATTS, G. F., COBLYN, J. S., WEINBLATT, M. E., MASSAROTTI, E. M., REMOLD-O'DONNELL, E., FARNDALE, R. W., WARE, J. & LEE, D. M. 2010. Platelets amplify inflammation in arthritis via collagen-dependent microparticle production. Science, 327**,** 580-3.

BOMPREZZI, R. 2015. Dimethyl fumarate in the treatment of relapsing-remitting multiple sclerosis: an overview. Ther Adv Neurol Disord, 8**,** 20-30.

BOULAFTALI, Y., HESS, P. R., GETZ, T. M., CHOLKA, A., STOLLA, M., MACKMAN, N., OWENS, A. P., 3RD, WARE, J., KAHN, M. L. & BERGMEIER, W. 2013. Platelet ITAM signaling is critical for vascular integrity in inflammation. J Clin Invest, 123**,** 908-16.

BOULAFTALI, Y., MAWHIN, M. A., JANDROT-PERRUS, M. & HO-TIN-NOE, B. 2018. Glycoprotein VI in securing vascular integrity in inflamed vessels. Res Pract Thromb Haemost, 2**,** 228-239.

BRILL, A., FUCHS, T. A., CHAUHAN, A. K., YANG, J. J., DE MEYER, S. F., KOLLNBERGER, M., WAKEFIELD, T. W., LAMMLE, B., MASSBERG, S. & WAGNER, D. D. 2011. von Willebrand factor-mediated platelet adhesion is critical for deep vein thrombosis in mouse models. Blood, 117**,** 1400-7.

BROWN, B. N., SICARI, B. M. & BADYLAK, S. F. 2014. Rethinking regenerative medicine: a macrophage-centered approach. Front Immunol, 5**,** 510.

BROWN, L. F., YEO, K. T., BERSE, B., YEO, T. K., SENGER, D. R., DVORAK, H. F. & VAN DE WATER, L. 1992. Expression of vascular permeability factor (vascular endothelial growth factor) by epidermal keratinocytes during wound healing. J Exp Med, 176**,** 1375-9.

BROWN, M., WEDGE, D. C., GOODACRE, R., KELL, D. B., BAKER, P. N., KENNY, L. C., MAMAS, M. A., NEYSES, L. & DUNN, W. B. 2011. Automated workflows for accurate mass-based putative metabolite identification in LC/MS-derived metabolomic datasets. Bioinformatics, 27**,** 1108-12.

BULTMANN, A., LI, Z., WAGNER, S., PELUSO, M., SCHONBERGER, T., WEIS, C., KONRAD, I., STELLOS, K., MASSBERG, S., NIESWANDT, B., GAWAZ, M., UNGERER, M. & MUNCH, G. 2010. Impact of glycoprotein VI and platelet adhesion on atherosclerosis--a possible role of fibronectin. J Mol Cell Cardiol, 49**,** 532-42.

CANENE-ADAMS, K. 2013. Preparation of formalin-fixed paraffin-embedded tissue for immunohistochemistry. Methods Enzymol, 533**,** 225-33.

CARBO, C., DEL CONDE, I. & DUERSCHMIED, D. 2009. Petechial bleeding after sunburn in a patient with mild thrombocytopenia. Am J Hematol, 84**,** 523.

CARRETERO, M., ESCAMEZ, M. J., GARCIA, M., DUARTE, B., HOLGUIN, A., RETAMOSA, L., JORCANO, J. L., RIO, M. D. & LARCHER, F. 2008. In vitro and in vivo wound healing-promoting activities of human cathelicidin LL-37. J Invest Dermatol, 128**,** 223-36.

CARTER, M. J., FYLLING, C. P. & PARNELL, L. K. 2011. Use of platelet rich plasma gel on wound healing: a systematic review and meta-analysis. Eplasty, 11**,** e38.

CHAIPAN, C., SOILLEUX, E. J., SIMPSON, P., HOFMANN, H., GRAMBERG, T., MARZI, A., GEIER, M., STEWART, E. A., EISEMANN, J., STEINKASSERER, A., SUZUKI-INOUE, K., FULLER, G. L., PEARCE, A. C., WATSON, S. P., HOXIE, J. A., BARIBAUD, F. & POHLMANN, S.

2006. DC-SIGN and CLEC-2 mediate human immunodeficiency virus type 1 capture by platelets. J Virol, 80**,** 8951-60.

CHALUPOWICZ, D. G., CHOWDHURY, Z. A., BACH, T. L., BARSIGIAN, C. & MARTINEZ, J. 1995. Fibrin II induces endothelial cell capillary tube formation. J Cell Biol, 130**,** 207-15.

CHAN, J. C., DUSZCZYSZYN, D. A., CASTELLINO, F. J. & PLOPLIS, V. A. 2001. Accelerated skin wound healing in plasminogen activator inhibitor-1-deficient mice. Am J Pathol, 159**,** 1681-8.

CHEN, L., MIRZA, R., KWON, Y., DIPIETRO, L. A. & KOH, T. J. 2015. The murine excisional wound model: Contraction revisited. Wound Repair Regen, 23**,** 874-7.

CHEN, S., LI, R., CHENG, C., XU, J. Y., JIN, C., GAO, F., WANG, J., ZHANG, J., ZHANG, J., WANG, H., LU, L., XU, G. T. & TIAN, H. 2018. Pseudomonas aeruginosa infection alters the macrophage phenotype switching process during wound healing in diabetic mice. Cell Biol Int, 42**,** 877-889.

CHICHARRO-ALCANTARA, D., RUBIO-ZARAGOZA, M., DAMIA-GIMENEZ, E., CARRILLO-POVEDA, J. M., CUERVO-SERRATO, B., PELAEZ-GORREA, P. & SOPENA-JUNCOSA, J. J. 2018. Platelet Rich Plasma: New Insights for Cutaneous Wound Healing Management. J Funct Biomater, 9.

CICVARIC, A., YANG, J., KRIEGER, S., KHAN, D., KIM, E. J., DOMINGUEZ-RODRIGUEZ, M., CABATIC, M., MOLZ, B., ACEVEDO AGUILAR, J. P., MILICEVIC, R., SMANI, T., BREUSS, J. M., KERJASCHKI, D., POLLAK, D. D., UHRIN, P. & MONJE, F. J. 2016. The brain-tumor related protein podoplanin regulates synaptic plasticity and hippocampus-dependent learning and memory. Ann Med, 48**,** 652-668.

CIPRIANI FRADE, M. A., BRUM CURSI, I., FORTES ARDRADE, F., COUTINHO NETTO, J. & MAGALHAAES BARBETTA, F. 2004. Management of diabetic skin wounds with a natural latex biomembrane. Med Cutan Iber Lat Am, 32**,** 157-162.

CLARK, S. R., MA, A. C., TAVENER, S. A., MCDONALD, B., GOODARZI, Z., KELLY, M. M., PATEL, K. D., CHAKRABARTI, S., MCAVOY, E., SINCLAIR, G. D., KEYS, E. M., ALLEN-VERCOE, E., DEVINNEY, R., DOIG, C. J., GREEN, F. H. & KUBES, P. 2007. Platelet TLR4 activates neutrophil extracellular traps to ensnare bacteria in septic blood. Nat Med, 13**,** 463-9.

CLAUSHUIS, T. A. M., DE VOS, A. F., NIESWANDT, B., BOON, L., ROELOFS, J., DE BOER, O. J., VAN 'T VEER, C. & VAN DER POLL, T. 2018. Platelet glycoprotein VI aids in local immunity during pneumonia-derived sepsis caused by gram-negative bacteria. Blood, 131**,** 864-876.

COMALADA, M., YERAMIAN, A., MODOLELL, M., LLOBERAS, J. & CELADA, A. 2012. Arginine and macrophage activation. Methods Mol Biol, 844**,** 223-35.

CONWAY, R., MURPHY, C. L., MADIGAN, A., KAVANAGH, P., GERAGHTY, L., REDMOND, N., HELBERT, L., CAREY, J. J., DUNNE, E., KENNY, D. & MCCARTHY, G. M. 2017. Increased platelet reactivity as measured by plasma glycoprotein VI in gout. Platelets**,** 1-6.

COTRAN, R. S. 1965. The Delayed and Prolonged Vascular Leakage in Inflammation. Ii. An Electron Microscopic Study of the Vascular Response after Thermal Injury. Am J Pathol, 46**,** 589-620.

COX, S., COLE, M. & TAWIL, B. 2004. Behavior of human dermal fibroblasts in three-dimensional fibrin clots: dependence on fibrinogen and thrombin concentration. Tissue Eng, 10**,** 942-54.

CRANE, M. J., DALEY, J. M., VAN HOUTTE, O., BRANCATO, S. K., HENRY, W. L., JR. & ALBINA, J. E. 2014. The monocyte to macrophage transition in the murine sterile wound. PLoS One, 9**,** e86660.

CROFT, A. P., NAYLOR, A. J., MARSHALL, J. L., HARDIE, D. L., ZIMMERMANN, B., TURNER, J., DESANTI, G., ADAMS, H., YEMM, A. I., MULLER-LADNER, U., DAYER, J. M., NEUMANN, E., FILER, A. & BUCKLEY, C. D. 2016. Rheumatoid synovial fibroblasts differentiate into distinct subsets in the presence of cytokines and cartilage. Arthritis Res Ther, 18**,** 270.

CRUZ, F. F., HORTA, L. F., MAIA LDE, A., LOPES-PACHECO, M., DA SILVA, A. B., MORALES, M. M., GONCALVES-DE-ALBUQUERQUE, C. F., TAKIYA, C. M., DE CASTRO-FARIA-NETO, H. C. & ROCCO, P. R. 2016. Dasatinib Reduces Lung Inflammation and Fibrosis in Acute Experimental Silicosis. PLoS One, 11**,** e0147005.

CUENI, L. N. & DETMAR, M. 2009. Galectin-8 interacts with podoplanin and modulates lymphatic endothelial cell functions. Exp Cell Res, 315**,** 1715-23.

DA SILVA, A. L., MAGALHAES, R. F., BRANCO, V. C., SILVA, J. D., CRUZ, F. F., MARQUES, P. S., FERREIRA, T. P., MORALES, M. M., MARTINS, M. A., OLSEN, P. C. & ROCCO, P. R.

2016. The tyrosine kinase inhibitor dasatinib reduces lung inflammation and remodelling in experimental allergic asthma. Br J Pharmacol, 173**,** 1236-47.

DAS, A., SINHA, M., DATTA, S., ABAS, M., CHAFFEE, S., SEN, C. K. & ROY, S. 2015. Monocyte and macrophage plasticity in tissue repair and regeneration. Am J Pathol, 185**,** 2596-606.

DAVIDSON, J. M., YU, F. & OPALENIK, S. R. 2013. Splinting Strategies to Overcome Confounding Wound Contraction in Experimental Animal Models. Adv Wound Care (New Rochelle), 2**,** 142-148.

DE GIORGIO-MILLER, A., BOTTOMS, S., LAURENT, G., CARMELIET, P. & HERRICK, S. 2005. Fibrin-induced skin fibrosis in mice deficient in tissue plasminogen activator. Am J Pathol, 167**,** 721-32.

DE WINDE, C. M., MATTHEWS, A. L., VAN DEVENTER, S., VAN DER SCHAAF, A., TOMLINSON, N. D., JANSEN, E., EBLE, J. A., NIESWANDT, B., MCGETTRICK, H. M., FIGDOR, C. G., TOMLINSON, M. G., ACTON, S. E. & VAN SPRIEL, A. B. 2018. C-type lectin-like receptor 2 (CLEC-2)-dependent dendritic cell migration is controlled by tetraspanin CD37. J Cell Sci, 131.

DEMERS, M., HO-TIN-NOE, B., SCHATZBERG, D., YANG, J. J. & WAGNER, D. D. 2011. Increased efficacy of breast cancer chemotherapy in thrombocytopenic mice. Cancer Res, 71**,** 1540-9.

DEUEL, T. F., SENIOR, R. M., CHANG, D., GRIFFIN, G. L., HEINRIKSON, R. L. & KAISER, E. T. 1981. Platelet factor 4 is chemotactic for neutrophils and monocytes. Proc Natl Acad Sci U S A, 78**,** 4584-7.

DEVALARAJA, R. M., NANNEY, L. B., DU, J., QIAN, Q., YU, Y., DEVALARAJA, M. N. & RICHMOND, A. 2000. Delayed wound healing in CXCR2 knockout mice. J Invest Dermatol, 115**,** 234-44.

DEVI, S., KULIGOWSKI, M. P., KWAN, R. Y., WESTEIN, E., JACKSON, S. P., KITCHING, A. R. & HICKEY, M. J. 2010. Platelet recruitment to the inflamed glomerulus occurs via an alphaIIbbeta3/GPVI-dependent pathway. Am J Pathol, 177**,** 1131-42.

DI GUIDA, R., ENGEL, J., ALLWOOD, J. W., WEBER, R. J., JONES, M. R., SOMMER, U., VIANT, M. R. & DUNN, W. B. 2016. Non-targeted UHPLC-MS metabolomic data processing methods: a comparative investigation of normalisation, missing value imputation, transformation and scaling. Metabolomics, 12**,** 93.

DIACOVO, T. G., PURI, K. D., WARNOCK, R. A., SPRINGER, T. A. & VON ANDRIAN, U. H. 1996. Platelet-mediated lymphocyte delivery to high endothelial venules. Science, 273**,** 252-5.

DICKNEITE, G., HERWALD, H., KORTE, W., ALLANORE, Y., DENTON, C. P. & MATUCCI CERINIC, M. 2015. Coagulation factor XIII: a multifunctional transglutaminase with clinical potential in a range of conditions. Thromb Haemost, 113**,** 686-97.

DING, Y., CUI, L., ZHAO, Q., ZHANG, W., SUN, H. & ZHENG, L. 2017. Platelet-Rich Fibrin Accelerates Skin Wound Healing in Diabetic Mice. Ann Plast Surg, 79**,** e15-e19.

DISKIN, C. & PALSSON-MCDERMOTT, E. M. 2018. Metabolic Modulation in Macrophage Effector Function. Front Immunol, 9**,** 270.

DOMBLIDES, C., LARTIGUE, L. & FAUSTIN, B. 2018. Metabolic Stress in the Immune Function of T Cells, Macrophages and Dendritic Cells. Cells, 7.

DOVI, J. V., HE, L. K. & DIPIETRO, L. A. 2003. Accelerated wound closure in neutrophil-depleted mice. J Leukoc Biol, 73**,** 448-55.

DREW, A. F., LIU, H., DAVIDSON, J. M., DAUGHERTY, C. C. & DEGEN, J. L. 2001. Wound-healing defects in mice lacking fibrinogen. Blood, 97**,** 3691-8.

DRISKELL, R. R., JAHODA, C. A., CHUONG, C. M., WATT, F. M. & HORSLEY, V. 2014. Defining dermal adipose tissue. Exp Dermatol, 23**,** 629-31.

DUNN, W. B., ERBAN, A., WEBER, R. J. M., CREEK, D. J., BROWN, M., BREITLING, R., HANKEMEIER, T., GOODACRE, R., NEUMANN, S., KOPKA, J. & VIANT, M. R. 2013. Mass appeal: metabolite identification in mass spectrometry-focused untargeted metabolomics. Metabolomics, 9**,** S44-S66.

DUTTING, S., BENDER, M. & NIESWANDT, B. 2012. Platelet GPVI: a target for antithrombotic therapy?! Trends Pharmacol Sci, 33**,** 583-90.

ECHTLER, K., STARK, K., LORENZ, M., KERSTAN, S., WALCH, A., JENNEN, L., RUDELIUS, M., SEIDL, S., KREMMER, E., EMAMBOKUS, N. R., VON BRUEHL, M. L., FRAMPTON, J., ISERMANN, B., GENZEL-BOROVICZENY, O., SCHREIBER, C., MEHILLI, J., KASTRATI, A., SCHWAIGER, M., SHIVDASANI, R. A. & MASSBERG, S. 2010. Platelets contribute to postnatal occlusion of the ductus arteriosus. Nat Med, 16**,** 75-82.

EGAN, K., DILLON, A., DUNNE, E., KEVANE, B., GALVIN, Z., MAGUIRE, P., KENNY, D., STEWART, S. & AINLE, F. N. 2017. Increased soluble GPVI levels in cirrhosis: evidence for early in vivo platelet activation. J Thromb Thrombolysis, 43**,** 54-59.

EISEMANN, T., COSTA, B., PETERZIEL, H. & ANGEL, P. 2019. Podoplanin Positive Myeloid Cells Promote Glioma Development by Immune Suppression. Front Oncol, 9**,** 187.

EKWALL, A. K., EISLER, T., ANDERBERG, C., JIN, C., KARLSSON, N., BRISSLERT, M. & BOKAREWA, M. I. 2011. The tumour-associated glycoprotein podoplanin is expressed in fibroblast-like synoviocytes of the hyperplastic synovial lining layer in rheumatoid arthritis. Arthritis Res Ther, 13**,** R40.

ELZEY, B. D., TIAN, J., JENSEN, R. J., SWANSON, A. K., LEES, J. R., LENTZ, S. R., STEIN, C. S., NIESWANDT, B., WANG, Y., DAVIDSON, B. L. & RATLIFF, T. L. 2003. Platelet-mediated modulation of adaptive immunity. A communication link between innate and adaptive immune compartments. Immunity, 19**,** 9-19.

EMING, S. A., KRIEG, T. & DAVIDSON, J. M. 2007. Inflammation in wound repair: molecular and cellular mechanisms. J Invest Dermatol, 127**,** 514-25.

ETULAIN, J. 2018. Platelets in wound healing and regenerative medicine. Platelets, 29**,** 556-568.

FADOK, V. A., BRATTON, D. L., KONOWAL, A., FREED, P. W., WESTCOTT, J. Y. & HENSON, P. M. 1998. Macrophages that have ingested apoptotic cells in vitro inhibit proinflammatory cytokine production through autocrine/paracrine mechanisms involving TGF-beta, PGE2, and PAF. J Clin Invest, 101**,** 890-8.

FEI, F., LEE, K. M., MCCARRY, B. E. & BOWDISH, D. M. 2016. Age-associated metabolic dysregulation in bone marrow-derived macrophages stimulated with lipopolysaccharide. Sci Rep, 6**,** 22637.

FINNEY, B. A., SCHWEIGHOFFER, E., NAVARRO-NUNEZ, L., BENEZECH, C., BARONE, F., HUGHES, C. E., LANGAN, S. A., LOWE, K. L., POLLITT, A. Y., MOURAO-SA, D., SHEARDOWN, S., NASH, G. B., SMITHERS, N., REIS E SOUSA, C., TYBULEWICZ, V. L. & WATSON, S. P. 2012. CLEC-2 and Syk in the megakaryocytic/platelet lineage are essential for development. Blood, 119**,** 1747-56.

FLANAGAN, M. 1998. The characteristics and formation of granulation tissue. J Wound Care, 7**,** 508-10.

FLETCHER, A. L., ACTON, S. E. & KNOBLICH, K. 2015. Lymph node fibroblastic reticular cells in health and disease. Nat Rev Immunol, 15**,** 350-61.

FRANCKE, A., HEROLD, J., WEINERT, S., STRASSER, R. H. & BRAUN-DULLAEUS, R. C. 2011. Generation of mature murine monocytes from heterogeneous bone marrow and description of their properties. J Histochem Cytochem, 59**,** 813-25.

FUTOSI, K., NEMETH, T., PICK, R., VANTUS, T., WALZOG, B. & MOCSAI, A. 2012. Dasatinib inhibits proinflammatory functions of mature human neutrophils. Blood, 119**,** 4981-91.

GALE, A. J. 2011. Continuing education course #2: current understanding of hemostasis. Toxicol Pathol, 39**,** 273-80.

GALVAN-PENA, S. & O'NEILL, L. A. 2014. Metabolic reprograming in macrophage polarization. Front Immunol, 5**,** 420.

GASIC, G. J., GASIC, T. B. & STEWART, C. C. 1968. Antimetastatic effects associated with platelet reduction. Proc Natl Acad Sci U S A, 61**,** 46-52.

GEERAERTS, X., BOLLI, E., FENDT, S. M. & VAN GINDERACHTER, J. A. 2017. Macrophage Metabolism As Therapeutic Target for Cancer, Atherosclerosis, and Obesity. Front Immunol, 8**,** 289.

GITZ, E., POLLITT, A. Y., GITZ-FRANCOIS, J. J., ALSHEHRI, O., MORI, J., MONTAGUE, S., NASH, G. B., DOUGLAS, M. R., GARDINER, E. E., ANDREWS, R. K., BUCKLEY, C. D., HARRISON, P. & WATSON, S. P. 2014. CLEC-2 expression is maintained on activated platelets and on platelet microparticles. Blood, 124**,** 2262-70.

GOERGE, T., HO-TIN-NOE, B., CARBO, C., BENARAFA, C., REMOLD-O'DONNELL, E., ZHAO, B. Q., CIFUNI, S. M. & WAGNER, D. D. 2008. Inflammation induces hemorrhage in thrombocytopenia. Blood, 111**,** 4958-64.

GROGER, M., NIEDERLEITHNER, H., KERJASCHKI, D. & PETZELBAUER, P. 2007. A previously unknown dermal blood vessel phenotype in skin inflammation. J Invest Dermatol, 127**,** 2893-900.

GROS, A., SYVANNARATH, V., LAMRANI, L., OLLIVIER, V., LOYAU, S., GOERGE, T., NIESWANDT, B., JANDROT-PERRUS, M. & HO-TIN-NOE, B. 2015. Single platelets seal neutrophil-induced vascular breaches via GPVI during immune-complex-mediated inflammation in mice. Blood, 126**,** 1017-26.

GUO, H., WANG, Y., ZHAO, Z. & SHAO, X. 2015. Platelet factor 4 limits Th17 differentiation and ischaemia-reperfusion injury after liver transplantation in mice. Scand J Immunol, 81**,** 129-34.

HAN, R., XIAO, J., ZHAI, H. & HAO, J. 2016. Dimethyl fumarate attenuates experimental autoimmune neuritis through the nuclear factor erythroid-derived 2-related factor 2/hemoxygenase-1 pathway by altering the balance of M1/M2 macrophages. J Neuroinflammation, 13**,** 97.

HANSON, A. J. & QUINN, M. T. 2002. Effect of fibrin sealant composition on human neutrophil chemotaxis. J Biomed Mater Res, 61**,** 474-81.

HECHLER, B. & GACHET, C. 2011. Comparison of two murine models of thrombosis induced by atherosclerotic plaque injury. Thromb Haemost, 105 Suppl 1**,** S3-12.

HERZOG, B. H., FU, J., WILSON, S. J., HESS, P. R., SEN, A., MCDANIEL, J. M., PAN, Y., SHENG, M., YAGO, T., SILASI-MANSAT, R., MCGEE, S., MAY, F., NIESWANDT, B., MORRIS, A. J., LUPU, F., COUGHLIN, S. R., MCEVER, R. P., CHEN, H., KAHN, M. L. & XIA, L. 2013. Podoplanin maintains high endothelial venule integrity by interacting with platelet CLEC-2. Nature, 502**,** 105-9.

HESS, P. R., RAWNSLEY, D. R., JAKUS, Z., YANG, Y., SWEET, D. T., FU, J., HERZOG, B., LU, M., NIESWANDT, B., OLIVER, G., MAKINEN, T., XIA, L. & KAHN, M. L. 2014. Platelets mediate lymphovenous hemostasis to maintain blood-lymphatic separation throughout life. J Clin Invest, 124**,** 273-84.

HICKE, L. & DUNN, R. 2003. Regulation of membrane protein transport by ubiquitin and ubiquitin-binding proteins. Annu Rev Cell Dev Biol, 19**,** 141-72.

HIGAZI, A. A., BARGHOUTI, II, AYESH, S. K., MAYER, M. & MATZNER, Y. 1994. Inhibition of neutrophil activation by fibrinogen. Inflammation, 18**,** 525-35.

HILLGRUBER, C., POPPELMANN, B., WEISHAUPT, C., STEINGRABER, A. K., WESSEL, F., BERDEL, W. E., GESSNER, J. E., HO-TIN-NOE, B., VESTWEBER, D. & GOERGE, T. 2015. Blocking neutrophil diapedesis prevents hemorrhage during thrombocytopenia. J Exp Med, 212**,** 1255-66.

HITCHCOCK, J. R., COOK, C. N., BOBAT, S., ROSS, E. A., FLORES-LANGARICA, A., LOWE, K. L., KHAN, M., DOMINGUEZ-MEDINA, C. C., LAX, S., CARVALHO-GASPAR, M., HUBSCHER, S., RAINGER, G. E., COBBOLD, M., BUCKLEY, C. D., MITCHELL, T. J.,

MITCHELL, A., JONES, N. D., VAN ROOIJEN, N., KIRCHHOFER, D., HENDERSON, I. R., ADAMS, D. H., WATSON, S. P. & CUNNINGHAM, A. F. 2015. Inflammation drives thrombosis after Salmonella infection via CLEC-2 on platelets. J Clin Invest, 125**,** 4429-46.

HO-TIN-NOE, B., BOULAFTALI, Y. & CAMERER, E. 2018. Platelets and vascular integrity: how platelets prevent bleeding in inflammation. Blood, 131**,** 277-288.

HO-TIN-NOE, B., CARBO, C., DEMERS, M., CIFUNI, S. M., GOERGE, T. & WAGNER, D. D. 2009. Innate immune cells induce hemorrhage in tumors during thrombocytopenia. Am J Pathol, 175**,** 1699-708.

HODIVALA-DILKE, K. M., MCHUGH, K. P., TSAKIRIS, D. A., RAYBURN, H., CROWLEY, D., ULLMAN-CULLERE, M., ROSS, F. P., COLLER, B. S., TEITELBAUM, S. & HYNES, R. O. 1999. Beta3-integrin-deficient mice are a model for Glanzmann thrombasthenia showing placental defects and reduced survival. J Clin Invest, 103**,** 229-38.

HOFFMAN, M., HARGER, A., LENKOWSKI, A., HEDNER, U., ROBERTS, H. R. & MONROE, D. M. 2006. Cutaneous wound healing is impaired in hemophilia B. Blood, 108**,** 3053-60.

HOFFMAN, M. & MONROE, D. M. 2012. The multiple roles of tissue factor in wound healing. Front Biosci (Schol Ed), 4**,** 713-21.

HONMA, M., MINAMI-HORI, M., TAKAHASHI, H. & IIZUKA, H. 2012. Podoplanin expression in wound and hyperproliferative psoriatic epidermis: regulation by TGF-beta and STAT-3 activating cytokines, IFN-gamma, IL-6, and IL-22. J Dermatol Sci, 65**,** 134-40.

HOPKINSON-WOOLLEY, J., HUGHES, D., GORDON, S. & MARTIN, P. 1994. Macrophage recruitment during limb development and wound healing in the embryonic and foetal mouse. J Cell Sci, 107 (Pt 5)**,** 1159-67.

HOU, T. Z., BYSTROM, J., SHERLOCK, J. P., QURESHI, O., PARNELL, S. M., ANDERSON, G., GILROY, D. W. & BUCKLEY, C. D. 2010. A distinct subset of podoplanin (gp38) expressing F4/80+ macrophages mediate phagocytosis and are induced following zymosan peritonitis. FEBS Lett, 584**,** 3955-61.

HOWDIESHELL, T. R., CALLAWAY, D., WEBB, W. L., GAINES, M. D., PROCTER, C. D., JR., SATHYANARAYANA, POLLOCK, J. S., BROCK, T. L. & MCNEIL, P. L. 2001. Antibody

neutralization of vascular endothelial growth factor inhibits wound granulation tissue formation. J Surg Res, 96**,** 173-82.

HUANG, X. Z., WU, J. F., FERRANDO, R., LEE, J. H., WANG, Y. L., FARESE, R. V., JR. & SHEPPARD, D. 2000. Fatal bilateral chylothorax in mice lacking the integrin alpha9beta1. Mol Cell Biol, 20**,** 5208-15.

HUR, J., JANG, J. H., OH, I. Y., CHOI, J. I., YUN, J. Y., KIM, J., CHOI, Y. E., KO, S. B., KANG, J. A., KANG, J., LEE, S. E., LEE, H., PARK, Y. B. & KIM, H. S. 2014. Human podoplanin-positive monocytes and platelets enhance lymphangiogenesis through the activation of the podoplanin/CLEC-2 axis. Mol Ther, 22**,** 1518-1529.

INDURUWA, I., MOROI, M., BONNA, A., MALCOR, J. D., HOWES, J. M., WARBURTON, E. A., FARNDALE, R. W. & JUNG, S. M. 2018. Platelet collagen receptor Glycoprotein VI-dimer recognizes fibrinogen and fibrin through their D-domains, contributing to platelet adhesion and activation during thrombus formation. J Thromb Haemost, 16**,** 389-404.

INOUE, O., SUZUKI-INOUE, K., MCCARTY, O. J., MOROI, M., RUGGERI, Z. M., KUNICKI, T. J., OZAKI, Y. & WATSON, S. P. 2006. Laminin stimulates spreading of platelets through integrin alpha6beta1-dependent activation of GPVI. Blood, 107**,** 1405-12.

JANDROT-PERRUS, M., LAGRUE, A. H., OKUMA, M. & BON, C. 1997. Adhesion and activation of human platelets induced by convulxin involve glycoprotein VI and integrin alpha2beta1. J Biol Chem, 272**,** 27035-41.

JENNINGS, L. K. 2009. Mechanisms of platelet activation: need for new strategies to protect against platelet-mediated atherothrombosis. Thromb Haemost, 102**,** 248-57.

JHA, A. K., HUANG, S. C., SERGUSHICHEV, A., LAMPROPOULOU, V., IVANOVA, Y., LOGINICHEVA, E., CHMIELEWSKI, K., STEWART, K. M., ASHALL, J., EVERTS, B., PEARCE, E. J., DRIGGERS, E. M. & ARTYOMOV, M. N. 2015. Network integration of parallel metabolic and transcriptional data reveals metabolic modules that regulate macrophage polarization. Immunity, 42**,** 419-30.

JUNG, S. M., TSUJI, K. & MOROI, M. 2009. Glycoprotein (GP) VI dimer as a major collagen-binding site of native platelets: direct evidence obtained with dimeric GPVI-specific Fabs. J Thromb Haemost, 7**,** 1347-55.

KAJI, C., TOMOOKA, M., KATO, Y., KOJIMA, H. & SAWA, Y. 2012. The expression of podoplanin and classic cadherins in the mouse brain. J Anat, 220**,** 435-46.

KANEKO, M. K., KATO, Y., KITANO, T. & OSAWA, M. 2006. Conservation of a platelet activating domain of Aggrus/podoplanin as a platelet aggregation-inducing factor. Gene, 378**,** 52-7.

KATO, K., KANAJI, T., RUSSELL, S., KUNICKI, T. J., FURIHATA, K., KANAJI, S., MARCHESE, P., REININGER, A., RUGGERI, Z. M. & WARE, J. 2003. The contribution of glycoprotein VI to stable platelet adhesion and thrombus formation illustrated by targeted gene deletion. Blood, 102**,** 1701-7.

KELTON, J. G., ARNOLD, D. M. & BATES, S. M. 2013. Nonheparin anticoagulants for heparin-induced thrombocytopenia. N Engl J Med, 368**,** 737-44.

KERRIGAN, A. M., DENNEHY, K. M., MOURAO-SA, D., FARO-TRINDADE, I., WILLMENT, J. A., TAYLOR, P. R., EBLE, J. A., REIS E SOUSA, C. & BROWN, G. D. 2009. CLEC-2 is a phagocytic activation receptor expressed on murine peripheral blood neutrophils. J Immunol, 182**,** 4150-7.

KERRIGAN, A. M., NAVARRO-NUNEZ, L., PYZ, E., FINNEY, B. A., WILLMENT, J. A., WATSON, S. P. & BROWN, G. D. 2012. Podoplanin-expressing inflammatory macrophages activate murine platelets via CLEC-2. J Thromb Haemost, 10**,** 484-6.

KESSNER, D., CHAMBERS, M., BURKE, R., AGUS, D. & MALLICK, P. 2008. ProteoWizard: open source software for rapid proteomics tools development. Bioinformatics, 24**,** 2534-6.

KEYES, B. E., LIU, S., ASARE, A., NAIK, S., LEVORSE, J., POLAK, L., LU, C. P., NIKOLOVA, M., PASOLLI, H. A. & FUCHS, E. 2016. Impaired Epidermal to Dendritic T Cell Signaling Slows Wound Repair in Aged Skin. Cell, 167**,** 1323-1338 e14.

KHO, S., BARBER, B. E., JOHAR, E., ANDRIES, B., POESPOPRODJO, J. R., KENANGALEM, E., PIERA, K. A., EHMANN, A., PRICE, R. N., WILLIAM, T., WOODBERRY, T., FOOTE, S., MINIGO, G., YEO, T. W., GRIGG, M. J., ANSTEY, N. M. & MCMORRAN, B. 2018. Platelets kill circulating parasites of all major Plasmodium species in human malaria. Blood.

KIM, M. H., LIU, W., BORJESSON, D. L., CURRY, F. R., MILLER, L. S., CHEUNG, A. L., LIU, F. T., ISSEROFF, R. R. & SIMON, S. I. 2008. Dynamics of neutrophil infiltration during cutaneous wound healing and infection using fluorescence imaging. J Invest Dermatol, 128**,** 1812-20.

KIM, S. J., KIM, S. H., KIM, J. H., HWANG, S. & YOO, H. J. 2016. Understanding Metabolomics in Biomedical Research. Endocrinol Metab (Seoul), 31**,** 7-16.

KITCHENS, C. S. & PENDERGAST, J. F. 1986. Human thrombocytopenia is associated with structural abnormalities of the endothelium that are ameliorated by glucocorticosteroid administration. Blood, 67**,** 203-6.

KLEINSCHNITZ, C., POZGAJOVA, M., PHAM, M., BENDSZUS, M., NIESWANDT, B. & STOLL, G. 2007. Targeting platelets in acute experimental stroke: impact of glycoprotein Ib, VI, and IIb/IIIa blockade on infarct size, functional outcome, and intracranial bleeding. Circulation, 115**,** 2323-30.

KREUTZMAN, A., COLOM-FERNANDEZ, B., JIMENEZ, A. M., ILANDER, M., CUESTA-MATEOS, C., PEREZ-GARCIA, Y., AREVALO, C. D., BRUCK, O., HAKANEN, H., SAARELA, J., ORTEGA-CARRION, A., DE ROSENDO, A., JUANES-GARCIA, A., STEEGMANN, J. L., MUSTJOKI, S., VICENTE-MANZANARES, M. & MUNOZ-CALLEJA, C. 2017. Dasatinib Reversibly Disrupts Endothelial Vascular Integrity by Increasing Non-Muscle Myosin II Contractility in a ROCK-Dependent Manner. Clin Cancer Res, 23**,** 6697-6707.

KRISHNAN, H., RAYES, J., MIYASHITA, T., ISHII, G., RETZBACH, E. P., SHEEHAN, S. A., TAKEMOTO, A., CHANG, Y. W., YONEDA, K., ASAI, J., JENSEN, L., CHALISE, L., NATSUME, A. & GOLDBERG, G. S. 2018. Podoplanin: An emerging cancer biomarker and therapeutic target. Cancer Sci, 109**,** 1292-1299.

KUBO, M., VAN DE WATER, L., PLANTEFABER, L. C., MOSESSON, M. W., SIMON, M., TONNESEN, M. G., TAICHMAN, L. & CLARK, R. A. 2001. Fibrinogen and fibrin are anti-adhesive for keratinocytes: a mechanism for fibrin eschar slough during wound repair. J Invest Dermatol, 117**,** 1369-81.

KUIJPERS, M. J., GILIO, K., REITSMA, S., NERGIZ-UNAL, R., PRINZEN, L., HEENEMAN, S., LUTGENS, E., VAN ZANDVOORT, M. A., NIESWANDT, B., EGBRINK, M. G. & HEEMSKERK, J. W. 2009. Complementary roles of platelets and coagulation in thrombus formation on plaques acutely ruptured by targeted ultrasound treatment: a novel intravital model. J Thromb Haemost, 7**,** 152-61.

LACCI, K. M. & DARDIK, A. 2010. Platelet-rich plasma: support for its use in wound healing. Yale J Biol Med, 83**,** 1-9.

LANGSTON, P. K., SHIBATA, M. & HORNG, T. 2017. Metabolism Supports Macrophage Activation. Front Immunol, 8**,** 61.

LAURENS, N., KOOLWIJK, P. & DE MAAT, M. P. 2006. Fibrin structure and wound healing. J Thromb Haemost, 4**,** 932-9.

LAX, S., RAYES, J., THICKETT, D. R. & WATSON, S. P. 2017a. Effect of anti-podoplanin antibody administration during lipopolysaccharide-induced lung injury in mice. BMJ Open Respir Res, 4**,** e000257.

LAX, S., RAYES, J., WICHAIYO, S., HAINING, E. J., LOWE, K., GRYGIELSKA, B., LALOO, R., FLODBY, P., BOROK, Z., CRANDALL, E. D., THICKETT, D. R. & WATSON, S. P. 2017b. Platelet CLEC-2 protects against lung injury via effects of its ligand podoplanin on inflammatory alveolar macrophages in the mouse. Am J Physiol Lung Cell Mol Physiol, 313**,** L1016-L1029.

LEBLANC, R. & PEYRUCHAUD, O. 2016. Metastasis: new functional implications of platelets and megakaryocytes. Blood, 128**,** 24-31.

LECKER, S. H., GOLDBERG, A. L. & MITCH, W. E. 2006. Protein degradation by the ubiquitin-proteasome pathway in normal and disease states. J Am Soc Nephrol, 17**,** 1807-19.

LEE, C. M. & HU, J. 2013. Cell density during differentiation can alter the phenotype of bone marrow-derived macrophages. Cell Biosci, 3**,** 30.

LEFRANCAIS, E., ORTIZ-MUNOZ, G., CAUDRILLIER, A., MALLAVIA, B., LIU, F., SAYAH, D. M., THORNTON, E. E., HEADLEY, M. B., DAVID, T., COUGHLIN, S. R., KRUMMEL, M. F., LEAVITT, A. D., PASSEGUE, E. & LOONEY, M. R. 2017. The lung is a site of platelet biogenesis and a reservoir for haematopoietic progenitors. Nature, 544**,** 105-109.

LI, B. & WANG, J. H. 2011. Fibroblasts and myofibroblasts in wound healing: force generation and measurement. J Tissue Viability, 20**,** 108-20.

LI, Y., FU, J., LING, Y., YAGO, T., MCDANIEL, J. M., SONG, J., BAI, X., KONDO, Y., QIN, Y., HOOVER, C., MCGEE, S., SHAO, B., LIU, Z., SONON, R., AZADI, P., MARTH, J. D., MCEVER, R. P., RUAN, C. & XIA, L. 2017. Sialylation on O-glycans protects platelets from clearance by liver Kupffer cells. Proc Natl Acad Sci U S A, 114**,** 8360-8365.

LI, Z., RUMBAUT, R. E., BURNS, A. R. & SMITH, C. W. 2006. Platelet response to corneal abrasion is necessary for acute inflammation and efficient re-epithelialization. Invest Ophthalmol Vis Sci, 47**,** 4794-802.

LIEVENS, D. & VON HUNDELSHAUSEN, P. 2011. Platelets in atherosclerosis. Thromb Haemost, 106**,** 827-38.

LINDHOLM, C. & SEARLE, R. 2016. Wound management for the 21st century: combining effectiveness and efficiency. Int Wound J, 13 Suppl 2**,** 5-15.

LISHKO, V. K., BURKE, T. & UGAROVA, T. 2007. Antiadhesive effect of fibrinogen: a safeguard for thrombus stability. Blood, 109**,** 1541-9.

LITTLEWOOD-EVANS, A., SARRET, S., APFEL, V., LOESLE, P., DAWSON, J., ZHANG, J., MULLER, A., TIGANI, B., KNEUER, R., PATEL, S., VALEAUX, S., GOMMERMANN, N., RUBIC-SCHNEIDER, T., JUNT, T. & CARBALLIDO, J. M. 2016. GPR91 senses extracellular succinate released from inflammatory macrophages and exacerbates rheumatoid arthritis. J Exp Med, 213**,** 1655-62.

LOCKYER, S., OKUYAMA, K., BEGUM, S., LE, S., SUN, B., WATANABE, T., MATSUMOTO, Y., YOSHITAKE, M., KAMBAYASHI, J. & TANDON, N. N. 2006. GPVI-deficient mice lack collagen responses and are protected against experimentally induced pulmonary thromboembolism. Thromb Res, 118**,** 371-80.

LONG, A. J., SAMPSON, E., MCCARTHY, R. W., HARRIS, C. M., BARNARD, M., SHI, D., CONLON, D., CALDWELL, R., HONOR, D., WISHART, N., HOEMANN, M., DUGGAN, L., FRITZ, D., STEDMAN, C., O'CONNOR, E., MIKAELIAN, I. & SCHWARTZ, A. 2016. Syk Inhibition Induces Platelet Dependent Peri-islet Hemorrhage in the Rat Pancreas. Toxicol Pathol, 44**,** 998-1012.

LORENZ, V., STEGNER, D., STRITT, S., VOGTLE, T., KIEFER, F., WITKE, W., SCHYMEINSKY, J., WATSON, S. P., WALZOG, B. & NIESWANDT, B. 2015. Targeted downregulation of platelet CLEC-2 occurs through Syk-independent internalization. Blood, 125**,** 4069-77.

LOWE, K. L., FINNEY, B. A., DEPPERMANN, C., HAGERLING, R., GAZIT, S. L., FRAMPTON, J., BUCKLEY, C., CAMERER, E., NIESWANDT, B., KIEFER, F. & WATSON, S. P. 2015a.

Podoplanin and CLEC-2 drive cerebrovascular patterning and integrity during development. Blood, 125**,** 3769-77.

LOWE, K. L., NAVARRO-NUNEZ, L., BENEZECH, C., NAYAR, S., KINGSTON, B. L., NIESWANDT, B., BARONE, F., WATSON, S. P., BUCKLEY, C. D. & DESANTI, G. E. 2015b. The expression of mouse CLEC-2 on leucocyte subsets varies according to their anatomical location and inflammatory state. Eur J Immunol, 45**,** 2484-93.

LOWE, K. L., NAVARRO-NUNEZ, L. & WATSON, S. P. 2012. Platelet CLEC-2 and podoplanin in cancer metastasis. Thromb Res, 129 Suppl 1**,** S30-7.

LUCAS, T., WAISMAN, A., RANJAN, R., ROES, J., KRIEG, T., MULLER, W., ROERS, A. & EMING, S. A. 2010. Differential roles of macrophages in diverse phases of skin repair. J Immunol, 184**,** 3964-77.

LUO, T. L., EISENBERG, M. C., HAYASHI, M. A. L., GONZALEZ-CABEZAS, C., FOXMAN, B., MARRS, C. F. & RICKARD, A. H. 2018. A Sensitive Thresholding Method for Confocal Laser Scanning Microscope Image Stacks of Microbial Biofilms. Sci Rep, 8**,** 13013.

MACKMAN, N. 2012. New insights into the mechanisms of venous thrombosis. J Clin Invest, 122**,** 2331-6.

MACRAE, F. L., DUVAL, C., PAPAREDDY, P., BAKER, S. R., YULDASHEVA, N., KEARNEY, K. J., MCPHERSON, H. R., ASQUITH, N., KONINGS, J., CASINI, A., DEGEN, J. L., CONNELL, S. D., PHILIPPOU, H., WOLBERG, A. S., HERWALD, H. & ARIENS, R. A. 2018. A fibrin biofilm covers blood clots and protects from microbial invasion. J Clin Invest, 128**,** 3356-3368.

MAHTAB, E. A., WIJFFELS, M. C., VAN DEN AKKER, N. M., HAHURIJ, N. D., LIE-VENEMA, H., WISSE, L. J., DERUITER, M. C., UHRIN, P., ZAUJEC, J., BINDER, B. R., SCHALIJ, M. J., POELMANN, R. E. & GITTENBERGER-DE GROOT, A. C. 2008. Cardiac malformations and myocardial abnormalities in podoplanin knockout mouse embryos: Correlation with abnormal epicardial development. Dev Dyn, 237**,** 847-57.

MAJNO, G. & PALADE, G. E. 1961. Studies on inflammation. 1. The effect of histamine and serotonin on vascular permeability: an electron microscopic study. J Biophys Biochem Cytol, 11**,** 571-605.

MANGIN, P. H., ONSELAER, M. B., RECEVEUR, N., LE LAY, N., HARDY, A. T., WILSON, C., SANCHEZ, X., LOYAU, S., DUPUIS, A., BABAR, A. K., MILLER, J. L., PHILIPPOU, H.,

HUGHES, C. E., HERR, A. B., ARIENS, R. A., MEZZANO, D., JANDROT-PERRUS, M., GACHET, C. & WATSON, S. P. 2018. Immobilized fibrinogen activates human platelets through glycoprotein VI. Haematologica, 103**,** 898-907.

MARTIN-VILLAR, E., FERNANDEZ-MUNOZ, B., PARSONS, M., YURRITA, M. M., MEGIAS, D., PEREZ-GOMEZ, E., JONES, G. E. & QUINTANILLA, M. 2010. Podoplanin associates with CD44 to promote directional cell migration. Mol Biol Cell, 21**,** 4387-99.

MARTIN-VILLAR, E., MEGIAS, D., CASTEL, S., YURRITA, M. M., VILARO, S. & QUINTANILLA, M. 2006. Podoplanin binds ERM proteins to activate RhoA and promote epithelial-mesenchymal transition. J Cell Sci, 119**,** 4541-53.

MARTIN, P., D'SOUZA, D., MARTIN, J., GROSE, R., COOPER, L., MAKI, R. & MCKERCHER, S. R. 2003. Wound healing in the PU.1 null mouse--tissue repair is not dependent on inflammatory cells. Curr Biol, 13**,** 1122-8.

MARTIN, P. & LEIBOVICH, S. J. 2005. Inflammatory cells during wound repair: the good, the bad and the ugly. Trends Cell Biol, 15**,** 599-607.

MATUS, V., VALENZUELA, G., SAEZ, C. G., HIDALGO, P., LAGOS, M., ARANDA, E., PANES, O., PEREIRA, J., PILLOIS, X., NURDEN, A. T. & MEZZANO, D. 2013. An adenine insertion in exon 6 of human GP6 generates a truncated protein associated with a bleeding disorder in four Chilean families. J Thromb Haemost, 11**,** 1751-9.

MCKENZIE, S. E., TAYLOR, S. M., MALLADI, P., YUHAN, H., CASSEL, D. L., CHIEN, P., SCHWARTZ, E., SCHREIBER, A. D., SURREY, S. & REILLY, M. P. 1999. The role of the human Fc receptor Fc gamma RIIA in the immune clearance of platelets: a transgenic mouse model. J Immunol, 162**,** 4311-8.

MCLAFFERTY, E., HENDRY, C. & ALISTAIR, F. 2012. The integumentary system: anatomy, physiology and function of skin. Nurs Stand, 27**,** 35-42.

MEIER, K. & NANNEY, L. B. 2006. Emerging new drugs for wound repair. Expert Opin Emerg Drugs, 11**,** 23-37.

MENDONCA, R. J., MAURICIO, V. B., TEIXEIRA LDE, B., LACHAT, J. J. & COUTINHO-NETTO, J. 2010. Increased vascular permeability, angiogenesis and wound healing induced by the serum of natural latex of the rubber tree Hevea brasiliensis. Phytother Res, 24**,** 764-8.

MICHAEL, B., YANO, B., SELLERS, R. S., PERRY, R., MORTON, D., ROOME, N., JOHNSON, J. K., SCHAFER, K. & PITSCH, S. 2007. Evaluation of organ weights for rodent and non-rodent toxicity studies: a review of regulatory guidelines and a survey of current practices. Toxicol Pathol, 35**,** 742-50.

MILLIEN, G., SPIRA, A., HINDS, A., WANG, J., WILLIAMS, M. C. & RAMIREZ, M. I. 2006. Alterations in gene expression in T1 alpha null lung: a model of deficient alveolar sac development. BMC Dev Biol, 6**,** 35.

MONROE, D. M., HOFFMAN, M. & ROBERTS, H. R. 2002. Platelets and thrombin generation. Arterioscler Thromb Vasc Biol, 22**,** 1381-9.

MONROE, D. M., MACKMAN, N. & HOFFMAN, M. 2010. Wound healing in hemophilia B mice and low tissue factor mice. Thromb Res, 125 Suppl 1**,** S74-7.

MONTAGUE, S. J., DELIERNEUX, C., LECUT, C., LAYIOS, N., DINSDALE, R. J., LEE, C. S., POULTER, N. S., ANDREWS, R. K., HAMPSON, P., WEARN, C. M., MAES, N., BISHOP, J., BAMFORD, A., GARDINER, C., LEE, W. M., IQBAL, T., MOIEMEN, N., WATSON, S. P., OURY, C., HARRISON, P. & GARDINER, E. E. 2018. Soluble GPVI is elevated in injured patients: shedding is mediated by fibrin activation of GPVI. Blood Adv, 2**,** 240-251.

MONTALESCOT, G. 2011. Platelet biology and implications for antiplatelet therapy in atherothrombotic disease. Clin Appl Thromb Hemost, 17**,** 371-80.

MOREIRA, C. F., CASSINI-VIEIRA, P., DA SILVA, M. F. & BARCELOS, L. S. 2015. Skin Wound Healing Model - Excisional Wounding and Assessment of Lesion Area. Bio-protocol, 5**,** e1661.

MORI, R., KONDO, T., OHSHIMA, T., ISHIDA, Y. & MUKAIDA, N. 2002. Accelerated wound healing in tumor necrosis factor receptor p55-deficient mice with reduced leukocyte infiltration. FASEB J, 16**,** 963-74.

MORRELL, C. N., AGGREY, A. A., CHAPMAN, L. M. & MODJESKI, K. L. 2014. Emerging roles for platelets as immune and inflammatory cells. Blood, 123**,** 2759-67.

MOTLEY, M. P., MADSEN, D. H., JURGENSEN, H. J., SPENCER, D. E., SZABO, R., HOLMBECK, K., FLICK, M. J., LAWRENCE, D. A., CASTELLINO, F. J., WEIGERT, R. & BUGGE, T. H. 2016. A CCR2 macrophage endocytic pathway mediates extravascular fibrin clearance in vivo. Blood, 127**,** 1085-96.

MOVAT, H. Z. 1979. Tissue injury and inflammation induced by immune complexes: the critical role of the neutrophil leukocyte. Exp Mol Pathol, 31**,** 201-10.

MUBBUNU, L., BOWA, K., PETRENKO, V. & SILITONGO, M. 2018. Correlation of Internal Organ Weights with Body Weight and Body Height in Normal Adult Zambians: A Case Study of Ndola Teaching Hospital. Anat Res Int, 2018**,** 4687538.

NACHMAN, R. L. & RAFII, S. 2008. Platelets, petechiae, and preservation of the vascular wall. N Engl J Med, 359**,** 1261-70.

NAGAE, M., MORITA-MATSUMOTO, K., KATO, M., KANEKO, M. K., KATO, Y. & YAMAGUCHI, Y. 2014. A platform of C-type lectin-like receptor CLEC-2 for binding O-glycosylated podoplanin and nonglycosylated rhodocytin. Structure, 22**,** 1711-1721.

NAGY, Z., VOGTLE, T., GEER, M. J., MORI, J., HEISING, S., DI NUNZIO, G., GAREUS, R., TARAKHOVSKY, A., WEISS, A., NEEL, B. G., DESANTI, G. E., MAZHARIAN, A. & SENIS, Y. A. 2019. The Gp1ba-Cre transgenic mouse: a new model to delineate platelet and leukocyte functions. Blood, 133**,** 331-343.

NAIK, B., KARUNAKAR, P., JAYADEV, M. & MARSHAL, V. R. 2013. Role of Platelet rich fibrin in wound healing: A critical review. J Conserv Dent, 16**,** 284-93.

NAKAZAWA, Y., SATO, S., NAITO, M., KATO, Y., MISHIMA, K., ARAI, H., TSURUO, T. & FUJITA, N. 2008. Tetraspanin family member CD9 inhibits Aggrus/podoplanin-induced platelet aggregation and suppresses pulmonary metastasis. Blood, 112**,** 1730-9.

NALDAIZ-GASTESI, N., GOICOECHEA, M., ALONSO-MARTIN, S., AIASTUI, A., LOPEZ-MAYORGA, M., GARCIA-BELDA, P., LACALLE, J., SAN JOSE, C., ARAUZO-BRAVO, M. J., TROUILH, L., ANTON-LEBERRE, V., HERRERO, D., MATHEU, A., BERNAD, A., GARCIA-VERDUGO, J. M., CARVAJAL, J. J., RELAIX, F., LOPEZ DE MUNAIN, A., GARCIA-PARRA, P. & IZETA, A. 2016. Identification and Characterization of the Dermal Panniculus Carnosus Muscle Stem Cells. Stem Cell Reports, 7**,** 411-424.

NAZARI, B., RICE, L. M., STIFANO, G., BARRON, A. M., WANG, Y. M., KORNDORF, T., LEE, J., BHAWAN, J., LAFYATIS, R. & BROWNING, J. L. 2016. Altered Dermal Fibroblasts in Systemic Sclerosis Display Podoplanin and CD90. Am J Pathol, 186**,** 2650-64.

NIESWANDT, B., PLEINES, I. & BENDER, M. 2011. Platelet adhesion and activation mechanisms in arterial thrombosis and ischaemic stroke. J Thromb Haemost, 9 Suppl 1**,** 92-104.

NISHIZAWA, T., KANTER, J. E., KRAMER, F., BARNHART, S., SHEN, X., VIVEKANANDAN-GIRI, A., WALL, V. Z., KOWITZ, J., DEVARAJ, S., O'BRIEN, K. D., PENNATHUR, S., TANG, J., MIYAOKA, R. S., RAINES, E. W. & BORNFELDT, K. E. 2014. Testing the role of myeloid cell glucose flux in inflammation and atherosclerosis. Cell Rep, 7**,** 356-65.

NUMATA, Y., TERUI, T., OKUYAMA, R., HIRASAWA, N., SUGIURA, Y., MIYOSHI, I., WATANABE, T., KURAMASU, A., TAGAMI, H. & OHTSU, H. 2006. The accelerating effect of histamine on the cutaneous wound-healing process through the action of basic fibroblast growth factor. J Invest Dermatol, 126**,** 1403-9.

NURDEN, A. T. 2011. Platelets, inflammation and tissue regeneration. Thromb Haemost, 105 Suppl 1**,** S13-33.

NYLANDER, A. N., PONATH, G. D., AXISA, P. P., MUBARAK, M., TOMAYKO, M., KUCHROO, V. K., PITT, D. & HAFLER, D. A. 2017. Podoplanin is a negative regulator of Th17 inflammation. JCI Insight, 2.

ODA, Y., HU, L., NGUYEN, T., FONG, C., TU, C. L. & BIKLE, D. D. 2017. Combined Deletion of the Vitamin D Receptor and Calcium-Sensing Receptor Delays Wound Re-epithelialization. Endocrinology, 158**,** 1929-1938.

ONO, S., EGAWA, G. & KABASHIMA, K. 2017. Regulation of blood vascular permeability in the skin. Inflamm Regen, 37**,** 11.

OSADA, M., INOUE, O., DING, G., SHIRAI, T., ICHISE, H., HIRAYAMA, K., TAKANO, K., YATOMI, Y., HIRASHIMA, M., FUJII, H., SUZUKI-INOUE, K. & OZAKI, Y. 2012. Platelet activation receptor CLEC-2 regulates blood/lymphatic vessel separation by inhibiting proliferation, migration, and tube formation of lymphatic endothelial cells. J Biol Chem, 287**,** 22241-52.

OURIEL, K. 2001. Peripheral arterial disease. Lancet, 358**,** 1257-64.

OZANNE, J., PRESCOTT, A. R. & CLARK, K. 2015. The clinically approved drugs dasatinib and bosutinib induce anti-inflammatory macrophages by inhibiting the salt-inducible kinases. Biochem J, 465**,** 271-9.

PAN, Y. & XIA, L. 2015. Emerging roles of podoplanin in vascular development and homeostasis. Front Med, 9**,** 421-30.

PAN, Y., YAGO, T., FU, J., HERZOG, B., MCDANIEL, J. M., MEHTA-D'SOUZA, P., CAI, X., RUAN, C., MCEVER, R. P., WEST, C., DAI, K., CHEN, H. & XIA, L. 2014. Podoplanin requires sialylated O-glycans for stable expression on lymphatic endothelial cells and for interaction with platelets. Blood, 124**,** 3656-65.

PARK-WINDHOL, C. & D'AMORE, P. A. 2016. Disorders of Vascular Permeability. Annu Rev Pathol, 11**,** 251-81.

PARK, N. J., ALLEN, L. & DRIVER, V. R. 2013. Updating on understanding and managing chronic wound. Dermatol Ther, 26**,** 236-56.

PASPARAKIS, M., HAASE, I. & NESTLE, F. O. 2014. Mechanisms regulating skin immunity and inflammation. Nat Rev Immunol, 14**,** 289-301.

PASTAR, I., STOJADINOVIC, O., YIN, N. C., RAMIREZ, H., NUSBAUM, A. G., SAWAYA, A., PATEL, S. B., KHALID, L., ISSEROFF, R. R. & TOMIC-CANIC, M. 2014. Epithelialization in Wound Healing: A Comprehensive Review. Adv Wound Care (New Rochelle), 3**,** 445-464.

PAYNE, H., PONOMARYOV, T., WATSON, S. P. & BRILL, A. 2017. Mice with a deficiency in CLEC-2 are protected against deep vein thrombosis. Blood, 129**,** 2013-2020.

PENCE, B. D. & WOODS, J. A. 2014. Exercise, Obesity, and Cutaneous Wound Healing: Evidence from Rodent and Human Studies. Adv Wound Care (New Rochelle), 3**,** 71-79.

PERTUY, F., AGUILAR, A., STRASSEL, C., ECKLY, A., FREUND, J. N., DULUC, I., GACHET, C., LANZA, F. & LEON, C. 2015. Broader expression of the mouse platelet factor 4-cre transgene beyond the megakaryocyte lineage. J Thromb Haemost, 13**,** 115-25.

PETERS, A., BURKETT, P. R., SOBEL, R. A., BUCKLEY, C. D., WATSON, S. P., BETTELLI, E. & KUCHROO, V. K. 2015. Podoplanin negatively regulates CD4+ effector T cell responses. J Clin Invest, 125**,** 129-40.

PIERRE, S., LINKE, B., SUO, J., TARIGHI, N., DEL TURCO, D., THOMAS, D., FERREIROS, N., STEGNER, D., FROLICH, S., SISIGNANO, M., MEYER DOS SANTOS, S., DEBRUIN, N., NUSING, R. M., DELLER, T., NIESWANDT, B., GEISSLINGER, G. & SCHOLICH, K. 2017.

GPVI and Thromboxane Receptor on Platelets Promote Proinflammatory Macrophage Phenotypes during Cutaneous Inflammation. J Invest Dermatol, 137**,** 686-695.

PINTO, N. R., UBILLA, M., ZAMORA, Y., DEL RIO, V., DOHAN EHRENFEST, D. M. & QUIRYNEN, M. 2018. Leucocyte- and platelet-rich fibrin (L-PRF) as a regenerative medicine strategy for the treatment of refractory leg ulcers: a prospective cohort study. Platelets, 29**,** 468-475.

POLLITT, A. Y., POULTER, N. S., GITZ, E., NAVARRO-NUNEZ, L., WANG, Y. J., HUGHES, C. E., THOMAS, S. G., NIESWANDT, B., DOUGLAS, M. R., OWEN, D. M., JACKSON, D. G., DUSTIN, M. L. & WATSON, S. P. 2014. Syk and Src family kinases regulate C-type lectin receptor 2 (CLEC-2)-mediated clustering of podoplanin and platelet adhesion to lymphatic endothelial cells. J Biol Chem, 289**,** 35695-710.

POULTER, N. S., POLLITT, A. Y., OWEN, D. M., GARDINER, E. E., ANDREWS, R. K., SHIMIZU, H., ISHIKAWA, D., BIHAN, D., FARNDALE, R. W., MOROI, M., WATSON, S. P. & JUNG, S. M. 2017. Clustering of glycoprotein VI (GPVI) dimers upon adhesion to collagen as a mechanism to regulate GPVI signaling in platelets. J Thromb Haemost, 15**,** 549-564.

QIANG, L., SAMPLE, A., LIU, H., WU, X. & HE, Y. Y. 2017. Epidermal SIRT1 regulates inflammation, cell migration, and wound healing. Sci Rep, 7**,** 14110.

QIAO, J., AL-TAMIMI, M., BAKER, R. I., ANDREWS, R. K. & GARDINER, E. E. 2015. The platelet Fc receptor, FcgammaRIIa. Immunol Rev, 268**,** 241-52.

QUINTANILLA, M., MONTERO-MONTERO, L., RENART, J. & MARTIN-VILLAR, E. 2019. Podoplanin in Inflammation and Cancer. Int J Mol Sci, 20.

RAMIREZ, M. I., MILLIEN, G., HINDS, A., CAO, Y., SELDIN, D. C. & WILLIAMS, M. C. 2003. T1alpha, a lung type I cell differentiation gene, is required for normal lung cell proliferation and alveolus formation at birth. Dev Biol, 256**,** 61-72.

RAMOS-VARA, J. A. 2017. Principles and Methods of Immunohistochemistry. Methods Mol Biol, 1641**,** 115-128.

RATH, M., MULLER, I., KROPF, P., CLOSS, E. I. & MUNDER, M. 2014. Metabolism via Arginase or Nitric Oxide Synthase: Two Competing Arginine Pathways in Macrophages. Front Immunol, 5**,** 532.

RAYES, J., JADOUI, S., LAX, S., GROS, A., WICHAIYO, S., OLLIVIER, V., DENIS, C. V., WARE, J., NIESWANDT, B., JANDROT-PERRUS, M., WATSON, S. P. & HO-TIN-NOE, B. 2018. The contribution of platelet glycoprotein receptors to inflammatory bleeding prevention is stimulus and organ dependent. Haematologica, 103**,** e256-e258.

RAYES, J., LAX, S., WICHAIYO, S., WATSON, S. K., DI, Y., LOMBARD, S., GRYGIELSKA, B., SMITH, S. W., SKORDILIS, K. & WATSON, S. P. 2017. The podoplanin-CLEC-2 axis inhibits inflammation in sepsis. Nat Commun, 8**,** 2239.

RETZBACH, E. P., SHEEHAN, S. A., NEVEL, E. M., BATRA, A., PHI, T., NGUYEN, A. T. P., KATO, Y., BAREDES, S., FATAHZADEH, M., SHIENBAUM, A. J. & GOLDBERG, G. S. 2018. Podoplanin emerges as a functionally relevant oral cancer biomarker and therapeutic target. Oral Oncol, 78**,** 126-136.

RINDER, H. M., BONAN, J. L., RINDER, C. S., AULT, K. A. & SMITH, B. R. 1991. Activated and unactivated platelet adhesion to monocytes and neutrophils. Blood, 78**,** 1760-9.

RIVERA, J., LOZANO, M. L., NAVARRO-NUNEZ, L. & VICENTE, V. 2009. Platelet receptors and signaling in the dynamics of thrombus formation. Haematologica, 94**,** 700-11.

ROBERTS, L. D., SOUZA, A. L., GERSZTEN, R. E. & CLISH, C. B. 2012. Targeted metabolomics. Curr Protoc Mol Biol, Chapter 30**,** Unit 30 2 1-24.

ROCHFORT, S. 2005. Metabolomics reviewed: a new "omics" platform technology for systems biology and implications for natural products research. J Nat Prod, 68**,** 1813-20.

RODRIGUES, S. F. & GRANGER, D. N. 2015. Blood cells and endothelial barrier function. Tissue Barriers, 3**,** e978720.

RODRIGUEZ-MERCHAN, E. C. 2012. Surgical wound healing in bleeding disorders. Haemophilia, 18**,** 487-90.

RODRIGUEZ-PRADOS, J. C., TRAVES, P. G., CUENCA, J., RICO, D., ARAGONES, J., MARTIN-SANZ, P., CASCANTE, M. & BOSCA, L. 2010. Substrate fate in activated macrophages: a comparison between innate, classic, and alternative activation. J Immunol, 185**,** 605-14.

ROMER, J., BUGGE, T. H., PYKE, C., LUND, L. R., FLICK, M. J., DEGEN, J. L. & DANO, K. 1996. Impaired wound healing in mice with a disrupted plasminogen gene. Nat Med, 2**,** 287-92.

RONFARD, V. & BARRANDON, Y. 2001. Migration of keratinocytes through tunnels of digested fibrin. Proc Natl Acad Sci U S A, 98**,** 4504-9.

RONO, B., ENGELHOLM, L. H., LUND, L. R. & HALD, A. 2013. Gender affects skin wound healing in plasminogen deficient mice. PLoS One, 8**,** e59942.

RUIFROK, A. C. & JOHNSTON, D. A. 2001. Quantification of histochemical staining by color deconvolution. Anal Quant Cytol Histol, 23**,** 291-9.

SAHNI, A. & FRANCIS, C. W. 2000. Vascular endothelial growth factor binds to fibrinogen and fibrin and stimulates endothelial cell proliferation. Blood, 96**,** 3772-8.

SCHACHT, V., DADRAS, S. S., JOHNSON, L. A., JACKSON, D. G., HONG, Y. K. & DETMAR, M. 2005. Up-regulation of the lymphatic marker podoplanin, a mucin-type transmembrane glycoprotein, in human squamous cell carcinomas and germ cell tumors. Am J Pathol, 166**,** 913-21.

SCHACHT, V., RAMIREZ, M. I., HONG, Y. K., HIRAKAWA, S., FENG, D., HARVEY, N., WILLIAMS, M., DVORAK, A. M., DVORAK, H. F., OLIVER, G. & DETMAR, M. 2003. T1alpha/podoplanin deficiency disrupts normal lymphatic vasculature formation and causes lymphedema. EMBO J, 22**,** 3546-56.

SCHINDELIN, J., ARGANDA-CARRERAS, I., FRISE, E., KAYNIG, V., LONGAIR, M., PIETZSCH, T., PREIBISCH, S., RUEDEN, C., SAALFELD, S., SCHMID, B., TINEVEZ, J. Y., WHITE, D. J., HARTENSTEIN, V., ELICEIRI, K., TOMANCAK, P. & CARDONA, A. 2012. Fiji: an open-source platform for biological-image analysis. Nat Methods, 9**,** 676-82.

SCHMIDT, B. A. & HORSLEY, V. 2013. Intradermal adipocytes mediate fibroblast recruitment during skin wound healing. Development, 140**,** 1517-27.

SCHONBERGER, T., ZIEGLER, M., BORST, O., KONRAD, I., NIESWANDT, B., MASSBERG, S., OCHMANN, C., JURGENS, T., SEIZER, P., LANGER, H., MUNCH, G., UNGERER, M., PREISSNER, K. T., ELVERS, M. & GAWAZ, M. 2012. The dimeric platelet collagen receptor GPVI-Fc reduces platelet adhesion to activated endothelium and preserves myocardial function after transient ischemia in mice. Am J Physiol Cell Physiol, 303**,** C757-66.

SCHRIMPE-RUTLEDGE, A. C., CODREANU, S. G., SHERROD, S. D. & MCLEAN, J. A. 2016. Untargeted Metabolomics Strategies-Challenges and Emerging Directions. J Am Soc Mass Spectrom, 27**,** 1897-1905.

SCHULZ, C., PENZ, S., HOFFMANN, C., LANGER, H., GILLITZER, A., SCHNEIDER, S., BRANDL, R., SEIDL, S., MASSBERG, S., PICHLER, B., KREMMER, E., STELLOS, K., SCHONBERGER, T., SIESS, W. & GAWAZ, M. 2008. Platelet GPVI binds to collagenous structures in the core region of human atheromatous plaque and is critical for atheroprogression in vivo. Basic Res Cardiol, 103**,** 356-67.

SCULLY, D., NASEEM, K. M. & MATSAKAS, A. 2018. Platelet biology in regenerative medicine of skeletal muscle. Acta Physiol (Oxf), 223**,** e13071.

SEMENIAK, D., KULAWIG, R., STEGNER, D., MEYER, I., SCHWIEBERT, S., BOSING, H., ECKES, B., NIESWANDT, B. & SCHULZE, H. 2016. Proplatelet formation is selectively inhibited by collagen type I through Syk-independent GPVI signaling. J Cell Sci, 129**,** 3473-84.

SEMPLE, J. W., ITALIANO, J. E., JR. & FREEDMAN, J. 2011. Platelets and the immune continuum. Nat Rev Immunol, 11**,** 264-74.

SEO, Y. K., SONG, K. Y., KIM, Y. J. & PARK, J. K. 2007. Wound healing effect of acellular artificial dermis containing extracellular matrix secreted by human skin fibroblasts. Artif Organs, 31**,** 509-20.

SHAH, D. R., DHOLAKIA, S. & SHAH, R. R. 2014. Effect of tyrosine kinase inhibitors on wound healing and tissue repair: implications for surgery in cancer patients. Drug Saf, 37**,** 135-49.

SHATERIAN, A., BORBOA, A., SAWADA, R., COSTANTINI, T., POTENZA, B., COIMBRA, R., BAIRD, A. & ELICEIRI, B. P. 2009. Real-time analysis of the kinetics of angiogenesis and vascular permeability in an animal model of wound healing. Burns, 35**,** 811-7.

SHAW, T. J. & MARTIN, P. 2009. Wound repair at a glance. J Cell Sci, 122**,** 3209-13.

SHEETS, A. R., DEMIDOVA-RICE, T. N., SHI, L., RONFARD, V., GROVER, K. V. & HERMAN, I. M. 2016. Identification and Characterization of Novel Matrix-Derived Bioactive Peptides: A Role for Collagenase from Santyl(R) Ointment in Post-Debridement Wound Healing? PLoS One, 11**,** e0159598.

SHI, G., FIELD, D. J., KO, K. A., TURE, S., SRIVASTAVA, K., LEVY, S., KOWALSKA, M. A., PONCZ, M., FOWELL, D. J. & MORRELL, C. N. 2014. Platelet factor 4 limits Th17 differentiation and cardiac allograft rejection. J Clin Invest, 124**,** 543-52.

SHIRAI, T., INOUE, O., TAMURA, S., TSUKIJI, N., SASAKI, T., ENDO, H., SATOH, K., OSADA, M., SATO-UCHIDA, H., FUJII, H., OZAKI, Y. & SUZUKI-INOUE, K. 2017. C-type lectin-like receptor 2 promotes hematogenous tumor metastasis and prothrombotic state in tumor-bearing mice. J Thromb Haemost, 15**,** 513-525.

SIMON, A. Y., SUTHERLAND, M. R. & PRYZDIAL, E. L. 2015. Dengue virus binding and replication by platelets. Blood, 126**,** 378-85.

SINDRILARU, A. & SCHARFFETTER-KOCHANEK, K. 2013. Disclosure of the Culprits: Macrophages-Versatile Regulators of Wound Healing. Adv Wound Care (New Rochelle), 2**,** 357-368.

SLATER, T. W., FINKIELSZTEIN, A., MASCARENHAS, L. A., MEHL, L. C., BUTIN-ISRAELI, V. & SUMAGIN, R. 2017. Neutrophil Microparticles Deliver Active Myeloperoxidase to Injured Mucosa To Inhibit Epithelial Wound Healing. J Immunol, 198**,** 2886-2897.

SMITH, C. A., WANT, E. J., O'MAILLE, G., ABAGYAN, R. & SIUZDAK, G. 2006. XCMS: processing mass spectrometry data for metabolite profiling using nonlinear peak alignment, matching, and identification. Anal Chem, 78**,** 779-87.

SMITH, E., PRASAD, K. M., BUTCHER, M., DOBRIAN, A., KOLLS, J. K., LEY, K. & GALKINA, E. 2010. Blockade of interleukin-17A results in reduced atherosclerosis in apolipoprotein E-deficient mice. Circulation, 121**,** 1746-55.

SOSROSENO, W., HERMINAJENG, E., BIRD, P. S. & SEYMOUR, G. J. 2004. L-arginine-dependent nitric oxide production of a murine macrophage-like RAW 264.7 cell line stimulated with Porphyromonas gingivalis lipopolysaccharide. Oral Microbiol Immunol, 19**,** 65-70.

STACK, J. R., MADIGAN, A., HELBERT, L., DUNNE, E., GARDINER, E. E., ANDREWS, R. K., FINAN, R., SMYTH, E., KENNY, D. & MCCARTHY, G. M. 2017. Soluble glycoprotein VI, a specific marker of platelet activation is increased in the plasma of subjects with seropositive rheumatoid arthritis. PLoS One, 12**,** e0188027.

STAVROU, E. X., FANG, C., BANE, K. L., LONG, A. T., NAUDIN, C., KUCUKAL, E., GANDHI, A., BRETT-MORRIS, A., MUMAW, M. M., IZADMEHR, S., MERKULOVA, A., REYNOLDS, C.

C., ALHALABI, O., NAYAK, L., YU, W. M., QU, C. K., MEYERSON, H. J., DUBYAK, G. R., GURKAN, U. A., NIEMAN, M. T., SEN GUPTA, A., RENNE, T. & SCHMAIER, A. H. 2018. Factor XII and uPAR upregulate neutrophil functions to influence wound healing. J Clin Invest, 128**,** 944-959.

STEGNER, D., HAINING, E. J. & NIESWANDT, B. 2014. Targeting glycoprotein VI and the immunoreceptor tyrosine-based activation motif signaling pathway. Arterioscler Thromb Vasc Biol, 34**,** 1615-20.

SUCHANSKI, J., TEJCHMAN, A., ZACHARSKI, M., PIOTROWSKA, A., GRZEGRZOLKA, J., CHODACZEK, G., NOWINSKA, K., RYS, J., DZIEGIEL, P., KIEDA, C. & UGORSKI, M. 2017. Podoplanin increases the migration of human fibroblasts and affects the endothelial cell network formation: A possible role for cancer-associated fibroblasts in breast cancer progression. PLoS One, 12**,** e0184970.

SUMNER, L. W., AMBERG, A., BARRETT, D., BEALE, M. H., BEGER, R., DAYKIN, C. A., FAN, T. W., FIEHN, O., GOODACRE, R., GRIFFIN, J. L., HANKEMEIER, T., HARDY, N., HARNLY, J., HIGASHI, R., KOPKA, J., LANE, A. N., LINDON, J. C., MARRIOTT, P., NICHOLLS, A. W., REILY, M. D., THADEN, J. J. & VIANT, M. R. 2007. Proposed minimum reporting standards for chemical analysis Chemical Analysis Working Group (CAWG) Metabolomics Standards Initiative (MSI). Metabolomics, 3**,** 211-221.

SUZUKI-INOUE, K., FULLER, G. L., GARCIA, A., EBLE, J. A., POHLMANN, S., INOUE, O., GARTNER, T. K., HUGHAN, S. C., PEARCE, A. C., LAING, G. D., THEAKSTON, R. D., SCHWEIGHOFFER, E., ZITZMANN, N., MORITA, T., TYBULEWICZ, V. L., OZAKI, Y. & WATSON, S. P. 2006. A novel Syk-dependent mechanism of platelet activation by the C-type lectin receptor CLEC-2. Blood, 107**,** 542-9.

SUZUKI-INOUE, K., INOUE, O. & OZAKI, Y. 2011. Novel platelet activation receptor CLEC-2: from discovery to prospects. J Thromb Haemost, 9 Suppl 1**,** 44-55.

SWAMYDAS, M. & LIONAKIS, M. S. 2013. Isolation, purification and labeling of mouse bone marrow neutrophils for functional studies and adoptive transfer experiments. J Vis Exp**,** e50586.

SZPADERSKA, A. M., EGOZI, E. I., GAMELLI, R. L. & DIPIETRO, L. A. 2003. The effect of thrombocytopenia on dermal wound healing. J Invest Dermatol, 120**,** 1130-7.

TAKAKUBO, Y., OKI, H., NAGANUMA, Y., SASKI, K., SASAKI, A., TAMAKI, Y., SURAN, Y., KONTA, T. & TAKAGI, M. 2017. Distribution of Podoplanin in Synovial Tissues in Rheumatoid Arthritis Patients Using Biologic or Conventional Disease-Modifying Anti-Rheumatic Drugs. Curr Rheumatol Rev, 13**,** 72-78.

TAKEMOTO, A., OKITAKA, M., TAKAGI, S., TAKAMI, M., SATO, S., NISHIO, M., OKUMURA, S. & FUJITA, N. 2017. A critical role of platelet TGF-beta release in podoplanin-mediated tumour invasion and metastasis. Sci Rep, 7**,** 42186.

TAMBELLA, A. M., ATTILI, A. R., DUPRE, G., CANTALAMESSA, A., MARTIN, S., CUTERI, V., MARCAZZAN, S. & DEL FABBRO, M. 2018. Platelet-rich plasma to treat experimentally-induced skin wounds in animals: A systematic review and meta-analysis. PLoS One, 13**,** e0191093.

TAMURA, S., SUZUKI-INOUE, K., TSUKIJI, N., SHIRAI, T., SASAKI, T., OSADA, M., SATOH, K. & OZAKI, Y. 2016. Podoplanin-positive periarteriolar stromal cells promote megakaryocyte growth and proplatelet formation in mice by CLEC-2. Blood, 127**,** 1701-10.

TANG, T., LI, L., TANG, J., LI, Y., LIN, W. Y., MARTIN, F., GRANT, D., SOLLOWAY, M., PARKER, L., YE, W., FORREST, W., GHILARDI, N., ORAVECZ, T., PLATT, K. A., RICE, D. S., HANSEN, G. M., ABUIN, A., EBERHART, D. E., GODOWSKI, P., HOLT, K. H., PETERSON, A., ZAMBROWICZ, B. P. & DE SAUVAGE, F. J. 2010. A mouse knockout library for secreted and transmembrane proteins. Nat Biotechnol, 28**,** 749-55.

TEJCHMAN, A., LAMERANT-FAYEL, N., JACQUINET, J. C., BIELAWSKA-POHL, A., MLECZKO-SANECKA, K., GRILLON, C., CHOUAIB, S., UGORSKI, M. & KIEDA, C. 2017. Tumor hypoxia modulates podoplanin/CCL21 interactions in CCR7+ NK cell recruitment and CCR7+ tumor cell mobilization. Oncotarget, 8**,** 31876-31887.

THOMAS, H., COWIN, A. J. & MILLS, S. J. 2017. The Importance of Pericytes in Healing: Wounds and other Pathologies. Int J Mol Sci, 18.

THOMAS, M. R. & STOREY, R. F. 2015. The role of platelets in inflammation. Thromb Haemost, 114**,** 449-58.

TOLSTIKOV, V. 2016. Metabolomics: Bridging the Gap between Pharmaceutical Development and Population Health. Metabolites, 6.

TSUKIJI, N., INOUE, O., MORIMOTO, M., TATSUMI, N., NAGATOMO, H., UETA, K., SHIRAI, T., SASAKI, T., OTAKE, S., TAMURA, S., TACHIBANA, T., OKABE, M., HIRASHIMA, M., OZAKI, Y. & SUZUKI-INOUE, K. 2018a. Platelets play an essential role in murine lung development through Clec-2/podoplanin interaction. Blood, 132**,** 1167-1179.

TSUKIJI, N., OSADA, M., SASAKI, T., SHIRAI, T., SATOH, K., INOUE, O., UMETANI, N., MOCHIZUKI, C., SAITO, T., KOJIMA, S., SHINMORI, H., OZAKI, Y. & SUZUKI-INOUE, K. 2018b. Cobalt hematoporphyrin inhibits CLEC-2-podoplanin interaction, tumor metastasis, and arterial/venous thrombosis in mice. Blood Adv, 2**,** 2214-2225.

TSUNEKI, M., MARUYAMA, S., YAMAZAKI, M., XU, B., ESSA, A., ABE, T., BABKAIR, H., CHENG, J., YAMAMOTO, T. & SAKU, T. 2013. Extracellular heat shock protein A9 is a novel interaction partner of podoplanin in oral squamous cell carcinoma cells. Biochem Biophys Res Commun, 434**,** 124-30.

UCHIYAMA, A., YAMADA, K., OGINO, S., YOKOYAMA, Y., TAKEUCHI, Y., UDEY, M. C., ISHIKAWA, O. & MOTEGI, S. 2014. MFG-E8 regulates angiogenesis in cutaneous wound healing. Am J Pathol, 184**,** 1981-90.

UHRIN, P., ZAUJEC, J., BREUSS, J. M., OLCAYDU, D., CHRENEK, P., STOCKINGER, H., FUERTBAUER, E., MOSER, M., HAIKO, P., FASSLER, R., ALITALO, K., BINDER, B. R. & KERJASCHKI, D. 2010. Novel function for blood platelets and podoplanin in developmental separation of blood and lymphatic circulation. Blood, 115**,** 3997-4005.

USSHER, J. R., ELMARIAH, S., GERSZTEN, R. E. & DYCK, J. R. 2016. The Emerging Role of Metabolomics in the Diagnosis and Prognosis of Cardiovascular Disease. J Am Coll Cardiol, 68**,** 2850-2870.

VAN DEN BOSSCHE, J., BAARDMAN, J., OTTO, N. A., VAN DER VELDEN, S., NEELE, A. E., VAN DEN BERG, S. M., LUQUE-MARTIN, R., CHEN, H. J., BOSHUIZEN, M. C., AHMED, M., HOEKSEMA, M. A., DE VOS, A. F. & DE WINTHER, M. P. 2016. Mitochondrial Dysfunction Prevents Repolarization of Inflammatory Macrophages. Cell Rep, 17**,** 684-696.

VAN EEUWIJK, J. M., STEGNER, D., LAMB, D. J., KRAFT, P., BECK, S., THIELMANN, I., KIEFER, F., WALZOG, B., STOLL, G. & NIESWANDT, B. 2016. The Novel Oral Syk Inhibitor,

Bl1002494, Protects Mice From Arterial Thrombosis and Thromboinflammatory Brain Infarction. Arterioscler Thromb Vasc Biol, 36**,** 1247-53.

VAN VULPEN, L. F. D., AMIN, S. N. & MAKRIS, M. 2018. Severe Wound Healing Impairment in a Patient with Dysfibrinogenaemia. Thromb Haemost, 118**,** 430-432.

VASAMSETTI, S. B., KARNEWAR, S., KANUGULA, A. K., THATIPALLI, A. R., KUMAR, J. M. & KOTAMRAJU, S. 2015. Metformin inhibits monocyte-to-macrophage differentiation via AMPK-mediated inhibition of STAT3 activation: potential role in atherosclerosis. Diabetes, 64**,** 2028-41.

VINAYAVEKHIN, N. & SAGHATELIAN, A. 2010. Untargeted metabolomics. Curr Protoc Mol Biol, Chapter 30**,** Unit 30 1 1-24.

WAGNER, E. F., SCHONTHALER, H. B., GUINEA-VINIEGRA, J. & TSCHACHLER, E. 2010. Psoriasis: what we have learned from mouse models. Nat Rev Rheumatol, 6**,** 704-14.

WALLENTIN, L. 2009. P2Y(12) inhibitors: differences in properties and mechanisms of action and potential consequences for clinical use. Eur Heart J, 30**,** 1964-77.

WANG, Y., GAO, H., SHI, C., ERHARDT, P. W., PAVLOVSKY, A., D, A. S., BLEDZKA, K., USTINOV, V., ZHU, L., QIN, J., MUNDAY, A. D., LOPEZ, J., PLOW, E. & SIMON, D. I. 2017. Leukocyte integrin Mac-1 regulates thrombosis via interaction with platelet GPIbalpha. Nat Commun, 8**,** 15559.

WATANABE, R., HILHORST, M., ZHANG, H., ZEISBRICH, M., BERRY, G. J., WALLIS, B. B., HARRISON, D. G., GIACOMINI, J. C., GORONZY, J. J. & WEYAND, C. M. 2018. Glucose metabolism controls disease-specific signatures of macrophage effector functions. JCI Insight, 3.

WATSON, S. P., HERBERT, J. M. & POLLITT, A. Y. 2010. GPVI and CLEC-2 in hemostasis and vascular integrity. J Thromb Haemost, 8**,** 1456-67.

WEBER, E. M., ALGERS, B., HULTGREN, J. & OLSSON, I. A. 2013. Pup mortality in laboratory mice--infanticide or not? Acta Vet Scand, 55**,** 83.

WELLER, K., FOITZIK, K., PAUS, R., SYSKA, W. & MAURER, M. 2006. Mast cells are required for normal healing of skin wounds in mice. FASEB J, 20**,** 2366-8.

WILGUS, T. A., ROY, S. & MCDANIEL, J. C. 2013. Neutrophils and Wound Repair: Positive Actions and Negative Reactions. Adv Wound Care (New Rochelle), 2**,** 379-388.

WONG, S. L., DEMERS, M., MARTINOD, K., GALLANT, M., WANG, Y., GOLDFINE, A. B., KAHN, C. R. & WAGNER, D. D. 2015. Diabetes primes neutrophils to undergo NETosis, which impairs wound healing. Nat Med, 21**,** 815-9.

XU, X. R., ZHANG, D., OSWALD, B. E., CARRIM, N., WANG, X., HOU, Y., ZHANG, Q., LAVALLE, C., MCKEOWN, T., MARSHALL, A. H. & NI, H. 2016. Platelets are versatile cells: New discoveries in hemostasis, thrombosis, immune responses, tumor metastasis and beyond. Crit Rev Clin Lab Sci, 53**,** 409-30.

XU, Z., XU, H., PLOPLIS, V. A. & CASTELLINO, F. J. 2010. Factor VII deficiency impairs cutaneous wound healing in mice. Mol Med, 16**,** 167-76.

YAMASHITA, Y., NAITOH, K., WADA, H., IKEJIRI, M., MASTUMOTO, T., OHISHI, K., HOSAKA, Y., NISHIKAWA, M. & KATAYAMA, N. 2014. Elevated plasma levels of soluble platelet glycoprotein VI (GPVI) in patients with thrombotic microangiopathy. Thromb Res, 133**,** 440-4.

YANG, H. S., SHIN, J., BHANG, S. H., SHIN, J. Y., PARK, J., IM, G. I., KIM, C. S. & KIM, B. S. 2011. Enhanced skin wound healing by a sustained release of growth factors contained in platelet-rich plasma. Exp Mol Med, 43**,** 622-9.

YERAMIAN, A., MARTIN, L., ARPA, L., BERTRAN, J., SOLER, C., MCLEOD, C., MODOLELL, M., PALACIN, M., LLOBERAS, J. & CELADA, A. 2006a. Macrophages require distinct arginine catabolism and transport systems for proliferation and for activation. Eur J Immunol, 36**,** 1516-26.

YERAMIAN, A., MARTIN, L., SERRAT, N., ARPA, L., SOLER, C., BERTRAN, J., MCLEOD, C., PALACIN, M., MODOLELL, M., LLOBERAS, J. & CELADA, A. 2006b. Arginine transport via cationic amino acid transporter 2 plays a critical regulatory role in classical or alternative activation of macrophages. J Immunol, 176**,** 5918-24.

YEUNG, J., LI, W. & HOLINSTAT, M. 2018. Platelet Signaling and Disease: Targeted Therapy for Thrombosis and Other Related Diseases. Pharmacol Rev, 70**,** 526-548.

YIN, T., HE, S. S., LIU, X. L., JIANG, W., YE, T. H., LIN, Z. Q., SANG, Y. X., SU, C., WAN, Y., SHEN, G. B., MA, X. L., YU, M., GUO, F. C., LIU, Y. Y., LI, L., HU, Q. C., WANG, Y. S. & WEI, Y. Q. 2015. Extravascular Red Blood Cells and Hemoglobin Promote Tumor Growth and Therapeutic Resistance as Endogenous Danger Signals. Journal of Immunology, 194**,** 429-437.

ZEILER, M., MOSER, M. & MANN, M. 2014. Copy number analysis of the murine platelet proteome spanning the complete abundance range. Mol Cell Proteomics, 13**,** 3435-45.

ZHANG, X., ZHU, X., WANG, C., ZHANG, H. & CAI, Z. 2016. Non-targeted and targeted metabolomics approaches to diagnosing lung cancer and predicting patient prognosis. Oncotarget, 7**,** 63437-63448.

ZHANG, Y., DAUBEL, N., STRITT, S. & MAKINEN, T. 2018. Transient loss of venous integrity during developmental vascular remodeling leads to red blood cell extravasation and clearance by lymphatic vessels. Development, 145.

ZHOU, J., MAY, L., LIAO, P., GROSS, P. L. & WEITZ, J. I. 2009. Inferior vena cava ligation rapidly induces tissue factor expression and venous thrombosis in rats. Arterioscler Thromb Vasc Biol, 29**,** 863-9.

ZIELINS, E. R., BRETT, E. A., LUAN, A., HU, M. S., WALMSLEY, G. G., PAIK, K., SENARATH-YAPA, K., ATASHROO, D. A., WEARDA, T., LORENZ, H. P., WAN, D. C. & LONGAKER, M. T. 2015. Emerging drugs for the treatment of wound healing. Expert Opin Emerg Drugs, 20**,** 235-46.

ZIMMERMANN, J., VOSS, H., SCHWAGER, C., STEGEMANN, J. & ANSORGE, W. 1988. Automated Sanger dideoxy sequencing reaction protocol. FEBS Lett, 233**,** 432-6.

Appendix

Publications arising from this thesis:

WICHAIYO, S., LAX, S., MONTAGUE, S. J., LI, Z., GRYGIELSKA, B., PIKE, J. A., HAINING, E. J., BRILL, A., WATSON, S. P. & RAYES, J. 2019. Platelet glycoprotein VI and C-type lectin-like receptor 2 deficiency accelerates wound healing by impairing vascular integrity in mice. Haematologica, 104, 1648-1660.

RAYES, J., JADOUI, S., LAX, S., GROS, A., **WICHAIYO, S.**, OLLIVIER, V., DENIS, C. V., WARE, J., NIESWANDT, B., JANDROT-PERRUS, M., WATSON, S. P. & HO-TIN-NOE, B. 2018. The contribution of platelet glycoprotein receptors to inflammatory bleeding prevention is stimulus and organ dependent. Haematologica, 103**,** e256-e258.

LAX, S., RAYES, J., **WICHAIYO, S.**, HAINING, E. J., LOWE, K., GRYGIELSKA, B., LALOO, R., FLODBY, P., BOROK, Z., CRANDALL, E. D., THICKETT, D. R. & WATSON, S. P. 2017. Platelet CLEC-2 protects against lung injury via effects of its ligand podoplanin on inflammatory alveolar macrophages in the mouse. Am J Physiol Lung Cell Mol Physiol, 313**,** L1016-L1029.

RAYES, J., LAX, S., **WICHAIYO, S.**, WATSON, S. K., DI, Y., LOMBARD, S., GRYGIELSKA, B., SMITH, S. W., SKORDILIS, K. & WATSON, S. P. 2017. The podoplanin-CLEC-2 axis inhibits inflammation in sepsis. Nat Commun, 8**,** 2239.